

Structure, mechanism and engineering of pyridoxal phosphate-dependent racemases

Amina Frese

PhD

University of York

Chemistry

May 2018

Abstract

The objective of this work is the investigation and structural characterisation of pyridoxal phosphate (PLP)-dependent racemases. In particular α -amino- ϵ -caprolactam racemases (ACLRs), such as the enzyme from *Achromobacter obae* (*AoACLR*) are of interest for this work, as they have been found to racemise amino acid derivatives. This can be beneficial for the use of enzymes for the application for the dynamic kinetic resolution (DKR) of amino acid derivatives. In this work focus was put on the racemisation of the model substrate phenylalanine methylester due to the potential of a biocatalytic DKR of amino acid esters to the corresponding amides.

In addition to *AoACLR*, two further enzymes were identified in a homology search. Racemases from *Rhizobium freirei* (*RfACLR*) and *Ochrobactrum anthropi* (*OaACLR*) were identified as targets for the evaluation of PLP-dependent racemases. These enzymes were heterologous expressed in *Escherichia coli* and purified.

The purified ACLRs were subjected to crystallisation trials and especially *RfACLR* was found to crystallise well. Intensive structural analysis of *RfACLR* gave structures of different reaction intermediates of the racemisation reaction. A reaction mechanism proceeding *via* the formation of a geminal diamine and an achiral quinonoid was proposed based on these results. Furthermore, the catalytic residues D210 and K267 were identified by mutational analysis.

The purified enzymes were subjected to activity assay to evaluate their substrate spectrum. Only *OaACLR* was found to be active towards phenylalanine methylester. With information obtained from the structure of *OaACLR*, structure-guided engineering of *OaACLR* resulted in 3.4-fold activity-improved variant. This variant, *OaACLR*-L293C, was characterised in detail and found to be an overall improved variant of *OaACLR*. *OaACLR*-L293C is therefore a promising biocatalyst for the application DKR of amino acid esters.

List of Contents

1	Introduction	1
1.1	Pyridoxal phosphate-dependent enzymes.....	1
1.1.1	Pyridoxal phosphate as catalyst.....	1
1.1.2	Reaction specificity of PLP-dependent enzymes	2
1.1.3	Fold type I PLP-dependent enzymes	8
1.1.4	Decarboxylases.....	9
1.1.5	Transaminases	11
1.1.6	Phospholyases	13
1.1.7	C-C bond formation.....	13
1.1.8	Other reactions catalysed by PLP-dependent enzymes	15
1.2	Amino acid racemisation in Nature	16
1.3	Racemases in Biocatalysis.....	18
1.3.1	Hydroxyl carbonyl derivative racemases	20
1.3.2	Amino acid racemases	23
1.3.3	Amino acid derivatives racemases	28
1.4	Aim of this work.....	37
2	Materials and Methods	39
2.1	Materials.....	39
2.1.1	Plasmids.....	39
2.1.2	Bacterial strains	40
2.1.3	Devices and equipment.....	40
2.2	Methods.....	41
2.2.1	Cloning synthetic genes into an expression vector.....	41
2.2.2	Gel electrophoresis	44
2.2.3	Site directed mutagenesis of ACLRs.....	45
2.2.4	Generation of site-saturation libraries with inverse PCR	48
2.2.5	Cell cultivation and heterologous protein expression.....	50
2.2.6	Chromatographic enzyme purification	53
2.2.7	Crystallisation.....	54
2.2.8	HPLC based activity assay	58
2.2.9	Photometric activity assay	59
2.2.10	Development of the photometric activity assay	61
2.2.11	Determination of protein concentration.....	62
3	Enzyme production and activity	64
3.1	Introduction	64
3.2	Material and Methods.....	65
3.3	Results and discussion.....	65

3.3.1	Cloning of the target genes	65
3.3.2	Heterologous gene expression in <i>E. coli</i>	66
3.3.3	Scale up of heterologous expression in recombinant <i>E. coli</i>	68
3.3.4	Chromatographic protein purification.....	68
3.3.5	Influence of storage condition on the enzyme activity	71
3.3.6	Determination of quaternary organisation of <i>Oa</i> ACLR by analytical SEC...	72
3.4	Conclusion	73
4	Characterisation of the racemisation activity of ACLRs	74
4.1	Introduction.....	74
4.2	Materials and methods	74
4.3	Results and discussion	74
4.3.1	Activity towards α -amino- ϵ -caprolactam.....	74
4.3.2	Activity towards phenylalanine amide.....	76
4.3.3	Activity towards phenylalanine methyl ester.....	77
4.3.4	Substrate screen for racemisation.....	82
4.3.5	Investigation of substrate hydrolysis.....	83
4.3.6	Inhibition of ACLRs by amino acids	86
4.3.7	Stability and activity in organic solvent.....	87
4.4	Conclusion	89
5	Structural analysis of <i>Rf</i> ACLR	90
5.1	Introduction.....	90
5.2	Materials and Methods.....	91
5.3	Results and discussion	91
5.3.1	Initial crystallisation trails.....	91
5.3.2	Structure of <i>Rf</i> ACLR	92
5.3.3	Mutational analysis of the reaction mechanism of <i>Rf</i> ACLR.....	99
5.4	Conclusion	109
6	Comparison of <i>Oa</i> ACLR and <i>Rf</i> ACLR	110
6.1	Introduction.....	110
6.2	Materials and Methods.....	110
6.3	Results and discussion	110
6.3.1	Structure of <i>Oa</i> ACLR	110
6.3.2	Comparison of <i>Rf</i> ACLR and <i>Oa</i> ACLR	111
6.3.3	Structure of <i>Oa</i> ACLR crystallised in presence of L-PheOMe.....	117
6.4	Conclusion	119
7	Photometric assay for the detection of AAER activity	121
7.1	Introduction.....	121
7.2	Materials and methods	122
7.3	Results and discussion	122

7.3.1	Development of a photometric assay for amino acid ester racemisation	122
7.4	Conclusion.....	128
8	Engineering of improved AAER activity	129
8.1	Introduction	129
8.2	Materials and methods.....	129
8.3	Results and discussion.....	129
8.3.1	Generation of saturation mutagenesis libraries	129
8.3.2	Cultivation and screening of <i>Oa</i> ACLR saturation mutant libraries	132
8.3.3	Purification and activity of positive hits from AAER screening.....	135
8.3.4	Comparison of <i>Oa</i> ACLR-L293C and wt <i>Oa</i> ACLR.....	137
8.4	Conclusion.....	144
9	Conclusions and future work.....	145
10	Appendix	148
10.1	Vector map of Lic3c vector.....	148
10.2	Gene sequences and corresponding amino acid sequences	148
10.3	Buffers for solubility screen	150
10.4	Data collection details for ACLR crystals.....	153
10.5	Kinetic parameters of <i>Oa</i> ACLR-L293C and <i>Oa</i> ACLR	156
	Abbreviations	157
	References	159

List of Figures

Figure 1: Chemical structure of PLP.....	1
Figure 2: Different types of PLP catalysed reactions.....	2
Figure 3: Formation of the external aldimine.	3
Figure 4: Different reaction types after formation of the external aldimine.....	4
Figure 5: Illustration of the Dunathan hypothesis.....	4
Figure 6: Reaction scheme of the two step conversion of dialkylglycine.....	5
Figure 7: Productive and non-productive conformations of D-amino acids.....	6
Figure 8: Reaction scheme for the racemisation of alanine catalysed by alanine racemase. ...	7
Figure 9: Structure of <i>Rf</i> ACLRL.....	9
Figure 10: Reaction scheme of PLP-dependent enzyme-catalysed decarboxylation.....	10
Figure 11: Reaction scheme of transaminase catalysed reaction.	11
Figure 12: First half reaction catalysed by glutamate aminotransferase.....	12
Figure 13: Serine hydroxymethyltransferase catalysed α -elimination and replacement.....	14
Figure 14: Different pathways for α/β -eliminations.....	15
Figure 15: Ind4 catalysed oxidation of a C-C bond of arginine. ⁷⁴	16
Figure 16: Phylogenetic tree of racemases and epimerases.	18
Figure 17: Two base reaction scheme of alanine racemase.....	19
Figure 18: Scheme of a DKR.....	20
Figure 19: Scheme of substrates favoured or disfavoured by mandelate racemase.....	21
Figure 20: Proposed reaction mechanism of lactate racemase.....	23
Figure 21: Process scheme of multi-enzyme system for the production of D-phenylalanine.....	25
Figure 22: Reaction scheme of one-pot fermentation of L-pipecolic acid.....	27
Figure 23: Scheme of D-hydantoin kinetic resolution to produce D-amino acids.....	29
Figure 24: Hydantoin process for the production of L-amino acids.....	30
Figure 25: DKR of <i>N</i> -acetyl amino acids to L-amino acids.....	31
Figure 26: DKR process for the production of L-lysine.....	32
Figure 27: Mechanism for the transamination of VAL catalysed by <i>Ao</i> ACLRL.....	34
Figure 28: Structure of <i>Ao</i> ACLRL.....	35
Figure 29: Dynamic kinetic resolution of racemic amino acid esters.....	37
Figure 30: Scheme of the N-terminal region of the target protein.....	39
Figure 31: Scheme of ligation independent cloning procedure.	42
Figure 32: Scheme of site directed mutagenesis using the Quikchange method.....	46
Figure 33: Scheme of site directed mutagenesis using inverse PCR.....	48
Figure 34: Scheme of different methods for vapour diffusion protein crystallisation.....	54
Figure 35: Scheme of MRC plate set up with CSS I and II crystallisation screen.....	55
Figure 36: Scheme of concentration variation in a 24 well crystallisation tray.	56
Figure 37: Crown ether used for chromatographic separation of amine enantiomers.	58
Figure 38: Scheme of the coupled enzyme assay for the detection of AAER activity.	60
Figure 39: Protein sequence alignment of <i>Oa</i> ACLRL, <i>Rf</i> ACLRL and <i>Ao</i> ACLRL.....	65
Figure 40: Agarose gel electrophoresis of the test restriction.....	66
Figure 41: SDS-PAGE of overexpression of <i>Ao</i> ACLRL, <i>Rf</i> ACLRL and <i>Oa</i> ACLRL.....	66
Figure 42: SDS-PAGE of test-expressions of <i>Oa</i> ACLRL in <i>E. coli</i> Rosetta.....	67
Figure 43: Growth curve of recombinant <i>E. coli</i> cells.....	68
Figure 44: Chromatogram of IMAC purification of <i>Rf</i> ACLRL.....	69
Figure 45: SDS-PAGE of fractions obtained from IMAC of <i>Rf</i> ACLRL.....	69
Figure 46: Chromatogram of SEC purification of <i>Rf</i> ACLRL.....	70
Figure 47: Purity of fractions obtained after SEC purification.....	70
Figure 48: Chromatogram of analytical size exclusion of <i>Oa</i> ACLRL.....	72
Figure 49: Calibration graph for D-ACL and L-ACL.....	75
Figure 50: Enzymatic racemisation of L-ACL.....	75
Figure 51: Calibration graph for determination of the concentration D- or L-PheNH ₂	76
Figure 52: Racemisation of L-PheNH ₂ catalysed by ACLRLs.....	76

Figure 53: Calibration graph for the determination of D- or L-PheOMe by chiral HPLC.....	78
Figure 54: Chromatogram of sample from reaction with <i>Oa</i> ACLR and L-Phe	79
Figure 55: Formation of D-Phe from the racemisation of L-PheOMe with ACLRs	79
Figure 56: Racemisation of L-PheOMe catalysed by <i>Oa</i> ACLR.....	80
Figure 57: Racemisation of L-PheOMe catalysed by <i>Oa</i> ACLR.....	81
Figure 58: Racemisation of L-PheOMe catalysed by <i>Oa</i> ACLR.....	81
Figure 59: Racemisation of L-PheOMe catalysed by <i>Oa</i> ACLR	81
Figure 60: Reaction scheme for a DKR of a racemic ester	82
Figure 61: Influence of the pH on hydrolysis of L-AAE-2.	84
Figure 62: Summary of racemisation of L-AAE-2 in ammonia solution	85
Figure 63: Influence of D-amino acid-2 on activity of <i>Oa</i> ACLR.....	86
Figure 64: Relative activities of <i>Oa</i> ACLR after incubation in MTBE.....	87
Figure 65: Racemisation reaction of L-PheNH ₂ catalysed by <i>Oa</i> ACLR in MTBE.....	88
Figure 66: Active site of <i>Ao</i> ACLR complexed with ϵ -caprolactam.....	90
Figure 67: <i>Rf</i> ACLR crystals obtained in crystal screening in MRC plates	92
Figure 68: Pictures of <i>Rf</i> ACLR crystals in hanging drops.	92
Figure 69: Quaternary structure of <i>Rf</i> ACLRs.	93
Figure 70: PLP-binding residues in the active site of <i>Rf</i> ACLR	93
Figure 71: <i>Rf</i> ACLR complexed with L-ACL.	94
Figure 72: View in active site of <i>Rf</i> ACLR modelled with L-Phenylalanine amide.....	95
Figure 73: Substrate binding site of <i>Rf</i> ACLR modelled with L-Phenylalanine amide.....	96
Figure 74: The binding site of <i>Rf</i> ACLR modelled with phenylalanine amide	96
Figure 75: Substrate binding of <i>Rf</i> ACLR.....	97
Figure 76: Conformational change of the C-terminal end	98
Figure 77: Substrate recognising residues of the substrate binding site of <i>Rf</i> ACLR.	99
Figure 78: SDS gels of test expression of <i>Rf</i> ACLR-Y137F in <i>E. coli</i> Rosetta cells.	100
Figure 79: Western blot of <i>Rf</i> ACLR-Y137A from soluble and insoluble fractions.....	100
Figure 80: Chromatogram of IMAC purification of <i>Rf</i> ACLR-Y137F	101
Figure 81: SDS gel of fractions obtained from IMAC of <i>Rf</i> ACLR-Y137F.	101
Figure 82: Active site of <i>Rf</i> ACLR-K241A mutant complexed with D-ACL	103
Figure 83: a) Change of the UV spectrum of <i>Rf</i> ACLR-D210A	104
Figure 84: Structure of the active site of <i>Rf</i> ACLR-D210A complexed with D-ACL.....	105
Figure 85: Aromatic cage in <i>Rf</i> ACLR for specific substrate binding.	106
Figure 86: Angle between Schiff base and C α -bond of ACL in the external aldimine.....	106
Figure 87: View in the active site of <i>Rf</i> ACLR variants complexed with ACL	107
Figure 88: Putative reaction mechanism of <i>Rf</i> ACLR.....	108
Figure 89: Pictures of <i>Oa</i> ACLR crystals.....	110
Figure 90: a) Quaternary structure of <i>Oa</i> ACLR.....	111
Figure 91: Comparison of structures of <i>Rf</i> ACLR and <i>Oa</i> ACLR	112
Figure 92: SDS-PAGE of solubility screening of <i>Rf</i> ACLR-W49A-M293L.....	113
Figure 93: Chromatogram of IMAC purification of <i>Rf</i> ACLR-W49A-M293L.	114
Figure 94: SDS PAGE gel after IMAC purification of <i>Rf</i> ACLR-W49A-M293L.....	114
Figure 95: Broom stick crystals obtained from <i>Rf</i> ACLR-W49A-M293L.....	115
Figure 96: Comparison of <i>Rf</i> ACLR and <i>Oa</i> ACLR.	116
Figure 97: Overlay of Y139 of <i>Oa</i> ACLR subunits A-D.	117
Figure 98: View in substrate binding site of <i>Oa</i> ACLR.....	118
Figure 99: Enzyme cascade for detection of PheOMe racemisation.....	122
Figure 100: TLC of alcalase catalysed reaction	123
Figure 101: Photometric detection PheOMe racemisation.....	124
Figure 102: Reaction of the photometric assay for AAER detection.....	125
Figure 103: Colour formation with the photometric assay	126
Figure 104: Optimisation of cell lysate concentration for the photometric assay	127
Figure 105: Bases in the target positions for saturation mutagenesis.....	131
Figure 106: Quality of saturation mutant libraries	131
Figure 107: Growth of <i>E. coli</i> BL21- <i>Oa</i> ACLR in 96 deep well plates.....	132

Figure 108: Cell growth of <i>E. coli</i> BL21 (DE3) cell overexpressing <i>OaACLR</i> mutants	133
Figure 109: Screening for activity-improved <i>OaACLR</i> mutants.....	134
Figure 110: Purified <i>OaACLR</i> variants after IMAC purification.....	135
Figure 111: Conversion of L-ACL to D-ACL catalysed by different <i>OaACLR</i> mutants.....	136
Figure 112: Relative activity of <i>OaACLR</i> mutants towards L-PheOMe	136
Figure 113: Conversion of L-PheOMe catalysed by purified <i>OaACLR</i>	138
Figure 114: Non-linear regression of activities measured for <i>OaACLR</i>	139
Figure 115: Non-linear regression of activities measured for <i>OaACLR</i> -L293C.....	140
Figure 116: a) Chromatogram of conversion of L-ACL by <i>OaACLR</i> -D210A.....	143
Figure 117: Separation of a mixture of D/L-ACL by chiral HPLC.	155
Figure 118: Separation of a mixture of D/L-PheNH ₂ by chiral HPLC.	155
Figure 119: Separation of a mixture of D/L-PheOMe by chiral HPLC.	156

List of Tables

Table 1: Overview of enzymes of investigated in this work.	37
Table 2: Racemase expression vectors1	39
Table 3: Bacterial strains.....	40
Table 4: Devices.....	40
Table 5: Reaction mixture for PCR.....	41
Table 6: Parameters of PCR for amplification of the target genes.....	41
Table 7: Primers used for ligation independent cloning.....	42
Table 8: Buffers used for western blotting.	45
Table 9: Primers used for site directed mutagenesis.	46
Table 10: PCR reaction components employed for site directed mutagenesis.....	47
Table 11: Program used for PCR for site directed mutagenesis.....	47
Table 12: Primers used for generation of site-saturation of <i>Oa</i> ACLR in position 51 or 293.....	49
Table 13: Components used for inverse PCR.....	49
Table 14: Touch down PCR program.....	49
Table 15: Components for the phosphorylation and ligation of the PCR product.	50
Table 16: Components for 1 L LB autoinduction medium.	50
Table 17: Components for 1 L TB autoinduction medium.	51
Table 18: Program for IMAC purification of his-tagged proteins.....	53
Table 19: Conditions tested for storage of purified <i>Rf</i> ACLR after purification.....	59
Table 20: Volumes and concentrations of the assay components	60
Table 21: Summary of chromatographic purifications of ACLRs.	70
Table 22: Relative activities of <i>Rf</i> ACLR obtained after storage under different conditions..	71
Table 23: Racemisation of PheOMe with cell lysate containing ACLRs	78
Table 24: Substrate screen of <i>Oa</i> ACLR.....	83
Table 25: Influence of reaction buffer on the chemical hydrolysis of L-AAE-2.....	85
Table 26: Comparison of initial activities and conversions.	88
Table 27: Summary of initial activities measured for ACLRs	89
Table 28: Conditions for crystallisation of ACLRs.....	91
Table 29: Activities for the racemisation of ACL with different <i>Rf</i> ACLR variants..	102
Table 30: Specific activities of <i>Rf</i> ACLR variants towards amino acid derivatives.	102
Table 31: Distances of residues relevant for catalysis to the substrate chiral centre.....	107
Table 32: Comparison of activities of <i>Oa</i> ACLR and <i>Rf</i> ACLR.....	112
Table 33: Comparison of activities measured with <i>Rf</i> ACLR and <i>Oa</i> ACLR variants.	113
Table 34: Activity of <i>Rf</i> ACLR variants towards ACL, PheNH ₂ and PheOMe.....	116
Table 35: Comparison of B-factors of tyrosine 137/ 139 of <i>Rf</i> ACLR and <i>Oa</i> ACLR.	118
Table 36: Summary of mutational evaluation of <i>Rf</i> ACLR and <i>Oa</i> ACLR	119
Table 37: Optimal assay conditions identified for the detection of AAER activity.	128
Table 38: Primers for the generation of a saturation mutagenesis library	130
Table 39: Purification yield and activity of best hits from AAER screening.....	135
Table 40: Summary of kinetic parameters determined for <i>Oa</i> ACLR.	140
Table 41: Conversions of different substrates with <i>Oa</i> ACLR and <i>Oa</i> ACLR-L293C.....	141
Table 42: Buffers used for solubility screen of <i>Rf</i> ACLR-W49A-M293L.....	150
Table 43: Data collection and refinement statistics.....	153
Table 44: Kinetic parameters obtained from curves with non-linear fitting.	156
Table 45: Kinetic parameters obtained from curves with non-linear fitting	156

Acknowledgements

First and foremost I would like to thank Gideon Grogan for giving me the opportunity to work on this project. I thank him for his excellent and friendly supervision which helped me to progress and personally grow during my PhD. I am greatly thankful for the freedom to work on different aspects of this project and the engagement in other projects. I am truly grateful for Gideon's support and encouragement throughout my whole PhD, especially when things did not work as planned.

I would also like to thank Peter Sutton for his engaging involvement and interest in my project and for his supervision during my placement at GSK. I would like to thank Joe Adams for taking over the supervision of my project and carrying on with the same interest in my progress. I thank Martin Fascione for taking up the role as my internal panel member and for the helpful and fruitful discussion and suggestions during my TAP meetings.

I appreciate the scientific support at the University of York and thank Amanda Dixon for training and help with HPLC equipment. I would like to thank Matthew Thompson from the University of Manchester for sharing his expertise in molecular cloning and screening of mutant libraries.

My gratitude goes to all members of YSBL for creating a welcoming and friendly work atmosphere. Special thanks go to the technical staff, Simon Grist, Louise Haigh and Juliet Borgia, for supporting every-ones research by running the labs so efficiently. My thanks also go to Johan Turkenburg and Sam Hart for collecting crystallographic data during night shifts at the synchrotron.

My great thanks go to all present and past members of the Grogan Group, who have made the time during my PhD so enjoyable. I am truly grateful for the scientific discussions that helped me with the progress of my work. I am even more thankful for all the non-scientific discussions during coffee and lunch breaks, group meals and social events. I enjoyed our group trips and nights out, particularly the pub quizzes! I thank Anibal Cuetos, Claudia Spandolf, Henry Man, Lilian Beloti, Mahima Sharma, Reza Danesh-Azari and Tamara Mielke for not only being colleagues but also good friends. Special thanks go to Muhiadin Omar, my mentor in the lab, who patiently answered all my questions when I started and always had true life advice for me. I thank Lilly Wells for her friendship and wholehearted conversations during our regular takeaway nights.

I thank my friends for supporting me during this time away from home in a different country. I thank Anabelle Schwarz, Dalia Bulut and Marion Zaworra for their regular visits in York, which made settling in to this new place a lot easier.

I am truly thankful for everything my partner Mark Petchey has done to support me during the time of my PhD. I thank him for his endless support, his inspiring curiosity for science and for always encouraging me to do my best.

I thank my father, Alan Jones, for supporting me wherever he can and for being an example and motivation for me to work hard for achieving my goals. I thank my sister, Julia Frese, her inquisitiveness has always been an inspiration for me. My biggest and deepest gratitude goes to my mother, Jutta Frese, for her support in everything I do. Without her love, support, and efforts I would not have been able to achieve this.

Declaration

I declare that this thesis is a presentation of original work and I am the sole author. This work has not previously been presented for an award at this, or any other, University. All sources are acknowledged as References in the main text.

All research carried out and presented within this thesis was completed by the author, with exception of collaborative work which is stated in the main text and listed below.

Work carried out or overseen by others:

- Initial homology search for *AoACLR* was carried out by Prof. Gideon Grogan
- Synthetic genes for ligation independent cloning were designed by Dr. Claudia Spandolf and synthesised by Invitrogen
- YSBLIC3C-vector for cloning was prepared by Dr. Henry Man
- Standards for analytical size exclusion chromatography were run by Mark Petchey
- Crystallographic data were collected by Dr. Johan Turkenburg and Sam Hart
- Gene sequencing was carried out by GATC Biotech
- Primer oligonucleotides were synthesised by Eurofins Genomics
- Competent bacteria cells were purchased from Merck or Novagen

1 Introduction

1.1 Pyridoxal phosphate-dependent enzymes

1.1.1 Pyridoxal phosphate as catalyst

Since the discovery of pyridoxal 5'-phosphate (PLP) in the 1940s the interest in PLP in chemical synthesis has not declined due to its vast versatility as catalyst.¹⁻² The biological activity of PLP as vitamin B₆ was first discovered in 1951 for bacteria, yeasts and rats.³ In living organisms PLP is recruited as a cofactor by apo-enzymes for biocatalytic activity as shown by Snell *et al.* for the first time in 1962.⁴ The biologically active form of vitamin B₆ is either PLP or pyridoxamine phosphate (PMP) and is covalently bound in the enzyme active site.

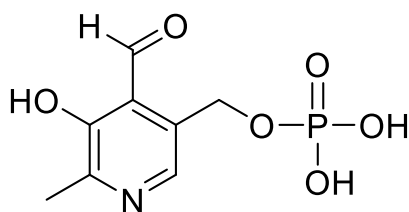


Figure 1: Chemical structure of PLP.

PLP-dependent enzymes take part in many different cellular processes, especially in the biosynthesis of amine containing metabolites, such as amino acids and their derivatives or amino sugars.⁵ Due to the significant role of PLP-dependent enzymes in cellular processes they are often drug targets for inhibitory inactivation. For example γ -aminobutyric acid aminotransferase or ornithine decarboxylase are targets for the treatment of epilepsy, respectively African sleeping sickness through inhibition of the enzymes.⁵ On the other hand, dysfunction in PLP-dependent enzymes can cause diseases like homocystinuria caused by deficiency of the cystathionine β -synthase.⁶

PLP can catalyse transaminations, decarboxylations, racemisations, eliminations and replacement reactions. Transamination, decarboxylation and racemisation are catalysed at the α position, elimination and replacement at the β or γ position as illustrated in Figure 2.¹

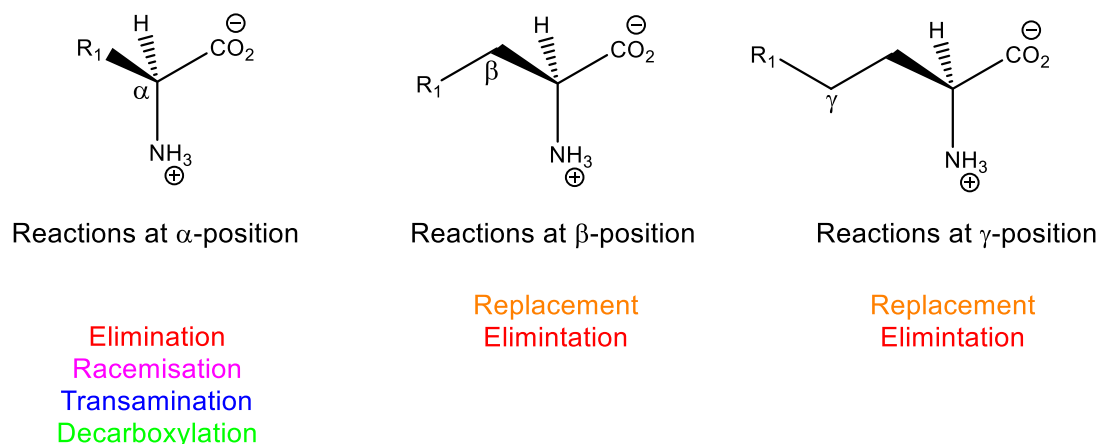


Figure 2: Different types of PLP catalysed reactions. The reactions are categorised according to the position of the bond breaking of the substrate.

The function of PLP as cofactor is identical in all the reactions: it stabilises the negative charge at the $C\alpha$ of the reaction intermediate. The transition state, namely the external aldimine is formed after a condensation reaction of the aldehyde group of PLP and the substrate amine forming a Schiff base. The negative charge of the formed carbanion is stabilised by the delocalisation of the negative charge over the π -system of the pyridine ring, which often is described as ‘electron sink’.⁵ The formation of the quinonoid enables the removal of the $C\alpha$ proton and thus allows for the subsequent chemistry for different reactions. PLP enables the deprotonation of the $C\alpha$ of amino derivatives under physiological conditions through the stabilisation of the negative charge of the carbanion. Under physiological conditions the pK_a at the $C\alpha$ is normally too high for proton abstraction.⁷ Outside biological systems, PLP can also work as catalyst in solution as the crucial step for catalysis is the formation of a stabilised intermediate. However, incorporation in an enzyme scaffold enhances reactivity and substrate specificity determines the type of the reaction that is catalysed.

1.1.2 Reaction specificity of PLP-dependent enzymes

All PLP-dependent, enzyme-catalysed reactions have the formation of an external aldimine intermediate of the cofactor and the substrate in common (Figure 3).

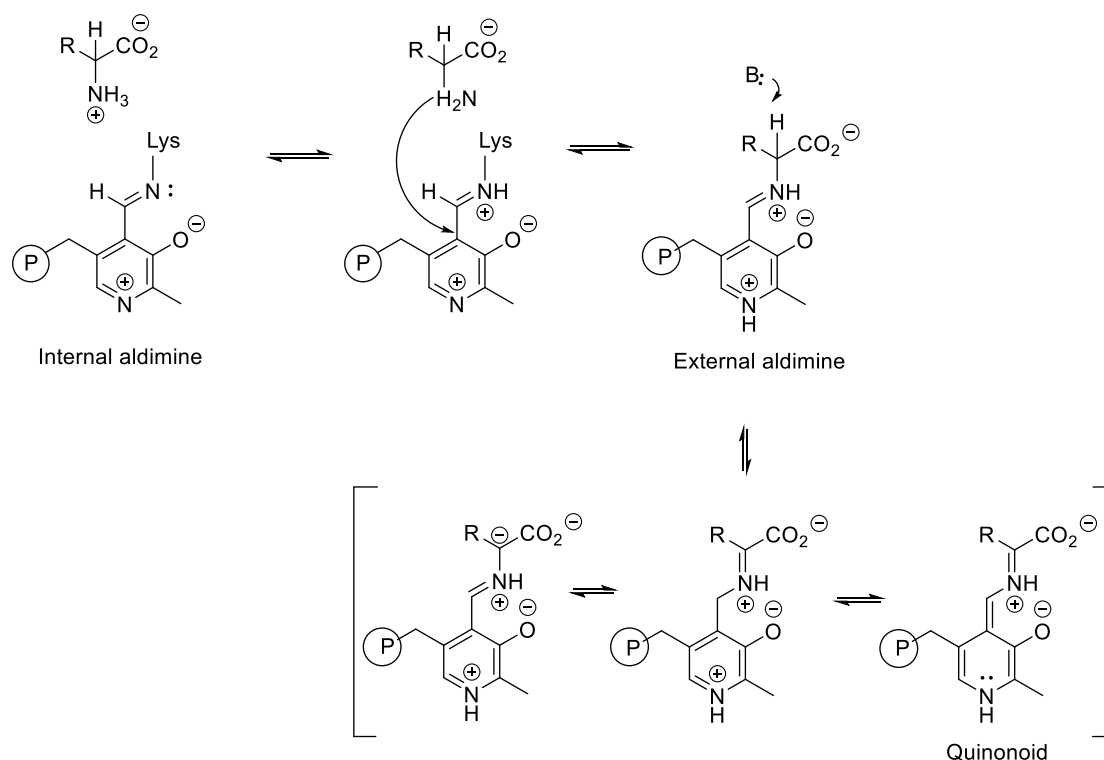


Figure 3: Formation of the external aldimine and the different resonance structures of the carbanionic intermediates.

The external aldimine is formed after attack of the protonated Schiff base, which is formed between an active site lysine ϵ -amine and the C4' of PLP. The Schiff base is attacked by the unprotonated amino group of the substrate resulting in the breaking of the bond between enzyme and cofactor and formation of a new Schiff base between substrate and cofactor.⁸ One intermediate state of the newly formed external aldimine is the so called quinonoid. Formation of the reaction intermediate is linked with the increase in electron delocalisation energy which increases the potential for bond breaking at the substrate C α .⁹

The external aldimine is the starting point to the many different reactions that are catalysed by PLP-dependent enzymes. The reaction type is determined by which bond of the external aldimine C α is broken.⁸ Theoretically, any of the three bonds at the C α can be broken (Figure 4) and different classes of PLP-dependent enzymes have evolved different scaffolds to control the specificity of the bond breaking.

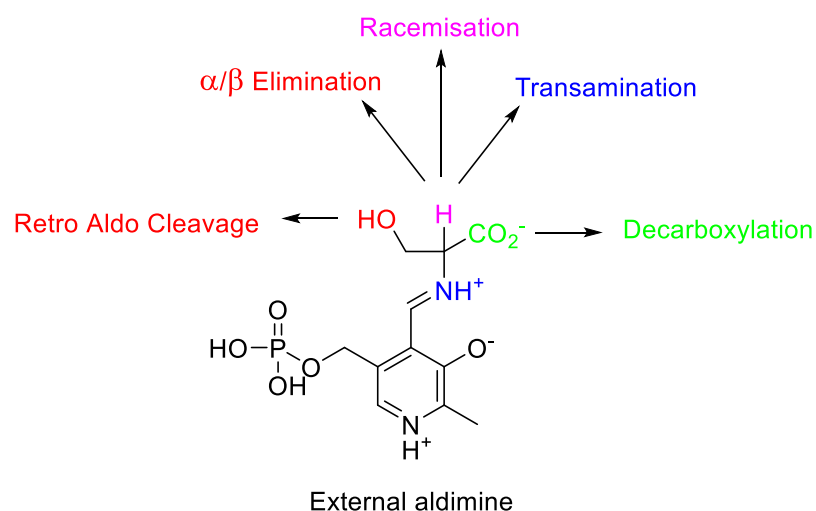


Figure 4: Different reaction types after formation of the external aldimine. Most reactions (elimination, racemisation, transamination) follow the proton abstraction at $C\alpha$. Adapted according to Toney *et al.*⁸

In 1966 Dunathan published a hypothesis to predict the type of reaction that is catalysed after formation of the external aldimine. The “Dunathan hypothesis” postulates that the conformation of the $C\alpha$ in relation to the pyridine ring of PLP determines the type of catalysed reaction. The bond that is at 90° angle to the pyridine ring, hence parallel to the π -system, is broken. This bond is destabilised through stereoelectronic effects of the π -system and the resulting carbanion is stabilised through the charge delocalisation through the π -system of the pyridine ring.⁹ Evidence for this hypothesis was later found in the solved structure of an aminotransferase complexed with phosphopyridoxyl aspartate. Jansonius *et al.* solved the structure of an aspartate aminotransferase to 2.8 \AA with substrate analogues revealing the catalytic residue, K258, and conformational changes that direct substrate specificity.¹⁰⁻¹²

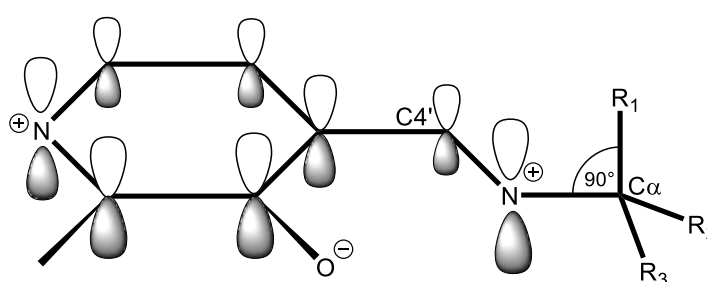


Figure 5: Illustration of the Dunathan hypothesis to predict the type of reaction that is catalysed after formation of the external aldimine. Picture is modified according to Toney *et al.*¹³

Once the carbanionic intermediate (Figure 3) is formed by deprotonation of the external aldimine at the $C\alpha$ it can go under different reactions.⁸ The simplest bond forming reaction is protonation at the opposite face of $C\alpha$ which is a racemisation reaction and gives the opposite enantiomer of the starting material as product. Protonation of the $C4'$ of the cofactor results in a ketimine intermediate and subsequent hydrolysis to give a ketone product as first half-

reaction of a transamination. The carbanionic intermediate can also act as a nucleophile which can result in α/β elimination, in the case of a good leaving group at C β . In a retro aldol condensation the α - β bond can be broken.⁸ In general three different principles determine the type of reaction that is catalysed after formation of the carbanionic intermediate which will be further discussed below.

1. Stereoelectronic effects determine bond breaking and making
2. The protonation state of PLP
3. The conformation of the active site and catalytic residues

1.1.2.1 Stereo-electronic effects: Specificity of dialkylglycine decarboxylase

The reaction specificity of PLP-dependent enzymes was in detail studied for dialkylglycine decarboxylase as this enzyme is able to catalyse two half reaction types: transamination and decarboxylation (Figure 6). The first half reaction is a decarboxylation reaction resulting in a ketone product and pyridoxamine phosphate (PMP). CO₂ is released from the substrate followed by the protonation of the C4' of PLP resulting in a ketimine intermediate. Subsequently, the intermediate is hydrolysed to the ketone product and PMP. This is a typical reaction mechanism for transamination as opposed to the C α protonation as typical for decarboxylation reactions. The second half-reaction is a typical transamination reaction where the generated PMP and pyruvate substrate react to the corresponding amino acid and PLP.¹³

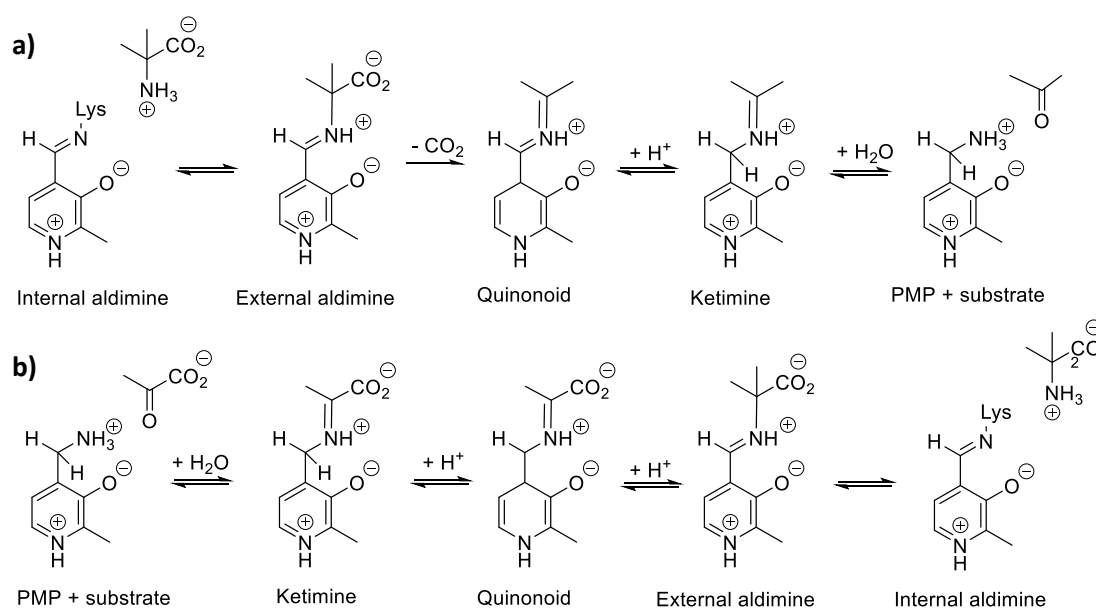


Figure 6: Reaction scheme of the two step conversion of dialkylglycine to amino acids catalysed by dialkylglycine decarboxylase. **a)** Decarboxylation half-reaction. **b)** Transamination half-reaction.

Crystal structures were obtained for dialkylglycine decarboxylase with substrates and different external aldimine intermediates.¹⁴⁻¹⁵ It was possible to designate three sites in the substrate binding pocket, named site A, B or C (see Figure 7). In the catalytic site A bond breaking and making is catalysed, whereas in site B carboxylate or larger alkyl groups are bound for the transamination half-reaction. Site C is restricted to bind only small alkyl groups.¹⁵ The activity and specificity towards the decarboxylation of a specific substrate is determined by sterical hindrance or preference in the site B.¹⁵⁻¹⁶

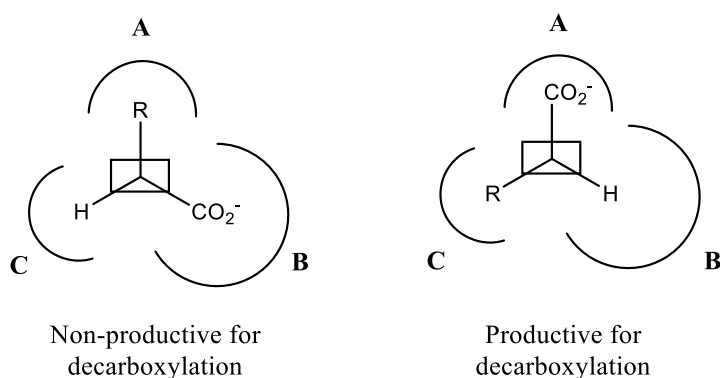


Figure 7: Productive and non-productive conformations of D-amino acids in the three different binding pockets of dialkylglycine decarboxylase.

Two different binding modes influence the specificity towards decarboxylation: it is promoted when the substrate carboxylate is located in the catalytic site A and prohibited when the carboxylate is accommodated in site B.¹⁵ This model explains the higher activity towards substrates with larger side chains. Binding of larger side chains is favoured in the larger site B, so that the carboxylate is bound in the catalytic site A.

1.1.2.2 Protonation state of PLP: Specificity of alanine racemase

Bacterial alanine racemase has been extensively studied due to its importance for bacterial growth and involvement of cell wall synthesis. Structural studies revealed the X-ray structure of the enzyme in complex with alanine.¹⁷ Based on the complex with alanine a reaction mechanism was proposed as summarised in Figure 8.

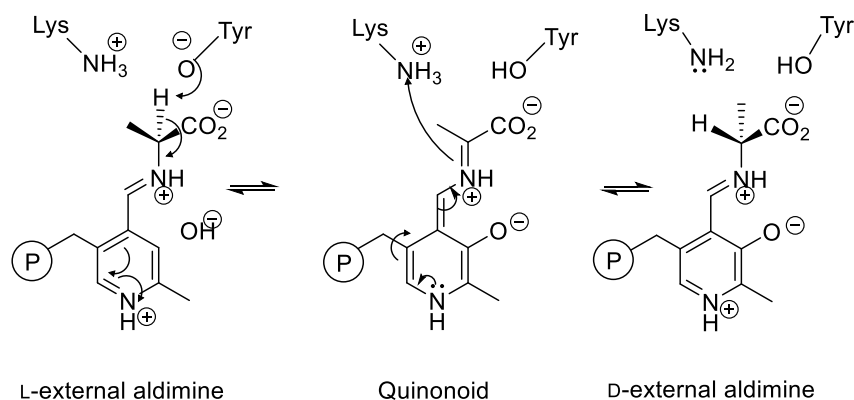


Figure 8: Reaction scheme for the racemisation of alanine catalysed by alanine racemase.

Y265 and K39 were identified as the catalytic acid/base pair by structural and mutational analysis.¹⁸ The residues are located at opposite faces of the C α , therefore enabling de- and reprotonation to give opposite enantiomers. An arginine is found in position 219 in alanine racemase; in aminotransferases a residue with a carboxylic group is often found in the homologous position. The pyridine nitrogen of PLP is protonated by the carboxylic group resulting in a more electrophilic pyridine, whereas arginine is unlikely to protonate the nitrogen.¹⁹⁻²⁰ The racemisation of D-alanine is catalysed *via* the formation of the D-external aldimine which is deprotonated by K39. The resulting carbanion is unstable due to the unprotonated state of the pyridine nitrogen. The carbanion is reprotonated by Y265 and the product is released by transamination.

1.1.2.3 Active site conformation

Reactions with solely PLP as catalyst showed that different reaction types were catalysed. Due to the lack of any conformational control during the catalysis, the specificity for a certain reaction type was low yielding a mixture of different products.²¹ PLP alone is an effective catalyst, however, the scaffold of the apoenzyme introduces high substrate and reaction specificity to the catalysis. This was shown by several mutational experiments that highlighted the importance of the active site environment on the reaction specificity.⁸

Replacing tyrosine with alanine in position 265 of the alanine racemase from *Geobacillus stearothermophilus* resulted in the 10⁵ fold increase of the aldolase activity and a 10³ decrease in the wild type racemase activity.²² In absence of the catalytic Y265, H166 takes over the role as the catalytic base during catalysis which leads to a change in reaction specificity to a retro-aldol condensation.

The rational design of an aspartate decarboxylase furthermore stresses the impact of active site residues on the reaction specificity. Based on differences in conserved amino acid residues in aspartate β -decarboxylases and aspartate transferases Wang *et al.* designed seven different

single mutants of an aspartate decarboxylase. The aminotransferase activity was introduced by the single mutation F204W into the aspartate decarboxylase and was 3.8 fold increased over decarboxylase activity.²³

Christen *et al.* were able to switch the reaction specificity of an aspartate aminotransferase from *Escherichia coli* (*E. coli*) into an aspartate decarboxylase by generating a triple mutant (Y225R/R292K/R386A). Investigation of the impact of the single mutation revealed that the arginine shift from R386A to Y225R was responsible for introduction of β -decarboxylase activity. In contrast, the mutation R293K reduced transferase activity of the enzyme by altering the substrate binding.²⁴

1.1.3 Fold type I PLP-dependent enzymes

All PLP-dependent enzymes can be classified into one of five different fold types (I-V). The fold type does not determine the type of reaction that is catalysed, but is a consequence of evolutionary process towards PLP-dependent enzymes. The majority of PLP-dependent enzymes are of fold type I.²⁵ A functional-phylogenetic analysis suggests that all fold types originate from a universal organism from ancestral enzymes.²⁶ The ancestral enzymes then evolved into the different fold type enzymes. Fold I type enzyme are diverse in their catalysed reaction but the majority were reported to catalyse reactions at the substrate C α .²⁶ As outlined above reactions at this position include racemisation, decarboxylation, elimination and transamination reactions.

The diversity of the fold type I group is due to the high number of enzymes belonging to this group. However the overall structure is conserved, and often referred to as aspartate aminotransferase superfamily.²⁵ All fold type I enzymes are dimers or higher order oligomers with one active site per subunit, which is located at the interface of the two subunits as illustrated in Figure 9.⁵

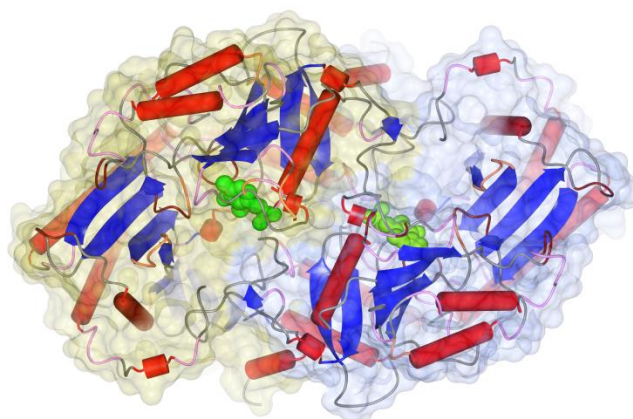


Figure 9: Structure of *RfACL*R (solved in this work) as representative of the fold type I of PLP-dependent enzymes. The secondary structure is represented in α -helices (red tubes) and blue β -sheets. The two subunits are represented as surface model in different colours (blue and gold). The active site is located at the interface of the dimers indicated by the cofactor PLP shown as green spheres.

Each monomer is built from a large and a small domain and the domains can undergo a conformational change after substrate binding, which might increase reactivity and determine substrate specificity.⁵ PLP binding is conserved in fold type I enzymes, as the *si*-face of PLP is buried in the PLP binding site and the bond making and breaking occurs on the buried *si*-face of the cofactor.²⁷ Even though the positioning of the PLP in its binding site is conserved within this group of PLP-dependent enzymes different residues are involved in the binding. The pyridine ring is often stacked between aromatic or hydrophobic residues, whereas charged or polar residues interact with the phosphate backbone of PLP.²⁸ Conserved throughout all PLP-dependent enzymes is the formation of the internal aldimine with a lysine that forms the Schiff base to the C4' of PLP.

1.1.4 Decarboxylases

Decarboxylases are of great physiological importance in living organisms. They are involved in the biosynthesis of amines and polyamines in prokaryotes and are used by bacteria for the intracellular and extracellular pH regulation through decarboxylation of amino acids.²⁹ In mammals they play a major role in the production of monoamine neurotransmitters. Some decarboxylases bind a pyruvoyl residue as prosthetic group in the active site, however, the majority of decarboxylases uses PLP as cofactor.³⁰ Decarboxylases were first classified by Christen *et al.* based on an alignment of nine different PLP-dependent enzymes which subdivided decarboxylases into four different classes (I-IV) with a different evolutionary background.³⁰ All decarboxylases of the groups I-III represent the fold type I; only members of the group IV exhibit the fold type III.²⁷ The structure of ornithine decarboxylase from *Lactobacillus* represents fold type I and, despite their low sequence homology, showed

similarity to fold type I aspartate transaminase, especially in the PLP binding motif.³¹ Comparing a bacterial and a mammalian ornithine decarboxylase revealed structural differences, especially in the stereochemistry of the enzyme-catalysed reaction, suggesting convergent evolution of bacterial and mammalian decarboxylases.²⁷

The reaction specificity in decarboxylases is controlled by the general stereo-electronic concept of PLP enzymes (Figure 10). After formation of the external aldimine, transaldimination results in the orientation of the α -carboxylate group parallel to the π -system of pyridine ring. The α - β or α - γ bond is then cleaved to release CO_2 resulting in the quinonoid, which is stabilised by electron delocalisation through the conjugated π -system.³² Depending on the conformation of the proton donor relative to the pyridine ring either retention or inversion of the configuration of the substrate is obtained. Retention occurs when the proton donor lies on the same side of the pyridine ring as the carboxylate group, inversion when the proton donor is on the opposite site of the pyridine ring of the leaving group.²⁷ Labelling experiments showed that the majority of decarboxylases catalyse reactions *via* retention,³³ however examples for inversion reactions have been reported as well.³⁴

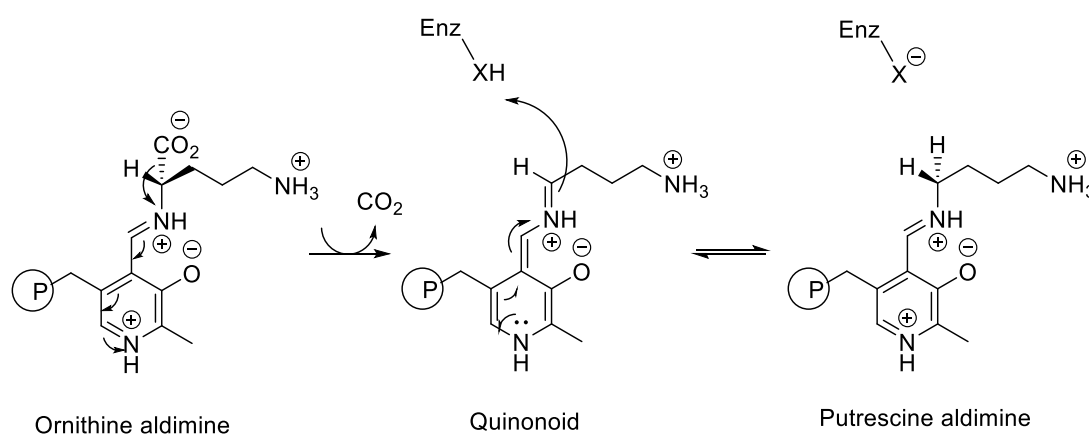


Figure 10: Reaction scheme of PLP-dependent enzyme-catalysed decarboxylation. Modified from Kirsch *et al.*⁵

Amino acid decarboxylases, such as L-3,4-dihydroxyphenylalanine (dopa) decarboxylase, glutamic acid decarboxylase or histidine decarboxylase catalyse the synthesis of neurologically active compounds and neurotransmitters in mammals.³⁵ Especially DOPA decarboxylase has been subjected to extensive research as it is involved in the synthesis of the monoamine neurotransmitters dopamine, serotonin, epinephrine and norepinephrine in mammals.³⁶ Deficiencies in DOPA decarboxylase catalysed reactions can result in diseases like Parkinson's disease or hypertension.³⁷ Another example for the neurologically key role of decarboxylases is glutamic acid decarboxylase which catalyses the decarboxylation of the named substrate to γ -aminobutyric acid (GABA). GABA is a key inhibitory neurotransmitter in mammals. Disorders of the GABA metabolism in the tricarboxylic acid cycle can lead to

dysfunctions of the central nervous system.³⁸ GABA has many functions, such as hypotensive, diuretic and tranquilising effects³⁹ and acts as secretion promoting compound for insulin.⁴⁰

In plants decarboxylases are involved in biosynthesis of secondary metabolites. Tryptophan decarboxylase and tyrosine decarboxylase are of interest due to their role in synthesis of tryptamine which is a precursor of different pharmaceutical alkaloids. Several metabolic engineering experiments have been carried out in order to give increased production of pharmaceutical compounds in plants.³⁷ Accumulation of tryptamine was achieved by introducing tryptophan decarboxylase into Tobacco.⁴¹ The tryptamine derivatives, serotonin and β -carboline alkaloids, were successfully accumulated in plant tissue cultures from *Peganum harmala*.⁴²

100% conversion to L-DOPA was achieved *in vitro* in a two-step reaction from catechol to dopamine with a lyase and tyrosine decarboxylase from *Streptococcus faecalis*.⁴³ GABA has been produced by fermentation from glutamate in different microorganisms such as *Lactobacillus strains* or *E. coli*.⁴⁴⁻⁴⁶ Cadaverine (1,5-diaminopentate) has been produced with 80 % conversion by whole-cell biotransformation with *E. coli* overexpressing an lysine decarboxylase.⁴⁷

1.1.5 Transaminases

Transaminases (TAs) are a class of important and very well investigated type of PLP-dependent enzymes.²⁵ In nature, TAs like acetylornithine transaminase or aspartate aminotransferase are involved in the nitrogen metabolism and conserved in prokaryotes and eukaryotes.⁴⁸⁻⁴⁹

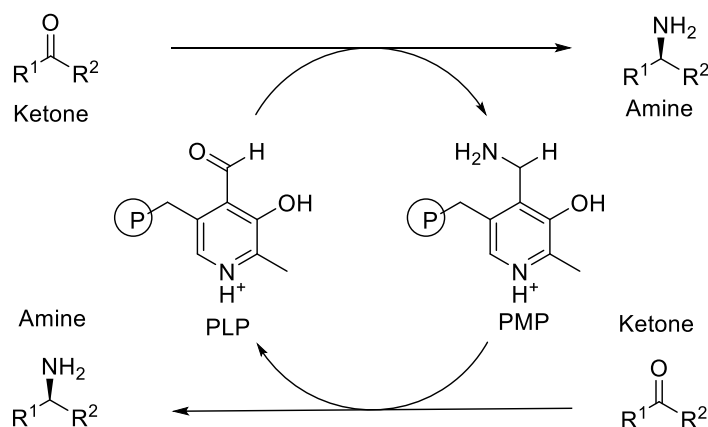


Figure 11: Reaction scheme of transaminase catalysed reaction.

This enzyme class is of biocatalytic interest as transaminases can be applied in the resolution of racemic compounds or, due to their enantioselectivity, also for the synthesis of chiral amines.⁵⁰⁻⁵¹ Transaminases catalyse the transfer of an amine group to an amine acceptor which commonly is a ketone or aldehyde (Figure 11). The reaction is catalysed in two half reactions. The first reaction is the oxidative deamination of the amine donor with transfer of the amine group to PLP to yield PMP. The second half reaction is the reductive amination of the amine acceptor and regeneration of PMP to PLP.^{8, 52}

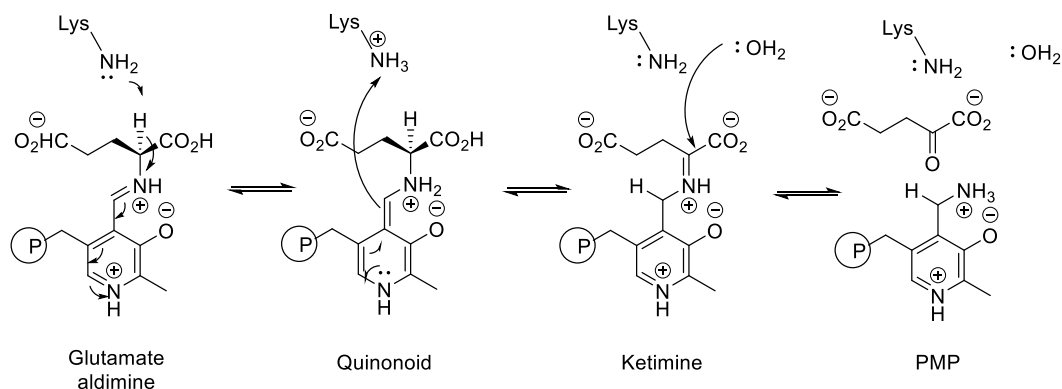


Figure 12: First half reaction catalysed by glutamate aminotransferase. Modified from Elliot *et al.*⁵

Transaminases (E.C 2.6.1.X) can be classified as α - and ω -transaminases, whereas α -TAs catalyse the transfer of an amine group from an α -amino acid to a α -keto acid. ω -transaminases are of interest as they are able to transfer amine groups from all non α -position.⁵²⁻⁵³ Most transaminases are member of the fold type I class of PLP-dependent enzymes. Transaminases of the class I-II and V exclusively represent the fold type I. Outside the fold type I class only class IV transaminases are classified in the fold type IV class.⁵⁴

ω -TAs are class III transaminases and of special interest for biocatalytic application as they can use substrates that are not α -keto acids or α -amino acids. Most of the known ω -transaminases show (*S*)-selectivity, however, a few (*R*)-selective ω -transaminases, like the ω -TA from *Arthrobacter sp.*,⁵⁵ are commercially available. Many different transaminases have been characterised and libraries covering broad substrate ranges are commercially available.⁵⁶ Additionally, various screens have been developed to screen for new ω -TAs.⁵⁷⁻⁵⁸ Chiral amines can be accessed with ω -TAs from either kinetic resolution or asymmetric synthesis. Drawbacks of kinetic resolution are the limitation to 50% yield and the reaction equilibrium favouring formation of the substrates.⁵⁶ Asymmetric synthesis is often the preferred route to the amine product as this would result in a theoretical yield of 100% product. However, this method suffers from drawbacks such as product inhibition and side product formation which require product removal and recovery.⁵⁶ Despite the drawback of both methods, ω -TAs are

very effective and versatile biocatalysis due to broad substrate specificity, enantioselectivity and natural cofactor regeneration.

ω -TAs have a great potential to help overcome difficulties in accessing chiral amines for the production of fine chemicals and pharmaceuticals. For example the application of an ω -TAs for the synthesis of a precursor of suvorexant, a dual orexin receptor for treatment of insomnia, reduced the environmental impact of the synthesis route as dichloromethane and a metal catalyst could be replaced by the biocatalytic step.⁵³ Other examples in which ω -TAs are used for pharmaceutical synthesis are the anti-diabetic drug Sitagliptin, the antihypertensive Dilevalol or the cholinergic agent Rivastigmine for dementia treatment.⁵³ Recent improvements that can even expand the application of ω -TAs are the use of smart amine donors, multienzyme cascades and rational enzyme design.⁵³

1.1.6 Phospholyases

Phospholyases are an interesting example for the variety of reactions that are catalysed by PLP fold type I enzymes. These enzymes belong to the class III of transaminases, but do not display any transamination activity. Only a few phospholyases have been characterised so far. A bacterial phospholyase was characterised by Tuner *et al.*⁵⁹⁻⁶⁰ and human AGXT2L1 and AGXT2L2 were investigated by Veiga-de-Cunha and co-workers.⁶¹ The first crystal structure of a phospholyase was solved for the enzyme A1RDF1 from *Arthrobacter aureescens* TC1.⁶² Solving the structure of this enzyme helped to prove former predictions on the mechanism of the reaction specificity. The PLP binding lysine K281 was identified as catalytic residue for hydrolysis of the substrate phosphoethanolamine. A positively charged pocket was identified in A1RDF1 to recognise and bind the phosphate moiety of the substrate.⁶² The protonation of the phosphate ester oxygen by K281 is possible due to the lack of the typical left-handed α -helix which has two amino acid deletions that seem to be characteristic for phospholyases.^{25, 62}

1.1.7 C-C bond formation

Aldolases catalyse the formation of a C-C bond *via* a reversible aldol reaction. They can also catalyse the breaking of the β bond by a retroaldol cleavage reaction.⁶³ They are highly specific to the donor substrate and different enzymes can use either dihydroxyacetone phosphate, acetaldehyde, glycine, pyruvate or phosphoenolpyruvate as donor.⁶⁴ Amongst the class of aldolases (EC 4.1.2.X) members of the subgroup I are cofactor-independent while some other aldolases need metal ions (Group II), PLP (Group IV) or lysine as cofactor.⁶⁴

Glycine-dependent aldolases are group IV aldolases that can catalyse the formation of β -hydroxyl α -amino carbonic acids by addition of glycine to an aldehyde. Only two types of glycine aldolases are known, serine and threonine aldolase. Both enzymes are involved in glycine synthesis from their respective amino acid substrate as revealed by labelling studies.⁶⁵

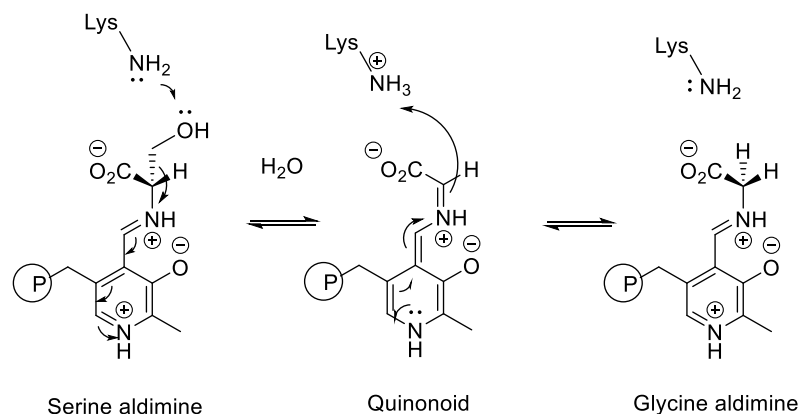


Figure 13: Serine hydroxymethyltransferase catalysed α -elimination and replacement. Adapted according to Eliot *et al.*⁵

Comparative studies of PLP-dependent threonine aldolases with racemases showed that they probably evolved from one ancestor and then further specialised in catalysing aldol or racemisation reactions over time.⁶³ Both reactions are very similar and require the same enzyme conformation in the active site. Homology between fold type I L-threonine aldolase and a fungal racemase and between a fold type III D-threonine aldolase and bacterial racemase has been reported.⁶³ The close relationship between PLP-dependent racemase and aldolases was shown by rational design of a racemase into an aldolase with just one single mutation of the active site.²²

Threonine aldolases have great potential for the application in biocatalysis. Due to the formation of two stereogenic centres of the product of the aldol reaction, four different stereoisomers can be obtained. D- or L-threonine aldolases are available with different substrate specificities, therefore giving access to a platform of different products.⁶⁶ The potential of aldolases for the synthesis of active pharmaceutical ingredients (APIs) has been shown by applying aldolases for the synthesis of precursors of thymine deoxypoloxin, an antifungal agrochemical⁶⁷ and the cardiac active compound digitoxin.⁶⁸ As aldolases are limited in their substrate specificity due to the high specificity towards the donor substrate, research has been conducted to expand the substrate scope of aldolases. Hilvert *et al.* used structure-guided protein engineering to expand the substrate scope and stereoselectivity of aldolases.⁶⁹⁻⁷⁰ Additionally to protein engineering enzyme discovery is a successful method for providing access to new aldolases with expanded substrate scope. PLP-dependent aldolases that accept fluorothreonine or methylserine were recently identified.^{71 72} Together, protein

engineering and enzyme discovery are excellent examples of expanding the applicability of enzymes for chemical synthesis. Due to extensive research novel aldolases with activity towards phenylserines, methylserines, fluorothreonine, alanine and aminobutyric acid as donor substrates were identified.

1.1.8 Other reactions catalysed by PLP-dependent enzymes

The versatility of PLP-dependent enzymes is illustrated by the broad variety of different reactions they catalyse. The most common reactions were described in the previous chapters, nonetheless, there are many other, more specific reactions. Some interesting examples are discussed in this section to further highlight the versatility of PLP-catalysed reactions.

α/β -eliminations are catalysed by PLP-dependent enzymes involved in amino acid metabolism, such as tyrosine phenol-lyase, tryptophan synthase or D-serine dehydrates.⁷³ Usually, PLP-dependent enzymes catalysed α/β -eliminations that undergo an E₁ *syn* elimination as poor leaving groups require the protonation of the β -position (Figure 14).⁷³

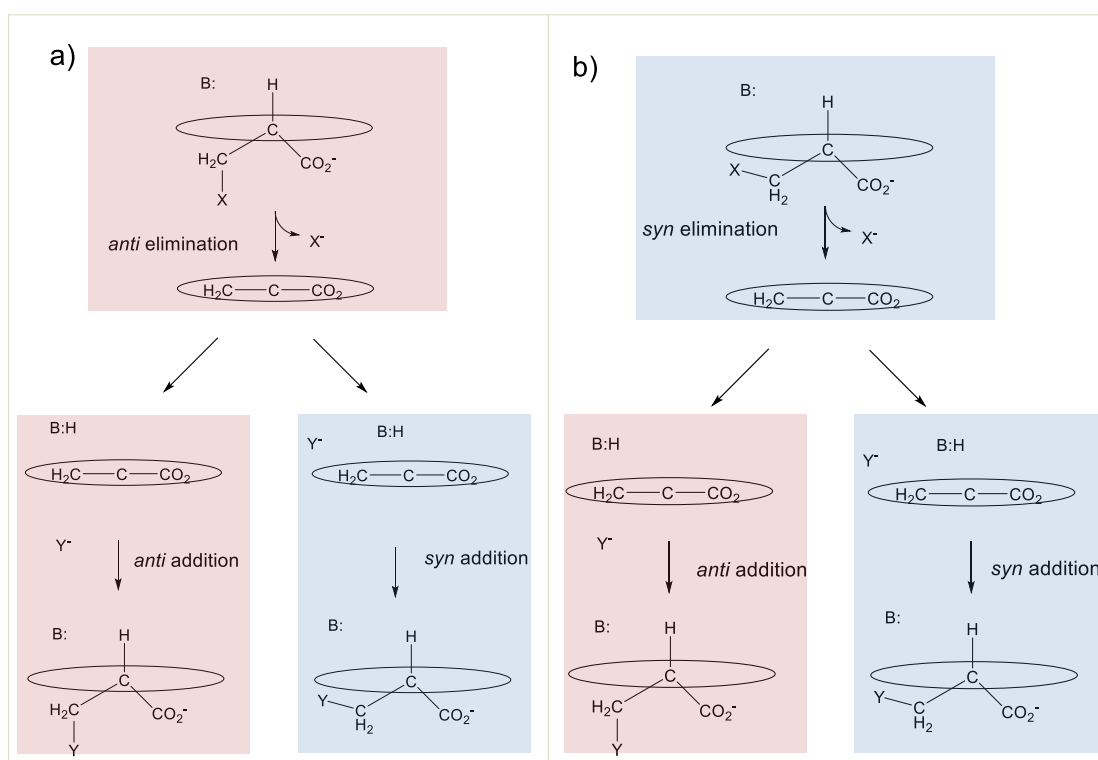


Figure 14: Different pathways for α/β -eliminations catalysed by PLP-dependent enzymes. View is on the substrate C α , the circle is representing the C4' of PLP. a) Pathways starting with *anti* elimination; b) Pathways starting with *syn* elimination. Figure was modified according to Tai *et al.*⁷³

O-acetylserine sulfhydrylase has been found to be an exception as it was suggested to catalyse α/β -eliminations without formation of the quinonoid and bond breaking does not occur on the

same side of the Schiff base. Therefore this reaction represents a rare exception from the Dunathan's hypothesis. This might be because the acetyl of *O*-acetyl-serine is a good leaving group which does not require protonation of the leaving group, hence is catalysed via E₂ mechanism.⁷³

Besides rare exceptions like acetylserine sulfhydrylase completely new reactions and therefore new classes are still discovered amongst the PLP-dependent enzymes. Recently a PLP-dependent enzyme able to catalyse the O₂ dependent oxidation was described by Du and colleagues⁷⁴. The discovered enzyme, Ind4, is able to combine the O₂ coupled oxidation with the anion stabilisation effect of PLP in order to oxidise an unactivated C-C bond in L-arginine. Ind4 catalyses the four-electron oxidation of L-arginine which is the initial step of the metabolic pathway to indolmycin (Figure 15). PLP-dependency of the catalysed reaction was confirmed, interestingly, the enzyme was also described to have similarity with a cofactor-independent oxidases.⁷⁴

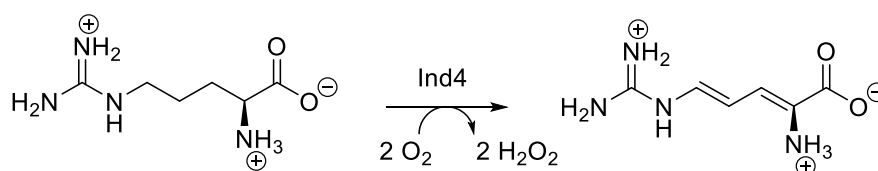


Figure 15: Ind4 catalysed oxidation of a C-C bond of arginine.⁷⁴

Another example is the enzyme cystathionine β -synthase, that catalyses a classical PLP-dependent condensation reaction converting homocysteine and serine to cystathionine. Remarkably, in humans and other organisms this enzyme binds heme and is the only known enzyme to bind PLP and heme as cofactors.⁷⁵ The heme is bound approximately 20 Å away from the active site and therefore it was proposed to be of a regulatory, non-catalytic function. The enzyme activity is regulated through redox changes of the iron, which suggest induction by signal molecules, such as CO or NO.⁷⁶

1.2 Amino acid racemisation in Nature

As described in the previous sections, most PLP-dependent enzymes catalysed reactions involve the conversion of amino acids or their derivatives. As building blocks of proteins L-amino acids are predominant in Nature. However, the D-enantiomer of amino acids is also present in living organisms. The most prominent examples are D-alanine and D-glutamate as

components of bacterial peptidoglycan. The availability of D-amino acids is not only crucial for the cell wall synthesis, but also influences processes such as capsule building, biofilm development or sporulation in microorganisms.⁷⁷ D-amino acids, such as D-valine or D-phenylalanine, are also often found in peptide containing antibiotics produced in several microorganisms.

Already 50 years ago, free D-amino acids, mainly D-forms of alanine or serine, were found in various animal tissues, however, explanation for their function was lacking.⁷⁸ With improvement of analytical techniques D-amino acids could be detected in peptides and even proteins in higher living organisms. The opioid peptide, dermorphin, was the first peptide containing D-alanine isolated from a vertebrate, the frog *Phyllomedusa sauvage*.⁷⁹ Other D-amino acid containing peptides were found in snails and the toxin of spiders.⁸⁰ Interestingly, the biological activity of equivalents with the L-amino acid was abolished or very low indicating the importance of the D-amino acid for biologic activity.

In humans D-aspartate has been found in proteins from several tissues, such as the brain, eye lens or skin.⁸⁰ D-aspartate was found in human proteins of tissues from elderly patients and explained by the naturally occurring racemisation of aspartyl residues over time. Free D-serine was identified in the mammal brain and was suggested to be a glutamate receptor regulator or synaptic modulator.⁸⁰ D-serine and D-aspartate were found in β -amyloid, the protein associated with Alzheimer's disease. The presence of D-amino acids in the β -amyloid might lead to failure of the natural degradation of this protein through proteinases.⁸¹ Recently, a connection between the severity of Alzheimer's disease and the level of D-amino oxidase, D-serine and D-glutamate in blood from Alzheimer's disease patients was reported and suggested as potential blood marker for Alzheimer's disease.⁸²

As D-amino acids can be found in living organisms, it is not surprising that accumulation of D-amino acids has been measured in the environment, in particular in oceans and grassland.⁷⁷ Release of D-alanine was observed from freshwater or marine bacteria environments under laboratory conditions. During the exponential growth phase up to 18% of the total produced D-alanine was released to the environment.⁸³ Accumulation of other D-amino acids, such as D-lysine, D-phenylalanine, and D-aspartic was also detected in the environment. 2-15% of the total amino acid concentration of soils from North America were determined as D-amino acids.⁸⁴ In addition to accumulation of D-amino acids through enzymatic activity, D-amino acids can also be produced by chemical racemisation. However, the chemical racemisation of L-amino acid is very slow and this principle is used in different research fields to estimate the age of samples. The field of amino acid geochronology describes the analysis of D/L ratio of amino acids in geological samples to estimate the age of the samples.⁸⁵ This technique can not

only be used for age estimation of geological samples, but also for biological samples, for example from the human dentin or sclera.⁸⁶

1.3 Racemases in Biocatalysis

As described above amino acid racemisation is very common and involved in various physiological processes in living organisms. This section will focus on the application of racemases for biocatalysis to produce natural and non-natural compounds. The controlled racemisation of organic compounds was reviewed two decades ago by Ebbers and co-workers.⁸⁷ Due to the importance of chirality in active compounds great emphasis is put on enantioselective processes in chemical synthesis. Racemisation has not only been overlooked but even avoided in synthesis as it is often seen as an inconvenient side reaction. Nevertheless, racemisation processes are highly valuable for the synthesis of enantiopure compounds, especially for the resolution of racemates. This potential has been discovered and exploited by the chemical industry and many racemisation processes are disclosed in patents.⁸⁷ Common chemical racemisation methods, like thermal, acid or base catalysed racemisation, often require harsh reaction conditions that facilitate side reactions.⁸⁸ Milder reaction conditions were investigated with racemisation catalysts, for example Schiff base forming aldehydes or ketones for the racemisation of amino acids and derivatives.^{87, 89}

The advantage of enzymatic over chemical routes is the high specificity and applicability at mild reaction conditions. Racemases are a small class of enzymes (EC 5.1.X.X) within the isomerases⁹⁰ as depicted in the phylogenetic tree in Figure 16.

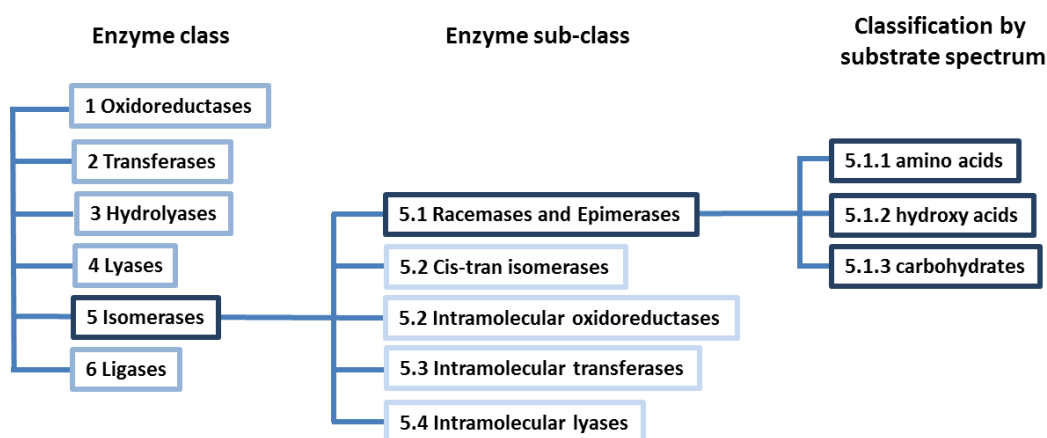


Figure 16: Phylogenetic tree of racemases and epimerases.

The major function of these enzymes in Nature is the racemisation of amino acids and α -hydroxyl acids as outlined in the previous section. Enzyme catalysed racemisation can be mediated by either one or two bases in the active site. Racemases can be classified according to the catalysed reaction mechanism, into one-base-system or two-base-system racemases.⁹¹ The general reaction scheme of enzyme catalysed two base mechanism is shown in Figure 17.

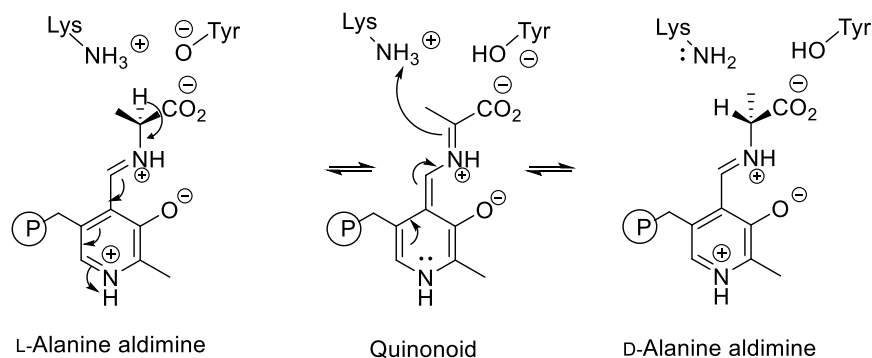


Figure 17: Two base reaction scheme of alanine racemase modified according to Elliot et al.⁵

Most racemases accept amino acids as substrates, however, other racemases have a relaxed substrate scope and accept amino acid derivatives or α -hydroxy acids.⁹¹ Most racemases recruit PLP as cofactor in the active site to facilitate catalysis, but there are also racemases that do not require a cofactor.⁹² As the reaction mechanism is still unknown for some racemases, it is more common to classify racemases by their substrate scope or PLP-dependency. As catalysts of stereo-inversion, racemases can be implemented as a useful tool for the synthesis of enantiopure chemicals. They represent an important instrument to enhance purity of the product and commonly are used in concert with an enantioselective enzyme. Racemases can be applied to improve yields of the enantiopure product in two different methods:

1. Kinetic resolution

In a kinetic resolution the racemic substrate is enantioselectively converted to the corresponding product yielding high enantiomeric excess (*ee*) of the desired enantiomer. A crucial disadvantage of a kinetic resolution is the limitation to 50% yield of the enantiomer of interest. Hence the product has to be separated and the undesired enantiomer has to be recycled in further steps.⁹³

2. Dynamic kinetic resolution

In-situ racemisation of the remaining enantiomer is an elegant way to avoid extensive recycling steps.⁹⁴ This process is called dynamic kinetic resolution (DKR) and has a theoretical yield of 100% of the enantiomer of interest. As reviewed by Huerta *et al.*⁹⁵ three conditions must be fulfilled for an efficient DKR:

- 1) Conversion of the enantiomer of interest must be significantly faster than the other.
- 2) Racemisation rate of the substrate must be higher than the conversion rate to product.
- 3) The product must not be racemised.

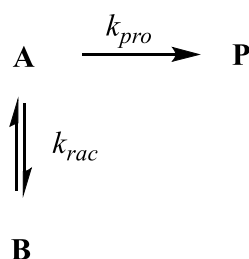


Figure 18: Scheme of a DKR. A, B enantiomers of the substrate, P: product, k_{pro} : rate constant of conversion of enantiomer A to product, k_{rac} : rate constant for racemisation of A and B. Modified according to Huerta *et al.* and Gruber *et al.* ⁹⁵⁻⁹⁶

When choosing a racemase for a specific process, the substrate spectrum and tolerance to given process conditions are crucial criteria. Selected racemases with different substrates scopes are highlighted in the following sections in order to illustrate their value for the synthesis of enantiopure compounds.

1.3.1 Hydroxyl carbonyl derivative racemases

With only two members known so far, hydroxyl carbonyl racemases are the smallest group within the sub-classes of racemases. Both representatives of this group, mandelate racemase and lactate racemase are PLP-independent but require cofactors of other nature. Both enzymes will be discussed in the section below.

1.3.1.1 Mandelate racemase

Mandelate racemase is isolated from *Pseudomonas putida* and has been investigated in detail. The enzyme activity is dependent on the presence of divalent ions, complete activity is achieved with Mg^{2+} but activity can also be restored with Co^{2+} , Ni^{2+} , Mn^{2+} and Fe^{2+} .⁹⁷ The divalent ions bind in the active site and facilitate proton abstraction by withdrawing electron density from the $\text{C}\alpha$ of the substrate.⁹⁷⁻⁹⁸ The structure of mandelate racemase revealed lysine and histidine as catalytic residues and confirmed a two-base reaction mechanism.⁹⁸ An achiral enol intermediate is formed after abstraction of the proton, which then is reprotonated from one of the catalytic residues resulting in two different enantiomers.

Mandelate racemase from *Pseudomonas putida* can easily be produced by fermentation in large amounts. More than 10^6 U of highly active enzyme were produced from a 10 L bioreactor.⁹⁹ Immobilisation on ionic resins increased activity of the enzyme and enhances application and recyclability in batch reactions.¹⁰⁰ Both, straightforward production and immobilisation of mandelate racemase increase the applicability of the enzyme for industrial purposes. Furthermore, the enzyme has a broad substrate scope and accepts derivatives of mandelate acid.¹⁰¹⁻¹⁰² Electron-withdrawing substituents in the *para* position of the benzyl ring increased activity, whereas substituents in the *meta* position decreased activity due to steric hindrance.¹⁰³ Presence of π -electron systems is essential for activity of mandelate racemase but it can be reduced to just one π -electron system as found in vinyl glycolate.¹⁰⁴ The enzyme retains 35% residual activity with this substrate. Contrarily, it is completely inactive with lactate which lacks any conjugated electrons. A model of substrates accepted by mandelate racemase and features that are favoured or disfavoured for catalysis is illustrated in Figure 19.

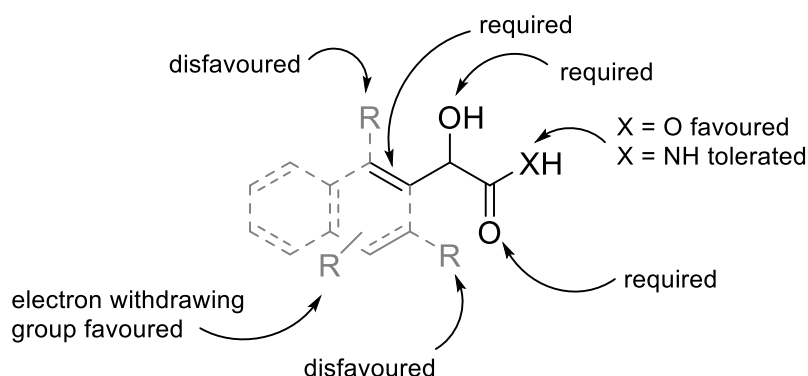


Figure 19: Scheme of substrates favoured or disfavoured by mandelate racemase. Features shown in black are the minimum requirements for racemisation, features shown in grey are not necessarily required for activity. Adapted according to Felfer *et al.*¹⁰²

Mandelate racemase has been applied in a kinetic resolution of racemic mandelate to (*S*)-*O*-acetyl mandelic acid.¹⁰⁵ The asymmetric synthesis of (*S*)-*O*-acetyl mandelic acid was carried out with a (*S*)-selective lipase from *Pseudomonas* in organic solvent. When the reaction was complete (50% yield of the product) the solvent and lipase were removed and mandelate racemase was added to racemise the remaining (*R*)-mandelate in aqueous buffer. Afterwards the lipase reaction was carried out again, repeating the two steps yielded 80% isolated product of excellent *ee*.¹⁰⁵

1.3.1.2 Lactate racemase

The first lactate racemisation was described in 1936 in *Clostridium butylicum*¹⁰⁶ after production of D-lactate was reported for some lactic acid bacteria.¹⁰⁷ Since then lactate racemases have been found in other microorganisms, such as streptobacteria species or the propionate producing *Mageshaera elsdenii*.¹⁰⁸⁻¹⁰⁹ Mandelate racemase and lactate racemase are the only known α -hydroxy acid racemases so far and both are PLP-independent. For lactate racemase, studies on activity towards other substrates than lactate or the application for chemical synthesis have not been reported to date. Lactate racemase requires Ni^{2+} for activity and therefore creates a new group of Ni-dependent enzymes.¹¹⁰ Due to the lack of an electron withdrawing group in its substrate, lactate, a hydride transfer was suggested as reaction mechanism.¹¹¹

Extensive research on the lactate racemase and lactate metabolism in *Lactobacillus plantarum* has been carried out by Hols and colleagues since the 2000s.^{110, 112-114} These efforts resulted in the publication of the first structure of a lactate racemase by the same group.¹¹⁰ The structure revealed that lactate racemase from *Lactobacillus plantarum* is a Ni^{2+} -dependent, dimeric enzyme of a novel α/β fold that has low similarity to other known structures.¹¹⁰ Molecular experiments of the same study investigated the maturation system of three other proteins that is required for building an active lactate racemase. The accessory proteins are necessary for the incorporation of Ni^{2+} and remarkably, also the metalcentre for coordination of Ni^{2+} , within the apo-form of lactate racemase.¹¹⁰

The antibiotic compound vancomycin abolishes cell wall synthesis and therefore microbial cell growth by forming a complex with the D-alanine incorporated in peptidoglycan of the cell walls. Replacing the terminal D-alanine of peptidoglycan with D-lactate is a modification in vancomycin resistant microorganisms against this attack mechanism.¹¹⁵⁻¹¹⁶ The racemisation activity of lactate racemase is induced by L-lactate and repressed by D-lactate.¹¹² In *Lactobacillus plantarum* D-lactate is normally produced by stereospecific lactate dehydrogenases and it is required for growth due to its incorporation in the cell wall.¹¹⁴ When lactate dehydrogenases are deleted, the presence of lactate racemase compensates this deletion by production of D-lactate in a rescue pathway for the synthesis of an intact cell wall and therefore ensures the survival of the organism.¹¹⁴

Further studies gave an insight into the reaction mechanism of lactate racemase. One study elucidated the uniqueness of lactate racemase as it is the only known enzyme that recruits a cofactor to form a tethered pincer complex with a metal ion. Evidence has been provided for the dependency of the racemisation activity on a nicotinic acid mononucleotide (NAMN).¹¹³

NAMN forms a metal-C bond and coordinates Ni^{2+} with this pincer complex in the active site which is common for chemical metal catalysts, but unprecedented for biocatalysts.¹¹³

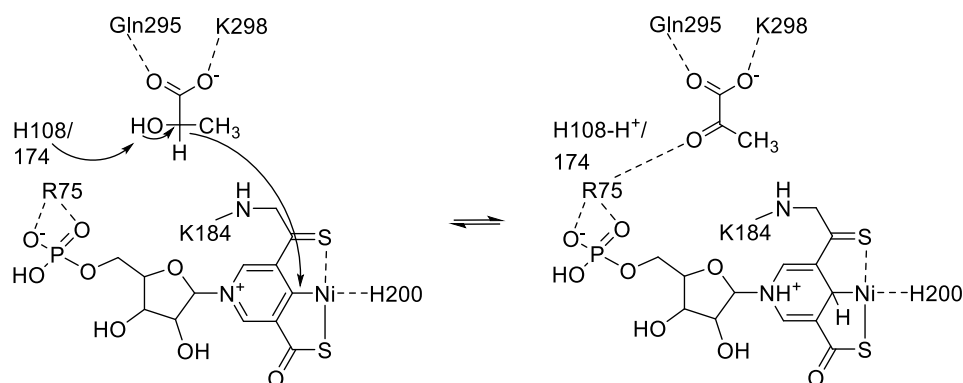


Figure 20: Proposed reaction mechanism of lactate racemase from *Lactobacillus plantarum* based on the structure solved by Desguin *et al.*¹¹³

The proposed reaction mechanism (see Figure 20) supports the hydride transfer hypothesis and suggests that NAMN takes up an analogous role to NAD in hydride transfer catalysis.¹¹³ Two conserved histidine residues, H108 and H174, are positioned at the opposite sides of the substrate and therefore could be catalytic residues.^{113, 117} Computational studies propose catalysis via a metastable NAMN-pyruvate intermediate destabilised by the less electrophilic Ni cofactor.¹¹⁷

1.3.2 Amino acid racemases

Amino acid racemases represent the largest and best known group within the racemases. Some members of this group have been investigated in detail in order to elucidate their biological role. In particular alanine racemase and glutamate racemase are well characterised as they are involved in the production of D-amino acid for the biosynthesis of bacterial peptidoglycan. However, especially in biocatalysis focus shifts towards identifying new amino acid racemases with a broader substrate acceptance.

1.3.2.1 Alanine racemase

Alanine racemase is a very well characterised PLP-dependent enzyme due to its importance for the biosynthesis of the bacterial cell wall. Alanine racemases have been isolated from many different bacterial sources, for example from *Clostridium* or *Streptomyces*, and are still subject of interest due to their potential as drug targets.¹¹⁸⁻¹²⁰ The alanine racemase reaction mechanism has been extensively studied as described in detail above (Chapter 1.1.2.2). Due

to their role in production of D-alanine for the incorporation in peptidoglycan, alanine racemases are highly specific to alanine. Nonetheless, an alanine racemase from *Salmonella typhimurium* was found to accept also serine, homoserine and cysteine as substrates.¹²¹ Efforts to expand the substrate acceptance of the alanine racemase from *Streptomyces coelicolor* by directed evolution resulted in a mutant that has new activity towards arginine and ornithine.¹²²

Despite the efforts to expand the substrate scope of alanine racemases, their application is still mostly restricted to the use for interconversion of their natural substrate. Alanine racemase has been applied for the synthesis of the ¹¹C-labelled aromatic amino acids, L-3,4-dihydroxy-phenylalanine (DOPA) and 5-hydroxy-L-tryptophan.¹²³ These amino acids are analogues to the neurotransmitters dopamine and serotonin and can be used to measure neuronal activity. Alanine racemase is applied in an auxiliary step of the multi-enzyme process. ¹¹C-labelled DL-alanine is oxidised by a D-amino acid oxidase to pyruvate which is then converted by a tryptophanase and indole to 5-hydroxyl-L-tryptophan.¹²³ Using the same concept with a tyrosinase and catechol results in ¹¹C-labelled DOPA.¹²³

1.3.2.2 Glutamate racemase

Similar to other amino acid racemases, the cofactor-independent glutamate racemase is also involved in the cell wall biosynthesis. Glutamate racemase synthesises D-glutamate which is an essential component of peptidoglycan of the bacterial cell wall.¹²⁴ Due to its conserved function across all bacteria in cell wall synthesis and the lack of an equivalent enzyme in humans, glutamate racemase has been targeted for discovery of new antibiotics.¹²⁴ Two Zn and Mn metal complexes from a compound library have been identified to inhibit activity of glutamate racemase from *Burkholderia sp.*, cause of severe lung infections, that can lead to irreversible bronchiectasis and respiratory failure.¹²⁵ Another important target is the glutamate racemase from *Mycobacterium tuberculosis*, a tuberculosis causing organism that has recently evolved multi and even total resistance against first and second-line antibiotics.¹²⁶⁻¹²⁷

Structures of glutamate racemases from Gram positive and negative bacteria were evaluated in order to elucidate its regulation and binding of potential inhibitors.^{126, 128} Glutamate racemases have a conserved dimeric α/β -fold, where the active site is situated at the interface of two subunits.¹²⁶ N-terminal and C-terminal residues were found to be catalytic, as well as an overall movement of the subunits that is essential for catalysis.¹²⁸ Regulation of the racemases can be negative, substrate mediated by D-glutamate or positive through a precursor of peptidoglycan.¹²⁸

Due to the specific physiological function in the synthesis of D-glutamate, glutamate racemases are highly substrate specific.⁸⁷ Therefore, their application in biocatalysis is limited

to this substrate. One obvious application of glutamate racemases is the production of D-glutamate from fermented L-glutamate. Kinetic resolution of L-glutamate was performed with glutamate racemases from different *Lactobacillus* species in combination with an L-selective glutamate decarboxylase to yield 50 g L^{-1} D-glutamate.¹²⁹⁻¹³⁰ This system exploits the different pH optima of the two enzymes. Adjusting the pH value to the respective optimum was used to control the sequence of the reactions.¹²⁹

A similar approach was demonstrated by using immobilised glutamate racemase and L-glutamate oxidase for the kinetic resolution of L-glutamate. In this case the enzymes had similar reaction optima. Immobilisation on carrier material and running the reaction in a flow reactor facilitated recycling steps.¹³¹ In a more sophisticated process, glutamate racemase was applied as an auxiliary enzyme to produce aromatic D-amino acids.¹³²⁻¹³³ A four enzyme multi-system was established to produce either D-phenylalanine or D-tyrosine from cheap L-glutamate.¹³² In the first step, glutamate racemase supplies D-glutamate from L-glutamate to the multi-enzyme system. In the second step, a D-amino acid transferase transfers the amine from D-glutamate to the respective pyruvate to produce D-phenylalanine or D-tyrosine. The α -ketoglutarate is recycled to L-glutamate by a dehydrogenase system using NADH and ammonia.

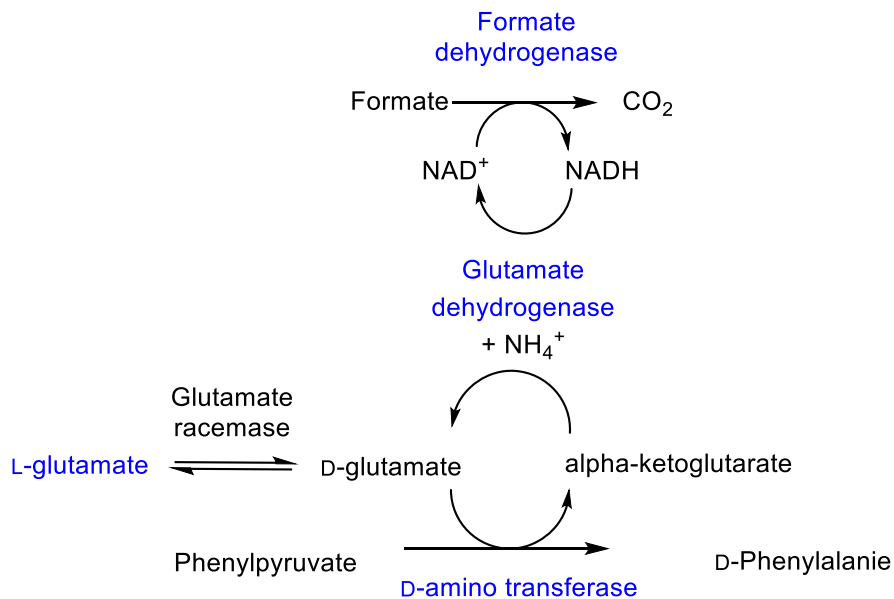


Figure 21: Process scheme of multi-enzyme system for the production of D-phenylalanine from L-glutamate. The process can also be applied to produce d-tyrosine by replacing phenylpyruvate with 4-hydroxyphenyl pyruvate¹³².

1.3.2.3 Broad spectrum amino acid racemase

Similar to alanine or glutamate racemases most amino acid racemases evolved high substrate specificity due to their specific physiological role. Unspecific racemisation of amino acids in the cell would lead to reduced availability of L-amino acid for protein biosynthesis¹²² and accumulation of D-amino acids could have toxic effects. Despite the need for high substrate specificity in nature, racemases with broad substrate spectra are highly desirable for biocatalytic purposes and have been isolated from *Pseudomonas* sp. and from *Aeromonas caviae* and.¹³⁴⁻¹³⁶ *Aeromonas caviae* amino acid racemase was the first known racemase to interconvert all three aromatic amino acids, however, with very low activity ($\leq 1\%$ of maximal activity with glutamine).¹³⁴ Several other broad-spectrum amino acid racemase (BSAAR) were isolated from *Pseudomonas* sp. in the 1980s.⁸⁸ More recently, amino acid racemases with broad substrate spectrum have been isolated and characterised from *E. coli* and *Bacillus subtilis*.¹³⁷ Nonetheless, especially the *E. coli* enzyme showed very low activity to most amino acids.¹³⁷ Thus, further investigations on the physiological role of these enzymes are necessary to assign them as broad-spectrum amino acid racemases.

As the natural role of BSAARs is still unknown a structural and bioinformatics study was carried out to clarify their classification in respect to other amino acid racemases.¹³⁸ A BSAAR from *Vibrio cholerae* was structurally compared to its closest homologue alanine racemase from *E. coli* to investigate the different background of BSAAR.¹³⁸ Indeed, structural features and conserved sequences were identified that allow distinguishing BSAARs from alanine racemases.¹³⁸ Based on these results it was suggested that BSAARs can be classified in a new subfamily of amino acid racemases.¹³⁸

The potential for industrial application of these enzymes was demonstrated for the production of L-tryptophan using BSAAR from *Pseudomonas putida*.¹³⁹ The racemase was used in concert with a tryptophan synthase to produce L-tryptophan from DL-serine and indole. The DKR was successfully performed at large scale in a 200 L reactor using whole cells as catalyst giving 91% yield of L-tryptophan.¹³⁹

1.3.2.4 Other biocatalytically relevant amino acid racemases

Many amino acid racemases have been identified and characterised emphasising their important role in different physiological processes like cell growth, second metabolism, neurotransmission or defence mechanisms. However, as mentioned in the examples above, amino acid racemases are often very restricted to a few substrates which hampers their wide application in biocatalysis. In this section a few examples of racemases with potential as biocatalyst and possible applications will be discussed.

Arginine racemase was isolated from *Pseudomonas graveolens* and was described to have activity towards several natural and non-natural amino acids.¹⁴⁰ Ornithine transamination and irreversible formation of PMP was observed as side reaction which has the inactivation of the enzymes as consequence.¹⁴⁰ Furthermore, the enzyme showed higher activity towards L-lysine than to L-arginine¹⁴⁰ leaving its classification as L-arginine racemase debatable. In accordance with these findings is the physiological role of arginine racemase that was recently found to be essential for the metabolism of D-lysine as carbon source in *Pseudomonas taetrolens*.¹⁴¹ Despite its broad substrate spectrum arginine racemase has no reported biocatalytic application yet.

The one-pot fermentation of optically pure L-pipecolic acid was recently performed with a recombinant *E. coli* strain overexpressing four heterologous enzymes, a piperidine-2-carboxylate reductase, L-lysine α -oxidase, lysine racemase and a glucose dehydrogenase.¹⁴² This system enables conversion of L-lysine to L-pipecolic acid with 87% yield and *in-situ* D-lysine recycling by the racemase and cofactor recycling by a dehydrogenase.¹⁴² Pipecolic acid is an important building block of many microbiological secondary metabolites and often essential for biological activity of APIs derived from natural products, for example rapamycin.¹⁴³

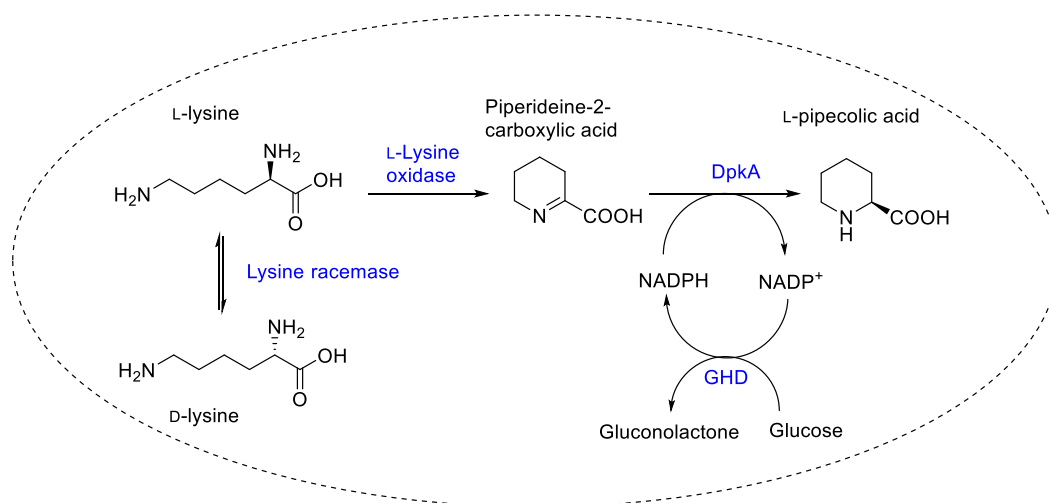


Figure 22: Reaction scheme of one-pot fermentation of L-pipecolic acid. The multienzyme system is overexpressed in a recombinant *E. coli* strain and L-lysine is converted to optically pure L-pipecolic. DpkA: piperidine-2-carboxylate reductase. Modified according to Tani *et al.*¹⁴²

Protein engineering is a powerful tool to give access to new enzyme activities, especially when supported by structural information. In experiments from Kourist and Miyamoyo a unique arylpropionate racemase was generated aided by structural information.¹⁴⁴ The low promiscuous racemisation activity of an arylmalonate decarboxylase could be significantly improved based on structural similarity to aspartate/glutamate racemases.¹⁴⁴ The new enzyme activity could be further improved by structure-guided engineering up to 40 fold giving an enzyme with efficient racemisation activity for application in chemical synthesis. The new

arylpropionate racemase accepts pyridyl, vinyl aliphatic and aryl carboxylic acids.¹⁴⁵ Especially aryl carboxylic acids are of pharmaceutical interest as they are common features of non-steroidal anti-inflammatory drugs, such as ibuprofen and naproxen.¹⁴⁶

1.3.3 Amino acid derivatives racemases

Amino acid derivative racemases are of special interest for the use in biocatalytic processes for production of enantiopure amino acids. Racemases of this sub-class present several examples for the application of racemases in chemical synthesis at industrial scale.

1.3.3.1 Hydantoin racemase

Hydantoin racemases have been implemented for the production of D-amino acids in the D-hydantoin process since the 1970s.¹⁴⁷ Today, this process is applied industrially by Degussa at multi-ton scale for the production of the D-amino acid containing side chains of the β -lactam antibiotics, amoxicillin and ampicillin.^{88, 91, 148} Racemic 5-monosubstituted hydantoins can be easily prepared from cheap starting materials.¹⁴⁸ Depending on the nature of the substituent racemisation of 5-monosubstituted hydantoins can be chemically (aromatic substituent) or enzymatically (aliphatic substituent) catalysed.¹⁴⁹ The D-hydantoin process includes three enzymatic steps (Figure 23). The first step is a ring opening reaction catalysed by a D-selective hydantoinase yielding the respective *N*-carbamoyl-D-amino acid from racemic 5-monosubstituted hydantoins. In the following step *N*-carbamoyl-D-amino acid is hydrolysed by a D-carbamoylase resulting in the corresponding D-amino acid. The last step is the recycling of the unreacted L-enantiomer which is racemised by hydantoin racemase. Hydantoin racemases have been discovered in *Arthrobacter* and *Pseudomonas*.¹⁵⁰⁻¹⁵¹ As this is a dynamic kinetic resolution with three different enzymes, reaction rates of the each step have to be carefully adjusted to shift the equilibrium to the product side.⁸⁸ Efforts were made to establish a process for the production of L-amino acids *via* the hydantoin process.¹⁴⁸ Developing an L-hydantoin process highly depends on the availability of a suitable L-hydantoinase. Only a few L-selective hydantoinases have been reported¹⁵² and their application was withheld by low activity and high catalyst costs.¹⁴⁸ For a feasible production of L-amino acids by this route catalysts costs were drastically decreased by improving the catalyst. In a first study the whole cell catalyst was improved by expressing and aligning activities of all three necessary enzymes in *E. coli*.¹⁵³ Additionally, the activity of the hydantoinase from *Arthrobacter sp* was further increased by inverting its natural D-selectivity to L-selectivity with 90% *ee*. This resulted in reducing catalysts cost so far that the process becomes now feasible for the production of the low cost amino acid L-methionine.¹⁵⁴ The catalyst optimisation aiming to enable an L-

hydantoin process is a great example of how protein and process engineering can be applied to overcome natural limitations of biocatalysts.

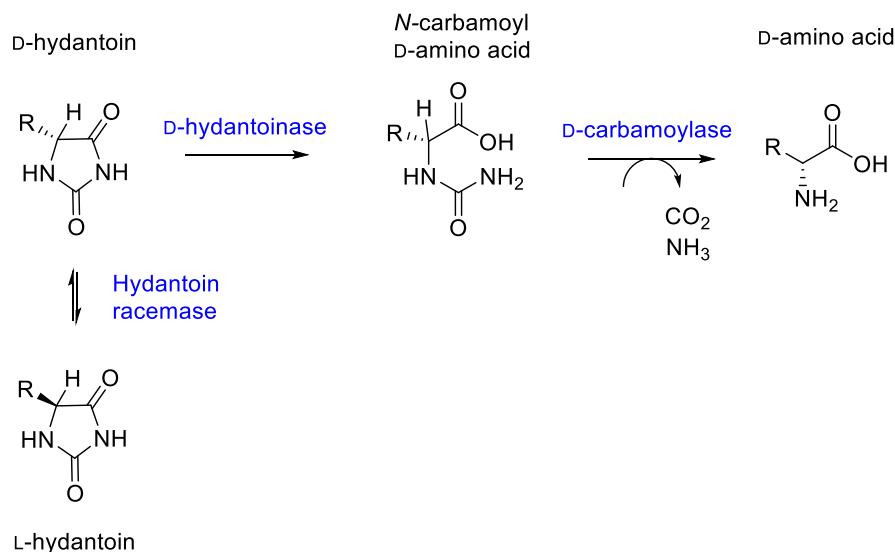


Figure 23: Scheme of D-hydantoin kinetic resolution to produce D-amino acids from the corresponding racemate of N-substituted hydantoin.¹⁴⁸

The industrial relevance of this enzyme is demonstrated by several patents filed for hydantoin racemase, for example for Degussa, DSM and Kaneka Corp. Several biochemical and biophysical characterisations of hydantoin racemases were carried out, however, a structure of the enzyme has not been published yet.^{151, 155-157} Nonetheless, the structure of the homologous enzyme allantoin racemase from *Pseudomonas* sp. has been solved.¹⁵⁸ Allantoin racemase shares 45% identity with the hydantoin racemase from *Pseudomonas* sp. and both enzymes belong to the aspartate/glutamate racemase superfamily. The structure of allantoin racemase is known as a α/β fold with subunits organised as a hexamer.¹⁵⁹ Two cysteines were identified as catalytic relevant residues which are conserved within the aspartate/glutamate racemase superfamily.¹⁵⁹ These conserved cysteine residues were also identified in hydantoin racemase from *Sinorhizobium meliloti* to be involved in catalysis.¹⁵⁵ The allantoin racemase enzyme has a role in the degradation of urate as part of the purine metabolism and nitrogen supply in bacteria.¹⁵⁹ Due to its narrow substrate specificity limited to (*S*)- or (*R*)-allantoin, this enzyme is not applied for any biocatalytic processes to date.

The power of combining enzymatic reactions in one process is illustrated by the recently optimised hydantoinase process for the production of optically pure L-amino acids with 100% yield.¹⁶⁰ The so-called double-racemase hydantoinase process uses *N*-acetyl amino acid racemase (NAAAR) in addition to hydantoin racemase to overcome selectivity limitations of the hydantoinase (Figure 24).

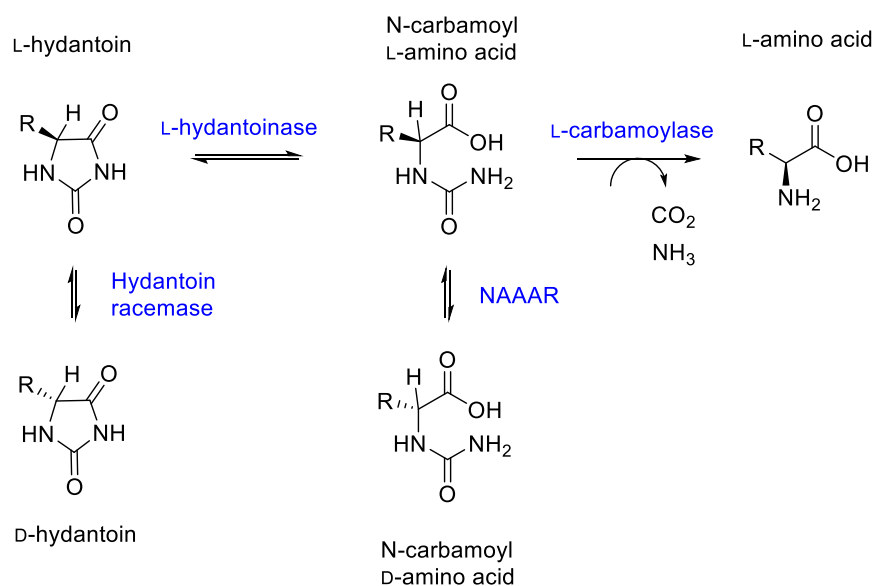


Figure 24: Hydantoin process for the production of L-amino acids. This process utilises two racemases to overcome the low reaction selectivity of L-hydantoinase towards N-carbamoyl-amino acids.

The process exploits the promiscuity of NAAAR which was shown to also racemise *N*-carbamoyl amino acids.¹⁶¹ The presence of NAAAR avoids accumulation of D-carbamoyl amino acid which is produced during the process due to the low enantioselectivity of L-hydantoinase.¹⁶⁰

1.3.3.2 N-acetyl amino acid racemase

Another process for the production of enantiopure amino acids is the acylase process which has been used by Degussa for the multi-ton production of L-methionine since 1970s.¹⁶² This biocatalytic process can be adapted to produce D-amino acids from *N*-acetyl-DL-amino acids using a D-acylase. A major drawback is the limitation to 50% yield so that the unreacted enantiomer has to be separated and chemically racemised under harsh thermal conditions.¹⁶³ To overcome this drawback emphasis was put on finding a highly selective racemisation catalyst for *N*-acetyl amino acid racemisation by various chemical companies. Enzyme screenings in different source organisms were carried out in order to isolate such a biocatalyst.¹⁶⁴⁻¹⁶⁵ The first *N*-acetyl amino acid racemase (NAAAR) activity was discovered by a soil sample screening in 1994.¹⁶³ This novel enzyme was isolated exclusively from Actinomycetes and showed racemisation activity against *N*-acetyl amino acids but not towards unprotected amino acids.¹⁶³ Due to its lack of activity towards amino acids NAAARs are very attractive catalyst to optimise the acylase process to a dynamic kinetic resolution by introducing *in situ* racemisation of the starting material.

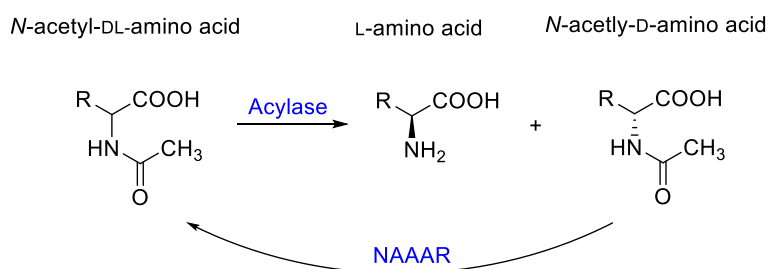


Figure 25: DKR of *N*-acetyl amino acids to *L*-amino acids. Modified according to Bommarius *et al.*¹⁶²

A NAAAR from *Amycolatopsis* sp. was heterologous expressed in *E. coli* and biochemically characterised.¹⁶⁶ This enzyme was promising for industrial application as it is thermostable and accepts various *N*-acetyl derivatives of valine, tyrosine and methionine.¹⁶⁷ Interestingly, activity towards alanyl-methionine dipeptide was detected but no activity could be measured towards amino acids, *N*-alkyl-amino acids or methyl or ethyl amino acid derivatives.¹⁶⁷ Despite its potential for biocatalytic application dependency on high concentrations of metal ions and substrate inhibition confined the application of the NAAAR from *Amycolatopsis* sp. for industrial processes.¹⁶⁸ The promiscuity of the *Amycolatopsis* sp. NAAAR was further investigated by an enzyme function-sequence analysis. The analysis suggested that NAAAR is a member of the enolase superfamily and the metabolic role is within the menaquinone biosynthesis.¹⁶⁸ *O*-succinylbenzoate synthase activity was measured to be 700 times higher than *N*-acetyl amino acid racemisation activity proving the catalytic promiscuity of this enzyme.¹⁶⁸ More recent studies indicate that NAAAR is a physiologically bifunctional enzyme as is also showed *N*-succinylamino acid racemase activity that could play a role in the amino acid metabolism.¹⁶⁹

To date, NAAARs have been isolated from Actinomycetes, Geobacillus and Streptomyces.¹⁷⁰ Structures of the NAAARs from *Deinococcus radioduran* and *Amycolatopsis* were solved in 2004.¹⁷¹⁻¹⁷² The crystal structure of *Deinococcus radioduran* NAAAR complexed with the ligand *N*-acetyl-L-glutamine revealed catalytic residues and binding sites of the ligand and Mg^{2+} . Two lysine residues were suggested as catalytic bases for proton abstraction in the racemisation reaction.¹⁷² The α/β fold is characteristic for enolases which supports the hypothesis that NAAARs belong to this enzyme superfamily.¹⁷¹

A genetic screening of 30 Actinomycetes strains identified a NAAAR from *Amycolatopsis orientalis* subsp *lurdia* that has similar properties to the *Amycolatopsis* sp. enzyme. The two NAAARs have high sequence similarity and are similar in their substrate spectrum, thermostability and metal ion dependency.¹⁷³ However, tolerance to high substrate concentrations is improved in the new enzyme and substrate concentrations up to 200 mM are tolerated¹⁷³ which is four fold higher than the limitation of the *Amycolatopsis* sp. NAAAR.

As an alternative approach to novel enzyme discovery protein engineering studies have been carried out by Campopiano *et al.* in collaboration with Dr. Reddy's. A double knockout *E. coli*

mutant strain was generated to detect NAAAR activity as selection system for directed evolution. The novel *E. coli* strain is L-methionine auxotroph and viability is dependent on NAAAR activity when cultivated in minimal medium supplied with *N*-acetyl-D-methionine.¹⁷⁴ Using this assay for directed evolution allowed to identify an improved NAAAR double mutant, that shows six fold activity compared to the wildtype *Amycolatopsis* sp. NAAAR.¹⁷⁴ A photometric assay was developed to further expand the screening capabilities to the determination of specific activities and substrates other than *N*-acetyl-D-methionine. The photometric assay is a coupled enzyme assay in which NAAAR activity is linked to the horseradish peroxidase catalysed oxidation of a photometric detectable dye.¹⁷⁵ Different substrates were tested with this assay confirming a novel activity towards *N*-acetyl-D-naphthylalanine¹⁷⁵.

The substrate scope for the acylase/racemase DKR system was recently extended to other amino acid derivatives.^{161, 176} Using a system of the thermostable enzymes from *Geobacillus* sp, L-*N*-carbamoylase and NAAAR, allows to use not only *N*-acetyl amino acids, but also *N*-formyl and *N*-carbamoyl amino acids as substrates to give yields of >95% of the optically pure L-amino acid.¹⁷⁶

1.3.3.3 α -amino- ϵ -caprolactam racemase

The α -amino- ϵ -caprolactam racemase from *Achromobacter obae* (AoACLR) has been commercially used in the Toray process for the industrial production of L-lysine from α -amino- ϵ -caprolactam (ACL) since the 1970s.¹⁷⁷ In this process L-ACL is hydrolysed by an L-ACL hydrolase from *Cryptococcus laurentii* whereas the remaining D-ACL is racemised *in situ* by ACLR.¹⁷⁸

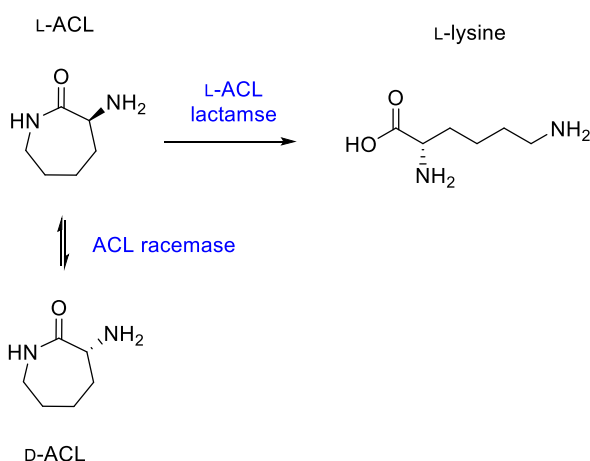


Figure 26: DKR process for the production of L-lysine using L-ACL lactamase and ACLR.

As this work focusses on this group of enzymes the state of the art of ACLRs will be detailed in this section with the example of AoACLR.

First biochemical characterisation of *Ao*ACLR

The PLP-dependent racemase *Ao*ACLR was investigated in detail in the 1980s by Soda *et al.*¹⁷⁹⁻¹⁸² and more recently re-discovered and intensely investigated by Asano and co-workers.¹⁸³⁻¹⁸⁵ Several ACLRs have been discovered and characterised from different organisms and especially from rhizobium bacteria.¹⁸⁶⁻¹⁸⁷ The natural role of ACLRs is unknown so far but ACLRs were mainly found in rhizobia which might indicate a role in plant root infection.¹⁸⁶ ACLRs belong to the enzyme class 5.1.1.15 and α -amino- ϵ -caprolactam is considered as the natural substrate for racemisation.^{179, 184} The monomer subunit of *Ao*ACLR was estimated to a molecular weight of 50 kDa and described to form a tight homodimer as tertiary structure.¹⁸² Originally, the *Ao*ACLR substrate scope was described as limited to cyclic amides of amino acids such as α -amino- ϵ -caprolactam from lysine and α -amino- δ -valerolactam (AVL) from ornithine.¹⁷⁹ *Ao*ACLR is competitively inhibited by AVL and was described to have no activity on amino acids or peptides.¹⁷⁹ Differently from the ACL racemisation pH optimum at 8.8, the pH optimum for AVL racemisation is pH 7.0. The difference in the pH optima was explained by the inactivation of *Ao*ACLR by AVL at pH values <8.0.¹⁸¹ Nevertheless, addition of PLP can reactivate or even protect *Ao*ACLR from inactivation by AVL, and α -keto acids, such as glyoxylate, can also prevent the inactivation.¹⁸¹ An explanation for this may be a transamination between AVL and PLP following the regeneration of pyridoxamine phosphate by transamination with the α -keto acid.¹⁸¹

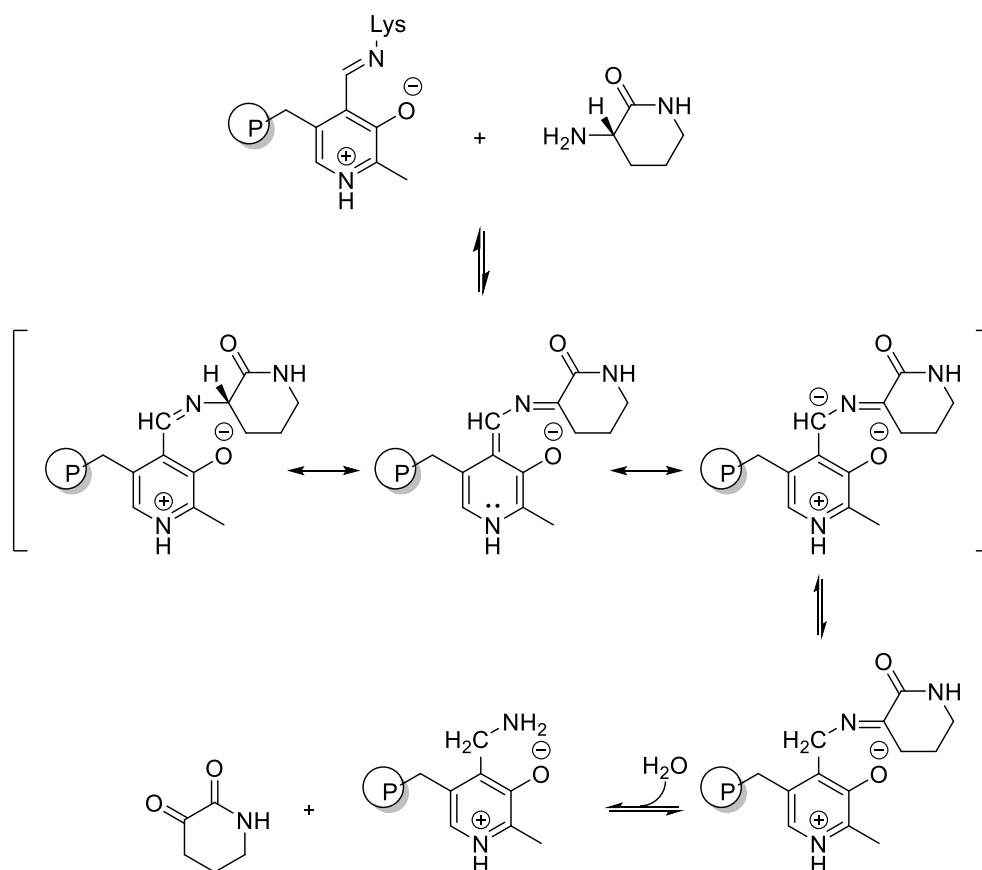


Figure 27: Mechanism for the transamination of VAL catalysed by *AoACLR* proposed by Ahmed et al. in 1985.¹⁸¹

L- α -amino- β -thio- ϵ -caprolactam was also discovered as substrate for *AoACLR* which is racemised 3-times faster than ACL but with a pH optimum of pH 10.0.¹⁸⁰ New interest on ACLRs arose in the 2000s due to the discovery of an expanded substrate scope and therefore a possible application in a DKR of amino acid amides to amino acids.¹⁸³

Structure and mechanism of *AoACLR*

The first reaction mechanism for ACLR catalysed racemisation was proposed in 1986.¹⁸² The determination of tritium incorporation during racemisation showed that tritium was incorporated in both D- and L-substrate suggesting a mechanism of deprotonation and subsequent reprotonation of the substrate using a hydrogen atom from the solvent.¹⁸² This deprotonation and reprotonation of the substrate-PLP complex was proposed to be mediated by a single active site base in a “swinging door” model which was found for another PLP-dependent (amino acid) racemase.¹⁸⁸

After the discovery of *Ao*ACLR it took more than 40 years until the first three-dimensional structure was published by Yamane and co-workers.¹⁸⁴ The structure was solved of native *Ao*ACLR (2.1 Å) and the enzyme in complex with ϵ -caprolactam (2.4 Å). The *Ao*ACLR monomer consists of an N-terminal domain from residues 3-43, a PLP-binding domain with residues 48-319 and a C-terminal domain containing residues 321-436. The active site is located around the PLP binding site in a cleft formed between PLP-binding site and the C-terminal domain.

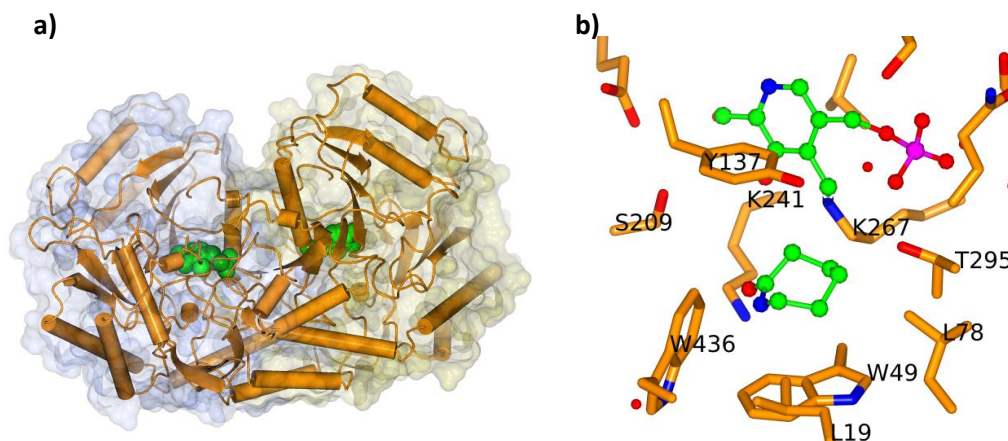


Figure 28: Structure of *Ao*ACLR (pdb code 2zuk) solved by Okazaki *et al.*¹⁸⁴ a) overall structure of the dimeric enzyme; b) view in the active site (orange cylinder representation) complexed with PLP and ϵ -caprolactam (green ball and stick representation).

The *Ao*ACLR crystal structure shows a homodimer in which the dimer formation between subunit A and B is stabilised by 48 interchain hydrogen bonds. As in other fold I PLP-dependent enzymes the N-terminal domain of the ACLR subunit A interacts with the PLP-binding site of subunit B. Various other interactions between both subunits indicate that the subunits form a dimer not only in the crystalline form but also in the dissolved enzyme.

As ϵ -caprolactam is an inhibitor of ACLR,¹⁷⁹ it is considered to interact with the active site of ACLR in a similar way as its natural substrates. The structure of the *Ao*ACLR- ϵ -caprolactam complex differs to the native ACLR structure only in the disordering of residues 151-158 in subunit B. ϵ -caprolactam is stacked between W49 and Y137 while the carbonyl oxygen is bound to K241 nitrogen by a hydrogen bond.

The C4' atom of PLP is covalently bond to the amino group of K267 forming the internal Schiff base linkage. The nitrogen of the PLP pyridine is connected to D238 by formation of a salt bridge. It is suggested that the bond of the PLP nitrogen and D238 stabilises the electron sink properties of PLP. The pyridine ring of PLP is complexed between Y137 and V240. Due to structural similarities to an alanine racemase it was proposed that racemisation is catalysed by an acid/base pair mechanism mediated by Y137, D210 or K267 as possible acid/base residues. Furthermore a racemisation mechanism via a quinonoid intermediate is suggested

due to the D238 mediated stabilisation of the pyridine nitrogen of PLP. *In silico* studies identified K241 as important for ACL racemase activity.¹⁸⁶ The aspartate in position 210 was suggested to be involved in amide recognition by hydrogen bonding with the lactam nitrogen of the substrate.¹⁸⁶

Substrate scope of *Ao*ACL

The *Ao*ACL catalysed racemisation of novel substrates, various amino acid amides, was described in detail in a recent study.¹⁸³ Among others L-2-aminobutyric acid amide, alanine amide, norvaline amide, norleucine amide, leucine amide, methionine amide and phenylalanine amide were tested as substrates for *Ao*ACL. Among the tested substrates L-2-aminobutyric acid amide was discovered to be accepted best with 2.7% relative activity (of 100% activity with ACL), lowest activity (0.052 %) was determined for L-phenylalanine amide.¹⁸³

Discovery of this expanded substrate scope disproved that ACLs are only active towards cyclic amino acid amide derivatives and created new potential applications of these racemases. DKRs for the production of various L-amino acids from the corresponding amides have been successfully applied with *Ao*ACL. In this process *Ao*ACL was used together with a D-amino peptidase from *Ochrobactrum anthropi* in one pot to resolve L-alanine amide to D-alanine with a yield of 99.7%.¹⁸³ An *Ao*ACL double mutant (L19V/L78T) was developed with improved activity towards L-phenylalanine amide for application in a DKR of phenylalanine amide to D-phenylalanine with yields >99% and excellent enantiomeric excess up to 99%.¹⁸⁵

The ongoing commercial interest in ACLs is demonstrated by a recent patent for the use of an ACL from *Ochrobactrum anthropi* (*Oa*ACL) for the production of enantiopure amino acids filed by DSM in 2008.¹⁸⁹ This patent describes the use of *Oa*ACL as amino acid amide racemase for the production of enantiopure amino acids from the corresponding racemic amino acid amides.

1.4 Aim of this work

The aim of this project is the evolution of a novel amino acid ester racemase (AAER) for the application in ester to amide DKRs as shown in Figure 29. Racemic amino acid esters are used in the desired DKR as substrate for a hydrolase-catalysed aminolysis towards the corresponding amino acid amide. The hydrolase-catalysed reaction is enantioselective, therefore it is of interest to racemise the unreacted enantiomer during the reaction. One criterion for the desired racemisation catalyst is high selectivity towards the ester substrate and low activity towards the amide product. Aim of this project is to evolve the desired AAER activity by structure-guided engineering starting from PLP-dependent ACLRs.

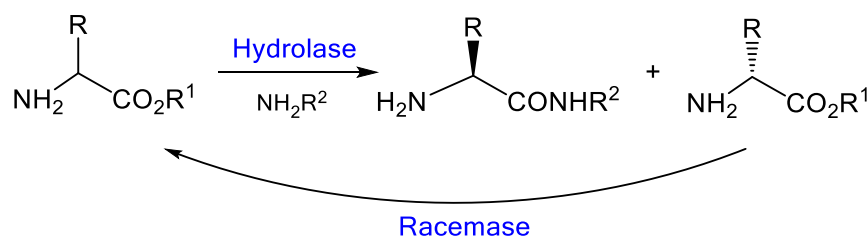


Figure 29: Dynamic kinetic resolution of racemic amino acid esters. A hydrolase and amino acid ester racemase are used *in-situ* to convert a racemic amino acid ester to the corresponding enantiopure amino acid amide.

The evolution of amino acid ester racemase activity will include structure-guided engineering experiments which require knowledge of the substrate binding and the reaction mechanism of ACLRs. This project will focus on exploring the three-dimensional structures and racemisation activity of amino acid amide racemases. As mentioned above racemisation activity towards amino acid amides was recently discovered for AoACL from *Achromobacter obae*.¹⁸³ Hence, AoACL will be subject of detailed investigations and two homologous enzymes, namely aminotransferase from *Rhizobium freirei* (RfACL) and amino acid amide racemase from *Ochrobactrum anthropi* (OaACL) will be explored within this work (Table 1).

Table 1: Overview of enzymes of investigated in this work.

Enzyme	AoACL	RfACL	OaACL
Origin organism	<i>Achromobacter obae</i>	<i>Rhizobium freirei</i>	<i>Ochrobactrum anthropi</i>
Enzyme function	amino-caprolactam-racemase	Class III aminotransferase	Amino acid amide racemase
Heterologous host	<i>Escherichia coli</i>	<i>Escherichia coli</i>	<i>Escherichia coli</i>
Gene length (bp)	1311	1311	1320
Size (kDa)	45.7	45.6	46.8
Cofactor	PLP	PLP	PLP
PDB code	2ZUK	5M46	n.a.

Attempts will be made to obtain X-ray structures of an ACLR-ligand complex to give insights of the substrate binding. Detailed knowledge of the ligand binding site will allow further conclusions about the mechanism of the racemisation reaction and will allow identification of key catalytic residues. All three ACLRs will be tested on their racemisation activity towards amino acid amides and esters. Once AAER activity is confirmed focus will be put on improving the racemisation activity of amino acid esters. The information gained from a crystal structure will facilitate the evolution of AAER activity by structure-guided engineering. In summary this work is aimed to characterize ACLRs according to three main objectives:

- Investigations into the structure and mechanism of ACLRs
- Characterisation of the racemisation activity
- Engineering of amino acid racemisation activity

2 Materials and Methods

2.1 Materials

All chemicals were of high analytical grade and purchased from Sigma-Aldrich, Fluka, Merck, Melford or Thermo Fisher Scientific. Restriction enzymes were supplied from New England Biolabs (NEB). Hotstart Turbo Pfu DNA polymerase was ordered from Agilent and KOD DNA polymerase was purchased from Merck. Enzymes for the photometric assay, alcalase, horse radish peroxidase and L-amino acid oxidase were purchased from Sigma-Aldrich. Premixed LB medium (high salt Miller's broth) was purchased from Melford. Crystallisation buffers were obtained from Hampton research (Index) or Molecular Dimensions (Pact, CSS I, CSS II). Oligonucleotides were synthesised by Eurofins Genomics or Invitrogen. Chemically competent bacteria cells were supplied by Merck, Clontech and Novagen.

2.1.1 Plasmids

A variant of the expression vector pET-28a was used for the molecular modification of expression hosts throughout this work. The YSBLI3C vector is an optimised pET-28a vector which features allow to use it for ligation independent cloning (LIC).¹⁹⁰ Amongst other features this plasmid encodes a gene encoding for kanamycin resistance, the T7 promotor and the lac operon. For protein modifications after protein expression it encodes an N-terminal hexa-histidine tag followed a cleavage site for a 3C protease (Figure 30). All vectors used for this work are listed in Table 2.

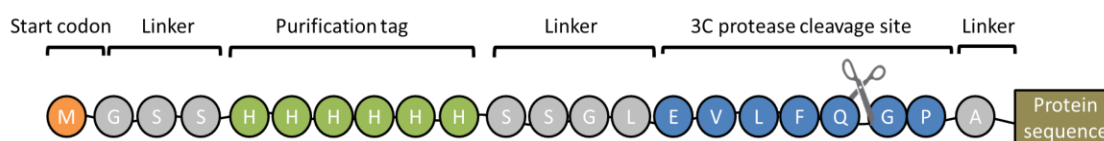


Figure 30: Scheme of the N-terminal region of the target protein encoded on the YSBLI3C vector.

Table 2: Racemase expression vectors. Gene sequences are shown in Appendix 10.2, vector map for YSBLI3C is shown in Appendix 10.1

Plasmid	Genotype	Supplier
YSBLI3C-vector	Modified from pET28a (ColE1 lacZ/KanR PT7 Plac)	YSBL
YSBLI3C- <i>Ao</i> ACLR	Recombinant with 1311 bp gene of ACLR	This work
YSBLI3C- <i>Rf</i> ACLR	Recombinant with 1311 bp gene of <i>Rf</i> ACLR	This work
YSBLI3C- <i>Oa</i> ACLR	Recombinant with 1320 bp gene of <i>Oa</i> ACLR	This work

2.1.2 Bacterial strains

Different strains of *Escherichia coli* (*E. coli*) were used for genetically modifications in order to produce the target proteins (Table 3).

Table 3: Bacterial strains

Bacterial strain	Genotype	Supplier
<i>E. coli</i> BL21(DE3)	F-ompThsdSb(rB-mB-) gal dcm	Merck
<i>E. coli</i> Rosetta TM (DE3)	F- ompT hsdSB(rB- mB-) gal dcm pRARE (CamR)	Novagen
<i>E. coli</i> Stellar (<i>E. coli</i> HST04)	F-, ara,Δ(lac-proAB) [Φ80d lacZΔM15], rpsL(str), thi, Δ(mrr-hsdRMS-mcrBC), ΔmcrA, dam, dcm	Clontech

2.1.3 Devices and equipment

Table 4: Devices

Technique	Device	Supplier
Centrifugation	GenFuge 24D	Progen
	Avanti J-20 XP Centrifuge	Beckmann Coulter TM
	Sigma 3-16 KL	Sigma
	LYNX 6000	Sorvall
Incubation	I 26 Shaker	New Brunswick Scientific
UV-Vis Spectroscopy	BioPhotometer plus	Eppendorf
	50 Bio UV Visible Spectrophotometer	Varian
	EPOCH	Tecan
	PolarStar	BMG Labtech
pH determination	pH 210 Microprocessor pH Meter	HANNAH Instruments
chromatography		
High pressure liquid	Dionex Ultimate Prominence HPLC system	LC Packings Shimadzu
DNA amplification	BIOER 2.01	LifeECO
Protein Purification	Akta Purifier	General Electrics
	Akta Pure	General Electrics
	Atka Start	General Electrics
X-ray crystallography	Mosquito® robot	TTP Labtech
	Micromax-007HF	Rigaku
	MAR345 imaging plate detector	Marresearch
Gel electrophoresis	SDS-PAGE	Biorad
	DNA electrophoresis	Amersham

2.2 Methods

2.2.1 Cloning synthetic genes into an expression vector

E. coli codon optimised synthetic genes for *Ao*ACL_R, *Rf*ACL_R and *Oa*ACL_R were purchased from Invitrogen and amplified by Polymerase Chain Reaction (PCR). Components of the reaction mixture are listed in Table 5 and a PCR program (Table 6) was run to amplify the gene of interest. Steps 2-5 were repeated in 35 cycles.

Table 5: Reaction mixture for PCR

Component	Concentration	Volume [μ L]	Final concentration
qH ₂ O		34	
dNTPs	each 2 mM	5	0.2 mM
KOD polymerase		5	
MgSO ₄	25 mM	2	1 mM
primer _{FWD}	20 pmol/ μ L	1	0.4 pmol/ μ L
primer _{REV}	20 pmol/ μ L	1	0.4 pmol/ μ L
DNA-template		1	
Total volume		50	

Table 6: Parameters of PCR for amplification of the target genes.

Reaction step	Temperature [$^{\circ}$ C]	Time [s]
Polymerase activation	94	120
Denature	94	30
Annealing	55	30
Extension	72	150
Final extension	72	180
Termination	10	-

Analysis and purification of the PCR product

The amplified PCR product was analysed on an agarose gel. The gel electrophoresis was carried out as described in Chapter 2.2.2. The dyed samples (60 μ L) were loaded onto the gel and after electrophoresis the DNA bands were visualised by blue light. A band of the expected size between 1000-1500 base pairs (bp) was visible for each sample. These bands were excised and the DNA was extracted from the agarose gel using a gel extraction kit (Sigma). After purification the DNA concentration of the samples was determined by UV absorption at a wavelength of 260 nm and the samples were stored at -20° C.

T4 polymerase digest of PCR product

Ligation independent cloning requires the specific restriction of the DNA fragment for the insertion into an expression vector.¹⁹⁰ Due to specific designed primers (Table 7) the restriction with a T4 DNA polymerase ($3' \rightarrow 5'$) will result in overhangs which are complementary to the overhangs of the vector. This allows for the insertion of the DNA fragment into the vector by simple annealing of the complementary overhangs (Figure 31). For the T4 polymerase treatment a DNA concentration of 0.2 pmol was used in a total reaction volume of 20 μ L. The reaction mixtures were incubated for 30 min at 20°C and then for 30 min at 75°C.

Table 7: Primers used for ligation independent cloning.

Primer	Nucleotide sequence
Forward primer ($5' \rightarrow 3'$)	GACCCGACGCGGTTA
Reverse primer ($5' \rightarrow 3'$)	CAGGGCGCCATG

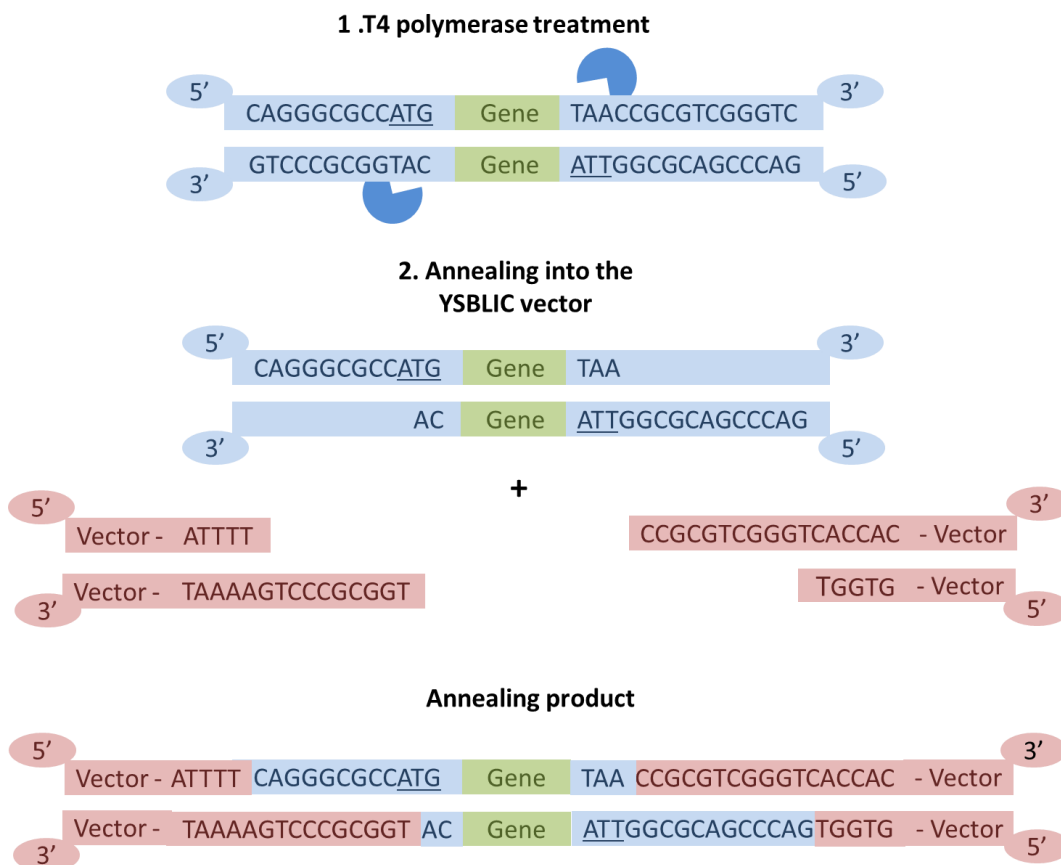


Figure 31: Scheme of ligation independent cloning procedure.

Annealing of the insert into an expression vector

After T4 polymerase treatment the PCR product was annealed into the YSBLIC3C vector. The vector was ready to use as it was linearised and treated with T4 polymerase before. 3 μ L of

insert and 3 μL of the YSBLIC3C-vector were pipetted into a reaction tube for the annealing reaction. The reaction was carried out for 10 min at room temperature and afterwards stopped by adding 1.5 μL EDTA (25 mM).

Transformation of chemically competent *E. coli* Stellar cells

1.5 μL of the respective YSBLIC3C-insert vector were added to 25 μL *E. coli* Stellar cells (Novagen). This mixture was incubated for 30 min on ice. Afterwards, the cells were heat shocked at 42°C for 20 s followed by incubation on ice for 5 min. 200 μL SOC medium were added to each preparation. This mixture was incubated at 37°C, 180 rpm for 60 min. The antibiotic kanamycin can be used to select recombinant *E. coli* cells containing the YSBLIC3C-vector as the vector encodes a gene for kanamycin resistance (Kan^R). Resistance against this antibiotic is based on the gene product of Kan^R, an enzyme that modifies kanamycin and therefore reduces its affinity to ribosomes.¹⁹¹ 200 μL of the cell culture were plated on LB-agar plates containing 35 $\mu\text{g mL}^{-1}$ kanamycin and incubated overnight at 37°C. The plates were stored in the fridge at 4°C until further use.

Amplification, purification and analysis of the YSBLIC3C-constructs

For amplification of YSBLIC3C-constructs in *E. coli* 5 mL overnight cell cultures were prepared. One single colony of recombinant *E. coli* Stellar cells was picked from the agar plate and used to inoculate the LB medium (containing kanamycin 30 $\mu\text{g mL}^{-1}$). The cultures were incubated at 37°C, 180 rpm overnight. The next day the *E. coli* cells were harvested by centrifugation at 4500 rpm at 4°C for 20 min. The plasmid DNA was isolated from the recombinant *E. coli* cells using a Quiagen Miniprep Kit according to the supplier's protocol. After purification the plasmid DNA was eluted in 50 μL water. The DNA concentration of the purified DNA construct was measured at 280 nm.

In order to analyse if the gene of interest was inserted into the YSBLIC3C-vector a test restriction digest was performed. The YSBLIC3C-vector was hydrolysed using the restriction enzymes NdeI and NcoI. The restriction site for NdeI is upstream (3') of the inserted gene whereas the restriction site for NcoI is located downstream (5') of the inserted gene. Possible restriction sites inside the gene sequence were checked with the program Serial Cloner 2.6.1. For the enzymatic restriction 7 μL YSBLIC3C-construct, 1 μL cutsmart buffer (NEB), 1 μL NcoI and 1 μL NdeI were pipetted into a reaction tube and incubated for 1 h at 37°C. After the incubation the samples were dyed with 1.7 μL sample dye. The complete volume of the

samples was loaded on an agarose gel and a gel electrophoresis was carried out at 110 V for 50 min.

2.2.2 Gel electrophoresis

Agarose gel electrophoresis

DNA fragments were analysed on an agarose gel. An agarose gel (1%) was prepared in triethanolamine (Tris-acetate-EDTA) buffer. The agarose was dissolved by heating the solution in a microwave. Safer Stain (Invitrogen) was added to the solution to allow visualisation of the DNA by UV or blue light. DNA samples were stained with sample dye (NEB) in a ratio of 1/6. 5 µL of 1 kb DNA ladder (NEB) were loaded on the gel. The dyed samples were loaded onto the gel. The electrophoresis chamber was connected to a power source and the gel electrophoresis was performed at 110 V for 30-55 min.

Sodium dodecyl sulphate polyacrylamide gel electrophoresis (SDS-PAGE)

Protein production and the purity of purified enzymes was analysed by SDS PAGE. Proteins were separated according to their size through a 12 % Bis-Tris SDS gel. The gels were prepared with resolving gel buffer (1,5 M Tris, 0.4 % SDS, pH 8.8) and stacking gel buffer (0.5 M Tris, 0.4 % SDS, PH 6.8) using a gel casting kit (Biorad). The protein sample was masked with an overall negative charge by SDS in the sample buffer and denatured by heating at 95°C. The gel electrophoresis was carried out for 45 min at 200 V in a gel tank (Biorad) using SDS running buffer (Tris-Glycine buffer, 5 % SDS).

Western blot

In order to identify the target protein of a sample run on a SDS gel, a western blot was prepared. This technique allows binding of his-tagged proteins with specific antibodies, transferring them onto a membrane to visualise them. A sheet of nitrocellulose membrane (Whatman) was soaked in methanol for about 2 min and afterwards soaked in transfer buffer for 10 min.

Table 8: Buffers used for western blotting.

Buffer	Concentration	Component
Transfer buffer	25 mM	Tris
	192 mM	Glycine
	20 % v/v	Methanol
10 x TBST·Cl	100 mM	Tris pH 7.5
	1 M	NaCl
	1 % v/v	Tween 20

Eight sheets of Whatman 3MM membranes were also soaked in transfer buffer. The SDS gel was washed with water and then with transfer buffer. Starting from the anode 4x Whatman paper, 1x cellulose membrane, SDS gel, 4x Whatman paper were placed into the western blot machine. Transfer of the proteins onto the nitrocellulose membrane was carried out at 25 V (500 mA) for 50 min. After running the transfer the membrane was rinsed with 5 mL TBST buffer (containing 5 % milk and 0.06 % v/v his-antibody). The marker was visualised and marked on the membrane by staining the membrane with Ponceau Red solution (Sigma) for 5 min. After removing the staining solution the membrane was washed in milk solution for a few minutes. The membrane was then transferred into the blocking solution (5 % milk in TBST buffer) and incubated under shaking for 1 h. The blocking solution was rinsed of with TBST buffer and the membrane was incubated with the primary antibody for 1h. After washing steps with TBST the membrane was incubated with the secondary antibody for 30 min. Protein bands were visualised using SigmaFast stain.

2.2.3 Site directed mutagenesis of ACLRs

Mutations were introduced into the DNA sequence of ACLRs using the site directed Quikchange method. With this method primers containing the desired change in the DNA sequence are used for a PCR, using the vector-gene construct as template DNA. The plasmid is amplified by PCR incorporating the primers with the mutation into the new construct. A round of amplification of the whole plasmid results in a new plasmid with staggered nicks. The newly amplified DNA then contains the mutation of interest and can be separated from the template DNA by performing a DpnI digestion of the methylated template DNA. The new plasmid is transformed into *E. coli* cells where the nicks are repaired (Figure 32).

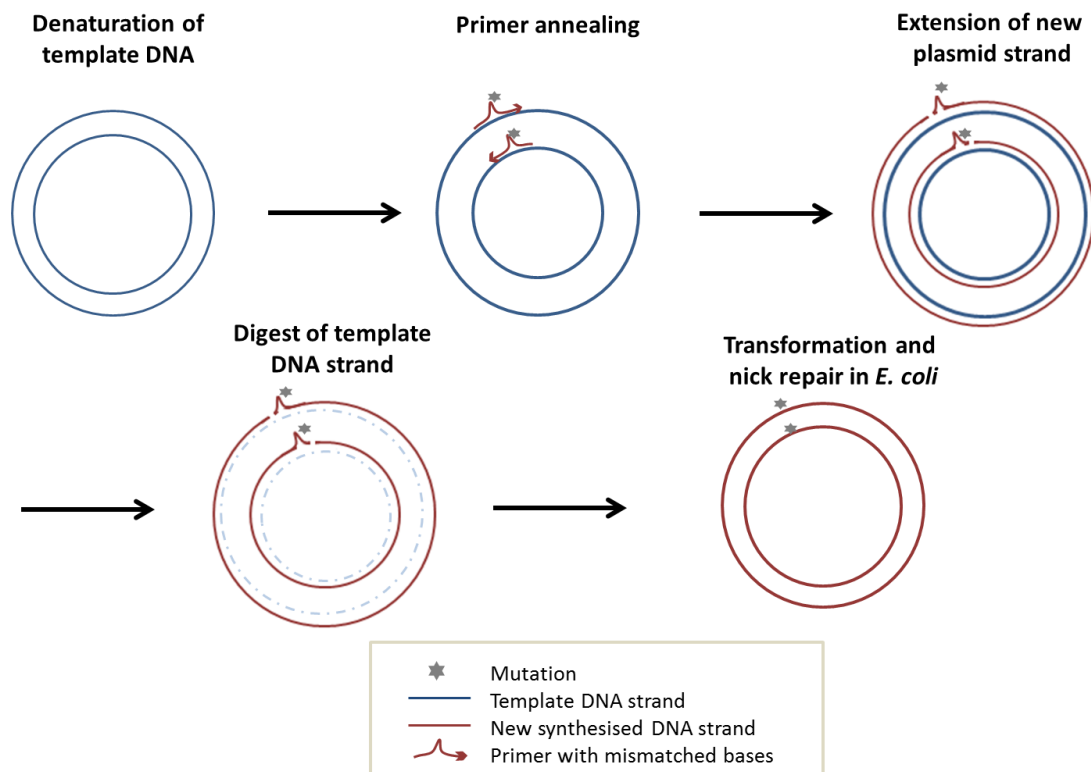


Figure 32: Scheme of site directed mutagenesis using the Quikchange method.

Within this work site directed mutagenesis (SDM) method using Hotstart Pfu Turbo DNA polymerase (Agilent) was carried out. Primers were designed using the online tool primerX and supplied from Eurofins Genomics. The sequences of all primers used for this work are listed in Table 9.

Table 9: Primers used for site directed mutagenesis.

Mutation	Forward primer (5' -> 3')	Reverse primer (5' -> 3')
<i>Rf</i> ACLR-Y137F	GCATTTATTGGTGCATTT CATGGTTGTACCGTTG	CAACGGTACAACCATGAAATGCA CCAATAAATGC
<i>Rf</i> ACLR-K241A	GGTCTGGTTGACGTTGAA GTAGTGT	TTAGTCCGGTGGTCGTGAGACTT AGCCA
<i>Rf</i> ACLR-D210A	CCGATTCAGAGTGCTGGT GGCCTGATTG	TTAGTCCGGTGGTCGTGAGACTT AGCCA
<i>Rf</i> ACLR-W49A	ATTGATCTGAGCGGTGCA GCAGGTGCAGCCAG	TGGGTCCGACCGACGTGGACGAC GTGGCGAGT
<i>Rf</i> ACLR-M293L	AGCGCATTTGCCTTGCA ACCCTGC	CGTCCCAGACGTTCCGTTTACGC GA
<i>Rf</i> ACLR-Y386T	CTGGGTCTGGTGCTGACC TATGTTGGTATGAATG	TAAGTATGGTTGTATCCAGTCGT GGTCTGGGTCA
<i>Oa</i> ACLR-A51W	ATTCTGGATCTGAGCGGT AGCTGGGGTCCGGCAGC ACTGGGTAT	ATAACCCAGTGCTGCCGGACCCC AGCTACCGCTCAGATCCAGAAT
<i>Oa</i> ACLR-L21V	CAGAAATTGGTTCGTGTGC GTTTTAGTCCGC	GCGGACTAAAACGCACACGACC AATTTCTG
<i>Oa</i> ACLR-L80T	GCAGGCGCAAGCCTGAC CCTGTATCCGAATGAAG	CTTCATTCGGATACAGGGTCAGG CTTGCGCCTGC
<i>Oa</i> ACLR-D210A	ACCGATTCTGAGTGCGGG TGGTCTGGTTG	TGTTGGTCTGGTGGGCGTGAGTC TTAGCC

A PCR was set up using the corresponding primers, the components of the PCR and the program that was run are listed in Table 10 and Table 11. Annealing temperatures were chosen 5°C below the according melting temperature of the primers. In case of poor yields from the PCR a Touchdown PCR with gradient of decreasing annealing temperatures was run.¹⁹²

Table 10: PCR reaction components employed for site directed mutagenesis.

Component	Stock concentration	Volume (μL)
Plasmid DNA template	100 ng μL^{-1}	1
Primer _{FWD}	20 pmol	1
Primer _{REV}	20 pmol μL^{-1}	1
dNTPs	2 mM (each nucleotide)	5
Pfu Turbo DNA polymerase buffer	10 x	5
Pfu Turbo DNA polymerase	1.0 U μL^{-1}	1
Filled up with H₂O to 50 μL		

Table 11: Program used for PCR for site directed mutagenesis. Steps 2-4 were repeated 35 cycles. The annealing temperature was adjusted according to the melting temperature of the primers.

Step	Temperature ($^{\circ}\text{C}$)	Time (s)
1. Initial denature	95	300
2. Denature	95	60
3. Annealing	5°C below melting temperature of primers	60
4. Extension	72	600
5. Final extension	72	300

After the PCR, DpnI (2 U) was added to the reaction mixture to hydrolyse the template DNA. DpnI specifically hydrolyses methylated DNA, which is methylated by *E. coli* deoxyadenosine methylase in the living organism. Therefore DNA generated *in vitro* is not methylated and is not hydrolysed by DpnI. The reaction mixture was incubated at 37°C for 4.5 h. A transformation of competent *E. coli* Stellar cells with a heat shock was carried out as described before (Chapter 2.2.1). The plasmid DNA was amplified and purified as described before (Chapter 2.2.1). The purified plasmid DNA was analysed by a test restriction using NcoI (1 μL), NdeI (1 μL), 4 μL of the purified plasmid, 1 μL cut smart buffer, in a total volume of 10 μL . The mixture was incubated for 1 h at 37°C and after incubation analysed on an agarose gel (Chapter 2.2.2). The desired mutation was verified by Sanger sequencing performed by GATC Biotech.

2.2.4 Generation of site-saturation libraries with inverse PCR

Site-saturation libraries of *Oa*ACLR were generated in position 51 (*Oa*ACLR-Sat-A51) or L293 (*Oa*ACLR-Sat-L293). To obtain a library of mutants with any of the 20 amino acid as replacement in a specific position, degenerate primers were used for amplification of the target gene. The primers NNK were selected, where N (nucleotide) stands for any of the four nucleotides (ACTG), and K (keto) is either Guanine (G) or Thymine (T). The combination NNK can result in 32 different codons and encodes for all 20 amino acids. The generation of site-saturation mutations is more challenging than single mutations, and success strongly depends on the DNA yield from PCR, therefore inverse PCR was chosen as cloning method. Primers for inverse PCR were designed such that the PCR product is linear and contains the desired mutation (Table 12). Due to the linearity of the PCR product the amplification yield is exponential. The linear PCR product is then phosphorylated by a kinase and re-circularised using a T4 ligase¹⁹³ (Figure 33).

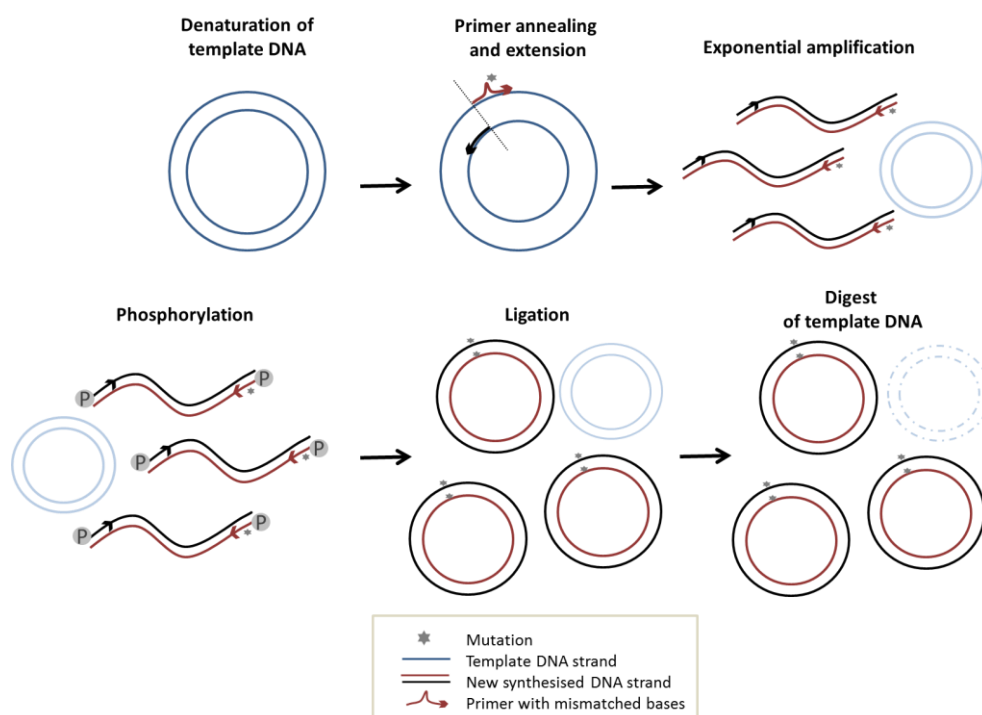


Figure 33: Scheme of site directed mutagenesis using inverse PCR.

As prediction of one specific melting temperature of primers with degenerate codons is not possible, PCRs were run as touchdown program. The touchdown method allows testing many different annealing temperatures in a single PCR reaction. For this the annealing temperature is reduced in every cycle over a certain range. The DNA is amplified at the optimal annealing temperature. In the second phase a standard PCR with the lowest annealing temperature of the selected range is run to further amplify the DNA.¹⁹⁴

Table 12: Primers used for generation of site-saturation of *Oa*ACL_R in position 51 or 293.

Mutation	Forward primer (5' -> 3')	Reverse primer (5' -> 3')
<i>Oa</i> ACL _R - Sat-A51	TGAGCGGTAGC NNKGGTC CGGCAGCA	GATCCAGAATGCTACGACCACC TT
<i>Oa</i> ACL _R -Sat-L293	CCGGCATTGTT NNKCAGA CCACCG	TGCATGATCCATCACCCACTGC

The PCR reaction was carried out as touchdown program, starting from 80°C decreasing to 65°C by -1°C per cycle (for 15 cycles).

Table 13: Components used for inverse PCR to generate site-saturation mutations in *Oa*ACL_R.

Volume (μL)	Component	Stock concentration
1	Plasmid	60 ng μL ⁻¹
0.75	Forward primer	20 pmol μL ⁻¹
0.75	Reverse primer	20 pmol μL ⁻¹
5	dNPTs	2 mM
5	Reaction buffer	10 x
3	MgSO ₄	25 mM
1.5	DMSO	
1	KOD Hot Start	1 U mL ⁻¹
Filled up to 50	H ₂ O	

Table 14: Touch down PCR program. Denature to extension steps were repeated with 15 cycles.

Step	Temperature (°C)	Time (s)
Phase 1		
Initial denature	95	180
Denature	95	30
Annealing	80 – 1 per cycle	45
Extension	72	60
Final extension	72	300
Phase 2		
Denature	95	30
Annealing	65	45
Extension	72	60
Final Extension	72	300

The PCR product was gel purified and 1.5 μL DpnI was added to 50 μL of the purified DNA and incubated for 1.5 h at 37°C. Ligation of the PCR product was performed at room temperature as listed in Table 15.

Table 15: Components for the phosphorylation and ligation of the PCR product.

Volume (μL)	Component
10	H ₂ O
4	purified DNA
2	NEB buffer 4
2	10x T4 ligase buffer
1	PNK T4 kinase
1	T4 ligase

E. coli Stellar cells (50 μL) were transformed with 3.5 μL of the mixture containing the ligation product. Plasmids were isolated from the pool of all obtained colonies by dissolving all colonies on the plate in a small amount of water. The cells were centrifuged and used for plasmid isolation. The purified plasmid was analysed by Sanger sequencing performed by GATC. The quality of the library was evaluated by estimating the percentage of the according base in the relevant positions by the peak height in the sequencing chromatogram. Additionally the quality was controlled by sequencing 15% of the library, which corresponds to 14 mutants. After confirmation of the library quality, competent *E. coli* BL21 (DE3) cells were transformed with the library plasmid.

2.2.5 Cell cultivation and heterologous protein expression

Large scale cultivations of *E. coli* for overexpression of the target gene were carried out in lysogenic broth (LB) medium (Table 16). When the cells reached the exponential growth phase (0.6-0.8 OD_{600 nm}) isopropyl β -D-1-thiogalactopyranoside (IPTG) was added at a final concentration of 1 mM to induce the overexpression of the target gene through the T7 expression system. Expression of the mutant libraries was carried out in terrific broth (TB) medium containing glucose and lactose (Table 17). This allows for the autoinduction of the expression of the target gene without adding an inducing agent. Glucose is a preferred carbon source and metabolised first, once it is completely consumed, the metabolism changes to the uptake of lactose. The presence of lactose in the cell induces then the overexpression of the target gene through the control of the lac operon.

Table 16: Components for 1 L LB autoinduction medium.

Amount (g)	Component
10	Tryptone
5	Yeast extract
10	NaCl
1.5	Tris/Tris HCl

Table 17: Components for 1 L TB autoinduction medium.

Amount (g)	Component
12	Tryptone
24	Yeast extract
0.5	Glucose
2.0	α - lactose
2.31	KH_2PO_4
12.33	K_2HPO_4

Preparation of glycerol stocks of recombinant *E. coli* cells

Chemically competent *E. coli* BL21 (DE3) cells were transformed with the previously prepared YSBLIC3C-vector containing the respective gene of interest (*Ao*ACL*R*, *Rf*ACL*R* or *Oa*ACL*R*). The transformation was carried out according to the procedure described before (Chapter 2.2.1). 1 μL of the respective YSBLIC3C-gene construct (YSBLIC3C-*Ao*CL*R*, YSBLIC3C-*Rf*ACL*R* or YSBLIC3C-*Oa*ACL*R*) was used for the transformation of 25 μL of competent cells. A single colony of the transformants was picked from the agar plate and used to inoculate 5 mL LB medium (containing 30 $\mu\text{g mL}^{-1}$ kanamycin). These cultures were incubated at 37°C, 180 rpm overnight. The next day glycerol stocks were prepared by adding 300 μL sterile glycerol to 700 μL of the cell culture. The glycerol stocks were stored at -80°C.

Test expressions

Overexpression of the target protein was carried out at different temperatures and with different IPTG concentrations. Overnight cultures were prepared by inoculating 5 mL LB medium (containing 30 $\mu\text{g mL}^{-1}$ kanamycin) with one single colony of the recombinant *E. coli* BL21 (DE3). The next day 15 mL cultures (LB medium containing 30 $\mu\text{g mL}^{-1}$ kanamycin) were inoculated with 150 μL of the overnight cultures. For each enzyme 3x 15 mL cultures were inoculated, one culture for induction with 1 mM IPTG, 0.1 mM IPTG and 0 mM IPTG as control. These main cultures were incubated at 37°C until 0.6-0.8 $\text{OD}_{600 \text{ nm}}$ was reached. The overexpression was induced with 1 mM IPTG or 0.1 mM IPTG. Then each of the 15 mL cultures was split into 3x 5 mL cultures (in 50 mL falcons) for incubation at 37°C, 27°C or 16°C. The cultures were incubated at the respective temperature at 180 rpm. 24 h after induction 1 mL of each culture was transferred into a reaction tube. The cells were harvested by centrifugation at 13000 rpm for 10 min. The cells were resuspended in 500 μL water and disrupted by sonication (30 s, 30 s pause, 3 cycles). The samples were again centrifuged at 13000 rpm for 10 min. The supernatant was transferred into a new reaction tube and the pellet was dissolved in 1 mL water or solubilisation buffer. Overexpression was analysed on a SDS gel as described in Chapter 2.2.2.

Buffer screening for optimisation of protein solubility

When the tested conditions for expression did not yield any soluble protein, screening for an appropriate buffer to solubilise the expressed protein was carried out according to Kohlstaedt and co-workers.¹⁹⁵ A 1 L culture of the recombinant *E. coli* BL21 (DE3) cells was induced with 0.1 mM IPTG (at 0.61 OD_{600 nm}) and incubated at 37°C overnight. The cells were harvested by centrifugation and resuspended in 30 mL Tris (100 mM NaCl, 1 mM EDTA, pH 8.5) and aliquoted into 30 reaction tubes. The cells were centrifuged and the pellet was resuspended in 1 mL of the 30 buffers of the buffer screen (Appendix 10.3). The cells were sonicated (30 s, 30 s pause, 3 cycles) and the soluble fractions were analysed by SDS-PAGE.

Protein expression at litre scale

Starter cultures were prepared for the inoculation of a main culture for overexpression of the gene of interest. 1 µL of the respective glycerol stock of *E. coli* BL21 (DE3)-YSBLIC3C-ACLR or a single colony from an agar plate was used to inoculate 10 mL LB medium (containing 30 µg mL⁻¹ kanamycin). The cultures were incubated at 37°C, 180 rpm overnight. The overnight cultures of recombinant *E. coli* BL21 (DE3) were used to inoculate 2 L LB medium (aliquoted to 2x 1 L LB medium in baffled 2 L shaker flasks). The medium was inoculated in a ratio of 1:1000. The cultures were incubated for approximately 3 h at 37°C, 180-200 rpm until an OD_{600nm} of 0.6-0.8 was reached. The overexpression of the target gene was induced with a final concentration of 1 mM IPTG. The cultures were then incubated at 16°C, 180 rpm. Samples were taken at different time points and the OD_{600 nm} was measured. 24 h after induction the cells were harvested by centrifugation at 4000 rpm, 20 min, 4°C, the cell pellet was stored at -20°C.

Expression of saturation mutagenesis libraries

In a 96 deep-well block 96x 700 µL LB medium (containing 30 µg mL⁻¹ kanamycin) were inoculated with different single colonies of recombinant *E. coli* BL21 (DE3) obtained after transformation with the saturation mutagenesis library plasmids (Chapter 2.2.4). After incubation at 37°C, 400 rpm for 18 h, 300 µL sterile glycerol was added to each well. The deep-well block was sealed, vortexed and then stored at -80°C.

For overexpression of the library, overnight cultures were prepared in a 96 deep-well block by inoculating 500 µL LB medium (containing 30 µg mL⁻¹ kanamycin) with 1 µL of the recombinant *E. coli* BL21 (DE3) glycerol stock. The plate was incubated at 350 rpm at 37°C overnight. 96x 1 mL of TB autoinduction medium in 96 deep-well blocks were inoculated

with 10 μ L per well of the respective overnight culture. The blocks were incubated at 400 rpm, 37°C. After incubation for 24 h the cells were pelleted by centrifugation at 4000 rpm, 4°C for 20 min. The supernatant was discarded and the cell pellets were stored at -20°C.

2.2.6 Chromatographic enzyme purification

Overexpressed enzymes were purified according to a standard protocol employing immobilised metal affinity chromatography (IMAC) followed by size exclusion chromatography (SEC). For IMAC purification of the target protein 5-20 g recombinant *E. coli* cells were weighed into a 50 mL reaction tube. The cells were resuspended in Tris buffer (50 mM, 300 mM NaCl, pH 7.5). The cells were disrupted by sonication for 8 cycles of 30 s sonication, following 45 s pause. Afterwards cell debris were centrifuged at 10000 rpm at 4°C for 40 min. The supernatant (crude cell extract) was loaded on a previously equilibrated (50 mM Tris, 300 mM NaCl, pH 7.5) nickel column (5 mL, HisTrap™ FF crude, GE) using a peristaltic pump with flowrate 2-3 mL min⁻¹. After loading the crude cell extract the column was connected to an Akta purification system. All purification buffers contained Tris buffer (50 mM, 300 mM NaCl, pH 7.5) and were filtered and degassed before use. For purification of the his-tagged target protein the program listed in Table 18 was run.

Table 18: Program for IMAC purification of his-tagged proteins.

Step	Imidazole concentration (mM)	Volume (mL)	Flow rate (mL min ⁻¹)
1. Initial wash	20	35	2.5
2. Wash	50	5	2.5
3. Elution	50-500	25	2.5
4 Final elution	500	35	2.5

The eluate obtained from step 3 was collected in 5 mL fractions. Fractions containing protein were analysed on a SDS gel. The presence of protein in the eluted fractions was determined by UV measurement at 280 nm during the purification. Fractions containing the target protein in appropriate purity were pooled and concentrated using 50 mL centricons (30000 MWM cut-off) to a final volume of 1-2 mL. The concentrated protein was loaded on a previously equilibrated (50 mM Tris, 300 mM NaCl, pH 7.5) S75, S200 column (GE) or a desalting column (5 mL HiTrap, GE). Size exclusion chromatography (SEC) was performed with an Akta purification system using an isocratic gradient of Tris buffer (50 mM, 300 mM NaCl, pH 7.5). Protein was eluted at a flowrate of 0.8-1 mL min⁻¹ for one column volume (CV). Fractions containing protein were analysed by SDS-PAGE. Fractions with appropriate purity of the target protein were pooled and the protein concentration was determined at 280 nm. The enzyme was directly used for crystallisation trials or stored at 4°C for later application in

racemisation reactions. In case enzyme was stored at -20°C , 10 % w/v glycerol was added as stabiliser in the buffer used for storage.

Analytical size exclusion of RfACLR and OaACLR

8.82 g of wet cells mass of *E. coli* Rosetta-OaACLR were resuspended in approximately 45 mL Tris buffer (50 mM, pH 7.5). The cells were disrupted by sonication (30s, 45s, 8 cycles). Cell debris were centrifuged at 10000 rpm for 40 min. The target protein was purified by IMAC with the standard program described above. Fractions containing the target protein were collected from IMAC purification. The pooled fractions were concentrated to approximately 500 μL and loaded through a 1 mL loop onto a Superdex 200 GL 10/300 SEC column (previously equilibrated with Tris, 50 mM, 300 mM NaCl, pH 7.5). The purification was run at a flowrate of 1.7 mL min^{-1} on an Akta pure system.

2.2.7 Crystallisation

Protein crystallisation was performed using the vapour diffusion method. For this crystallisation technique a reservoir of crystallisation solution is used in a closed container to create a saturated atmosphere. The crystallisation solution contains precipitants, salts and buffer salts to adjust to a specific pH value. As the protein solution is mixed with the crystallisation solution the protein drop has a lower concentration than the crystallisation solution in the reservoir. The protein drop is placed within the closed container, either as sitting drop or as hanging drop. The difference in concentration leads to diffusion of water from the protein drop into the atmosphere and eventually into the crystallisation solution. Due to the water diffusion out of the protein drop, the concentration increases over time until an equilibrium between protein drop and the reservoir is reached. During the adjustment of the equilibrium the concentration for supersaturation in the protein drop, where crystal formation can occur, is also reached.

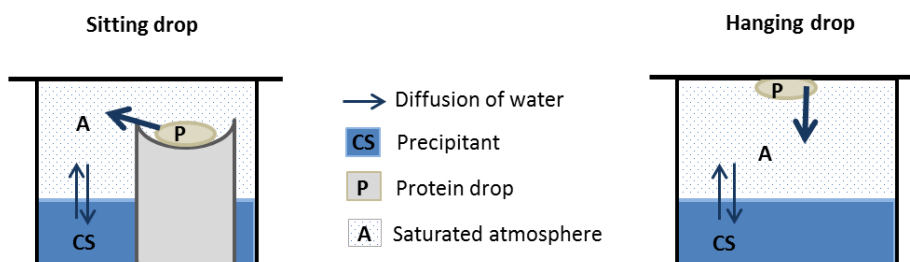


Figure 34: Scheme of different methods for vapour diffusion protein crystallisation.

Initial crystal screening in sitting drops

Initial crystallisation trials were carried out with commercially available crystallisation screens in 96 well plates for the preparation of sitting drops. Freshly purified *Ao*ACLR, *Rf*ACLR or *Oa*ACLR was concentrated to approximately 10 mg mL⁻¹ in an approximately volume of 100 µL. The commercially available crystal screens Index, Pact and CSS II and I were used for crystallisation trials. The theoretical isoelectric point of the enzymes was calculated from their amino acid sequence using the program ExPASy ProtParam. The theoretical isoelectric point of *Ao*ACLR, *Rf*ACLR and *Oa*ACLR was calculated between pH 5.7-5.8, buffers with a pH near this isoelectric point were selected to add to the crystal screens CSS I and II. Tris-HCl pH 6.0 and BisTris pH 5.5 were added to a final concentration of 0.1 M to the CSS screen mother liquor. 54, respectively 60 µL of mother liquor were pipetted into the reservoir of a MRC plate (96 wells). 150 nL mother liquor and 150 nL enzyme were pipetted together into a sitting drop using the mosquito robot (Figure 35). The wells of the MRC plate were sealed air tight and stored at 18°C. Formation of crystals was followed over several weeks.

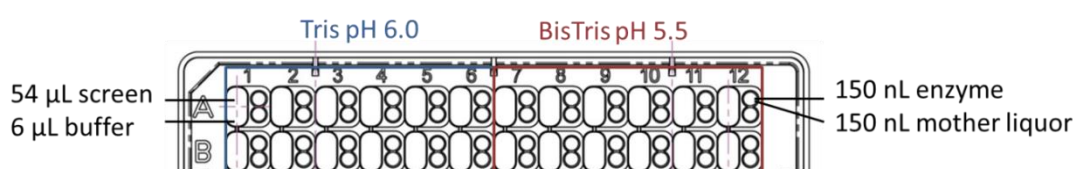


Figure 35: Scheme of MRC plate set up with CSS I and II crystallisation screen

Scale up and optimisation of crystals

After obtaining crystals from the initial screening, optimisation of the crystallisation conditions was carried out. The condition giving crystals was used for crystallisation by the hanging drop method using a 24 well plate and bigger protein drops (2-3 µL) to slow down crystal growth. The concentration of salt and PEG was varied around the screen condition to identify the optimal condition (Figure 36). Where necessary the impact of the additives (glycerol, ethylene glycol, 1,4 butanediol) on the crystal growth was investigated.

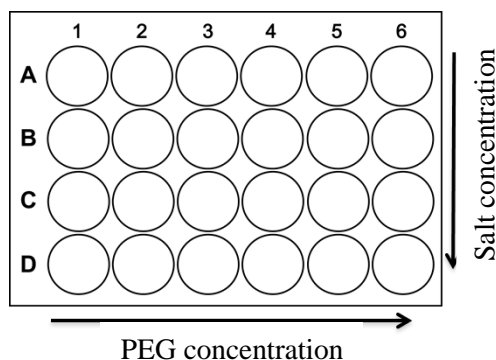


Figure 36: Scheme of concentration variation in a 24 well crystallisation tray.

The enzyme solution was prepared by concentrating it to approximately 100 μL with a concentration of 2-10 mg mL^{-1} . 1 μL of mother liquor was pipetted on a siliconised cover slip (18 x 18 mm). 1-2 μL of enzyme solution was added into 1 μL of the mother liquor drop and mixed by gently pipetting up and down. The cover slip was put upside down onto the greased edges to close the well air tight.

Crystallisation of enzyme-ligand complexes

For standard co-crystallisation with ligands 10 μL of L-ACL, L-PheNH₂, L-Phe or L-PheOMe (20-80 mM final concentration) were added to 90 μL enzyme solution (2-10 mg mL^{-1}) and incubated on ice for 30-60 min. The enzyme solution was then used to prepare hanging drops in 24 well plates as described before.

To optimise ligand binding to the enzyme co-crystallisation with mother liquor containing the ligand (40 mM L-PheNH₂ or 100 mM L-PheOMe) was carried out. Enzyme (approximately 3 mg mL^{-1}) was used for crystallisation in 96 MRC plates using the previously mentioned crystallisation screens. The ligand stock solution was dispensed into the mother liquor wells of the MRC plates using a respective program on the Mosquito.

Crystal micro-seeding

Crystal seed stocks were prepared using the Seed Bead™ kit according to the supplier's recommendations (Hampton Research). 50 μL of the respective crystallisation solution were pipetted into the reaction tube containing a seed bead. Crystals obtained in sitting or hanging drops were transferred into to the seed bead reaction tube. The mixture was then vortexed for 3 minutes. This solution was used as seed stock to set up crystallisation trials. For crystallisation in 24 well plates a 1:1 ratio of fresh protein and seed stock was used to set up hanging drops. For 48 well plates 500 nL protein were aliquoted, then 70 nL of the seed stock

were added to the protein drop, then 430 nL of the mother liquor were copied to each of the protein drops using the Mosquito robot.

Crystal freezing and data collection

Crystals were either frozen directly from the crystallisation drop or transferred into a cryo protectant solution before freezing in liquid nitrogen. If cryo protectant solution was used, it was prepared with the condition of the mother liquor containing glycerol (10% v/v), 1 mM PLP and an appropriate concentration of the ligand. Diffraction of the crystals was tested in house on a Rigaku Micromax-007HF fitted with Osmic multilayer optics and a Marresearch MAR345 imaging plate detector. When the resolution was considered as sufficient ($< 3 \text{ \AA}$) the complete dataset was collected from the synchrotron.

Solving the structure and molecular replacement

Full datasets were collected on beamlines I02 or I04 at the Diamond Light Source, Didcot, Oxfordshire, UK. Data were processed and integrated using XDS and scaled using SCALA within the Xia2 processing system. The number of molecules in the asymmetric unit was calculated with the Matthews Coefficient. The coefficient relates the crystal volume per asymmetric unit to the molecular weight of the protein. The statistical analysis of this relation of over more than 100 x-ray structures gave a coefficient to estimate the volume of solvent contained in the asymmetric unit and therefore allows prediction of the number of proteins per unit¹⁹⁶

X-ray structures were solved by molecular replacement which is based on solving the phase problem by using phase information of a homologous X-ray structure that has already been solved. The homologous model structure is fitted into the experimental electron density and the model sequence is aligned with the new sequence. The new structure is calculated by a three-dimensional rotational search and translational search according to the fitted known structure. Differences such as deviations in sequence, flexibility (B factors) or exposure of the residues are taken in account for the calculations.¹⁹⁷ Within this work molecular replacements were carried out with MOLREP¹⁹⁷ using the structure of *Ao*ACL_R (PDB code 2ZUK) or *Rf*ACL_R (solved in this work) as molecular replacement model. The structure was refined using iterative cycles of the programs COOT¹⁹⁸ and REFMAC5.¹⁹⁹ REFMAC implements a maximum likelihood function to calculate intensities from the experimental reflections in order to generate the electron density map (omit map, F_o).¹⁹⁹ A theoretical map (F_c) is calculated according to the input structure and compared to F_o . A difference map ($F_o - F_c$) is

generated to improve fitting of the atomic structure into the electron density and determine the quality of the fitting. COOT was used to manually refine positions of the atom structure according to the new calculated electron density obtained as output from REFMAC. After building of the protein backbone and side chains, residual density of the omit map in the active site was modelled as PLP or substrate.

2.2.8 HPLC based activity assay

For determination of the enzyme activity, the racemisation of L-enantiomer to D- and L-enantiomer was measured by chiral HPLC. The enantiomers were separated using a chiral Crownpak (+) column (Daicel) on a Shimadzu Prominence HPLC system. Under acidic conditions enantiomers of compounds containing an ammonium ion near the chiral centre can be separated by the column material, crown ether (Figure 37). Hence, amino acids or compounds containing an amino group in proximity to the chiral centre can be separated according to their enantiomeric conformation.²⁰⁰

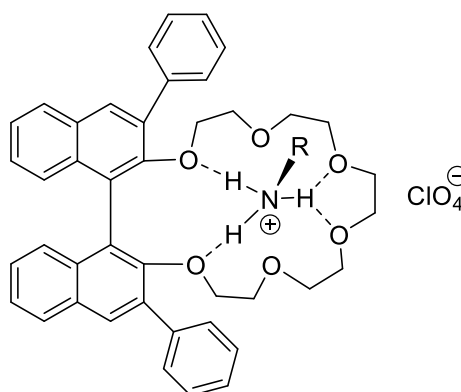


Figure 37: Crown ether used for chromatographic separation of amine enantiomers.

Standard reactions were carried out at 1-2 mL or 100-200 μL total reaction volume in KPi buffer (100 mM) at 30°C, 500 rpm. 200 μL , respectively 20 μL samples were taken at continuous time points, quenched with 2 N HClO_4 and diluted in water (1:4 ratio). The samples were analysed by chiral HPLC using a Crownpak (+) column with an isocratic gradient (60 mM HClO_4 , 10 % MeOH) at a flowrate of 1 mL min^{-1} . Peaks of the separated compounds were detected at 190 nm. Peak areas of the separated enantiomers were determined and the ratio of enantiomers was calculated as relative peak areas or the concentration was calculated according to a standard curve. Formation of the opposite enantiomer was plotted against the reaction time. The slope of the graph was used to calculate specific activities (U mg^{-1}), defined as conversion of 1 μmol substrate per min per mg of enzyme. The protein concentration was measured by UV or Bicinchoninic acid (BCA) method (Chapter 2.2.11).

Influence of storage condition on the enzyme activity

Inactivation of the enzyme by snap freezing was observed during the course of this work. Therefore different conditions were tested to find optimal storage conditions. After purification of *Rf*ACLR the enzyme was stored at different conditions as listed in Table 19. Aliquots of an enzyme solution (1.4 μL) with the same protein concentration (1.2 mg mL^{-1}) were prepared, 20 % (v/v) Tris buffer (50 mM, pH 7.5) or glycerol was added. After 24 h storage the enzyme solutions were quickly thawed and used for a racemisation activity assay using L-PheNH₂ as substrate. Specific activities (U mg^{-1}) were calculated from the conversion of substrate per minute, related to the applied amount of enzyme.

Table 19: Conditions tested for storage of purified *Rf*ACLR after purification.

Protein concentration After storage (mg mL^{-1})	Additive	Storage condition
0.96	600 μL Tris (50 mM, pH 7.5)	Stored at 4°C
0.81	600 μL glycerol	Stored at -20°C
1.17	600 μL Tris (50 mM, pH 7.5)	Snap frozen, stored at -20°C
0.84	600 μL glycerol	Snap frozen, stored at -20°C

Determination of kinetic parameters

Kinetic parameters were determined for the conversion of L-PheOMe by *Oa*ACLR variants. For this purpose the specific activity of *Oa*ACLR was measured at eight different L-PheOMe concentrations (1-60 mM) using the HPLC assay. The activities were plotted against the concentration and a graph was fitted according to the respective kinetic model (Michaelis-Menten or substrate inhibition). The kinetic parameters K_m and V_{max} were derived from the fitted graphs. K_{cat} was calculated from V_{max} and the enzyme molarity.

2.2.9 Photometric activity assay

A coupled enzyme activity assay was developed for the detection of PheOMe racemisation for the photometric measurement of enzymatic racemisation activity. The assay was adapted according to a colorimetric assay for the detection of *N*-acetyl amino acid racemase activity.¹⁷⁵ In the previously developed assay the production of the L-enantiomer was coupled to the deacetylation and amino acid oxidation, which was then coupled to the oxidation of *o*-dianisidine. The colour of the produced *o*-dianisidine can be detected photometrically at a wavelength of 436 nm.

For detection of PheOMe racemisation activity the production of L-PheOMe from D-PheOMe was coupled to the H_2O_2 coupled oxidation of *o*-dianisidine catalysed by peroxidase from horseradish in one pot as illustrated in Figure 38.

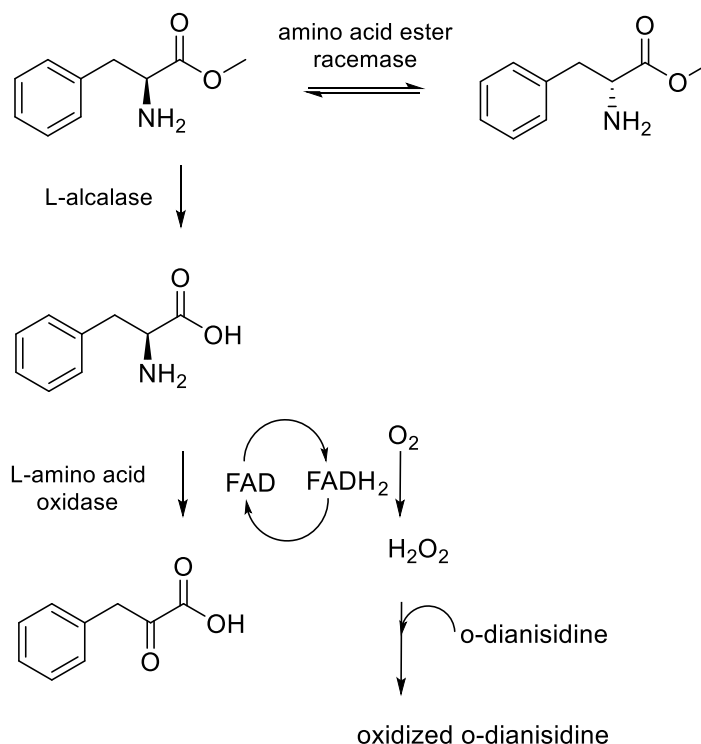


Figure 38: Scheme of the coupled enzyme assay for the detection of AAER activity.

Reactions were carried out in a total volume of 200 μL (100 mM KPi buffer, pH 5.8) in 96 well plates. The enzyme was applied as cell lysate from *E. coli* BL21 (DE3) containing overexpressed ACLR (or an empty vector as control). D-PheOMe (5 mM) was used as substrate for the ACLR catalysed racemisation reaction. The produced L-PheOMe was hydrolysed to the corresponding amino acid by the L-selective alcalase from *Bacillus Licheniformis* (0.26 U mL^{-1}). L-phenylalanine was then oxidised by L-amino acid oxidase (L-AAO) from *Crotalus atrox* (60 mU mL^{-1}). The oxidation of the amino acid was detected by coupling the production of H_2O_2 , side product of the reaction. It is used as co-substrate by horseradish peroxidase (28 U mL^{-1}) to oxidise *o*-dianisidine (0.2 mg mL^{-1}). The concentration of oxidised *o*-dianisidine was detected by absorption at 436 nm, which can be correlated to the concentration of produced D-PheOMe.

Table 20: Volumes and concentrations of the assay components for colorimetric detection of PheOMe racemisation.

Assay component	Volume (μL)	Final concentration
Alcalase	10	0.26 U mL^{-1}
L-AAO	10	60 mU mL^{-1}

HRP	0.6	28 U mL ⁻¹
KPi buffer (pH 5.8)	9.4	50 mM
D-PheOMe	30	5 mM
<i>o</i>-dianisidine	40	0.2 mg mL ⁻¹
cell lysate	100	

The assay was used in 96 well plates to detect PheOMe racemisation of saturation mutants of *Oa*ACLR (Chapter 2.2.5). *E. coli* BL21 (DE3) cells containing the overexpressed saturation mutant libraries (Chapter 2.2.5) were resuspended in 500 μ L KPi buffer (100 mM, pH 7.0) and disrupted by sonication for 3 min (1 s on, 1 s off) with a 24 probe sonicator. The cell debris were centrifuged at 4000 rpm, 4°C for 20 min. A master mix of all components except *o*-dianisidine and cell lysate was prepared and aliquoted as 60 μ L per well. Enzymes were prepared in KPi buffer (100 mM, pH 7.0), D-PheOMe was prepared in KPi buffer (100 mM, pH 5.8). 40 μ L *o*-dianisidine were added to each well and the reaction was started by adding the 100 μ L cell lysate to the wells. Reactions were run with cell lysate from *E. coli* BL21 (DE3)-YSBLIC3C-*Oa*ACLR as positive control and *E. coli* BL21 (DE3) harbouring an empty YSBLIC3C vector as negative control. After incubation at 30°C for 1 h, absorbance at 436 nm was measured in a plate reader (EPOCH). The concentration of the oxidised *o*-dianisidine was calculated from the Lambert-Beer law using $\epsilon = 8700$ for oxidised *o*-dianisidine at 436 nm. The path length was calculated as 0.62 cm from the radius (0.32 cm) and volume (200 μ L) in the wells. To calculate specific activities, the produced amount of D-PheOMe was related to the protein concentration in the reactions, which was measured with the BCA method.

2.2.10 Development of the photometric activity assay

Alcalase catalysed hydrolysis of L-PheOMe

The efficiency of the alcalase reaction was tested using the enzyme at different concentrations (2.6 and 0.26 U mL⁻¹). The alcalase catalysed hydrolysis of PheOMe was carried out at 30°C for 2 h, in a total reaction volume of 1 mL (50 mM KPi buffer, pH 7.0). The conversion of D- or L-PheOMe (10 mM) to phenylalanine was analysed by Thin Layer Chromatography (TLC) using aluminium oxide silica plates and a butanol/ammonium acetate mixture (7:3) as mobile phase.

Testing different concentrations of HRP and L-AAO

The previously established colorimetric assay was transferred to a 96-well plate format at 200 μ L scale. The assay was tested with L-Phe (10 mM) to confirm efficiency of the signal output. L-AAO and HRP, were used at different concentrations to identify optimal concentrations of both enzymes to give a detectable signal within a suitable time range. Reactions were carried

out in a total reaction volume of 200 μL (50 mM KPi buffer, pH 7.0, 0.2 mg mL^{-1} *o*-dianisidine) using 10 mM L-Phe as substrate. Six different concentrations of L-AAO (0-2 U mL^{-1}), respectively HRP (0-47.3 U mL^{-1}) were tested. When the enzyme concentration was not varied, reactions contained 47.3 U mL^{-1} HRP or 2 U mL^{-1} L-AAO. 100 mg of recombinant *E. coli* BL21 (DE3) harbouring an empty YSBLIC3C vector were resuspended in 1 mL Tris buffer (100 mM, pH 7.5). A 1:10 dilution was prepared to disrupt the cells by sonication (3 cycles of 30 s on, 30 s pause). Cell debris were centrifuged at 13000 rpm for 10 min, resulting in clear supernatant used as cell lysate. The cell lysate was added to the reaction mixture to start the reaction. The reaction was incubated at 30°C and the formation of oxidised σ -dianisidine was followed at different time points.

Testing different PheOMe concentrations

The assay was tested with different L-PheOMe concentrations (0-91 mM) to find the optimal substrate concentration. To prevent hydrolysis of L-PheOMe the assay was performed at pH 5.8 (50 mM KPi buffer). Assay conditions were as listed in Table 20 and cell lysate from *E. coli* cells harbouring an empty YSBLIC3C vector or containing overexpressed *Oa*ACLR was produced as described before.

Testing different cell lysate dilutions

The assay was carried out under standard conditions (Chapter 2.2.9) with different cell lysate dilutions to evaluate the optimum to overcome the background reaction. Cell lysate was prepared from *E. coli* BL21 (DE3) harbouring an empty YSBLIC3C vector or *E. coli* Rosetta-YSBLIC3C-*Oa*ACLR by weighing in 100 mg cells and resuspension in 1 mL Tris buffer (50 mM, pH 7.5). The cells were sonicated as described before and the resulting cell lysate was diluted to different ratios with buffer. The assay was tested with the different dilutions of cell lysate. Reactions were started by adding the cell lysate to the standard reaction mixture, the absorption of oxidised *o*-dianisidine was measured at 450 nm after 3.5 h.

2.2.11 Determination of protein concentration

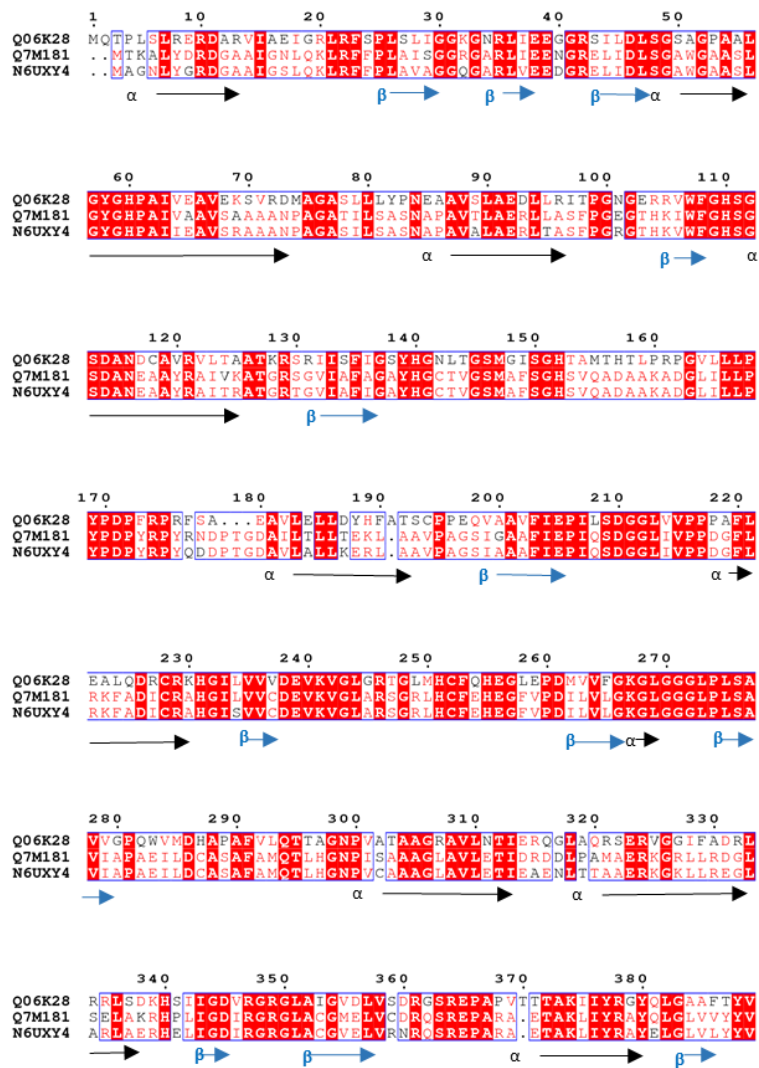
Protein concentrations were estimated by UV method for crystallisation trails or after protein purification. The absorbance of aromatic amino acids in the protein was measured at 280 nm in a spectrophotometer (Eppendorf BioPhotometer plus). The enzyme concentration was calculated according to the Lambert-Beer law using a path length of 1 cm.

The BCA method was used for determination of the protein concentration from protein used for kinetic measurements or from cell lysates. The assay is based on the biuret reaction, in which Cu^{+2} is reduced to Cu^{+1} by peptide bonds under alkaline conditions. Cu^{+1} forms a purple complex with BCA, which can be measured photometrically and related to the protein concentration.²⁰¹ The assay was carried out using the Pierce™ assay kit according to the supplier's recommendations (Thermo Scientific). For every measurement a standard curve of different BSA (bovine serum albumin) concentrations was prepared in the range of 0-2 mg mL^{-1} . The protein concentration of the measured samples was calculated according to the slope of the standard curve.

3 Enzyme production and activity

3.1 Introduction

As outlined in Chapter 1.4 of the introduction, the subject of this work is to evaluate the potential of ACLRs for the application in a DKR from amino acid esters to amides. The ACLR from *Achromobacter obae* (AoACL) has been proven to be an effective biocatalyst for the DKR of amino acid derivatives.^{183, 185} In preliminary work a data bank search (blast search) was performed to find homologous enzymes of AoACL. As result the homologous enzymes from *Rhizobium freirei* (RfACL) and *Ochrobactrum anthropi* (OaACL) were identified as putative ACLRs (Figure 39).



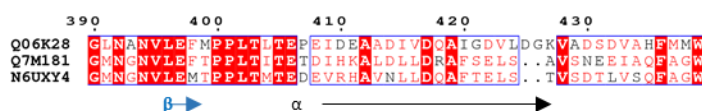


Figure 39: Protein sequence alignment of *Oa*ACL (Q06K28), *Rf*ACL (N6UXY4) and *Ao*ACL (Q7M181) calculated with the protein sequence alignment tool Clustal Omega.

The bioinformatic analysis of the protein sequences showed that *Rf*ACL and *Ao*ACL are close homologues with 85 % sequence identity. Additionally, *Oa*ACL was selected because it is a more distant homologue (53% sequence identity with *Ao*ACL) and therefore increases the sequence space that is investigated.

The aim of the work described in this section was to produce the three homologous ACLs by heterologous expression in recombinant *E. coli*. For this purpose the synthetic genes of *Ao*ACL, *Rf*ACL, and *Oa*ACL were synthesised (Gentech, Invitrogen), amplified and cloned into an expression vector. *E. coli* cells with the T7 overexpression system were transformed with the recombinant vector in order to synthesise the respective ACL. Optimal conditions for overexpression were investigated and once found the enzyme was overexpressed under these conditions. Following, the target enzyme was isolated and purified from the *E. coli* cells.

3.2 Material and Methods

Gene cloning, expression and protein purification were carried out as described in Materials and Methods, Chapter 2.2.1, 2.2.5 and 2.2.6.

3.3 Results and discussion

3.3.1 Cloning of the target genes

DNA sequences encoding the respective genes for *Ao*ACL, *Rf*ACL or *Oa*ACL and respective primer oligonucleotides were designed for ligation independent cloning and supplied by Eurofins genomics. After DNA amplification and cloning into the expression vector pET-YSBLIC3C a test restriction of the purified DNA constructs was performed using the restriction enzymes NdeI and NcoI to analyse the insertion of the target gene into the expression vector. Expected lengths of DNA fragments for the constructs were predicted with the program SerialCloner as 5400 bp (pET-YSBLIC3C-vector backbone), in case of the *Ao*ACL gene 690 and 629 bp, for the *Rf*ACL gene 690, 443, 178 bp and for the *Oa*ACL gene 1320 bp.

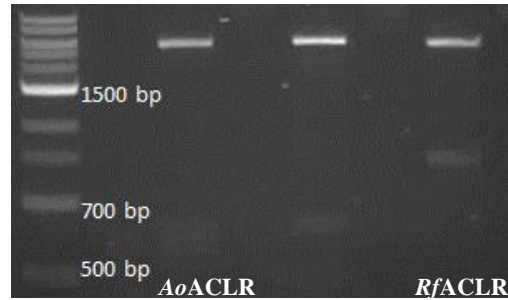


Figure 40: Agarose gel electrophoresis of the test restriction of YSBLIC3C-*AoACL*R, YSBLIC3C-*RfACL*R, YSBLIC3C-*OaACL*R.

The agarose gel shown in Figure 40 reflects the expected length of the DNA fragments after the enzymatic double digest. All DNA constructs show bands of approximately 5400 bp, which represents the pET-YSBLIC3C-vector backbone. In each case bands occur of the expected length of the (hydrolysed) target gene, indicating that the genes were inserted into the pET-YSBLIC3C-vector. The correct DNA sequence of the inserted genes was verified by Sanger sequencing performed by GATC Biotech.

3.3.2 Heterologous gene expression in *E. coli*

Chemically competent *E. coli* BL21 (DE3) cells were transformed with the respective pET-YSBLIC3C-gene construct resulting in recombinant *E. coli* BL21 (DE3) harbouring plasmids encoding for *AoACL*R, *RfACL*R or *OaACL*R. Overexpression of the target gene was tested in 10 mL cultures at different temperatures (16, 27, 37°C) and two different IPTG concentrations (0.1 mM, 1 mM). Overexpression of the target gene was compared and confirmed with a negative control without expression induction (0 mM IPTG). After cell disruption by sonication insoluble and soluble protein fractions were separated and analysed by SDS-PAGE.

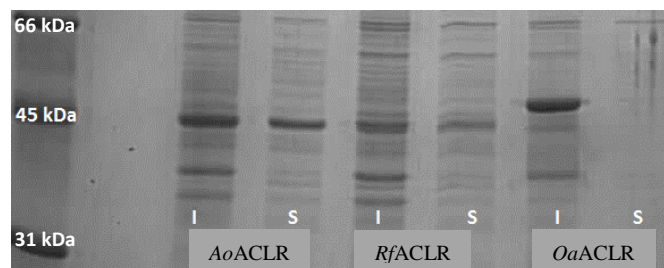


Figure 41: SDS-PAGE of overexpression of *AoACL*R, *RfACL*R and *OaACL*R in *E. coli* BL21 (DE3) at 16°C, induction with 1 mM IPTG. I: insoluble protein; S: soluble protein.

The SDS gel in Figure 41 illustrates the overexpression of each of the tested target genes in recombinant *E. coli* BL21 (DE3) cells at optimal conditions. Sufficient yields of soluble protein were obtained after cultivation at 16°C and induction with 1 mM IPTG. Bands of approximately 45 kDa occurred for each of the overexpressed enzymes (size of *Ao*ACL_R 45.67 kDa, *Rf*ACL_R 45.64 kDa, *Oa*ACL_R 46.81 kDa). The solubility of the produced enzymes varies, especially in the case of overexpressed *Oa*ACL_R most of the enzyme aggregated in inclusion bodies. *Oa*ACL_R was hardly expressed as soluble protein at any of the tested conditions. *Ao*ACL_R was best expressed as soluble protein at 37 and 16°C, induced with 1 mM. *Rf*ACL_R expression gave best yields of soluble protein under the same conditions.

As the tested conditions confirmed low expression of soluble *Oa*ACL_R in *E. coli* BL21 (DE3) test expressions were repeated with *E. coli* Rosetta (DE3)-*Oa*ACL_R cells. This *E. coli* BL21 (DE3) derivatives strain is known to improve protein expression by using codons that are rarely used in *E. coli* bacteria. The expression of *Oa*ACL_R was tested at 16°C and 27°C (induction with 0.1 mM IPTG) and protein production was monitored during the cultivation (20 and 40 h) by SDS PAGE (Figure 42).

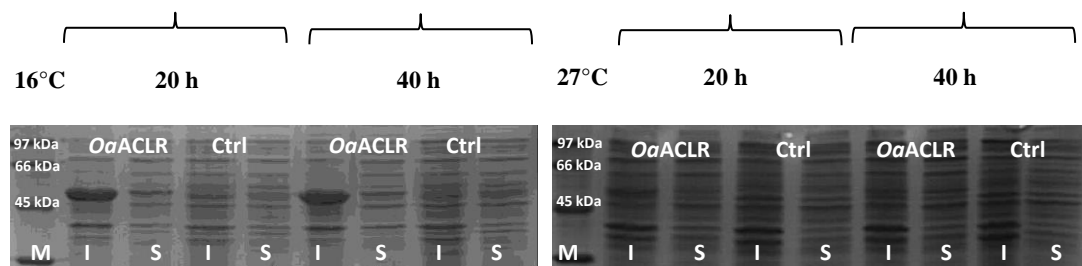


Figure 42: SDS-PAGE of test-expressions of *Oa*ACL_R in *E. coli* Rosetta (DE3) cells. Recombinant cells were incubated at 16 and 27°C, overexpression was induced with 0.1 mM IPTG. A control (ctrl) was run for each condition with recombinant cells without induction of the overexpression. I: insoluble fraction, S: soluble fraction, M: Marker.

Highest yields of soluble *Oa*ACL_R were obtained at 16°C after incubation time of 20 h. Despite the fact that slightly higher yields of soluble *Oa*ACL_R were produced at 27°C, all further cultivations were performed at 16°C, as the ratio of soluble/insoluble protein was found to be higher at this temperature. Highest yields of soluble *Oa*ACL_R were obtained after incubation for 20 h, longer incubation (40 h) only yielded increase in insoluble protein but not more production of soluble *Oa*ACL_R.

3.3.3 Scale up of heterologous expression in recombinant *E. coli*

Based on the previous results recombinant *E. coli* cells transformed with the respective vector were cultivated at the optimal condition (16°C, 1 mM IPTG) at 2 L scale to obtain sufficient amounts of cells for enzyme purification.

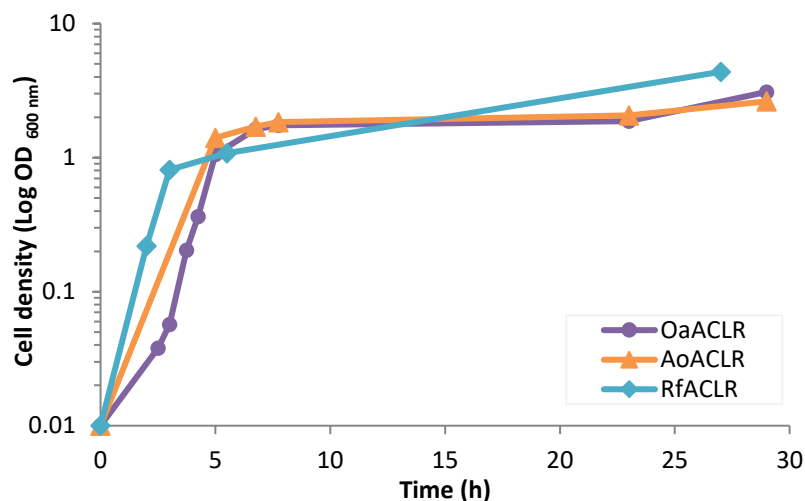


Figure 43: Growth curve of recombinant *E. coli* cells cultivated at 16°C, 180 rpm, 27-30 h. Start OD_{600 nm} was 0.01 of incubation (37°C), after induction the temperature was reduced to 16°C. Overexpression was induced at 0.4-0.8 OD_{600 nm} 3-4.25 h after starting incubation.

The bacterial growth was followed by measuring the OD_{600 nm} at continuous time points (Figure 43). The growth curves represent the typical progression of bacterial growth with the exponential phase followed by a stationary phase. After stopping the cultivation OD_{600 nm} of 2.6 (*AoACL*), 4.4 (*RfACL*) 3.0 (*OaACL*) were measured. Cultivation under given conditions gave wet cell yields of 3.8 g L⁻¹ for *AoACL*, 4.7 g L⁻¹ of *RfACL* and 4.5 g L⁻¹ of *OaACL*.

3.3.4 Chromatographic protein purification

E. coli cells from cultivation at the optimal conditions were harvested and disrupted to obtain a crude cell extract. The target protein was purified from the crude cell extract by IMAC by elution with an imidazole concentration of 90-200 mM as shown for the purification of *RfACL* (Figure 44). Presence of the target protein in the collected fractions and purity of the protein was controlled by SDS PAGE (Figure 45).

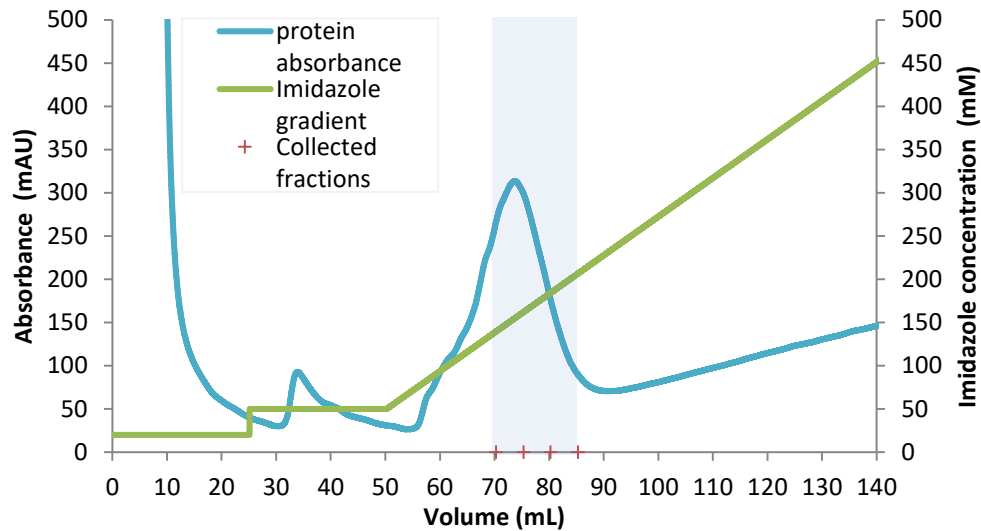


Figure 44: Chromatogram of IMAC purification of *RfACLR*. After two washing steps with imidazole (20 and 50 mM) a linear gradient was run to an imidazole concentration of 500 mM. The blue highlighted box indicates the fractions that were collected for the second purification step.

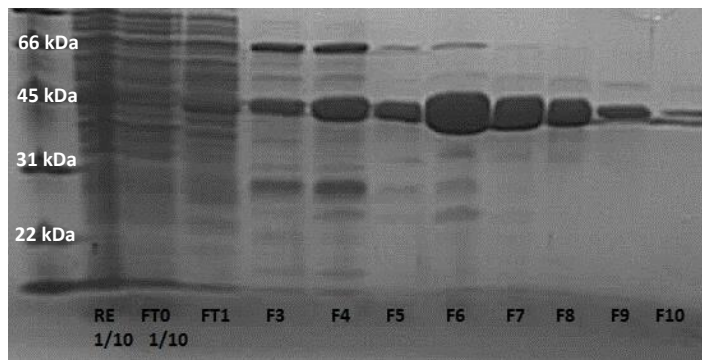


Figure 45: SDS-PAGE of fractions obtained from IMAC of *RfACLR*. 10 μ L of each fraction were dyed with 10 μ L SDS-sample dye and loaded on a SDS-gel. RE: crude cell extract; FT: Flow through, both were loaded in a 1:10 dilution.

During the wash steps with low imidazole concentrations (20 and 50 mM) most of the unspecific bound proteins were eluted from the column. Both, the chromatogram and the SDS-PAGE show that fractions 4-8 contained high concentrations of the target enzyme, whereas only in fraction 6-8 the enzyme was of high purity. The SDS-PAGE analysis of the fractions shows partly purified *RfACLR*. If the protein was subjected to crystallisation trials, SEC purification was carried out to further improve the purity of the enzyme. In this case fractions 6-8 were pooled and purified by SEC (Figure 46).

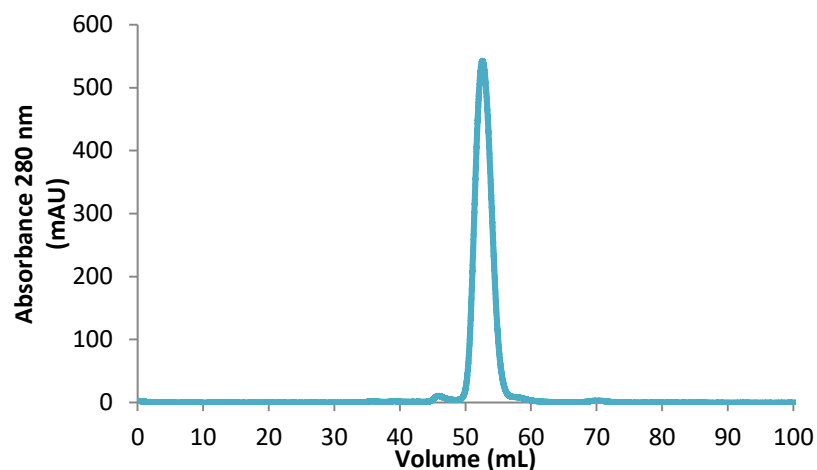


Figure 46: Chromatogram of SEC purification of *RfACL*. Proteins were eluted with an isocratic gradient according to their size. Presence of protein in the collected fractions was followed by absorbance at 280 nm.

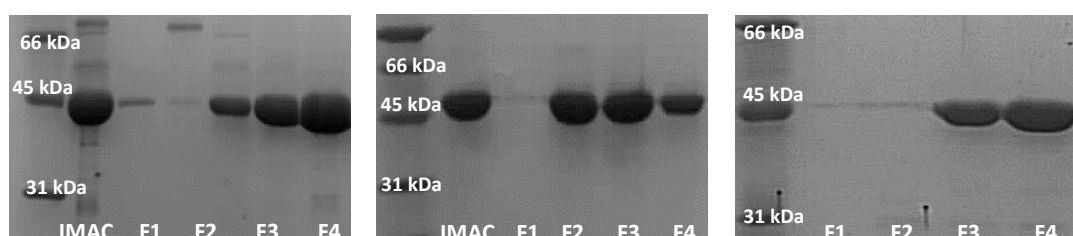


Figure 47: Purity of fractions (F) obtained after SEC purification Left: *AoACL*, middle: *RfACL*, right: *OaACL*. IMAC: partly purified enzyme after IMAC purification.

The SDS-PAGE after SEC purification shows that the partially purified enzyme obtained from IMAC was purified to homogeneity by SEC (Figure 46). Yields for the purification procedure were calculated from the total amount of purified enzyme correlated to the mass of cells used for the purification. A summary of the purification yields for all three ACLRs is listed in Table 21.

Table 21: Summary of chromatographic purifications of *AoACL*, *RfACL* and *OaACL*. Total yields were calculated from the total amount of protein determined after SEC in correlation to the amount of wet cells or cell culture used for the purification.

Purification step		Unit	<i>AoACL</i>	<i>RfACL</i>	<i>OaACL</i>
Culture		L	2	4	4
Wet cell		g	12.3	4.8	17.8
IMAC	Protein concentration	mg ml ⁻¹	n.d.	0.4	0.5
	Volume	mL	n.d.	25.0	25.0
	Total amount of protein	mg	n.d.	10.0	11.6
SEC	Protein concentration	mg ml ⁻¹	3.6	0.4	0.4
	Volume	mL	10.0	10.0	6.0
	Total amount of protein	mg	30.6	4.4	2.6
Total yield		mg g ⁻¹	2.9	0.9	0.2
		mg L ⁻¹	15.3	2.2	0.8

The production of the enzymes yielded 2.9 mg *Ao*ACLR 0.9 mg *Rf*ACLR and 0.2 mg *Oa*ACLR purified enzyme per g wet cells. Lowest yield of purified enzyme was obtained for *Oa*ACLR, although cell cultivation gave good yield of wet cells. This is in accordance with the poor expression of soluble *Oa*ACLR investigated in the test expression before (Chapter 3.3.2). During the two-step purification loss in the amount of enzyme was observed after SEC purification. 44% of *Rf*ACLR and only 23% of *Oa*ACLR obtained after IMAC could be recovered after SEC purification. This is due to further purification of the target protein but also due to precipitation of the enzyme, which was observed during concentration of the target protein before SEC.

3.3.5 Influence of storage condition on the enzyme activity

Significant loss of enzyme activity was observed between experiments for measuring the racemisation activity. The loss of activity through storage at 4°C was first observed for *Oa*ACLR. After 1 d storage at 4°C *Oa*ACLR showed activity of 9.7 U mg⁻¹ towards L-PheNH₂. After further storage for 5 d less than 1 U mg⁻¹ activity was retained. Also, activity seemed to be almost completely lost after snap freezing the protein, after which the specific activity was less than 1 U mg⁻¹. For *Rf*ACLR a loss in activity of 67 % was determined after storage at 4°C for 6 d (38.5 U mg⁻¹ after 1 d, 12.8 U mg⁻¹ after 6 d storage).

For a more detailed investigation different conditions were tested to find optimal conditions for storage of purified ACLRs. The decrease of activity towards L-PheNH₂ was determined with purified *Rf*ACLR as described in Chapter 2.2.8.1. The enzyme solution was stored at 4 or -20°C, with glycerol or in buffer solution. Relative activities were calculated after 24 h storage (Table 22).

Table 22: Relative activities of *Rf*ACLR obtained after storage under different conditions.

Additive	Storage condition	Relative activity [%]
20% (v/v) Tris buffer	Stored at 4°C	63.1
20% (v/v) Glycerol	Stored at -20°C	100.0
20% (v/v) Tris buffer	Snap frozen, stored at -20°C	34.8
20% (v/v) Glycerol	Snap frozen, stored at -20°C	63.7

Under the tested conditions, storage with 20% (v/v) glycerol at -20°C was determined as the optimal storage condition, as this gave highest activity after 24 h storage duration. Snap

freezing in liquid nitrogen negatively affected the enzyme activity. Snap frozen enzyme lost 36.3% activity compared to enzyme just frozen to -20°C . Snap freezing the enzyme without glycerol resulted in a drastic decrease in activity to only 34.6%. Storage at 4°C and snap freezing with glycerol gave similar relative activities of 63.1, respectively 63.7%. The high loss of $>40\%$ during 24 h storage at 4°C points out that the duration of storage needs to be considered when comparing activities determined in this work. Stability tests of enzyme stored at -20°C with glycerol should be carried out to find optimal conditions to retain enzyme activity.

3.3.6 Determination of quaternary organisation of *Oa*ACLR by analytical SEC

The higher order structure of *Oa*ACLR was estimated by running an analytical SEC (

Figure 48). In this chromatographic technique proteins are separated according to their molecular size on a gel matrix with defined pore size. The elution time can then be compared to standards and the molecular weight of the protein can be estimated. As the molecular size of *Oa*ACLR was calculated as 49.13 kDa by calculations from the sequence, this can be used to estimate the quaternary structure of the analysed protein.

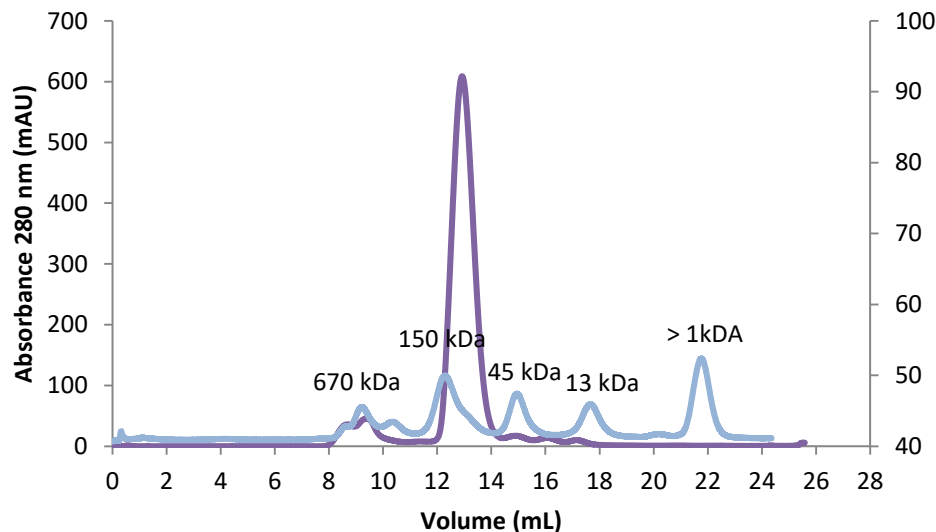


Figure 48: Chromatogram of analytical size exclusion of *Oa*ACLR. Graph for *Oa*ACLR is shown in purple, the graph for protein standards run on the same gel filtration column is shown on blue.

The analytical SEC confirms that *Oa*ACLR in solution is between 45-150 kDa compared to standards from Aldolase (150 kDa) eluting at 12 mL and conalbumin (45 kDa) at eluting at 15 mL. This suggests that *Oa*ACLR is organised as dimers in solution. Furthermore no significant

aggregation during the purification process could be determined for *Oa*ACLR. The chromatogram shows minor impurities (8-10 mL) with proteins of the size (640 kDa), which also were determined in the SDS-PAGE of the IMAC purification of *Oa*ACLR.

3.4 Conclusion

Three homologues ACLRs have been successfully produced by cloning, recombinant expression in *E. coli* and chromatographic protein purification methods. Optimal conditions for the expression in recombinant *E. coli* BL21 (DE3) cells were evaluated. A cultivation temperature of 16°C and induction with 1 mM IPTG were found to give highest amounts of soluble protein for *Ao*ACLR and *Rf*ACLR. In the case of *Oa*ACLR low yields of soluble protein could be overcome by choosing a different overexpression strain (*E. coli* Rosetta) and a lower induction with 0.1 mM IPTG. For each of the ACLRs highly pure enzyme was obtained after two chromatographic purification steps in moderate to good yields. with *Ao*ACLR yielded highest amounts of purified enzyme (15.3 mg L⁻¹), as this enzyme is also expressed in higher levels of soluble protein. On the other hand about 20-fold lower yields were obtained from the lower expressed *Oa*ACLR. The molecular weight and quaternary organisation of *Oa*ACLR was analysed by an analytical SEC with the result that the enzyme is of a size between 75-150 kDa and hence organised as dimers in solution. All three enzymes will be characterised in detail with focus on their racemisation activity.

4 Characterisation of the racemisation activity of ACLRs

4.1 Introduction

After successful cloning, expression and purification of *Ao*ACLR, *Rf*ACLR and *Oa*ACLR, the enzymes were characterised in respect to their potential for the use in a DKR towards amino acid amides. The racemases were tested with different amino acid derivatives which are of interest for the application in the production of pharmaceutically relevant building blocks or APIs. As activity towards ACL and phenylalanine amide was demonstrated for *Ao*ACLR,¹⁸³ these substrates were tested with *Rf*ACLR, *Oa*ACLR and repeated with *Ao*ACLR. Phenylalanine methylester was selected as model substrate to investigate amino acid ester racemisation activity of the ACLRs. Other substrates, relevant for a DKR with potential for industrial application, were tested with ACLRs. Additional factors, like substrate inhibition or activity in organic solvents, were tested to evaluate the applicability of these enzymes.

4.2 Materials and methods

Enzyme activity towards different substrates was determined using the HPLC based assay described in Chapter 2.2.8.

4.3 Results and discussion

4.3.1 Activity towards α -amino- ϵ -caprolactam

The racemisation activity towards α -amino- ϵ -caprolactam (ACL) was tested with *Ao*ACLR, *Rf*ACLR and *Oa*ACLR. Reactions were run and the formation of D-ACL was analysed by chiral HPLC (see Appendix 10.6 for HPLC chromatograms for the separation of ACL enantiomers). In control reactions insignificant racemisation of L-ACL by PLP (1 μ M) was observed (4.1 % conversion after 48 h), however all enzymatic racemisations were carried out without supplementing PLP to the reaction solution. The concentration of produced D-ACL and depleted L-ACL was calculated according to a calibration graph measured from different ACL concentrations of standard solution in the range of 1.25-30 mM (Figure 49). As HPLC samples of reactions were diluted in a ratio of 1:4, all standard solutions also were diluted in this ratio (Figure 50).

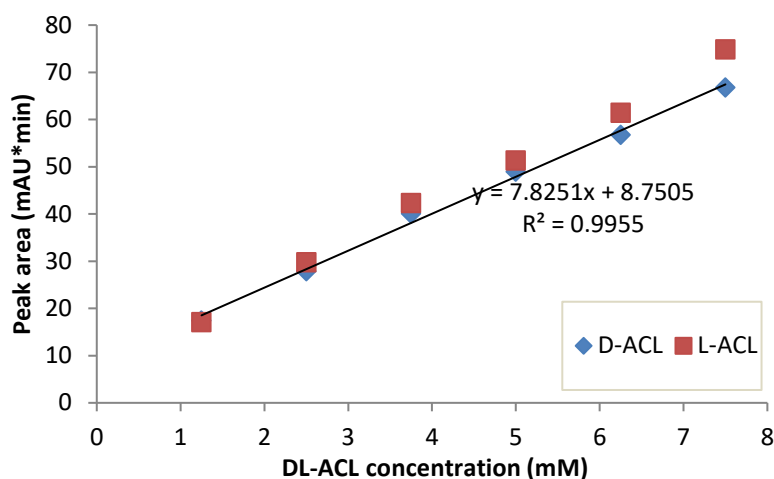


Figure 49: Calibration graph for D-ACL and L-ACL in the range of 1.25-8 mM.

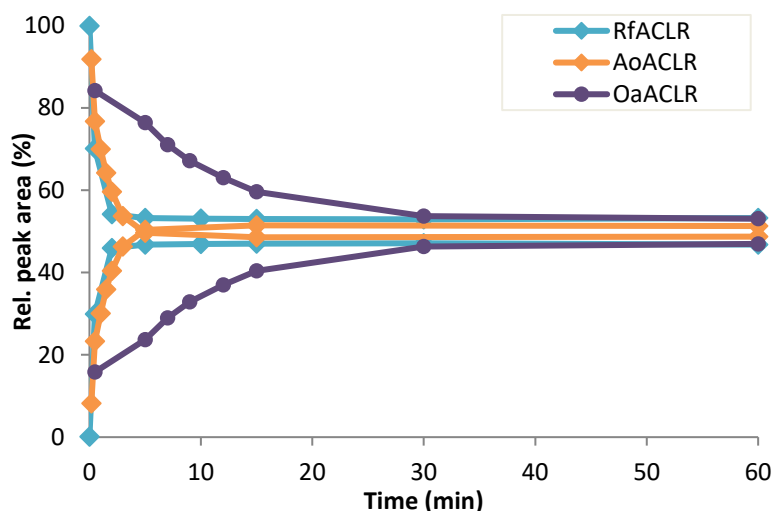


Figure 50: Enzymatic racemisation of L-ACL (50 mM) in a total reaction volume of 2.5 mL (100 mM KPi, pH 7.0, 30°C). 0.55 mg mL⁻¹ AoACL, 0.75 mg mL⁻¹ RfACL or 0.81 mg mL⁻¹ OaACL were used for the racemisation reaction.

The AoACL catalysed racemisation was complete after 5 min with an enantiomeric excess (*ee*) of 0.8%. RfACL also racemised L-ACL very fast, the reaction was almost complete with production of 46 % D-ACL after 2 min. However, even after longer reaction time the *ee* of the RfACL catalysed reaction did not decrease 4.4% *ee*. OaACL showed slow substrate racemisation with completion of the reaction after 30 min (53% D-ACL). In the case of OaACL the *t*₀ sample contained already an unusual high amount of the D-enantiomer (15%), which might be due to contamination with enzyme of the reaction mixture before starting the reaction. The results confirm that each of the tested enzymes has racemisation activity towards L-ACL which is considered as natural substrate for ACLRs. Racemisation activity could be determined for both, RfACL and OaACL, although in the case of OaACL the reaction was slower catalysed than by the other two ACLRs.

4.3.2 Activity towards phenylalanine amide

After confirming racemisation activity towards the natural substrate ACL, phenylalanine amide (PheNH₂) was tested as substrate for *Ao*ACLR, *Rf*ACLR and *Oa*ACLR. Phenylalanine amide was selected as model substrate for testing amino acid amide racemisation activity, due to its similarity with phenylalanine methylester, for which amino acid ester racemisation activity shall be evolved. The concentration of product and depleted substrate was calculated according to a calibration graph obtained from different PheNH₂ concentrations in the range of 0-4 mM (Figure 51).

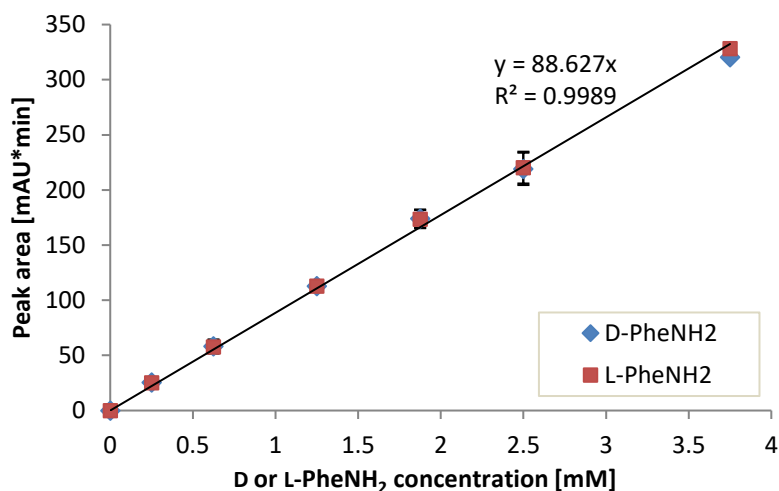


Figure 51: Calibration graph for determination of the concentration D- or L-PheNH₂ in HPLC samples analysed by chiral HPLC.

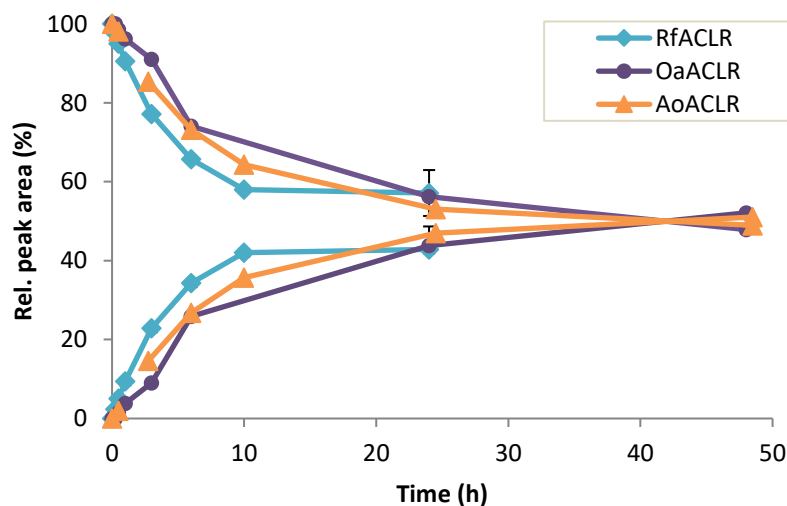


Figure 52: Racemisation of L-PheNH₂ catalysed by *Ao*ACLR (orange), *Rf*ACLR (turquoise) or *Oa*ACLR (purple). L-PheNH₂ (10 mM) was racemised by purified *Ao*ACLR (~0.921 mg), *Rf*ACLR (~1.56 mg) or *Oa*ACLR (~4.55 mg) in a total reaction volume of 2.5 mL (100 mM KPi, pH 7.0). Reactions were carried out at 30°C for 48 h, samples were analysed by chiral HPLC.

Testing the racemisation reaction verified that each of the enzymes is active on L-PheNH₂ (Figure 52). Different from control reactions with L-ACL and PLP, L-PheNH₂ was significantly racemised by PLP (1 μM), after 25 min, approximately 20 % D-PheNH₂ was racemised from 10 mM L-PheNH₂. However, the tested enzymatic reactions (enzyme concentrations 8-40 μM) were significantly faster, after 25 min each reaction reached more than 40 % conversion.

From the slope of the graphs in the area from 0-3 h starting velocities for the reaction (μM min⁻¹) were calculated. Considering the enzyme concentration in the reaction mixture, specific activities (U mg⁻¹) could be calculated for the enzymes. 1 Unit (U) was defined as the amount of enzyme that is required to convert 1 μmol substrate within 1 min. Highest activity was observed with *Rf*ACLR (20.4 U/mg), followed by *Ao*ACLR (11.9 U/mg) and *Oa*ACLR (5.2 U/mg). *Ao*ACLR was stored at -20°C before use, whereas *Rf*ACLR and *Oa*ACLR were stored at 4°C after purification (1 d). This could have affected the enzyme activity and the actual activity of *Ao*ACLR towards L-PheNH₂ might be higher. Many different factors of the storage, like duration, temperature, buffers or enzyme concentration, can affect enzyme stability and therefore lead to a decrease of the activity. As investigations in Chapter 3.3.5 showed, storage conditions had a great effect on the enzyme activity of *Rf*ACLR.

4.3.3 Activity towards phenylalanine methyl ester

Engineering of amino acid ester racemisation is the main objective of this work and phenylalanine methylester (PheOMe) was designated as model substrate for this purpose. A minimal starting activity is necessary in order to evolve novel activities in enzymes. All three ACLRs were tested for the racemisation of PheOMe to evaluate their potential as starting point for the evolution of amino acid ester racemisation.

To preclude that PheOMe racemisation activity is lost during the purification process or storage of the enzyme, the racemisation reaction was carried out with freshly prepared cell lysate from recombinant *E. coli* cells expressing the respective genes (*Ao*ACLR, *Rf*ACLR or *Oa*ACLR) or containing an empty YSBLIC3C-vector as control (Table 23). The cell lysate was used for reactions under standard condition with 5 mM L-PheOMe, samples were taken after 24 h and formation of D-PheOMe was measured according to a calibration graph (Figure 53).

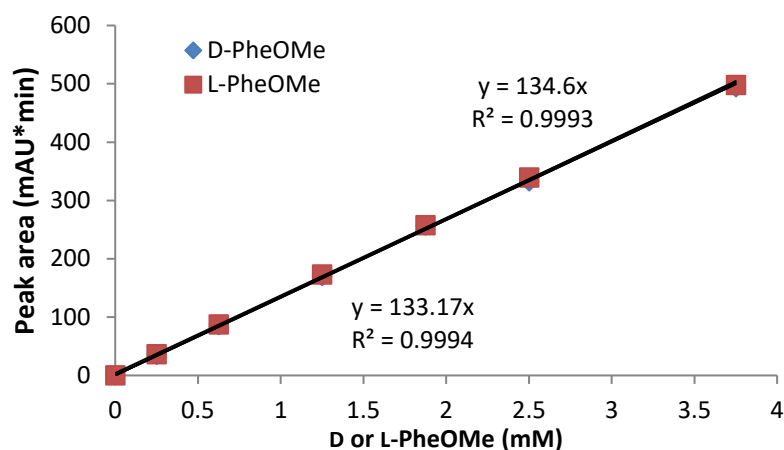


Figure 53: Calibration graph for the determination of D- or L-PheOMe by chiral HPLC.

Table 23: Racemisation of PheOMe with cell lysate containing ACLRs. Total peak area (mAU*min) obtained from racemisation reactions with cell lysate from recombinant *E. coli* (0.1 g mL⁻¹) expressing *Ao*ACLR, *Rf*ACLR or *Oa*ACLR. Listed total peak areas were determined from samples taken after 24 h reaction with 5 mM L-PheOMe in total reaction volume of 2.5 mL (KPi, 100 mM, pH 7.0) at 30°C.

Enzyme	D-Phe	D-PheOMe	L-Phe	L-PheOMe
<i>Ao</i> ACLR	0.00	0.00	147.55	23.79
<i>Rf</i> ACLR	0.00	0.00	118.97	43.13
<i>Oa</i> ACLR	17.64	16.08	105.32	23.71
Control	0.00	0.00	159.77	27.73

*Ao*ACLR and *Rf*ACLR catalysed reactions gave no D-product (D-Phe or D-PheOMe), likewise in the control reaction. Racemisation activity was observed with *Oa*ACLR, as both D-products, D-Phe and D-PheOMe, were detected in *Oa*ACLR-cell lysate catalysed reaction. Noteworthy is the hydrolysis of PheOMe to the phenylalanine (Phe) which was also observed in the control reaction with cell lysate of *E. coli* cells containing an empty YSBLIC3C-vector. It is to investigate if the hydrolysis is catalysed by a component of the cell lysate or if it occurs chemically (Chapter 4.3.5).

4.3.3.1 Confirmation of *Oa*ACLR activity towards L-PheOMe

In the first instance activity of *Oa*ACLR and *Rf*ACLR towards L-Phe was tested as this was produced in the reactions with cell lysate and L-PheOMe. No transformation of L-Phe was observed when using purified *Rf*ACLR or *Oa*ACLR in the reactions (Figure 54).

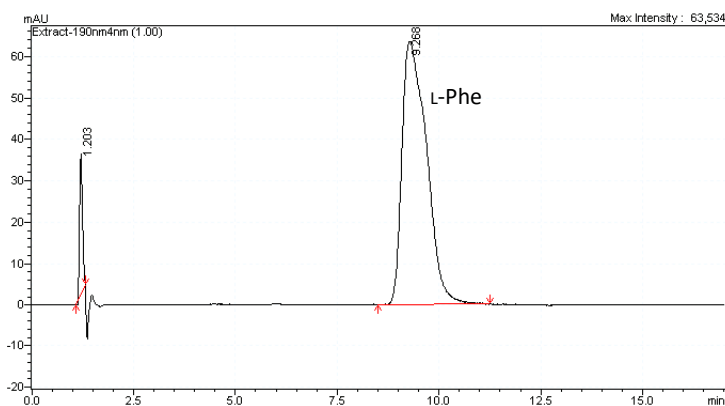


Figure 54: Chromatogram of sample from reaction with *Oa*ACLR and 10 mM L-Phe (retention time 9.2 min) after 6 h reaction time.

This result rules out that L-Phe is racemised or otherwise converted by *Oa*ACLR or *Rf*ACLR. This means that detected D-Phe in the reaction samples is the hydrolysis product of D-PheOMe and not a racemisation product of L-Phe. Phe and PheOMe showed similar signal response when run at the HPLC under same conditions. L-Phe (10 mM) resulted in an average of 403 ± 125 mAU*min peak area, L-PheOMe (10 mM) gave an average 441 ± 108 mAU*min peak area under same HPLC conditions. Consequently, peak areas of D-products (PheOMe and Phe), respectively L-products (PheOMe and Phe) can be combined to estimate how much D-PheOMe was produced before it hydrolysed to D-Phe.

In the next step, purified ACLRs were used for the racemisation reaction of L-PheOMe. Not surprisingly *Rf*ACLR and *Ao*ACLR did not show activity towards PheOMe. Formation of >2% D-product was measured after a reaction of 24 h for both enzymes, but similar rates were observed with control reactions and inactivated enzyme (Figure 55).

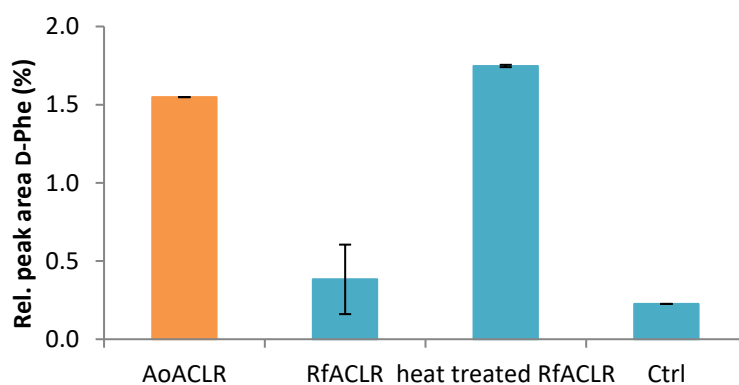


Figure 55: Formation of D-Phe from the racemisation of L-PheOMe with ACLRs. D-PheOMe could not be detected due to hydrolysis; therefore D-Phe was measured. The reaction was carried out with 10 mM L-PheOMe in a total reaction volume of 2.5 mL (100 mM KPi buffer) at 30°C for 24 h. The control reaction (Ctrl) was run under same conditions but without enzyme.

Due to the hydrolysis of D-PheOMe during the reaction only D-Phe could be determined as racemisation product. Unexpectedly, a highest conversion of L-PheOMe to the D-product was observed with heat deactivated *Rf*ACLR. The heating process (90°C for 2h) might have led to release of PLP in the solution or exposure of non-catalytic lysine residues by denaturation. These factors could give an explanation for higher racemisation rates with deactivated enzyme than with untreated enzyme. The conversion of L-PheOMe obtained with deactivated *Rf*ACLR is significantly higher than with untreated *Rf*ACLR. This result clearly shows that the conversion of L-PheOMe detected for untreated *Rf*ACLR is not catalysed in the active site, but may be referred to non-specific racemisation. The lack of activity towards PheOMe of *Ao*ACLR and *Rf*ACLR might be due to inhibition by phenylalanine or due to a narrower substrate spectrum of these enzymes.

The reaction was then performed with purified *Oa*ACLR at pH 7.0 and pH 5.8 to investigate the effect of the pH on hydrolysis of the substrate (also see Chapter 4.3.5) and the enzyme activity (Figure 56-59). The pH of 5.8 was selected as a condition where the substrate is relatively stable²⁰² and where activity of the homologous *Ao*ACLR was reported as sufficient (approximate 20-40% residual activity for ACL racemisation).¹⁷⁹

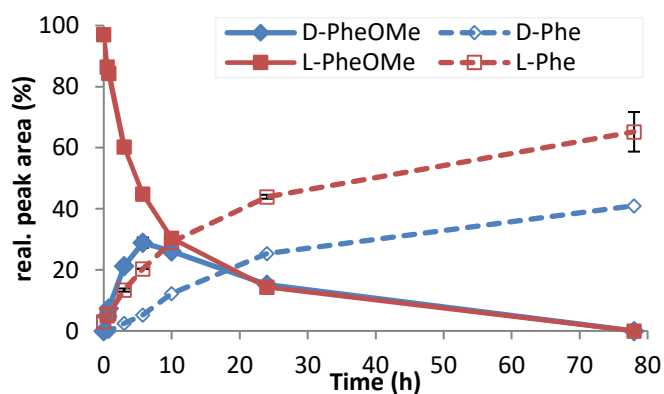


Figure 56: Racemisation of L-PheOMe catalysed by *Oa*ACLR. The activity of freshly purified *Oa*ACLR (0.5 mg) was tested with 5 mM L-PheOMe in a total reaction volume of 2.0 mL (100 mM KPi, pH 7.0). The reaction was carried out for 78 h at 30°C, the reaction components were analysed by chiral HPLC.

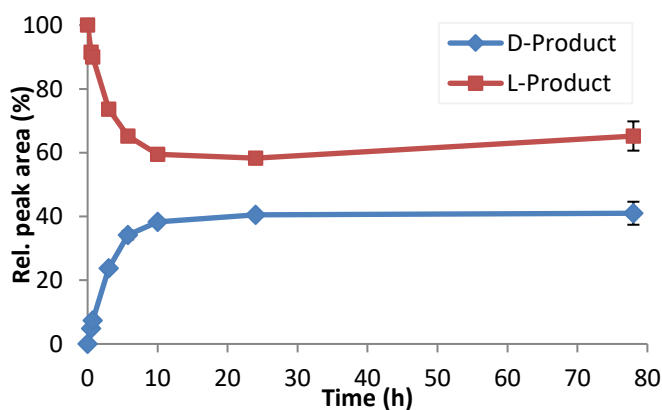


Figure 57: Racemisation of L-PheOMe catalysed by *OaACLR*. Data from Figure 56 are summarized as D-product (D-PheOMe and D-Phe) and L-product (L-PheOMe and L-Phe).

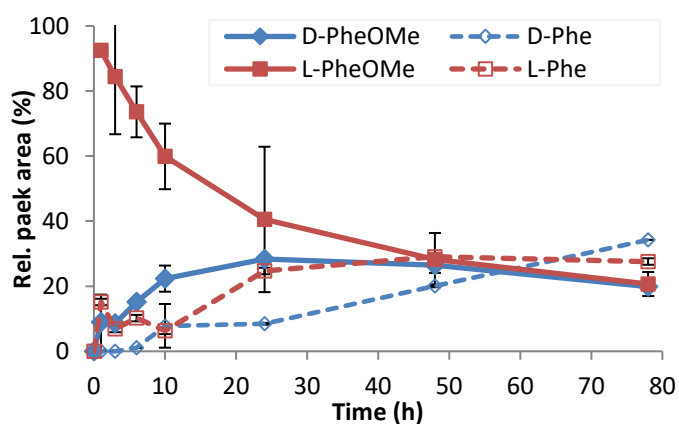


Figure 58: Racemisation of L-PheOMe catalysed by *OaACLR*. The activity of freshly purified *OaACLR* (1.1 mg) was tested with 5 mM L-PheOMe in a total reaction volume of 2.0 mL (100 mM KPi, pH 5.8). The reaction was carried out for 78 h at 30°C, the reaction components were analysed by chiral HPLC.

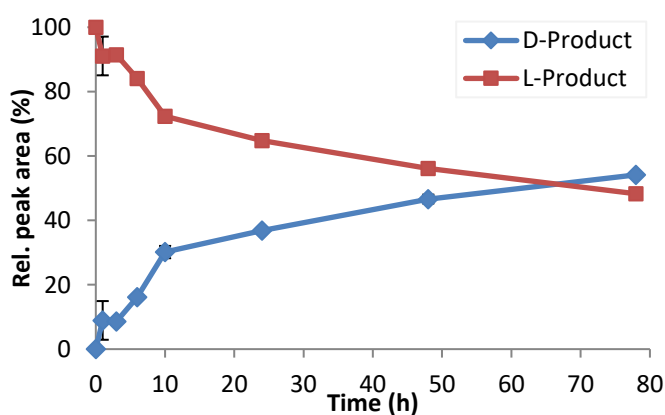


Figure 59: Racemisation of L-PheOMe catalysed by *OaACLR*. Data from Figure 58 are summarized as D-product (D-PheOMe and D-Phe) and L-product (L-PheOMe and L-Phe).

The results shown in Figure 56 to Figure 59 confirm that *OaACLR* catalyses the racemisation of L-PheOMe to D/L-PheOMe. Activities of 15.3 ± 0.7 U mg⁻¹ (pH 7.), respectively 1.7 ± 0.5

U mg^{-1} (pH 5.8) were calculated for the racemisation reaction of L-PheOMe catalysed by *Oa*ACLR.

Hydrolysis of the substrate and product was reduced by using pH 5.8 instead of pH 7.0, as D-PheOMe but no D-Phe could be detected. After 24h reaction time 43.9% L-Phe were obtained in the reaction at pH 7.0 and only 27.0% L-Phe in the reaction at pH 5.8. The reaction at pH 7.0 suggests enzyme inhibition by the hydrolysis products, as formation of the D-product converged to an *ee* of 22%. This effect was not observed in the reaction at pH 5.8, where less phenylalanine accumulated during the reaction.

In the control reaction (without enzyme) only hydrolysis of L-PheOMe to L-Phe, but no racemisation of L-PheOMe to the D-enantiomer was observed. This confirms that the hydrolysis is chemically catalysed and that there is no significant racemisation background reaction. Applying purified *Oa*ACLR for the reaction verifies that the previously observed racemisation of PheOMe of the cell lysate was specific activity of *Oa*ACLR.

4.3.4 Substrate screen for ACLR racemisation

After confirming the activity of *Oa*ACLR towards phenylalanine methylester the racemisation of two different amino acid esters and the corresponding amides was tested. These substrates were selected in collaboration with GSK as they are relevant for a DKR towards an API of interest for the pharmaceutical industry. The amide or ester substrates can be enzymatically converted to a biologically active D-amide product. In the DKR the racemate of the substrates can be used as the amide formation is selectively catalysed (Figure 60). The application of a racemase for this DKR is of high interest because it allows to selectively racemise the substrate during the reaction.

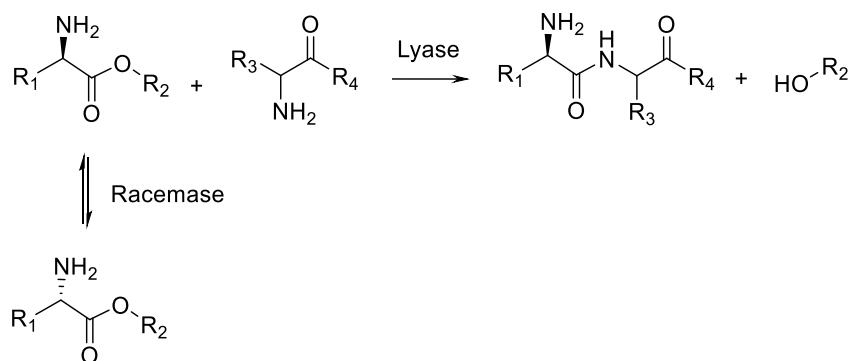


Figure 60: Reaction scheme for a DKR of a racemic ester and an amine donor to the D-amide product. The D-ester is enzymatically converted to the D-amide product. Simultaneously, the remaining L-enantiomer is racemised by a racemase.

The racemisation of both enantiomers of two amino acid esters (AAE) and the corresponding amino acid amides (AAA) was tested with purified *Oa*ACLR (Table 24).

Table 24: Substrate screen of *Oa*ACLR for the racemisation of amino acid amides and esters. Reaction condition: 5 mM substrate in KPi buffer (100 mM, pH 6.5) in a total reaction volume of 0.1 mL. Enantiomeric excess (*ee*) was calculated only from the D/L-ratio of the substrates, not the hydrolysis products.

Substrate	Relative peak area (%)				<i>ee</i> (%)	Reaction time (h)
	D-amino acid	L-amino acid	D-substrate	L-substrate		
L-PheNH ₂	0.0	0.0	41.5	58.5	7	1
L-AAA-1	0.0	0.0	49.4	50.6	1.3	24
D-AAA-1	0.0	0.0	39.8	60.2	20.3	24
L-AAA-2	0.0	0.0	40.1	59.9	19.7	24
D-AAA-2	0.0	0.0	56.7	43.3	13.4	24
L-AAE-1	0.0	41.5	0.0	58.5	100	24
D-AAE-1	32.1	44.5	23.4	0.0	-100	24
L-AAE-2	12.3	64.6	8.3	14.9	28.6	24
D-AAE-2	64.2	11.8	16.3	8.7	35.7	24

*Oa*ACLR showed high activity to all tested amides and AAE-2, but low activity towards AAE-1. Determination of activity towards the tested esters was difficult, as hydrolysis to the corresponding amino acid was observed during the course of the reaction. The chemical hydrolysis of AAE-1 was found to be much faster than for AAE-2 which might explain why the bulkier substrate AAE-2 is converted by *Oa*ACLR but AAE-1 only with very low activity.

This result indicates the potential of *Oa*ACLR as racemisation catalyst in a DKR to yield the desired amide product. However, the chemical hydrolysis of the substrate is detrimental for this reaction and might lead to reduced activity of the enzyme. The hydrolysis and its effects on the enzyme were investigated in detail in the following section.

4.3.5 Investigation of substrate hydrolysis

As mentioned above, the hydrolysis of L-PheOMe to L-Phe was observed during racemisation reactions (>40% hydrolysis after 24 h). From negative control reactions without enzyme it was concluded that the ester hydrolysis is chemical and not caused by catalytic activity of the enzyme. Studies on the effect of the pH on the hydrolysis of L-PheOMe were published before.²⁰² Maximal stability of L-PheOMe was determined at pH 2.90 with lowest reaction rates for the demethylation, at pH 7.49 the reaction rate was > 300 times higher, indicating fast hydrolysis of the ester at a natural pH value. Within this work the hydrolysis of PheOMe was investigated at pH 7.0 and 5.8 as outlined in the previous chapter (Chapter 4.3.3.1).

High background hydrolysis to the corresponding amino acid was also found for the substrates AAE-1 and AAE-2 and complicated the determination of enzymatic racemisation (Chapter 4.3.4). As no literature values could be found for these substrates, the influence of the pH on the hydrolysis was investigated. Reactions at different pH values with and without enzyme were carried out and the production of the hydrolysis product was quantified by HPLC (Figure 61).

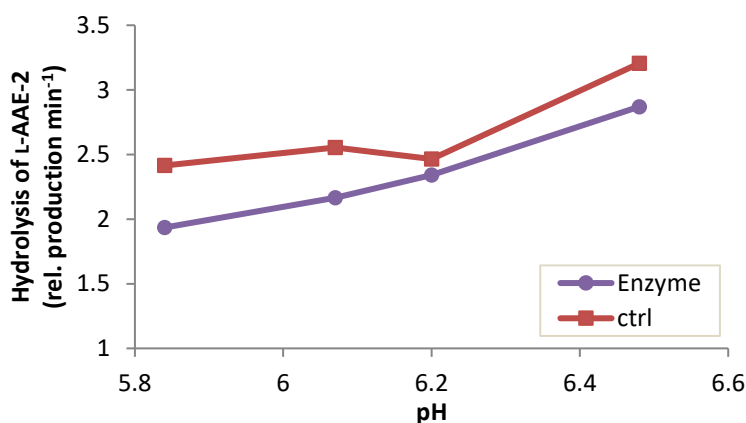


Figure 61: Influence of the pH on hydrolysis of L-AAE-2. The production of the hydrolysis product, L-amino acid-2, was followed during the reaction in KPi buffer (100 mM) at 30°C. Enzymatic reaction was carried out with *Oa*ACLR. The control reaction (ctrl) was carried out under same conditions but without enzyme.

The comparison of the hydrolysis in reactions with and without enzyme illustrates that the hydrolysis is not enzyme catalysed. Slightly lower production of the hydrolysis product was measured when enzyme is present in the reaction, probably because the enzyme binds the substrate for the racemisation reaction. This is important for further reaction optimisation and conditions for the reduction of the chemical hydrolysis need to be investigated. Lower reaction rates were determined with reaction buffer at lower pH values, hence these pH values have a stabilising effect on AAE-2.

In preliminary tests ammonia solution was found to be stabilising for the substrate. Thus, the effect of buffer salt in solution was investigated. The effect of different buffers on the hydrolysis of L-AAE-2 was investigated. The influence of the presence KPi buffer and Tris buffer was also evaluated in ammonia solution.

Table 25: Influence of reaction buffer on the chemical hydrolysis of L-AAE-2. Values of relative L-amino acid-2 production were measured after 4 h reaction time. Hydrolysis of L-AAE-2 (5 mM) in ammonia solution (pH 6.6) containing no buffer salt, 25 mM KPi or 25 mM Tris was determined after 4 h.

	KPi (pH 6.5)	Tris (pH 6.5)	NH ₄ OH (pH 6.6)
Relative amount of hydrolysis product (%)	20.8	25.9	10.4

Both, KPi and Tris buffer increase the reaction rate of the hydrolysis in ammonia solution (20.8-25.9% hydrolysis). The hydrolysis rate in ammonia solution was the lowest under the tested conditions, giving 10 % hydrolysis product after 4 h. Therefore this buffer should be used in reactions testing the enzymatic racemisation of AAE-2. As ammonia solution (pH 6.6) was found as a condition in which the hydrolysis of L-AAE-2 was reasonable slow, activity of *Oa*ACLR was tested in this reaction buffer. The production of D-AAE-2 from L-AAE-2 catalysed with different *Oa*ACLR concentrations was determined after 24 h reaction time. Racemisation without catalyst was followed as negative control, as positive control the racemisation using PLP was monitored (Figure 62).

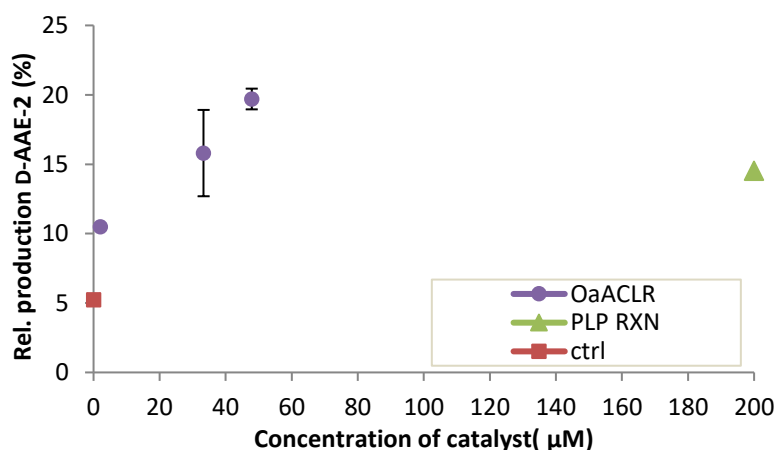


Figure 62: Summary of racemisation of L-AAE-2 in ammonia solution. Shown is the relative peak area of D-AAE-2 determined after 24 h reaction time with different concentrations of enzyme or PLP. The control reaction did not contain any catalyst.

Increasing the enzyme concentration resulted in an increase in conversion of L-AAE-2 to D-AAE-2, confirming that *Oa*ACLR is active in ammonia solution and catalysing the racemisation of AAE-2. The enzymatic reaction required a lower concentration of catalyst, with 50 µM enzyme a conversion of ~20% was obtained, whereas a similar conversion (15%) was achieved with 200 µM PLP. This result illustrates that *Oa*ACLR retains enzymatic activity in ammonia solution and is a more effective catalyst than PLP.

4.3.6 Inhibition of ACLRs by amino acids

The hydrolysis of phenylalanine methylester at neutral pH is competitive with the enzymatic catalysed racemisation. In racemisation reactions starting from L-PheOMe, production of D-phenylalanine can be either explained with hydrolysis of D-PheOMe to the amino acid or racemisation activity of the enzyme on L-phenylalanine obtained from the hydrolysis reaction. The latter can be excluded as L-phenylalanine was described as inhibitor of *Ao*ACLR^{179, 181} and no conversion could be measured with either *Rf*ACLR or *Oa*ACLR (Chapter 4.3.3.1). One possible reason for low yields of D-product in the reactions with amino acid esters might be enzyme inhibition due to the presence of the inhibitor amino acids. In the following, the inhibitory effect of the hydrolysis product of AAE-2 was evaluated for *Oa*ACLR (Figure 63). For this purpose *Oa*ACLR was incubated with amino acid-2 (final concentrations from 1-20 mM) for 1 h. The activity of *Oa*ACLR was assayed after the incubation under standard conditions with L-ACL.

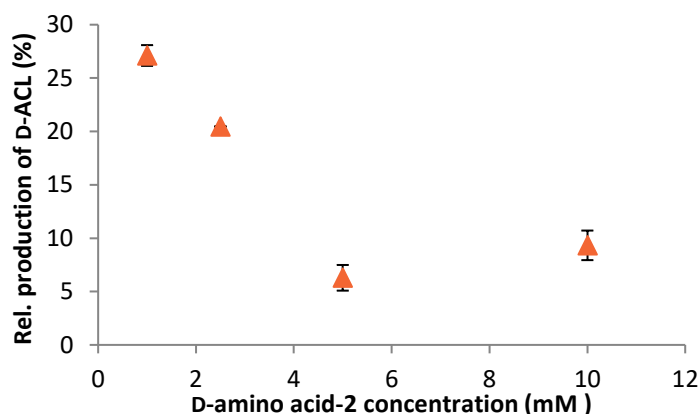


Figure 63: Influence of concentration of the hydrolysis product (D-amino acid-2) of D-AAE-2 on racemisation activity of *Oa*ACLR. The enzyme was pre-incubated with different concentrations of amino acid-2. The activity was assayed for the racemisation of 50 mM L-ACL in 100 μ L KPi buffer (100 mM, pH 6.5).

The result illustrates the inhibition of the racemisation activity of *Oa*ACLR in the presence of amino acid-2. With higher concentrations of amino acid-2, less D-ACL was produced in the assay reaction. This outcome stresses the importance to reduce the substrate hydrolysis in the reaction. The substrate hydrolysis not only reduces the concentration of available substrate of interest, but also the enzyme activity during the reaction.

4.3.7 Stability and activity in organic solvent

Organic solvents were considered as alternative to ammonia solution as reaction medium. This would counter the substrate hydrolysis, enhance product work up and avoid enzymatic side reactions in case a lipase is used for the amide formation reaction. MTBE was selected as organic solvent for initial trials due to its easy handling and previously reported stability of PLP-dependent transaminases.²⁰³ The tolerance of *Oa*ACLR to MTBE was tested by incubating the enzyme in the solvent with different buffer content (2-67 % Tris buffer, pH 7.5) following the activity determination in the standard assay in aqueous buffer (Figure 64).

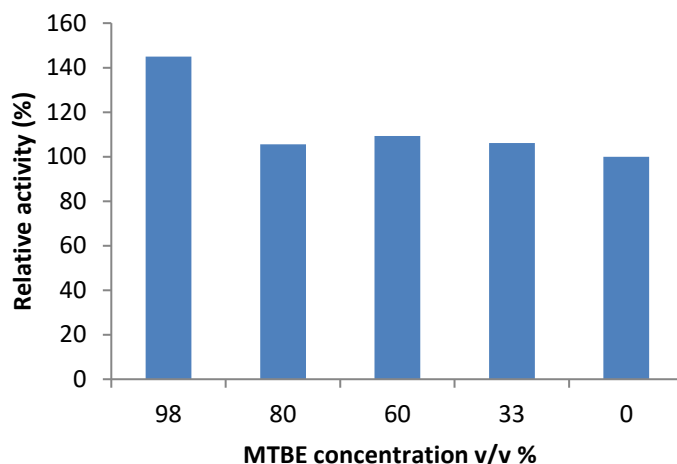


Figure 64: Relative activities of *Oa*ACLR after incubation in MTBE (20 min at 30°C). 100 % is related to the activity of enzyme incubated in Tris buffer (0 % MTBE) instead of organic solvent. The activity was tested with 50 mM L-ACL in a total volume of 2.0 mL (100 mM KPi, pH 7.0) at 30°C.

After incubation in MTBE retaining or even improvement of the *Oa*ACLR activity was observed. Within the broad range of solvent/buffer ratios of 33-80% no significant impact on the racemisation activity of *Oa*ACLR towards ACL was detected. Unexpectedly, the activity was increased to 145% relative activity in case of very low amounts of buffer (2%) in the reaction system. The result of this experiment proposes that the enzyme activity is either not affected by organic solvent or can be recovered by incubation in aqueous buffer.

In the next step the racemisation activity of the enzyme was tested in MTBE containing 2% Tris buffer. *Oa*ACLR (dissolved in 50 μ L Tris buffer, pH 7.5) was applied in a total reaction volume of 2 mL MTBE to racemise L-phenylalanine amide and the formation of the opposite enantiomer was monitored by HPLC (Figure 65).

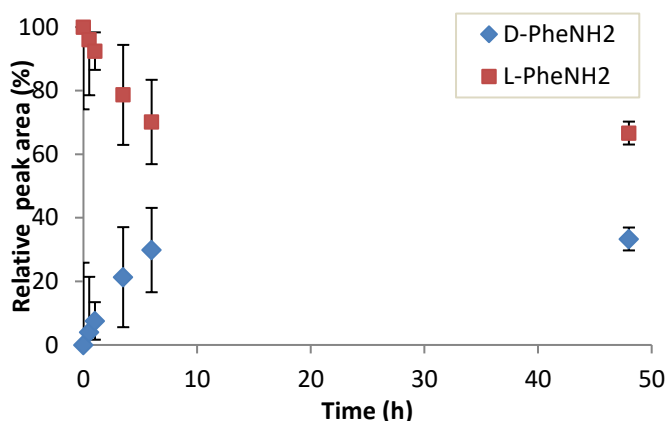


Figure 65: Racemisation reaction of L-PheNH₂ (10 mM) catalysed by *OaACLR* in MTBE (containing 2% Tris buffer, pH 7.5) at 30°C.

The initial reaction rate of *OaACLR* with the substrate L-PheNH₂ was calculated as 11.3 ± 2.6 U/mg in MTBE which is 146% of the activity in aqueous buffer. This is in accordance with the increase of 145% activity after incubation the enzyme in the same solvent/buffer system (Figure 64).

Table 26: Comparison of initial activities and conversions (after 6 h reaction time) of *OaACLR* in aqueous buffer and organic solvent (containing 2% Tris buffer, pH 7.5).

Substrate	Aqueous system		Organic system	
	Specific activity	Conversion	Specific activity	Conversion
L-PheNH ₂	5.2 ± 1.6 U mg ⁻¹	26.8 %	11.3 ± 2.6 U mg ⁻¹	31.5 %
L-PheOMe	15.3 ± 0.7 U mg ⁻¹	38.2 %	n.d.	20.6 %

The *OaACLR* catalysed racemisation of L-PheNH₂ normally was finished after 48 h in an aqueous reaction system (Chapter 4.3.2). In organic solvent substrate conversion reached a plateau after 6 h and conversion converged to approximately 30%. This suggests that the enzyme was inhibited during the reaction. Inhibition could be due to the organic solvent reaching the enzyme surface and stripping the hydration shell from the enzyme's surface. Otherwise, the sample taking might have had an impact on the enzyme, as for each time point 200 μ L of the total reaction mixture (2 mL) was removed. This could have an effect on the composition of the solvent/buffer ratio, resulting in critical amounts of aqueous buffer. Due to problems with sample recovery and therefore detection of L-PheOMe in the samples initial rates could not be calculated, however the conversion after 6 h was measured as 20.6% which is slightly lower than 38% conversion obtained in aqueous buffer. All together the results of stability and activity studies of *OaACLR* in MTBE implicate that the enzyme performance is not affected in organic solvent and similar conversion rates of racemisation can be retained in MTBE.

4.4 Conclusion

Three ACLRs have been tested with regards to the racemisation of different amino acid derivatives as summarised in Table 27. The racemisation of amino acid esters is of particular interest as a starting point for evolution of an amino acid ester racemase. All tested enzymes demonstrated activity towards ACL and phenylalanine amide.

Table 27: Summary of initial activities measured for ACLRs for the racemisation of different amino acid derivatives.

Enzyme	Specific activity toward Substrate (U mg ⁻¹)		
	L-ACL	L-phenylalanine amide	L-phenylalanine ester
<i>Ao</i> ACLR	30117 ± 972	11.9 ± 5.2	0
<i>Rf</i> ACLR	26469 ± 5425	20.4 ± 0.8	0
<i>Oa</i> ACLR	2337 ± 291	5.2 ± 1.6	15.3 ± 0.7

Interestingly, only *Oa*ACLR showed activity towards phenylalanine methylester. Further focus was put on the characterisation of the racemisation reaction of *Oa*ACLR with different substrates. *Oa*ACLR was also active on other amino acids amides and esters. Hydrolysis of all tested esters was observed which results in the accumulation of the corresponding amino acid in the reaction mixture. The influence of the hydrolysis product was found to inhibit the racemisation activity of *Oa*ACLR. The nature of the hydrolysis was further investigated and alternative reaction systems were established to reduce the accumulation of amino acid in the reaction mixture. *Oa*ACLR was active in alternative reaction systems, ammonia solution or organic solvent, which aided to reduce the ester hydrolysis. In summary, *Oa*ACLR has been identified as an amino acid ester racemase with potential for industrial application. Even though the activity towards phenylalanine methylester is comparatively low, it provides a promising starting point for engineering higher activities towards this substrate.

5 Structural analysis of RfACLR

5.1 Introduction

First investigations on ACLRs were carried out in the early 1980s. Among these was a labelling experiment on the exchange of the C α -proton with the solvent.¹⁸² The single base mechanism was proposed based on the high rate of internal return of the same proton at the C α position after racemisation. The deprotonation and reprotonation of the substrate-PLP complex was proposed to be mediated by a single active site base in swinging door model which was found for a PLP-dependent amino acid racemase.¹⁸⁸

So far the only structure of an ACLR was solved for the enzyme from *Achromobacter obae* in 2009.¹⁸⁴ From this study a two base reaction mechanism was suggested, with Y137 acting as one residue of the catalytic acid/base pair. D210 was suggested as substrate recognising residue and the interaction of D238 with the PLP pyridine ring suggests a reaction *via* a quinonoid intermediate.¹⁸⁴ Drawing detailed conclusions from the *Ao*ACLR structure is hampered by the inhibitor-complex with poor ligand density (Figure 66). The proposed reaction mechanism lacks experimental proof for intermediates and catalytic residues. The attempt to further investigate the mechanism of ACLRs was made in a mutational evaluation which suggested D210 and the PLP binding K267 as catalytic acid/base pair and identified other conserved residues like D238 or K241.¹⁸⁶

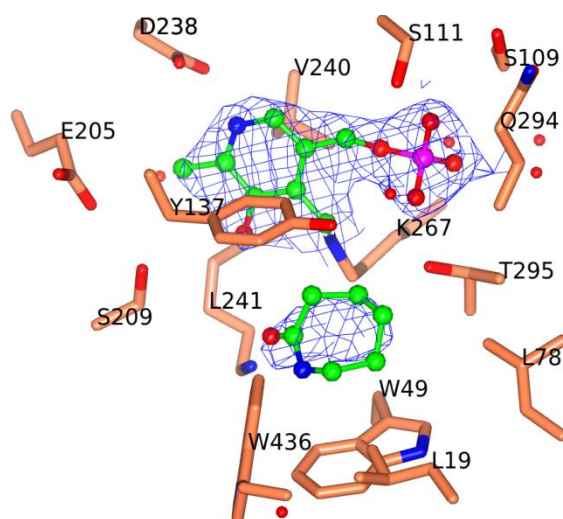


Figure 66: Active site of *Ao*ACLR complexed with ϵ -caprolactam solved at 2.4 Å. The structure was solved by Okazaki *et al.* and deposited a PDB as 2ZUK.¹⁸⁴ Electron density of the $2F_o-F_c$ map is shown corresponding to a level of 1σ .

The purpose of the work outlined in this chapter was to investigate the reaction mechanism of ACLRs by capturing reaction intermediates in activity reduced mutants. In the first instance crystallisation trials with the wildtype (wt) enzymes were carried out to identify residues important for racemisation activity. The putative catalytic residues were replaced to reduce activity of the enzyme and the mutants were subjected to crystallisation trials with the aim to depict reaction intermediates in the enzyme structure.

5.2 Materials and Methods

ACLRs were produced as outlined in Chapter 2.2.5 and 2.2.6 and purified to high purity (Chapter 3.3.4). Crystallisation trials were carried out according to the procedure described in Chapter 2.2.7. *Rf*ACLR mutants were prepared as described in Chapter 2.2.3 and the activity of the mutants was determined with the standard HPLC assay (Chapter 2.2.8).

5.3 Results and discussion

5.3.1 Initial crystallisation trials

Purified *Ao*ACLR, *Rf*ACLR and *Oa*ACLR were used in a concentration of approximately 10 mg mL⁻¹ for initial crystallisation screening. To obtain an enzyme-ligand-complex ACL stock solution (final concentration 20 mM) was added to concentrated enzyme and incubated on ice for 30 min. The commercial crystal screens Index, Pact and CSS were used for screening crystallisation conditions in 96-well plates. The conditions giving crystals are summarised in Table 28.

Table 28: Conditions for crystallisation of ACLRs.

Enzyme	Crystallisation condition	Composition
<i>Ao</i> ACLR	Index G12	0.2 mM MgCl ₂ 0.1 mM HEPES (pH 7.0) 25 % w/v PEG 3350
<i>Rf</i> ACLR	IndexG12	0.2 mM MgCl ₂ 0.1 mM HEPES (pH 7.0) 25 % w/v PEG 3350
	Index G3	0.2 M Lithium sulfate monohydrate 0.1 M Bis-Tris (pH 6.5) 25% w/v PEG 3350
	Pact B3	0.1 M MIB 25 % w/v PEG 1500
<i>Oa</i> ACLR	Pact E12	0.2 M Sodium malonate dibasic monohydrate 20 % w/v PEG 3350
	Pact F2	0.2 M NaBr 0.1M Bis-Tris propane (pH 6.5) 20 % w/v PEG 3350
	Index E12	0.05 M MgCl ₂ 0.1 m HEPES (pH 7.0) 30 % w/v PEG MME 550

From the three tested ACLRs best crystals were obtained for *RfACLR*. Several conditions were found as successful crystallisation conditions.

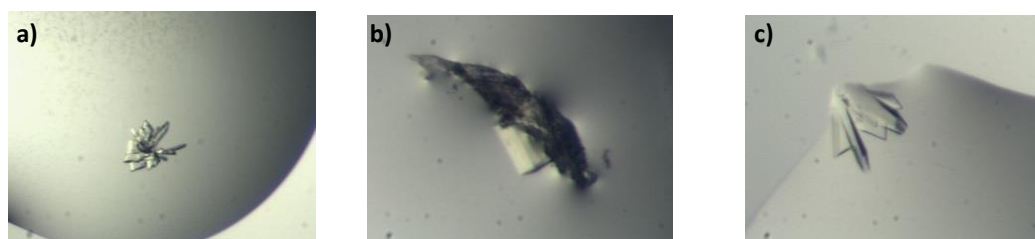


Figure 67: *RfACLR* crystals obtained in crystal screening in MRC plates. A) and B) Index G3, C) Pact B3.

The conditions Index G12 and G3 were scaled up in 24 well plates and the concentrations were slightly varied (Chapter 2.2.7). The original conditions of Index G12 were identified as best condition for crystal formation. Similar crystals formed in hanging drops (2 μ L) as on smaller scale (300 nL). *RfACLR* crystallised in fast growing crystal clusters in usually less than two days (Figure 68 A-B). After a longer incubation time additional single square plates or cubes were formed (Figure 68 C). Most crystals had a slightly yellow colour suggesting that PLP was retained in the protein during the crystallisation process.



Figure 68: Pictures of *RfACLR* crystals in hanging drops with crystallisation conditions from Index G12 (0.2 mM MgCl₂, 0.1 mM HEPES, pH 7.0, 25 % w/v PEG 3350). Approximately 10 mg mL⁻¹ purified *RfACLR* was co-crystallised with L-ACL.

5.3.2 Structure of *RfACLR*

RfACLR crystals were harvested, flash cooled in liquid nitrogen and the diffraction data was collected as described in Chapter 2.2.7. The structure of native *RfACLR* was solved with a resolution of 1.7 Å, the data collection details are listed in Appendix 10.4. The structure was solved using the *AoACLR* structure (PDB entry 2ZUK¹⁸⁴) as molecular replacement model. The quaternary structure of *RfACLR* represents a homodimer with two active sites per dimer

as depicted in Figure 69. The active site is located in the interface of the two dimers. Due to its high sequence similarity, the overall structure of *Rf*ACLR is very similar to *Ao*ACLR and therefore also represents a fold type I of the PLP-dependent racemases.

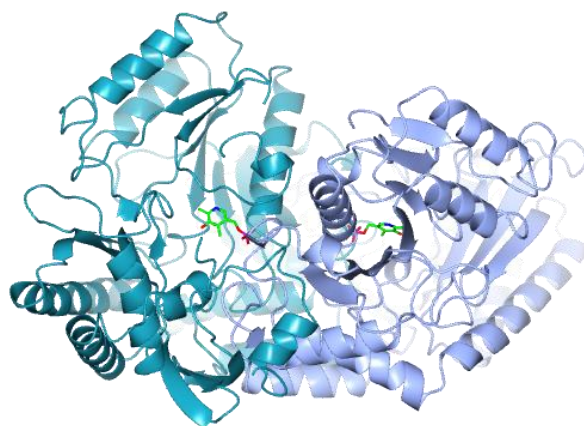


Figure 69: Quaternary structure of *Rf*ACLR. The homodimer is formed of two identical subunit A (cyan) and subunit B (blue). PLP indicates the location of the active site, which is in the interface of both subunits.

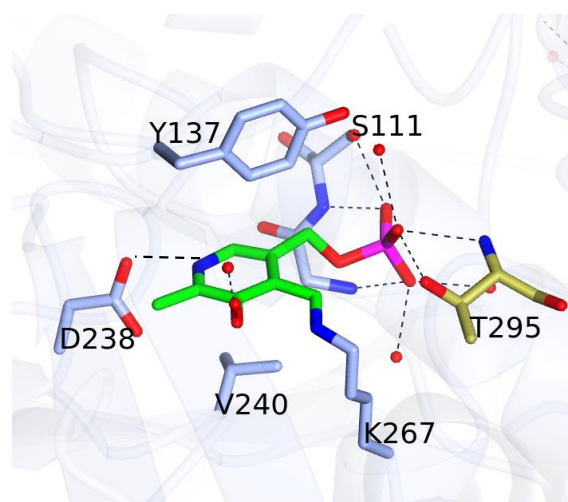


Figure 70: PLP-binding residues in the active site of *Rf*ACLR. Residues in blue belong to subunit A, gold residue are of subunit B.

Interactions for PLP binding were closely investigated as illustrated in Figure 70. In the active site PLP is covalently bond to the amine group of K267 building an internal aldimine. The position of PLP is stabilised by stacking interaction between Y139 and V249, a salt bridge between D238 and the pyridine nitrogen. During the catalysis, this salt bridge can destabilise the carbanion after formation of the external aldimine. The protonation of the pyridine nitrogen suggests that the reaction proceeds *via* the quinonoid intermediate (Introduction 1.1.2.2). The phosphate backbone of PLP is stabilised by hydrogen bonds to S113, T295 (from the other subunit) and two conserved water molecules. The binding of PLP seems to be conserved within ACLRs as the same residues were described for *Ao*ACLR¹⁸⁴ and *Oa*ACLR within this work (Chapter 6.3.1).

5.3.2.1 RfACLR in complex with ACL

The three-dimensional structure of a RfACLR-ACL complex was solved from crystals grown in clusters (Figure 68b). The structure was solved and refined using the previously solved structure of native RfACLR as replacement model.

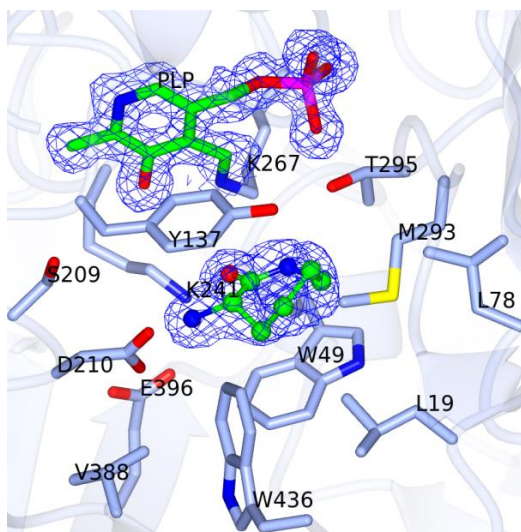


Figure 71: RfACLR complexed with L-ACL (ball and stick model). Residues shown are in the distance $>5 \text{ \AA}$ from ACL. Electron density of the $F_o - F_c$ map at a level of 1σ before adding of the ligand into the structure is shown in blue wire representation.

The high resolution structure (1.5 \AA) of RfACLR complexed with ACL shows the active site. The ligand density of the substrate allowed modelling of both enantiomers into the map with 50% occupancy, however, here the L-enantiomer of ACL is represented. Residues with a distance of 5 \AA to the chiral centre of the substrate are represented in Figure 71. The substrate stacked between the aromatic residues Y137 and W49 and binding is further stabilised by interactions with several hydrophobic residues like W436, L19, L78 and M293. The structure also reveals amino acid residues that might interact with the substrate. Y137, T295, K241 and D210 are in distance $>5 \text{ \AA}$ to the chiral centre of ACL and therefore could take part in the catalysis. As described above T295 is involved in PLP binding, which makes it unlikely be involved in the reaction mechanism. Putative acid/base catalytic residues for the racemisation reaction are D210 (3.9 \AA), K241 (4.7 \AA) and Y137 (5.1 \AA) with close distance of to the chiral centre of ACL.

5.3.2.2 RfACLR modelled with phenylalanine in the active site

Aiming towards the evolution of a more active amino acid ester racemase it was of interest to solve a structure of the enzyme complexed with a similar compound. As discussed in detail in

the previous chapter (Chapter 4.3.3) *RfACLR* was not active towards the model substrate phenylalanine methylester. Therefore emphasis was put on growing crystals with phenylalanine amide as *RfACLR* activity was confirmed for this substrate (Chapter 4.3.2). Crystals obtained from co-crystallisation of *RfACLR* with L-phenylalanine amide (20 mM) diffracted at 1.2 Å and the three-dimensional structure was determined from the collected data using the native *RfACLR* structure as molecular replacement model (Figure 72). Electron density for the ligand was not detected, therefore the ligand was modelled into the active site during the refinement process.

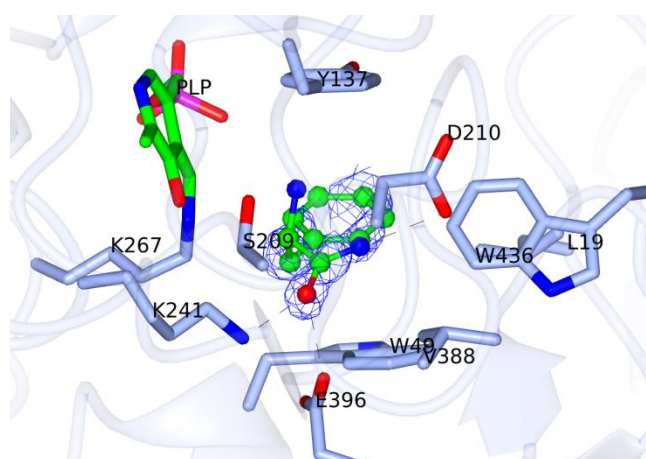


Figure 72: View in active site of *RfACLR* modelled with L-Phenylalanine amide (ball and stick model in green). Shown residues are in the vicinity (> 5 Å) to the substrate. Ligand density (blue wire) is shown after modelling and refining the ligand in the structure corresponding to $F_o - F_c$ at 0.9σ .

The view of the active site of *RfACLR* fitted with PheNH_2 depicts amino acid side chains close to the substrate that might interact with the substrate. Due to the lack of electron density for the ligand, PheNH_2 was modelled into the active site. Nonetheless, the conformation of PheNH_2 can be compared to ACL in the active site and confirms findings from the *RfACLR*-ACL structure. Y137, K241, K267 and D210 are residues that are located in the vicinity of the chiral centre of the substrate and therefore might be possible catalytic residues. The residues D210, K241 and E396 are near to the amide group (> 3.2 Å), so they might be involved in amide recognition. D210 and E396 are connected through a salt bridge, the distances of D210 to the amide group nitrogen (3.2 Å) and E396 to the amide group oxygen (2.8 Å) are close enough to form hydrogen bonds. D210 and K241 have been suggested as amide recognising residues or catalytic residues in *AoACLR* before.^{186 184} D210 and K241 are promising targets for mutational analysis in order to investigate their function in the enzyme catalysis.

The view of phenylalanine amide bound to the substrate binding pocket provides information on the low activity towards this substrate. The spherical conformation of phenylalanine amide reveals that it occupies most of the space in the binding pocket, leaving less space for

conformational changes during the catalysis (Figure 73 and Figure 74). Directed evolution experiments showed that mutations resulting in a bigger substrate binding pocket increased activity of the mutant *Ao*ACLR-L19V-L78T towards phenylalanine amide significantly.¹⁸⁵ The present structure gives explanation for this as the double mutation L19V/L78T results in opening the substrate binding site where the phenyl ring of the substrate is located.

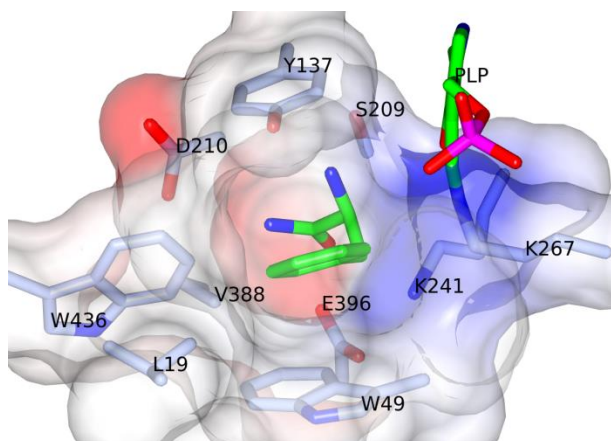


Figure 73: Substrate binding site of *Rf*ACLR modelled with L-Phenylalanine amide and PLP (green cylinder representation). The surface of the residues near to the substrate ($> 5 \text{ \AA}$) are represented according to their electrical charge (red: negative, blue: positive, white: uncharged).

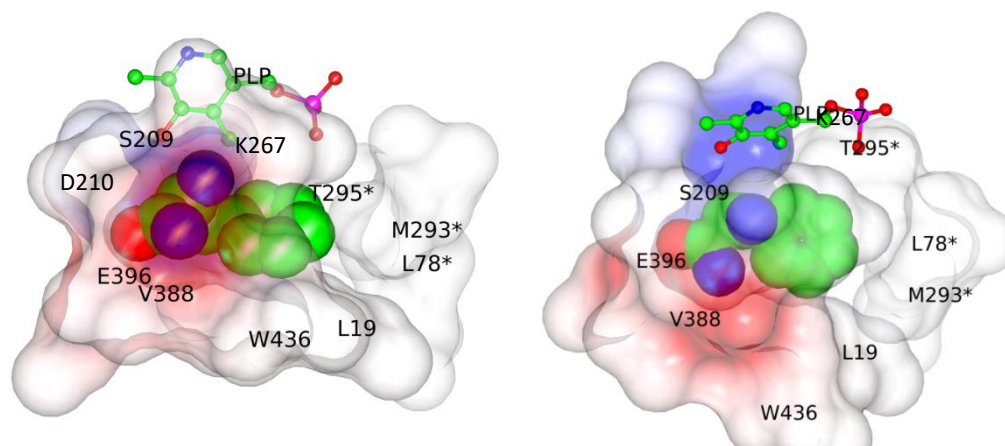


Figure 74: Spatial occupation of the binding site of *Rf*ACLR modelled with phenylalanine amide. The surface of the residues near to the substrate ($> 5 \text{ \AA}$) are represented according to their electrical charge (red: negative, blue: positive, white: uncharged). PLP is represented as ball and stick model. L-Phenylalanine is shown as sphere model. Residues assigned with * belong to subunit B.

As the enzyme is inactive towards phenylalanine methylester and therefore has no or only low affinity towards the substrate, a crystal structure of *Rf*ACLR complexed with PheOMe could not be obtained. Nonetheless, from the insight given from the *Rf*ACLR-PheNH₂ complex conclusions can be drawn for the conformation of PheOMe in the active site. The space in the active site is fully occupied by PheNH₂, suggesting that the active site would not provide enough space for the methyl group of PheOMe. Besides recognition of the ester group, steric hindrance might also be a reason for the inactivity of *Rf*ACLR towards PheOMe. Expanding

the substrate binding pocket for the methyl group of PheOMe might facilitate substrate access to the active site and therefore increase the enzyme activity towards it. Possible targets for mutations to obtain a larger pocket in that area are V338 and W436, whereas W436 should be retained as it closes the substrate binding site during catalysis. The double mutation of L19V/L78T might also increase activity towards PheOMe.

5.3.2.3 Substrate binding of RfACL

This section summarises observations made for the substrate binding in the active site of RfACL. Visualising the surface of RfACL enabled to locate the entrance to the active site. Two tunnels to the active site were found. In both structures, with and without enzyme, the entrance of one tunnel is blocked by the opposite subunit. Hence only one of the two channels leading to the active site allows the substrate to enter the active from the solution (Figure 75 a). The active site is divided into two binding pockets, a hydrophobic pocket where the PLP pyridine ring is located and the PLP C4 is bound to K267 and a more hydrophilic pocket where the substrate is bound (Figure 75 b).

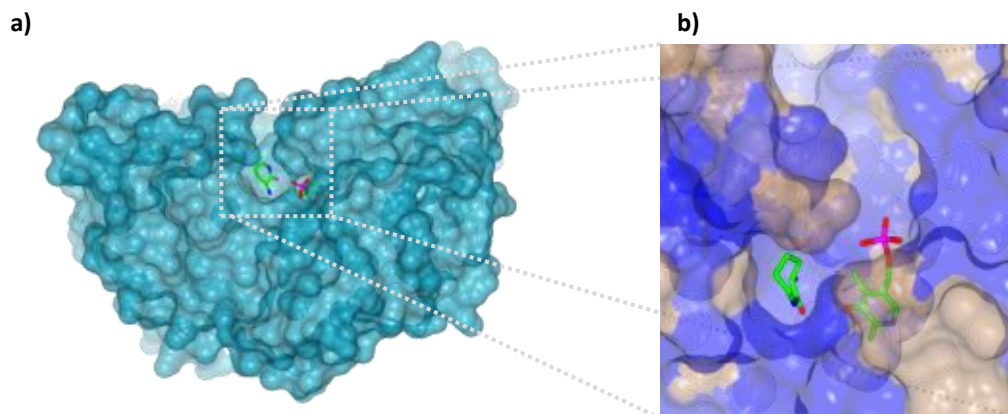


Figure 75: Substrate binding of RfACL a) Surface model of RfACL subunit A showing the entrance to the active site. b) Zoom into the substrate and PLP binding site of RfACL. The surface of the residues is illustrated according to their hydrophobicity: hydrophobic (yellow), hydrophilic (blue).

Comparing the structure of native RfACL and the structure complexed with ligand (ACL or phenylalanine amide) shows a flexible C-terminal loop in the structure from D421-W436, the last C-terminal residue (Figure 76).

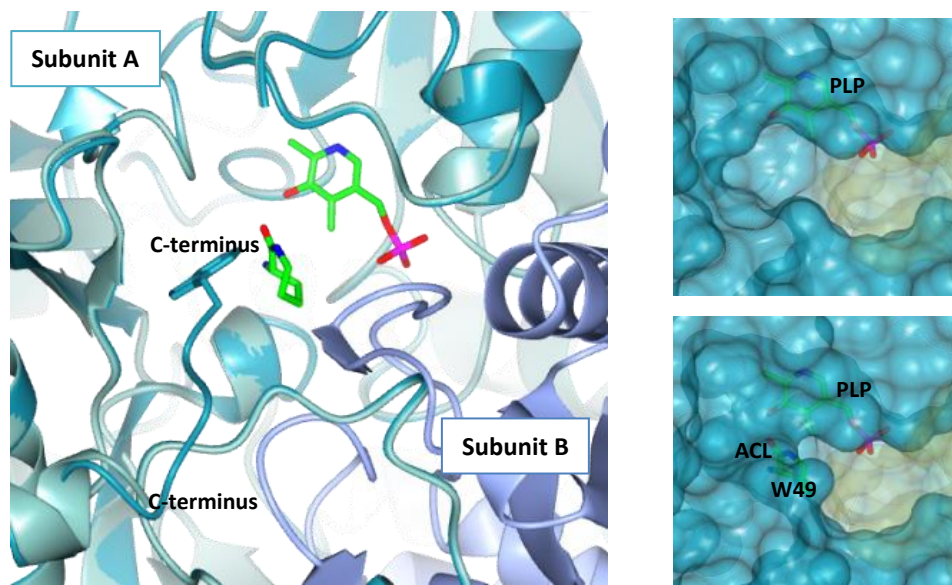


Figure 76: Conformational change of the C-terminal end initiated by substrate binding. Right: Superimposed model of native *RfACLR* (light cyan) and *RfACLR-ACL* complex (cyan). Left: Closing of the entrance to the active site by W436. Subunit A is represented in cyan, subunit B in gold.

The conformation of the C-terminal loop could only be identified in structures complexed with substrate, meaning that without substrate this loop is in a flexible conformation. When substrate is bound to the active site, the C-terminal loop undergoes a conformational change, so that the entrance to the active site is closed by W436. The observation of this conformational change caused by substrate binding is in accordance with previous results from structural studies on *AoACLR*.¹⁸⁴

5.3.2.4 Substrate recognition

When the substrate is bound to the active site several interaction of the substrate with active site residues were observed. The functional groups of the substrate interact with the active site residues K241 and D210 as depicted in Figure 77.

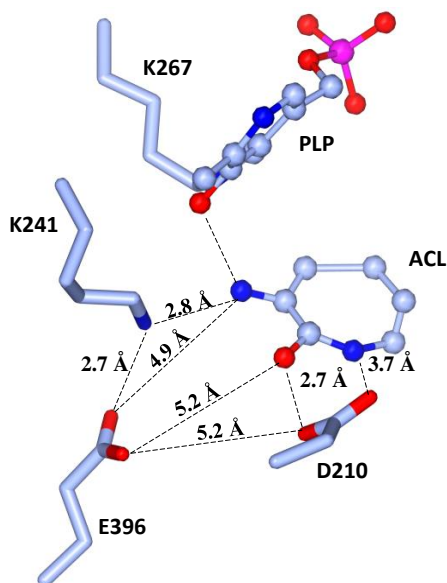


Figure 77: Substrate recognising residues of the substrate binding site of *RfACL*.

K241 interacts with the amino group of the substrate and D210 interacts with the amide oxygen on the opposite site. K241 forms a salt bridge with E396 which might stabilise the position of K241. As glutamate is a residue of high flexibility, during catalysis it might also alter its position to interact with D210. D210 stabilises the positioning of the substrate by a hydrogen bond with the amide imine, but also interacts with the amide oxygen. Hence, D210 is likely to be the residue to recognise the amide functionality of the substrate. K241 is a possible residue for the amino group recognition. In combination K241 and D210 are putative residues for the recognition of amino acid amides. Interactions of both these residues with E396 during the catalysis might help to position the residue in the correct conformation. With 3.1 Å from the PLP C4 to the amino group of ACL is close enough for the attack of the Schiff base between K267 and PLP. This attack would initialise the catalysis by forming a new Schiff base between the C4 of PLP and the substrate amino group.

5.3.3 Mutational analysis of the reaction mechanism of *RfACL*

The structure of wt *RfACL* revealed amino acid residues that might interact with the substrate during the catalysis. Y137, D210, K241 and K267 were identified as putative acid/base catalytic residues for the racemisation reaction. To investigate the reaction mechanism and identify amino acid residues that are catalysing the racemisation, *RfACL* mutants with alanine or phenylalanine replacing these residues were generated. These mutants were analysed in terms of their racemisation activity and structural differences.

5.3.3.1 Expression of *RfACLR*-Y137F

RfACLR-Y137 would not be expressed as soluble protein under standard conditions (in *E. coli* BL21 (DE3), 16°C, 1 mM IPTG). Test expressions performed in *E. coli* BL21 (DE3) did not identify a suitable overexpression condition. Test expression were repeated in a different strain, *E. coli* Rosetta, at 16, 27, 37°C with 0.1 or 1 mM IPTG (Figure 78).

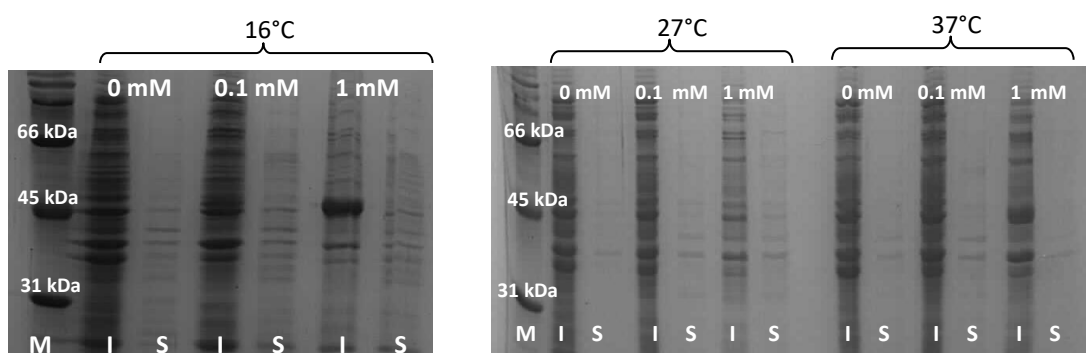


Figure 78: SDS gels of test expression of *RfACLR*-Y137F in *E. coli* Rosetta cells.

Highest amounts of soluble protein were expressed at 16°C with 1 mM IPTG induction. The identity of the protein expressed at these conditions with a molecular weight of approximately 45 kDa was verified by western blotting against the his-tag of *RfACLR*.

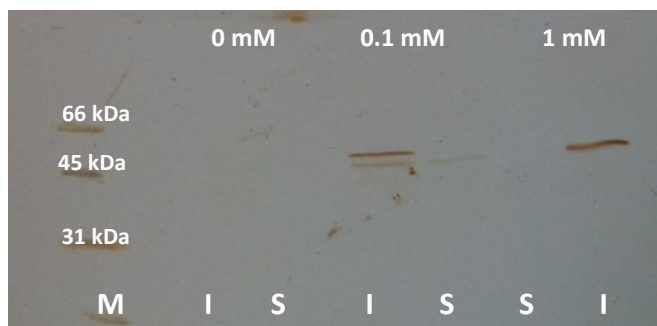


Figure 79: Western blot of *RfACLR*-Y137A from soluble and insoluble fractions after overexpression of *RfACLR* in *E. coli* Rosetta cells at 16°C.

The western blot shows that overexpression of *RfACLR*-Y137F was poor and yielded in very small amounts of produced protein. Most of the small amounts of expressed *RfACLR*-Y137 was synthesised as insoluble protein and minor amounts of soluble protein were detected by the western blot. Nonetheless, a purification of *RfACLR*-Y137F from a large scale cultivation (4 L, 1 mM IPTG, 16°C, 24 h) of recombinant *E. coli* Rosetta cells (17.6 g) was performed (Figure 80 and Figure 81).

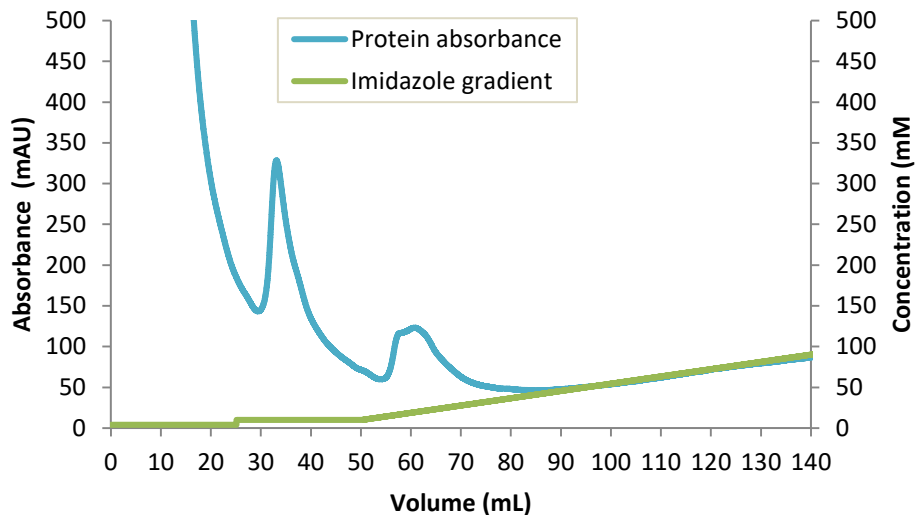


Figure 80: Chromatogram of IMAC purification of *RfACLR*-Y137F expressed in recombinant *E. coli* Rosetta cells.

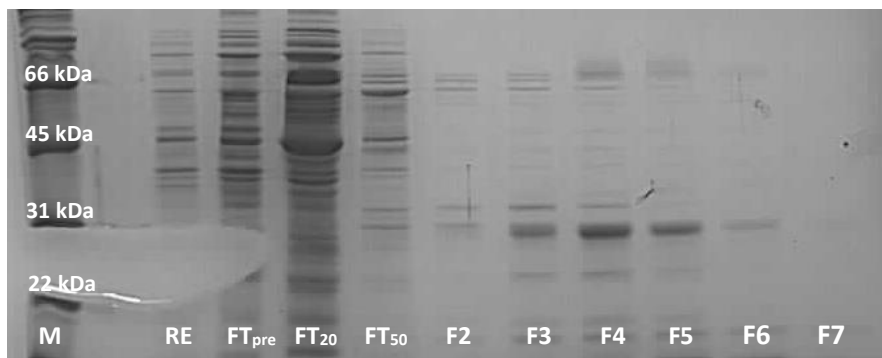


Figure 81: SDS gel of fractions obtained from IMAC of *RfACLR*-Y137F. RE, FT_{pre} (wash from loading cell lysate), FT₂₀ (20mM wash) FT₅₀ (50 mM wash) were diluted 1:10.

The chromatogram and the SDS-PAGE analysis show that *RfACLR*-Y137F did not bind the IMAC column and could not be purified from the cell lysate. In the 20 mM imidazole wash a big band of 45 kDa was observed on the SDS gel. This might correlate to incorrectly folded *RfACLR*-Y137F. The purification did not yield any purified *RfACLR*-Y137F indicating that the soluble protein expressed in *E. coli*-Rosetta cells was folded incorrectly. Even though the expression of *RfACLR*-Y137F was not successful, this result provides the valuable information that Y137 is crucial for correct folding of the enzyme. This might be because it is crucial for defining the substrate binding site or for the catalytic activity of the enzyme.

5.3.3.2 Characterisation of *RfACLR*-K241 and *RfACLR*-D210

RfACLR-D210A and *RfACLR*-K241A were expressed as soluble protein and purified from recombinant *E. coli* cells under same conditions as wt *RfACLR* (Chapter 2.2.6). The

racemisation activity of the mutants *RfACLR-K241A*, and *RfACLR-D210A* was tested with D- or L-ACL and compared to the activity obtained with the wt enzyme as listed in Table 29.

Table 29: Activities for the racemisation of 50 mM ACL with different *RfACLR* variants. The reaction was carried out in a total reaction volume of 1 mL (100 mM KPi, pH 7.0) at 30°C for 30 min. Production of the opposite enantiomer was determined by chiral HPLC and related to the amount of enzyme used in the reaction to calculate specific activities.

		<i>RfACLR</i>	<i>RfACLR-K241A</i>	<i>RfACLR-D210A</i>
Specific activity (U mg⁻¹)	D-ACL	14441.3 ± 3346	1246.8 ± 42.2	6.4 ± 2.1
	L-ACL	22966.5	2371.0 ± 148.1	2.4 ± 2.5
Relative activity (%)	D-ACL	62.9	5.4	0.03
	L-ACL	100.0	10.3	0.01

RfACLR and *RfACLR-K241A* show slightly higher activity towards the L-enantiomer of ACL than D-ACL which is in accordance with previous results for *AoACLR*.¹⁸³ *RfACLR-K241A* is reduced in its racemisation activity by a factor of 10 compared to wt activity. Racemisation activity of *RfACLR-D210A* is almost abolished and six orders of magnitudes smaller than the wt activity. This mutant seems to be more active towards the D-enantiomer of ACL. However, as the activity of *RfACLR-D210A* is so low it is difficult to make a reliable statement about preference of an enantiomer from these results. Altogether, the very low activity of *RfACLR-D210A* is less than 0.03 % wt activity. The detected racemisation might be background activity or might be a result of catalysis through unspecific residues. High standard deviations with the same order of magnitude as the average value indicate a non-specific activity. To get a general overview of the activity spectrum of the variants, activity was determined for ACL, PheOMe and PheNH₂ with *RfACLR-K241A* and *RfACLR-D210A* as summarised in Table 30.

Table 30: Specific activities of *RfACLR* variants towards amino acid derivatives. The reaction was carried out in a total reaction volume of 2 mL (100 mM KPi, pH 7.0) at 30°C. 50 mM L-ACL, 10 mM L-PheOMe or L-PheNH₂ were used in the reaction. Production of the opposite enantiomer was determined by chiral HPLC and related to the amount of enzyme used in the reaction to calculate specific activities.

Substrate	Specific activity (U mg⁻¹)		
	wt <i>RfACLR</i>	<i>RfACLR-K241A</i>	<i>RfACLR-D210A</i>
L-ACL	31733 ± 4620	678.6 ± 16.3	2.0 ± 0.06
L-PheNH₂	10.8 ± 3.1	0.0	0.0
L-PheOMe	0.0	0.0	0.0

Both mutants are drastically reduced in their activity to ACL, *RfACLR-K241A* with 2.1% relative activity and *RfACLR-D210A* with 0.006% relative activity. Racemisation of L-PheNH₂ or L-PheOMe could not be detected with either of the *RfACLR* variants.

In summary, both *RfACLR* variants were reduced in their activity, whereas this effect is very drastic for *RfACLR*-D210A. Both variants do not convert the more challenging substrates, phenylalanine amide and phenylalanine methylester. Both *RfACLR* mutants show residual activity towards ACL, but in case of the very low activity of *RfACLR*-D210A it is questionable if this is catalytic or unspecific activity. K241 and D210 seem to be crucial for the full function of the enzyme. Especially D210 seems to be a crucial residue as its replacement with alanine resulted in more than 10000 fold reduction in racemisation activity.

5.3.3.3 Structural analysis of *RfACLR* mutants

The structure of *RfACLR*-K241A shows the external aldimine

After evaluating activity of *RfACLR*-K241A, it was subjected to crystallisation trials as described in Chapter 2.2.7. *RfACLR*-K241A crystallised in the same condition as the wt enzyme. Diffraction data was collected from crystals grown from *RfACLR*-K241A co-crystallised with L-ACL. The structure of the mutant *RfACLR*-K241A was solved to a resolution of 1.9 Å by using wt *RfACLR* as molecular replacement model.

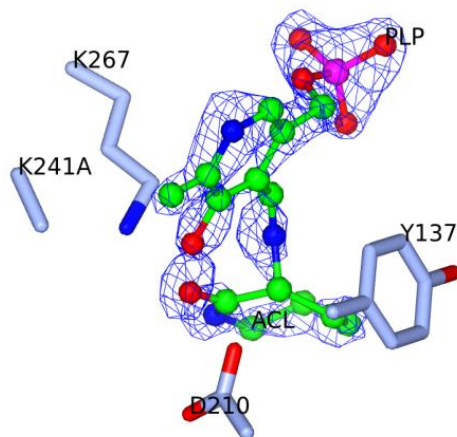


Figure 82: Active site of *RfCALR*-K241A mutant complexed with D-ACL showing the external aldimine formed by PLP and ACL. Ligands are illustrated in the ball and stick model. Electron density (blue wire) corresponds to the F_o-F_c map at a level of 1σ before adding of the ligand into the structure.

The external aldimine, PLP bound to the substrate, is present in the active site of the activity reduced *RfACLR*-K241A (Figure 82). Both, PLP and the substrate move towards each other to enable formation of the imine bond to form the external aldimine. Clear electron density around the imine bond confirms the formation of the imine between C4 of PLP and the ACL amine. The imine bond is in perpendicular position to the π -system of the PLP pyridine ring and therefore in the correct conformation for cleavage. The structure of *RfACLR*-K241A shows residues in distance to the chiral centre of ACL, which are Y137 (4.5 Å), D210 (2.8 Å)

and K267 (4.2 Å). This strongly suggests that K267, which is the PLP binding residue for the internal aldimine, is the catalytic residue for deprotonation at the substrate chiral centre. After releasing PLP and formation of the external aldimine K267 becomes a possible catalytic residue, as it is in proximity to the chiral centre (≤ 4.2 Å). Reprotonation could be mediated by D210 or Y137 as these residues are located on the re-face of the substrate. K267 and D210 might serve as catalytic acid/base pair during the racemisation. These residues are close enough to interact with the chiral centre. Additionally, these two residues are in a good position to de-/re-protonate C α of the substrate from the re-/si-face. K241 was described to be involved in substrate recognition of ACLRs before.¹⁸⁶ Interaction of K241 with the amide group was suggested for previous *RfACLR* structures (Chapter 5.3.2.4), lacking substrate recognition might give an explanation for the reduced activity of the *RfACLR*-K241A mutant.

The structure of *RfACLR*-D210A shows the geminal diamine

Crystallisation trials were also performed with *RfACLR*-D210A and L-ACL. After adding the substrate to the enzyme solution a change in colour from the usual yellow to a pink colour was observed. The change in colour was measured by UV spectrophotometry for enzyme solution with and without added substrate. Crystals obtained from *RfACLR*-D210A with ACL were also pink (Figure 83).

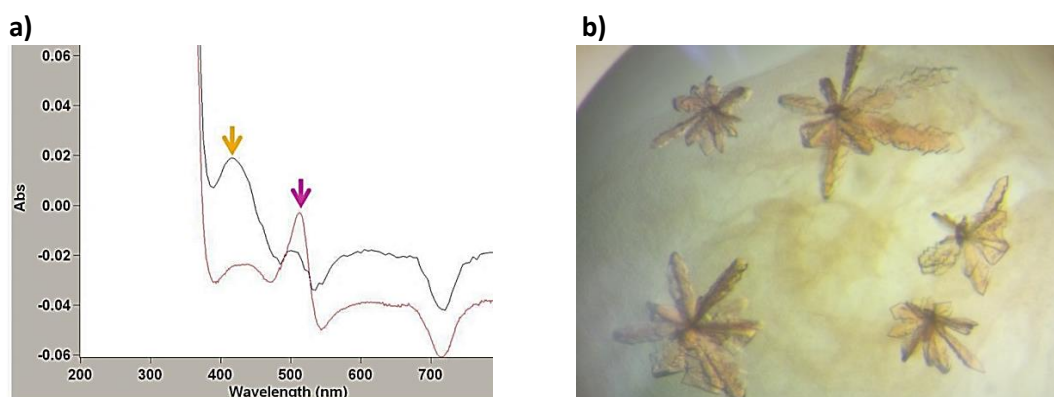


Figure 83: a) Change of the UV spectrum of *RfACLR*-D210A without substrate (black line) and *RfACLR* with 10 mM L-ACL (red line). Yellow arrow indicates characteristic λ_{\max} for the external aldimine, pink arrow indicates characteristic λ_{\max} for the quinonoid. b) Protein crystals grown from *RfACLR*-D210A with ACL.

The change in colour suggests that when adding ACL to the enzyme solution the quinonoid is partially formed and present in the solution.¹⁸ The UV spectrum for *RfACLR*-D210A incubated with substrate showed a characteristic peak at 510 nm which corresponds to the absorption maximum (λ_{\max}) for the quinonoid.^{8, 204} The fact that this can be measured in the UV spectrum indicates that the reaction rate of this mutant is drastically reduced. The structure of *RfACLR*-D210A was solved and refined to a resolution of 1.5 Å (Figure 84).

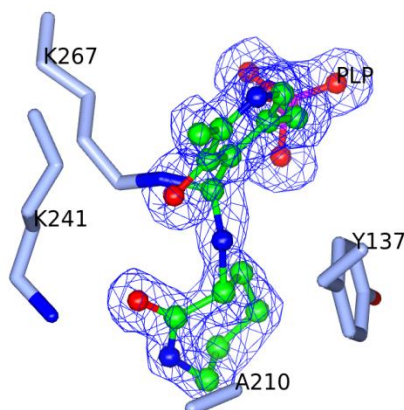


Figure 84: Structure of the active site of *RfACLR-D210A* complexed with D-ACL. This structure shows the geminal diamine, a chiral intermediate formed by PLP, ACL and K267. Ligands are illustrated in the ball and stick model. Electron density (blue wire) corresponds to the $F_o - F_c$ map at a level of 1σ before adding of the ligand into the structure.

The ligand density in the active site of *RfACLR-D210A* represents the state of the geminal aldimine. The geminal aldimine is an intermediate of the replacement reaction at the chiral centre, in which PLP is bound to the PLP binding residue K267 and the substrate exocyclic amine at the same time. This state can be captured after proton replacement at the chiral carbon, but before the substrate release. This would explain the D-configuration of ACL in the *RfACLR-D210A* structure, although it was co-crystallised with L-ACL. During the crystallisation process racemisation of L-ACL was catalysed and due to the very slow reaction rate of the *RfACLR-D210A* mutant it was possible to capture the reaction intermediate before the substrate release.

Reaction specificity of *RfACLR*

As described in Chapter 1.1.2 of the introduction, PLP dependent enzymes provide a specific scaffold to position the substrate in relation to PLP in the active site. Catalysis occurs at the bond of the substrate that is perpendicular positioned to PLP. This bond is destabilised by the π system of the PLP pyridine ring and can therefore be broken. In the case of PLP catalysed racemisation of ACL the perpendicular alignment of the Schiff base and the PLP pyridine ring would result in a reduced pK_a of the C α which can then be deprotonated. In *RfACLR* ACL is highly specifically bound in the active site in an aromatic cage formed of three aromatic residues (Figure 85).

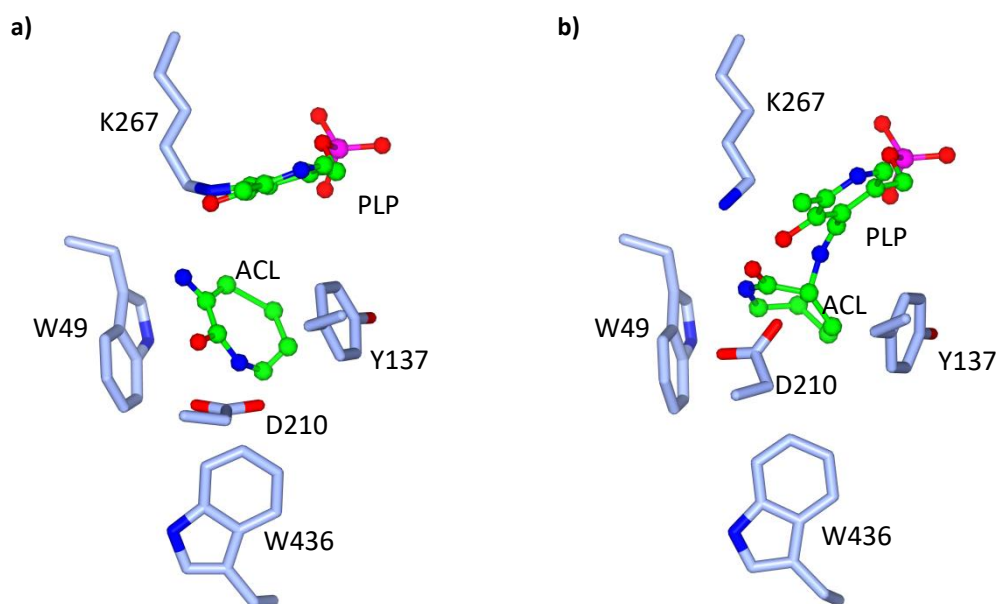


Figure 85: Aromatic cage in *RfACLR* for specific substrate binding, a) wt *RfACLR* complexed with ACL, b) *RfACLR*-K241A complexed with ACL.

The specific substrate binding is mediated by the aromatic residues W49, Y137 and W436. ACL is stacked between W49 and Y137. As discussed above, the role of the C-terminal residue W436 is the closing the entrance of the active site. Furthermore, W436 completes the aromatic cage in the closed conformation. PLP acts as an aromatic opponent of W436 on the other side of the substrate. The three aromatic residues together with PLP act as four aromatic entities that allow very specific binding and positioning of the substrate. During catalysis a conformational change of ACL was observed, where ACL is no longer parallel but perpendicular orientated to W49 and Y137. The Schiff base of the external aldimine should be perpendicularly orientated to PLP to allow deprotonation at the C α . The movement of ACL that was observed from the different crystal structures suggest that the Schiff base approximates to a perpendicular alignment to PLP.

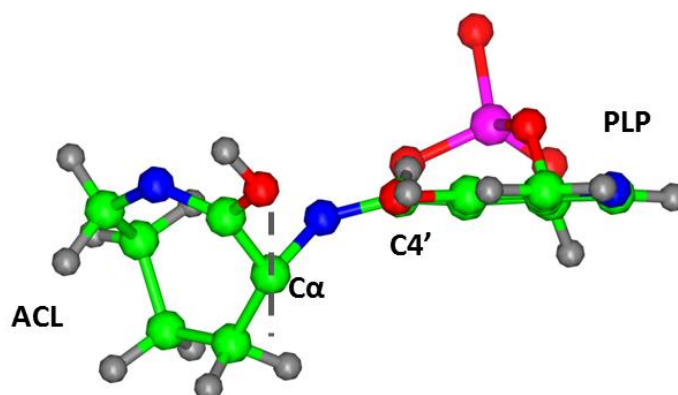


Figure 86: Angle between Schiff base and C α -bond of ACL in the external aldimine with view onto the methyl group of the PLP pyridine ring. The dashed line through C α indicates the angle that is 90° to the PLP pyridine ring.

5.3.3.4 Reaction mechanism derived from structural analysis

Evaluation of *RfACLR*-K241A and *RfACLR*-D210A gave insight into the role of the active site residues in the reaction mechanism. The PLP binding lysine, K267, was identified as one catalytic residue of the acid/base pair. Y137 was found to be essential for the production of soluble enzyme and also a possible catalytic residue in the de/reprotonation. However, tyrosine has a pK_a of 10.1 similar to the pK_a of 10.9 of lysine. D210 is a more likely candidate for the reprotonation of the chiral centre, due to its perfect position opposite to K267 and an acidic pK_a of 3.7. Therefore these two residues are suited to act as acid/base pair in the catalysis. D210 might also be involved in amide recognition, possibly in combination with K241. Listing the distances of the respective residues to the chiral centre of ACL in the solved structures emphasises the role of D210 (2.8 Å to chiral centre) and K267 (3.6 Å to chiral centre) in the reaction mechanism (Table 31).

Table 31: Distances of residues relevant for catalysis to the substrate chiral centre.

Distance of residue to chiral centre	wt <i>RfACLR</i> Internal aldimine	<i>RfACLR</i> -K241A External aldimine	<i>RfACLR</i> -D210A Geminal diamine
Y137	5.6 Å	4.5 Å	4.8 Å
D210	4.6 Å	2.8 Å	/
K241	4.2 Å	/	5.2 Å
K267	3.9 Å	4.2 Å	3.6 Å
Relative activity (%)	100	10.3	0.01

Comparing the structures solved for the different *RfACLR* variants complexed with ACL illustrates the rotation of the substrate during the catalysis and movement of involved residues in the active site (Figure 87).

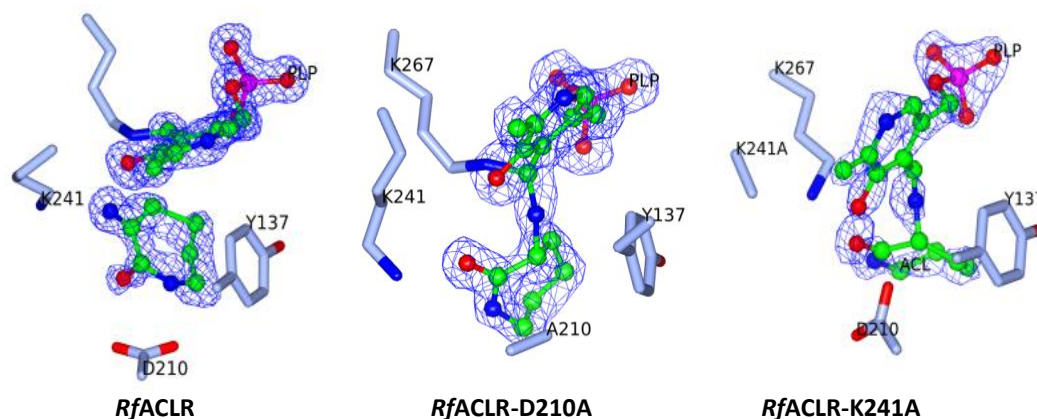


Figure 87: View in the active site of *RfACLR* variants complexed with ACL.

In order to form the external aldimine (*Rf*ACLR-K421A structure) ACL rotates about 90° to form a Schiff base to PLP. Through the formation of the imine bond of PLP and ACL, the binding of K267 and PLP is released. This results in the amine group of K267 pointing away from the substrate that is present as external aldimine with PLP. Looking at the geminal diamine (*Rf*ACLR-D210A), K267 is now again pointing towards PLP, forming a bond between PLP, ACL and K267. Before the substrate is released, it again rotates slightly (about 45°) in order to build the geminal aldimine with PLP and K267. The results from the structural analysis permitted to propose a reaction mechanism, in which the quinonoid and the geminal diamine serve as intermediates (Figure 88).

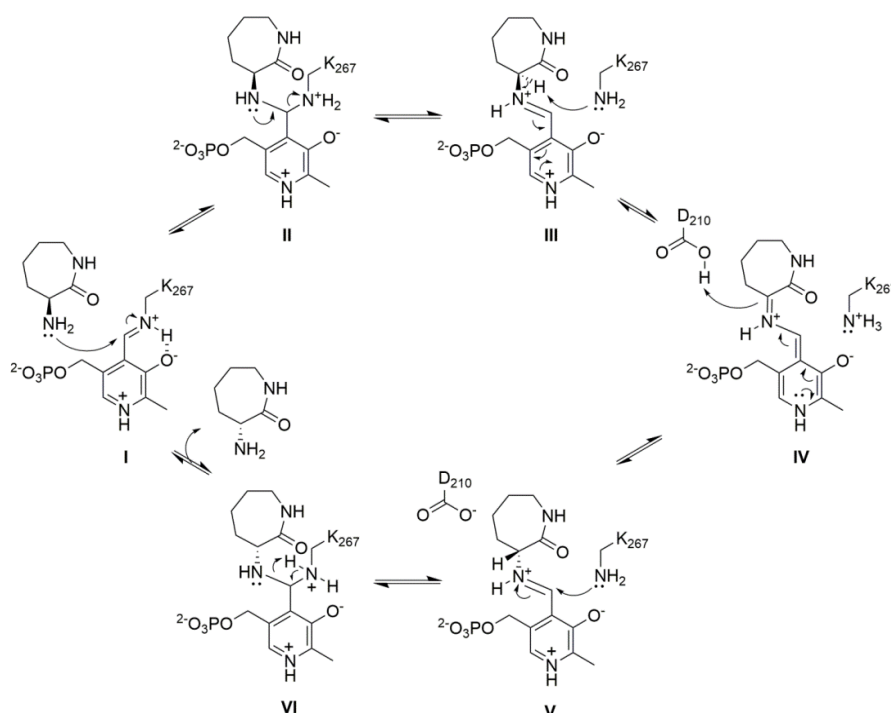


Figure 88: Putative reaction mechanism of *Rf*ACLR based on intermediates obtained from structural analysis. I) Attack of the internal aldimine, II) Formation of the geminal aldimine by PLP, III) and VI) ACL and K267, III) Deprotonation of the chiral carbon by K267, IV) Formation of the achiral quinonoid, V) Reprotonation to the opposite enantiomer by D210, VI) Formation of the geminal aldimine and substrate release. Figure was adapted according to Frese *et al.* ²⁰⁵

The internal aldimine is attacked by the exocyclic amine of ACL (I). This results in the formation of the geminal diamine, a chiral intermediate, in which PLP is bound to both, L-ACL and K267 (II). After deprotonation of the chiral carbon of L-ACL by K267 acting as catalytic base residue (III), an achiral intermediate, the quinonoid, is obtained (IV). Reprotonation by the catalytic acid residue D210A results in the D-configuration of the substrate (V) and the geminal diamine, is formed (VI) before the release of the substrate.

5.4 Conclusion

Analysis of crystal structures obtained from *Rf*ACLR complexed with substrate revealed amino acid residues that are involved in the reaction mechanism. Y137, D210, K241 and K267 were identified as residues that might be involved either as catalytic residue or in amide recognition. These findings are in accordance with previous structural and *in silico* studies on other ACLRs.^{184, 186}

Evaluation of enzyme-substrate complexes gave insight into the substrate binding. A hydrophilic substrate binding pocket and a hydrophobic cofactor binding pocket are located in the active site. Also, the entrance to the active site and a closing mechanism were found by comparison of native and complexed *Rf*ACLR structures. The analysis of the structure of the *Rf*ACLR modelled with PheNH₂ elucidated a steric hindrance of the substrate in the substrate binding site. This result is in accordance with studies in which *Ao*ACLR was engineered and optimised for PheNH₂ racemisation activity by expanding the substrate binding site.¹⁸⁵

The structural analysis of the *Rf*ACLR mutants, *Rf*ACLR-K214A and *Rf*ACLR-D210A, shed light into the reaction mechanism of ACLRs. The mutated enzymes revealed structures of reaction intermediates that were formed during the catalysed racemisation reaction. A reaction mechanism was proposed based on the structures from the different reaction intermediates. Proposed was a two base reaction mechanism in which D210 and K267 are the catalytic residues. These residues act as proton donor/acceptor at the *re*- and *si*-face of the substrate chiral centre. The racemisation is catalysed *via* the achiral quinonoid intermediate and the chiral geminal diamine, from which the structure was solved in the *Rf*ACLR-D210A mutant complexed with ACL.

6 Comparison of *Oa*ACLR and *Rf*ACLR

6.1 Introduction

After the detailed structural investigation of *Rf*ACLR focus was put on the structure of *Oa*ACLR. Differences between these two ACLRs are of special interest because only *Oa*ACLR displayed activity towards L-phenylalanine methylester. The structure of *Oa*ACLR was evaluated and compared to *Rf*ACLR. Mutational analysis of differing substrate binding residues of the two enzymes was carried out to get insight into the background of the different substrate scopes. A rational design approach was used to introduce PheOMe racemisation activity in *Rf*ACLR by using *Oa*ACLR active site residues as template.

6.2 Materials and Methods

Crystallisation techniques were performed as described in Chapter 2.2.7. Mutations were introduced by site directed mutagenesis as outlined in Chapter 2.2.3. Genes were overexpressed and enzymes purified according to Chapter 2.2.5 and 2.2.6. Activities for the racemisation reaction were measured according to the standard HPLC assay (Chapter 2.2.8).

6.3 Results and discussion

6.3.1 Structure of *Oa*ACLR

Three successful conditions were found in initial crystallisation screenings to grow *Oa*ACLR crystals (Chapter 5.3.1). Index E12, Pact E12 and Pact F2 gave conditions for the formation of small crystals in 96 well screening plates. Each condition was used to scale the crystallisation up to 2 μ L in hanging drops. The condition Pact E12 (0.2 M Na malonate, 20 % PEG 3350) gave best crystals from *Oa*ACLR at a protein concentration of 1-2 mg mL⁻¹.

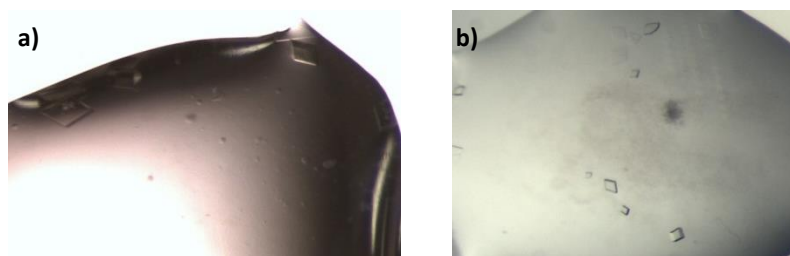


Figure 89: Pictures of *Oa*ACLR crystals obtained in condition PACT E12 (0.2 M Na malonate, 20 % PEG 3350).

Crystals were tested for diffraction and diffraction data were collected for the best crystal (Figure 89a). The structure of native *Oa*ACLR was solved at 2.0 Å using *Rf*ACLR as

molecular replacement model. Even though *Oa*ACLR shares only 52% sequence homology with *Rf*ACLR, the overall structure is very similar and both enzymes represent a structural organisation of the PLP-enzyme type fold I. Different from *Rf*ACLR the quaternary structure of crystalline *Oa*ACLR is a homotetramer, formed of four identical subunits from which two build a dimer with the active site at their interface (Figure 90).

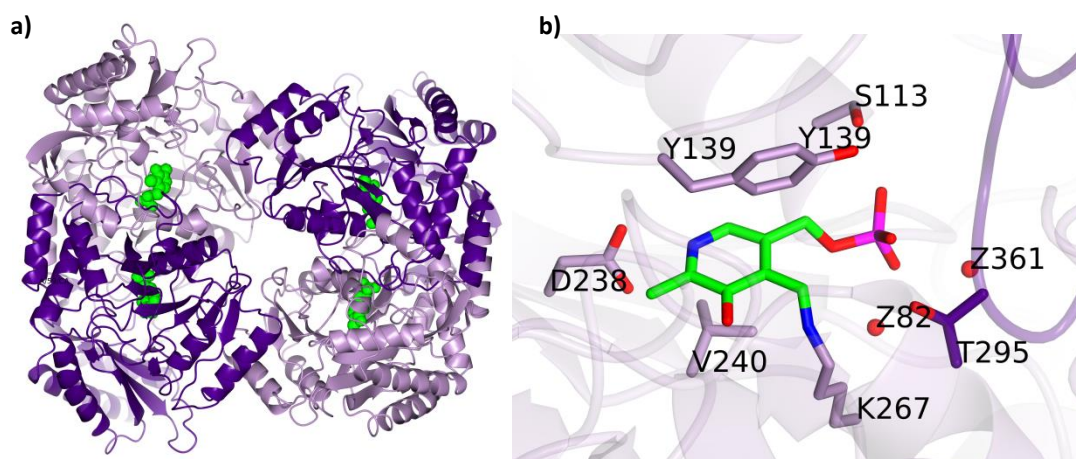


Figure 90: a) Quaternary structure of *Oa*ACLR. Each two subunits form a dimer of which two build a homotetramer. Purple: subunit A and C, orange: subunit B and D. b) Binding of PLP in the active site of *Oa*ACLR. PLP is represented in green cylinder model, purple residues belong to subunit A, residues illustrated in coral are of subunit B.

The cofactor PLP is covalently bound to the amine group of K267 building an internal aldimine via a Schiff base in the active site. The position of PLP is stabilised by the same interactions as described for *Rf*ACLR (Chapter 5.3.2). Residues interacting with the PLP pyridine ring are Y139, V249 and D238. Hydrogen bonds with S113, T295 and water molecules position the phosphate backbone in the binding site. The residues of PLP binding seem to be highly conserved in ACLRs as the same residues were identified in *Ao*ACLR,¹⁸⁴ *Rf*ACLR and *Oa*ACLR. This PLP binding motifs is partly conserved in other PLP-dependent enzymes. The residues V239, T297, D238 and K268 were also found to bind PLP in an aminomutase and a polyketide synthase with the exception of threonine in position 118 instead of serine.²⁸ However, a serine with the function to stabilise the PLP phosphate backbone is not unusual in PLP-dependent enzymes and was found a peptide synthetase and a decarboxylase.²⁸

6.3.2 Comparison of *Rf*ACLR and *Oa*ACLR

The racemisation activity of *Oa*ACLR and *Rf*ACLR have been characterised in detail in Chapter 3. It was found that both enzymes have different activity profiles (Table 32). *Rf*ACLR is 3.9 times more active towards PheNH₂ than *Oa*ACLR, but only *Oa*ACLR showed activity towards PheOMe.

Table 32: Comparison of activities of *Oa*ACL_R and *Rf*ACL_R.

Substrate	Specific activity (U mg ⁻¹)	
	<i>Oa</i> ACL _R	<i>Rf</i> ACL _R
L-ACL	2337 ± 291	26469 ± 5425
L-PheNH ₂	5.2 ± 1.6	20.4 ± 0.8
L-PheOMe	15.3 ± 0.7	0

Solving the structure of both enzymes and comparing them gives a closer insight into the different performance of these similar enzymes (Figure 91). Focusing on the active site gives some explanation for the lower activity of *Oa*ACL_R towards ACL and PheNH₂. Tryptophan in position 49 in *Rf*ACL_R is replaced by an alanine residue in the equivalent position (A51) in *Oa*ACL_R. This could affect binding of smaller substrates as the interacting residue for aromatic stacking is not present. In the *Rf*ACL_R structure the substrate is located between Y137 and W49, whereas for *Oa*ACL_R the substrate would be located between Y139 and A51. However, the presence of the alanine instead of tryptophan might result in a bigger substrate binding pocket, which permits bulkier substrates, like PheOMe, to be converted by *Oa*ACL_R. To verify this hypothesis a structure of an *Oa*ACL_R-substrate complex would be beneficial. Additionally, mutational analysis might identify the function of W49/A51 in binding of the substrate of both enzymes.

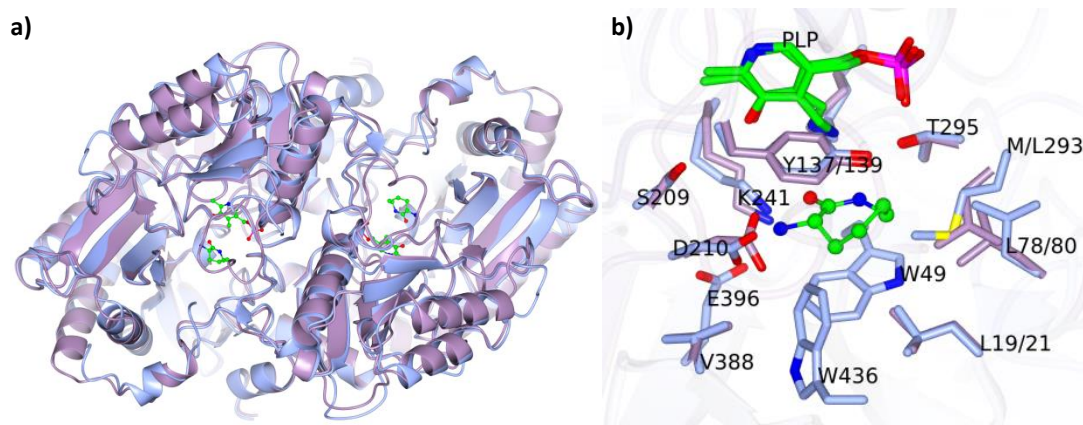


Figure 91: Comparison of structures of *Rf*ACL_R and *Oa*ACL_R. A) Overlay of quaternary structure b) Overlay of active site structure. Blue: *Rf*ACL_R, purple: *Oa*ACL_R

6.3.2.1 Investigation of the role of W49 and M293 by mutational analysis

The active site residues of *Rf*ACL_R and *Oa*ACL_R only differ in position 49/51, where a tryptophan (*Rf*ACL_R) is changed to an alanine in *Oa*ACL_R and in position 293, where the *Rf*ACL_R methionine is replaced by a leucine in *Oa*ACL_R. The mutants *Oa*ACL_R-A51W and *Rf*ACL_R-W49A were generated, overexpressed and purified to evaluate the influence of the

residue 49/51 on the activity towards PheOMe. The alanine in this position (A51) in *OaACLR* might give more space for binding bulky substrates like PheOMe. On the other hand, tryptophan in position 49 in *RfACLR* might help increase substrate affinity by stronger and more specific binding through π -electron stacking. The activity of the different *RfACLR* and *OaACLR* variants was tested with ACL, PheNH₂ and PheOMe.

Table 33: Comparison of activities measured with *RfACLR* and *OaACLR* variants.

Substrate	Specific activity (U mg ⁻¹)	
	<i>OaACLR</i> -A51W	<i>RfACLR</i> -W49A
L-ACL	79.5 ± 0.3	596.2
L-PheNH ₂	0	0
L-PheOMe	0	0

Changing alanine in position 51 to tryptophan in *OaACLR* resulted in 29 times reduced activity of the enzyme towards L-ACL and activity towards the tested phenylalanine derivatives was completely abolished. Replacing the tryptophan by alanine in position 49 of *RfACLR* did not result in increased activity towards bulkier substrates like PheOMe. This mutation gave an enzyme that was reduced in its activity (2.3 % residual activity), and even the activity towards L-PheNH₂ was lost by this mutation.

In the next step the double mutation W49A and M293L was introduced into *RfACLR* in order to introduce the same active site residues in *RfACLR* as in *OaACLR*. The overexpression of *RfACLR*-W49A-M293L did not yield soluble protein and the enzyme could not be purified from crude cell extract from *E. coli* cells harbouring only insoluble *RfACLR*-W49A-M293L. In order to improve the yield of soluble protein, test expressions and solubility screening with different buffers were carried out as described by Kohlstaedt and co-workers.¹⁹⁵ The soluble and insoluble fractions were analysed by SDS-PAGE (Figure 92).

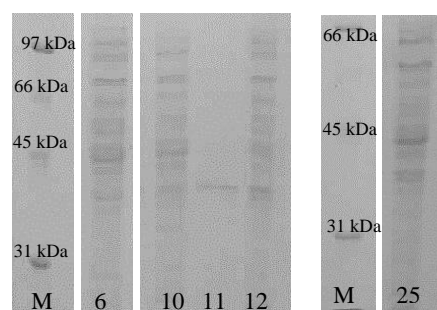


Figure 92: SDS-PAGE of solubility screening of *RfACLR*-W49A-M293L. Lanes with samples with the highest content of soluble protein are shown here. Numbers at the bottom designate the buffer that was used for solubilisation.

The 30 different tested buffers are listed in the Appendix (10.3). Results from screening the different solubilisation buffers suggested that the enzyme is most soluble in the buffers 6, 10, 12 and 25. Buffer 25 (50 mM Tris, 100 mM, sodium glutamate, 10 mM DTT, pH 8.0) was selected as solubilisation buffer for a IMAC purification of *RfACLR-W49A-M293L* overexpressed at 4 L scale in recombinant *E. coli* BL21 (Figure 93 and Figure 94).

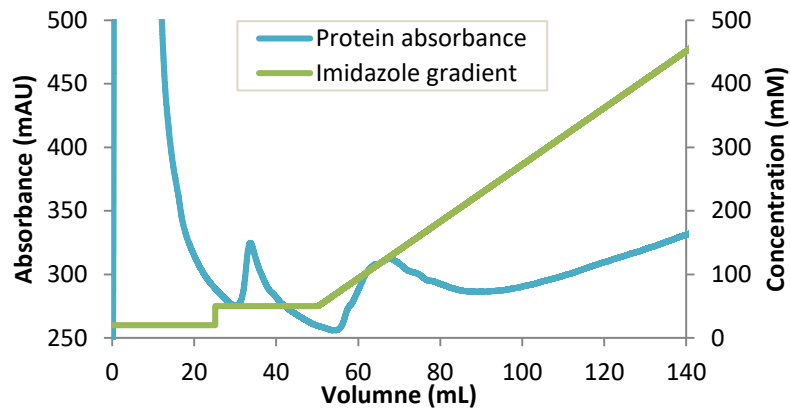


Figure 93: Chromatogram of IMAC purification of *RfCALR-W49A-M293L*.

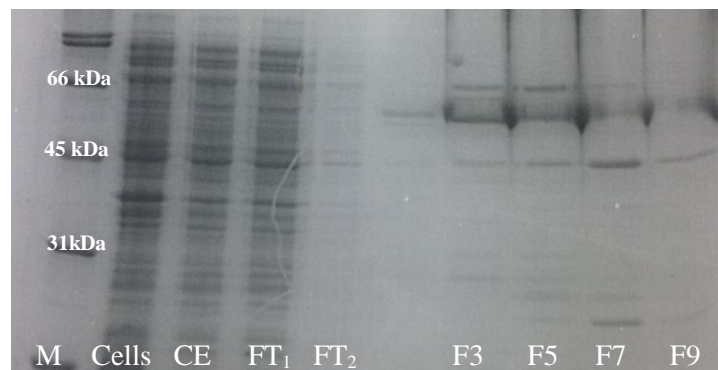


Figure 94: SDS PAGE gel of different fractions obtained after IMAC purification of *RfACLR-W49A-M293L*.

The total yield of 6 mg partly purified *RfACLR-W49A-M293L* was isolated from 8.5 g *E. coli* cells resulting in a yield of 0.7 mg g^{-1} . Due to the low yield of enzyme *RfACLR-W49A-M293L* was not further purified by SEC, but the buffer was exchanged (50 mM Tris, 300 mM NaCl, pH 7.5) to remove imidazole from the solution. *RfACLR-W49A-M293L* (3 mg mL^{-1}) was used for co-crystallisation trials with 20 mM L-ACL in hanging drops in a 24 well plate.



Figure 95: Broom stick crystals obtained from *RfACLR*-W49A-M293L in Index G12 (0.2 mM MgCl₂, 0.1 mM HEPES pH 7.0, 25 % w/v PEG 3350).

The same crystallisation condition was used for crystallisation of the double mutant as used for wt *RfACLR* (Index G12). Crystals exclusively formed broom stick morphology (Figure 95). The racemisation activity of purified *RfACLR*-W49A-M293L was tested for L-ACL, L-PheNH₂ and L-PheOMe to further characterise this *RfACLR* variant. *RfACLR*-W49A-M293L did not show racemisation activity towards any of the tested substrates; even no residual racemisation activity could be detected for L-ACL. Even though protein was purified after optimisation of the solubility, the enzyme might still be misfolded and therefore inactive. The low yield of purified enzyme and lack of its typical yellow colour (indicating the lack of PLP binding) and the unusual crystal shape support this hypothesis.

6.3.2.2 Impact of the aromatic residues W49 and Y386

A constellation of aromatic residues that interact by π -system interactions was found in and around the active site of *RfACLR*. The interaction of these residues of this so called aromatic cage with the substrate was in discussed in the previous chapter. When comparing *RfACLR* and *OaACLR* it becomes noticeable that not only the aromatic residue in position 51 is replaced by a non-aromatic residue, but also the complete series of aromatic residues is not present in *OaACLR* (Figure 96). This might result to lower substrate binding affinity due to less binding interactions. This also might lead to lower substrate specificity and a more relaxed substrate spectrum of the enzyme, because substrates could bind more flexibly in this less restricted substrate binding pocket. The influence of the aromatic residues W49 and Y386 in *RfACLR* was investigated by replacing them with the corresponding *OaACLR* residue and testing the activity of the *RfACLR* mutant.

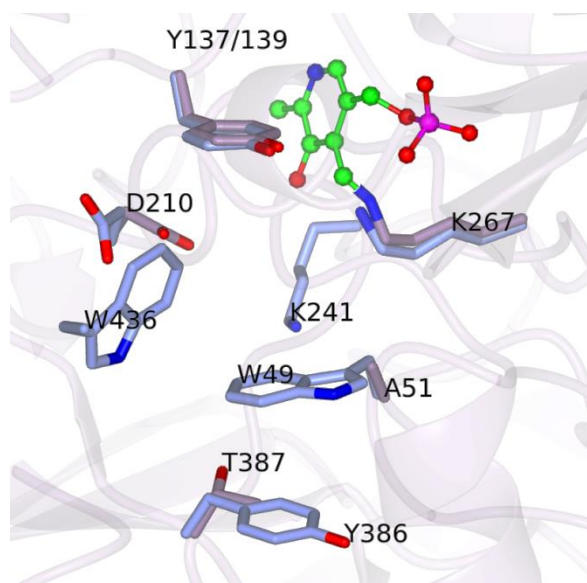


Figure 96: Comparison of *RfACL* (blue) and *OaACL* (purple) vicinity of the active site. The *RfACL* active site is formed by a series of aromatic residues.

RfACL-W49A-Y386T was expressed in *E. coli* and purified by IMAC purification. During the concentration of the enzyme in centricons yellow flow through was observed. The protein concentration of the flow through was measured as 0.4 mg mL^{-1} suggesting that not protein but unbound PLP was washed out into the flow through giving the yellow colour. Storing the enzyme after purification overnight at 4°C resulted in significant precipitation of the enzyme. Hence, IMAC purification was repeated and the purified enzyme was directly used for crystallisation trials and activity determination. Hanging drops for the crystallisation of *RfACL*-W49A-Y386T (3 mg mL^{-1}) were prepared in a 24 well tray with the condition Index G12. Even after long incubation time (>3 months) no crystallisation was observed. The racemisation activity of *RfACL*-W49A-Y386T was determined by HPLC with the standard substrates ACL, PheNH₂ and PheOMe.

Table 34: Activity of *RfACL* variants towards ACL, PheNH₂ and PheOMe.

Substrate	Specific activity (U mg^{-1})	
	<i>RfACL</i> -W49A	<i>RfACL</i> -W49A-Y386T
L-ACL	596.2	622.3 U/mg
L-PheNH ₂	0	0
L-PheOMe	0	0

The *RfACL* mutant is reduced in its activity towards L-ACL, activity towards L-PheNH₂ and L-PheOMe was completely abolished. This result is very similar to the substrate scope of the single mutant *RfACL*-W49A. Even though the enzyme was purified at higher yields (3.3 mg g^{-1}) observations during the purification process, such as the release of PLP from the enzyme, suggest that the double mutation affected the folding and stability of *RfACL*-W49A-Y386T.

In summary, reciprocal mutagenesis of the active site of *Rf*ACLR was performed to gain *Oa*ACLR activity, PheOMe racemisation, in *Rf*ACLR. Several mutants of *Rf*ACLR that replaced residues with *Oa*ACLR residues were tested for the racemisation activity towards PheOMe. Unfortunately, the evaluation of these mutants could not give explanation for the different substrate spectrum of the enzymes. All of the tested variants were reduced in activity towards the natural substrate, in the case of *Rf*ACLR-W49A-M293L no residual activity was measured at all. Activity towards PheNH₂ and PheOMe was completely abolished in each of the tested mutants. The influence of the second shell residue Y386 in *Rf*ACLR was tested, but this again gave an activity reduced mutant.

6.3.3 Structure of *Oa*ACLR crystallised in presence of L-PheOMe

Previous crystallisation trials failed to give crystals of *Oa*ACLR in the presence of substrate (ACL, PheNH₂ or PheOMe). Therefore previously obtained native *Oa*ACLR crystals were used for crystal seeding experiments. The crystal seeding method was successful and resulted in crystal growth in presence of 20 mM L-PheOMe at various crystallisation conditions. The structure of *Oa*ACLR in presence of L-PheOMe was solved from these crystals. The solved structure was very similar to the structure of native *Oa*ACLR but ligand density for L-PheOMe could not be identified. However, some changes in the structure were observed. Different conformations of Y139 were found in the different subunits and the density map for Y139 allowed fitting the residue in alternative conformations (Figure 97).

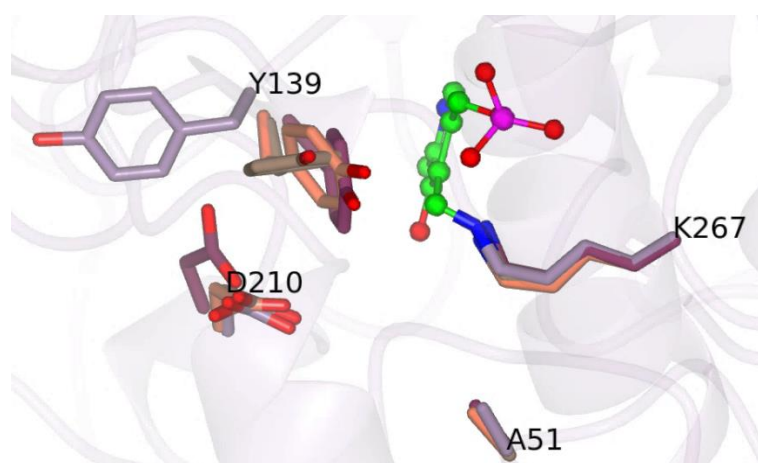


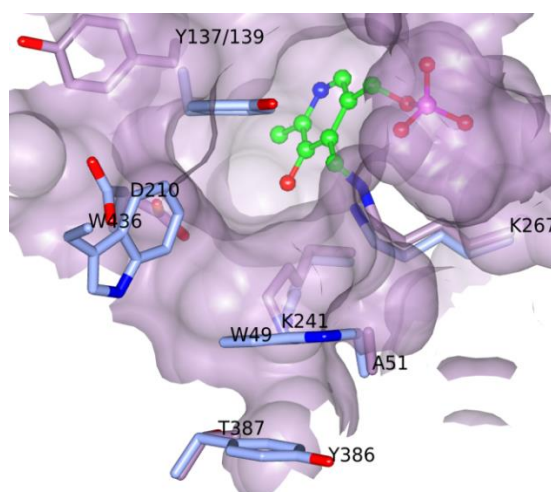
Figure 97: Overlay of Y139 of *Oa*ACLR subunits A-D. The subunits are depicted as cylinder model in different colours, PLP is illustrated in green as stick and ball model.

This is remarkable considering that the conformation of Y137 in all solved *Rf*ACLR structures was found to be highly conserved. This is also represented in the B-factors of the tyrosine in position 137 or 139 in *Rf*ACLR and *Oa*ACLR (Table 35).

Table 35: Comparison of B-factors of tyrosine 137/ 139 of *Rf*ACLR and *Oa*ACLR. In the case of two or four subunits, B-factors for all respective tyrosine are listed.

B-factor	Native <i>Rf</i> ACLR	<i>Rf</i> ACLR-ACL	<i>Oa</i> ACLR
Y137/139	28	10, 11	36, 37, 39, 55
Overall side chain	22	17	32
Overall main chain	17	14	22

The flexibility of Y137 in the active site of *Rf*ACLR is with a B-factor of 28 significantly lower than Y139 of *Oa*ACLR which has a maximal B-factor of 55. The conformation of Y137 in *Rf*ACLR seems to be further stabilised when substrate is bound to the active site. The *Rf*ACLR substrate binding pocket is framed by Y137, W49 and W436 building an aromatic cage. The position of W49 is stabilised by further aromatic stacking with Y386. Comparing this to the substrate binding of *Oa*ACLR reveals the lack of an aromatic cage for substrate binding in the *Oa*ACLR (Figure 98).

**Figure 98: View in substrate binding site of *Oa*ACLR (purple). *Rf*ACLR substrate binding site residues are superimposed and shown in blue.**

The lack of substrate binding trough aromatic residues might result in weaker and less specific substrate binding. This would provide an explanation for the lower activity of *Oa*ACLR towards ACL, the natural substrate of ACLRs. With a different substrate scope and only 53% sequence similarity the ACLR from *Ochrobactrum anthropi* clearly differs from *Rf*ACLR and *Ao*ACLR. ACL racemisation might be a result of the substrate promiscuity of this enzyme which was classed as amino acid amide racemase in the Unitprot data base. The substrate promiscuity of *Oa*ACLR is permitted by its flexible substrate binding pocket which enhances the binding of bulky substrates due to less steric hindrance. Additionally, the new observed conformation of Y139 pointing away from the substrate binding site results in even more space for substrate binding in the active site.

6.4 Conclusion

The structure of *OaACL* was solved at 2.0 Å and showed high overall similarity to the *RfACL* structure. Both enzymes are interesting targets for a detailed comparison as they are similar in their structure but have different substrate scopes. The enzymes were compared by reciprocal mutagenesis with the aim to introduce the PheOMe racemisation activity of *OaACL* into *RfACL*. Residues of *RfACL* of the substrate binding site were replaced by *OaACL* and their effect on the racemisation activity was measured (Table 36). The racemisation activity towards PheOMe and PheNH₂ was abolished in all of the generated mutants. Racemisation activity towards the natural substrate ACL was decreased 30-40 fold. Besides the reduction in activity other effects such as reduced stability (*RfACL*-W49-Y386T) or incorrect folding (*RfACL*-M293L) were observed especially for double mutants. This stresses the complexity of structural interactions between residues that impact the correct function of the enzyme. Only two residues differ in the active site of *OaACL* and *RfACL*. However, the negative results of the reciprocal mutagenesis emphasise that with only 53% sequence similarity not only active site residues but also other structural aspects, such as second shell residues, conformational changes and flexible regions contribute to the full function of the enzyme.

Table 36: Summary of mutational evaluation of active site residues of *RfACL* and *OaACL* with respect to the racemisation activity.

Enzyme	Specific activity (U mg ⁻¹)		
	L-ACL	L-PheNH ₂	L-PheOMe
<i>OaACL</i>	2337 ± 291	5.2 ± 1.6	15.3 ± 0.7
<i>RfACL</i>	26469 ± 5425	20.4 ± 0.8	0
<i>OaACL</i> -A51W	79.5 ± 0.3	0	0
<i>RfACL</i> -W49A	596.2	0	0
<i>RfACL</i> -W49A-M293L	0	0	0
<i>RfACL</i> -W49A-Y386T	622.3	0	0

The analysis of the structure solved for *OaACL* crystallised in the presence of L-PheOMe gave new details on the acceptance of PheOMe as substrate by *OaACL*. The tyrosine in the position 139 that is directly involved in substrate binding was found in different conformational states. In one conformation it is pointing away from the substrate binding site and creates a larger binding site as with Y139 in the usual conformation. The flexibility of this residue was noticed for the first time in *OaACL* and was not found in *RfACL* or *AOACL*. Even though no ligand density was obtained for this *OaACL* structure, the conformational change of Y139 might be induced by the presence of PheOMe and might be one reason for the

expanded substrate acceptance of *OaACLR*. The general lack of aromatic residues, that form an aromatic cage for specific substrate binding in *RfACLR*, might give an explanation for the different substrate spectrum of *OaACLR*.

7 Photometric assay for the detection of AAER activity

7.1 Introduction

The information gained from the investigation into the reaction mechanism of ACLRs can be used for the structure-guided evolution of improved amino acid ester racemases. After a rational design approach proved to be unsuccessful (Chapter 6) a semi-rational approach was pursued. In the semi-rational engineering method small, selected mutant libraries of the enzyme of interest are generated and screened for improved activity. For this purpose it is necessary to develop a high throughput assay for the photometric detection of amino acid ester racemisation activity.

A photometric assay for the detection of *N*-acetyl amino acid racemase activity was recently developed by Campopiano and co-workers.¹⁷⁵ For the photometric detection of the reaction the racemisation of a *N*-acetyl amino acid was coupled to the deacetylation and following oxidation of the amino acid. The oxidation of the amino acid can be detected by coupling it to a H₂O₂ mediated oxidation of *o*-dianisidine. The red colour of oxidized *o*-dianisidine can then be detected at 436 nm. Within this work a photometric activity assay for the detection of PheOMe racemisation activity was developed in a similar way.

Four enzymatic reactions are coupled in the assay for detection of amino acid ester racemisation activity (Figure 99). The first reaction, the reaction to be detected, is the racemisation of D-PheOMe. Only when D-PheOMe is racemised to L-PheOMe further course of the cascade is possible, as all following reactions are catalysed by L-selective enzymes. The next step requires the hydrolysis of the ester to the corresponding amino acid. The endoproteinase of the serine type and the major component of subtilisin has been reported to be an enantioselective L-phenylalanine methyl ester hydrolase.²⁰⁶ This L-selective hydrolase, the alcalase from *Bacillus licheniformis*, is hence used in the second reaction to hydrolyse L-PheOMe to L-phenylalanine.

The hydrolysis of PheOMe has been investigated within this work (Chapter 4). As D-PheoMe is used as substrate the hydrolysis would result in D-Phenylalanine which is not converted by the L-selective amino acid oxidase (L-AAO) in the next step of the cascade.

The third reaction is the detection reaction, coupled of two enzymatic reactions. First, L-phenylalanine is oxidised to phenylpyruvate by L-AAO from *Crotalus atrox*. Flavin adenine dinucleotide (FAD) present in the cell lysate is used as electron acceptor during this reaction and reduced to FADH₂. The cofactor is recycled by the oxidation of O₂ to H₂O₂ also catalysed

by L-AAO. The production of H_2O_2 can be detected by horse radish peroxidase (HRP) catalysed oxidation of *o*-dianisidine. Despite its reduced form, oxidized *o*-dianisidine has a maximum in absorbance at 436 nm.

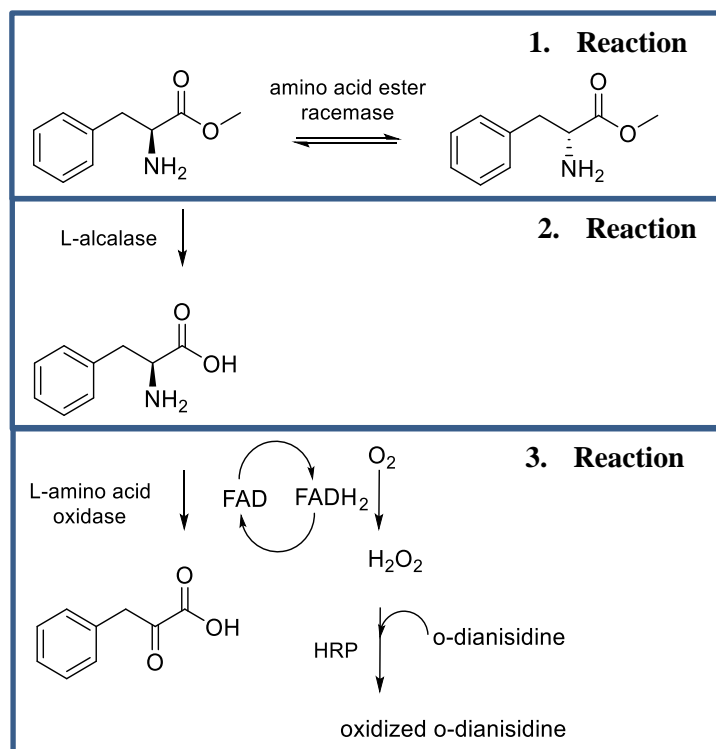


Figure 99: Reaction scheme of the enzyme cascade for detection of PheOMe racemisation activity.

7.2 Materials and methods

The photometric activity assay to measure amino acid ester racemisation activity was developed and used to screen mutant libraries as outlined in Chapter 2.2.9.

7.3 Results and discussion

7.3.1 Development of a photometric assay for amino acid ester racemisation

For preliminary tests of the different assay conditions similar as described by Campopiano *et al.*¹⁷⁵ were used in a total reaction volume of 1 mL. Progression of the absorbance at 436 nm was followed at subsequent time points. Reactions were carried out in plastic cuvettes and incubated at 30°C. Different components of the assay were tested in their functionality and for optimisation of the assay.

7.3.1.1 Preliminary test of the different assay reactions

Alcalase catalysed hydrolysis of phenylalanine methylester

To verify the suitability of alcalase for the second reaction of the assay cascade, the activity and selectivity of the enzyme was tested under assay conditions. The alcalase catalysed hydrolysis of D- or L-PheOMe was analysed by TLC (Figure 100). The reaction was carried out in Tris buffer (50 mM, pH 7.5) at 30°C for 2 h (Chapter 2.2.10) with 10 mM substrate and 0.26 mU L⁻¹ alcalase (Reaction 4-5).

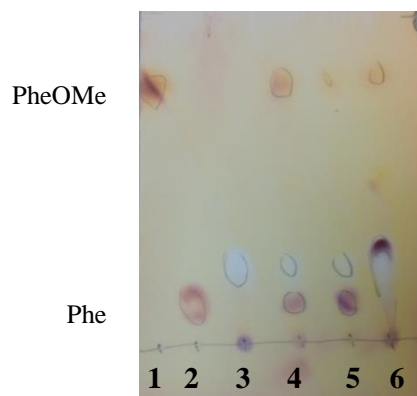


Figure 100: TLC of alcalase catalysed reaction. 1: L-PheOMe standard (3 mg ml⁻¹), 2: L-Phenylalanine standard (1 mg/ml⁻¹), 3: Alcalase in Tris buffer (50 mM, pH 7.5), 4: Reaction with D-PheOMe, 5: Reaction with L-PheOMe, 6: Reaction with D/L-PheOMe. 10 mM PheOMe were used for reactions, 2.6 mU L-alcalase (reaction 4-5), respectively 0.26 U mL⁻¹ L-alcalase (reaction 6) were applied.

The result of the TLC verifies that alcalase catalyses the hydrolysis of L-PheOMe. A preference of alcalase to the L-enantiomer was observed (Reaction 5) as L-PheOMe is almost completely converted to phenylalanine, whereas a larger amount of PheOMe remained unconverted in the reaction with D-PheOMe (Reaction 4). The production of phenylalanine detected for the reaction with D-PheOMe can be explained with the chemical hydrolysis of the ester (Chapter 4.3.3). Nonetheless, alcalase was identified as an effective hydrolase for the hydrolysis of L-PheOMe which can be applied to catalyse the second reaction in the assay enzyme cascade.

Testing of the detection reaction of L-AAO and HRP

The detection reaction was tested by using L-phenylalanine, L-AAO, HRP and *o*-dianisidine in a 1 mL reaction. The formation of oxidized *o*-dianisidine could clearly be detected by eye through the change in colour from yellow to red. The colour formation also gave a strong signal at 436 nm. After 20 min incubation time an absorbance of 1.04 mAU was measured, whereas for the reaction with same components but without phenylalanine only 0.33 mAU was detected.

After confirming that a signal can be measured with the detection reaction (L-AAO, HRP and *o*-dianisidine) the reaction was carried out with D- or L-PheOMe but without racemisation catalyst (Figure 101). Cell lysate from *E. coli* cells with empty YSBLIC3C-vector (ctrl cell lysate) was used in the reactions.

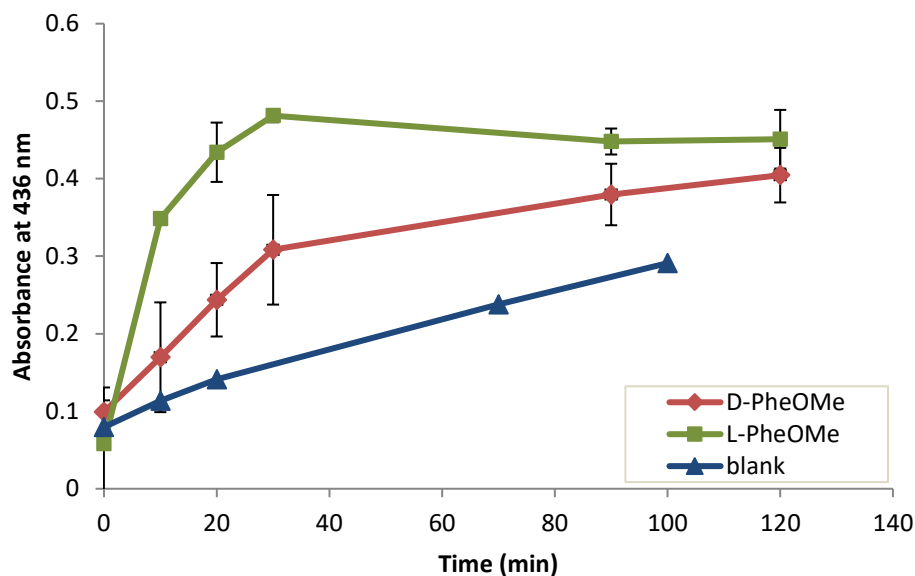


Figure 101: Photometric detection PheOMe racemisation (10 mM). Assay cascade (alcalase, L-AAO, HRP) with oxidised *o*-dianisidine giving a response at 436 nm. The reaction was run with ctrl lysate and the increase of absorbance was followed at 30°C for 2 h.

The positive control, containing L-PheOMe, control cell lysate, alcalase, L-AAO, HRP and *o*-dianisidine confirmed the correct function of the enzyme cascade. The selected enzymes can be used in combination to detect the presence of L-PheOMe. Therefore, the production of L-PheOMe in a racemisation reaction can be measured by coupling this reaction to the signal reaction of the cascade.

Also the negative reaction (D-PheOMe, control cell lysate, alcalase, L-AAO and HRP and *o*-dianisidine) gave the expected result. The signal produced by the oxidation of *o*-dianisidine is 1.5 fold lower than for the positive control. Even though the positive signal in the positive control is much stronger, there is still a rather high increase of absorbance in the negative control. The increase in absorbance might come from unselective hydrolysis of D-PheOMe through alcalase or an *E. coli* hydrolase. Produced D-phenylalanine could then be racemised by a broad spectrum amino acid racemase from *E. coli*.¹³⁷ The formation of L-phenylalanine would result in the progression of the cascade and detection of *o*-oxidised dianisidine.

A high background reaction was detected in the blank reaction where buffer was used instead of PheOMe (control cell lysate, alcalase, L-AAO, HRP and *o*-dianisidine). Cell lysate from *E. coli* without any overexpressed enzyme was used for this reaction. Many metabolic enzymes

convert FAD/FADH₂ as cofactor. As long as FADH₂ is produced in background reactions HRP can use the cofactor together with O₂ to oxidise *o*-dianisidine. This background reaction has to be taken into account when calculating the concentration of oxidised *o*-dianisidine.

With these preliminary tests a colorimetric, easy and rapid method was found to test amino acid ester racemase activity. Nevertheless, more detailed investigations of the influence of the assay component concentrations and reaction times are necessary to develop this assay for amino acid ester racemase activity screenings.

7.3.1.2 Optimisation of the assay for the application in 96 well plates

Different L-AAO and HRP concentrations

The previously established colorimetric assay was transferred to 96-well plate format. At first the assay was tested with L-phenylalanine (10 mM) to test optimal enzyme concentrations for the detection reaction. The enzymes in of the detection reaction, L-AAO) (0-2 U mL⁻¹) and HRP (0-47.3 U mL⁻¹) were used in different concentrations to identify optimal concentrations of both enzymes to give a response in an appropriate time frame.

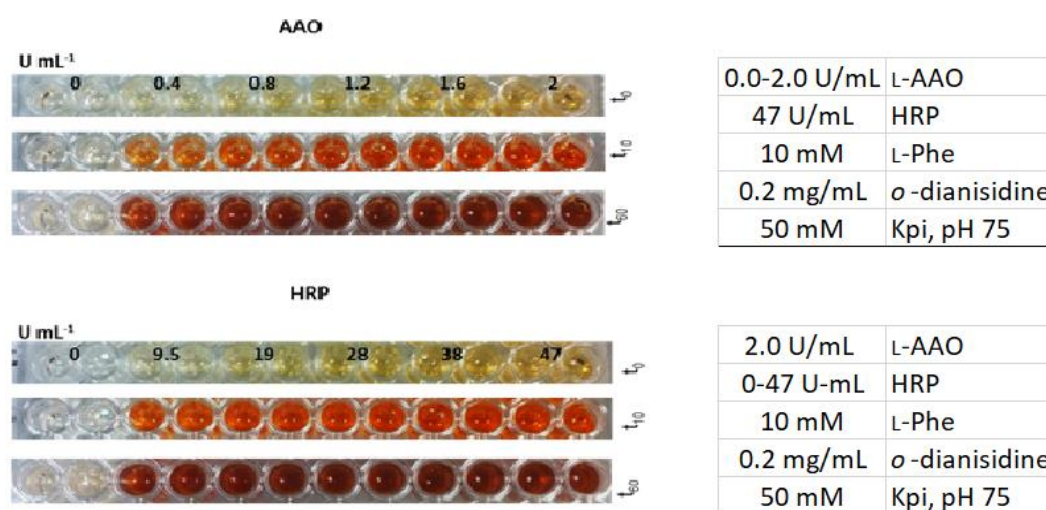


Figure 102: Colour formation in detection reaction of the photometric assay for AAER detection. Different concentrations of AAO and HRP were tested to find the concentrations for optimal colour formation.

Colour formation occurred immediately after adding all components (reaction was started with addition of *o*-dianisidine at t_0). The increase in colour formation was followed for 60 min after which saturation in colour formation was observed. It is necessary that the detection reaction gives an immediately signal after the hydrolysis of L-PheOMe to L-phenylalanine to ensure the signal formation is not limited by the activity of the reporting enzymes. However, for practical and cost reasons the enzyme concentration should not largely exceed the sufficient

concentrations. Optimal increase in absorbance was detected with the combination of 60 mU mL⁻¹ L-AAO and 28 U mL⁻¹ HRP.

Testing different PheOMe concentrations

The assay was tested with different L-PheOMe or D-PheOMe concentrations to evaluate the optimal substrate concentration. To prevent ester hydrolysis the assay was performed at pH 5.8. Both, ctrl cell lysate and *Oa*ACLR cell lysate were tested with different PheOMe concentrations (0-91 mM). The colour formation was measured after 19 h incubation time (Figure 103).

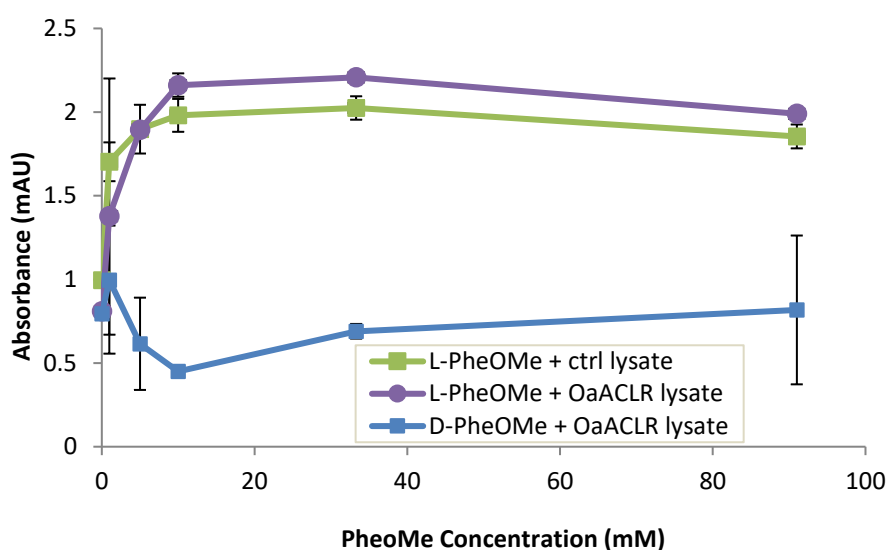


Figure 103: Colour formation with the photometric assay at different PheOMe concentrations after incubation at 30°C for 19 h. The assay was carried out in 200 µL of 50 mM KPi buffer (pH 5.8) (containing 0.06 U mL⁻¹ AAO, 28 U mL⁻¹ HRP, 0.26 U mL⁻¹ alcalase, 0.02 mg mL⁻¹ *o*-dianisidine, cell lysate) 0-90 mM L- or D-PheOMe were used as substrate.

Using L-PheOMe with either control cell lysate or cell lysate containing *Oa*ACLR gave a high response in absorbance. This confirms that the complete assay with all three reactions is suitable to detect L-PheOMe. The maximum in absorbance was reached with 10 mM substrate, however at this and higher substrate concentrations precipitation was observed in the reaction wells. When using PheOMe concentrations ≥ 10 mM in the standard HPLC assay precipitation was not observed, therefore this observation might be caused by the conditions in the photometric assay. The photometric assay contains many different components, two substrates, four enzymes and cell lysate. The concentration of components in solution is very high in the assay, which facilitates substrate precipitation at high concentrations.

Using D-PheOMe in the reactions with *Oa*ACLR resulted in a lower colour formation. From these results it is not clear if the *Oa*ACLR catalysed reaction is distinguishable from the

background reaction. So far optimal concentrations of the enzymes L-AAO, HRP and the substrates L-PheOMe and *o*-dianisidine were found. Hence, optimal conditions were found for all assay components except for the concentration of *Oa*ACLR. To finalise the assay optimisation and to clarify if it can be used for the detection of the racemisation of D-PheOMe, it was then tested with different *Oa*ACLR concentration.

Testing the assay with different cell lysate concentrations

The efficiency of the assay to measure the production of D-PheOMe from ACLR catalysed racemisation was tested by using cell lysate from *E. coli* cells overexpressing *Oa*ACLR. This reaction was compared to the background reaction by using control cell lysate under same reaction conditions. The assay was carried out with different cell lysate concentrations to find an appropriate concentration to overcome the background reaction.

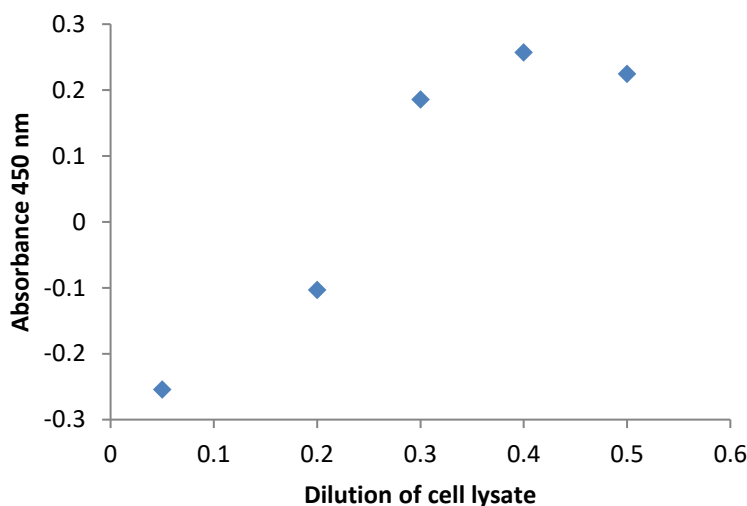


Figure 104: Optimisation of cell lysate concentration for the photometric assay. Absorption of oxidised *o*-dianisidine was measured after 3.5 h reaction time. 5 mM D-PheOMe was used in 50 mM KPi buffer (pH 5.8) with 0.06 U mL⁻¹ L-AAO, 28 U mL⁻¹ HRP, 0.26 U mL⁻¹ alcalase and 0.02 mg mL⁻¹ *o*-dianisidine. Different dilutions of cell lysate (from *E. coli* Rosetta-*Oa*ACLR) were used and blanks from control cell lysates (from *E. coli* BL21- empty YSBLIC3C vector) with corresponding concentrations were subtracted.

Testing the assay with D-PheOMe and cell lysate containing *Oa*ACLR confirmed the ability of the assay to detect the racemisation reaction. Nonetheless, the margin of the detected racemisation reaction and the background is narrow due to the high background and the slowly catalysed racemisation. To overcome the background reaction a higher cell lysate concentration needs to be applied, a 1:3 dilution of the cell lysate (100 mg cells mL⁻¹) gave a sufficient conversion to detect formation of L-PheOMe under the tested conditions. After subtracting the background reaction absorbance >0.2 was measured with these higher concentrations of *Oa*ACLR cell lysate.

The amount of *Oa*ACL_R can be calculated to 0.006 mg *Oa*ACL_R in the assay when using the respective 1:3 dilution from the cell lysate assuming that 0.2 mg *Oa*ACL_R are expressed in 1 g cells (Chapter 3.3.4). For the mutant library screening cell lysate from *E. coli* cells cultivated in 2 mL TB will be used for the assay. According to the results from Chapter 3, 0.8 mg *Oa*ACL_R is expressed in 1 L cell culture in LB medium. This correlates to 0.0016 mg in a 2 mL culture. From the present results this amount would not be enough to overcome the background reactions. However, the expression yields can not be directly compared as the cultivation conditions are not comparable. For the assay, the cells are cultivated in a different container, other medium, at higher shaking rate and temperature. The expression of *Oa*ACL_R in the 2 mL culture in TB medium can be expected to be higher than under the conditions used before (Chapter 2.2.5).

With all conditions optimised the assay was carried out in repeats with wt *Oa*ACL_R enzyme. For the 16 measured repeats the average absorbance was 0.239 with a deviation of 0.056, which corresponds to a percentage deviation of 23.4 %.

7.4 Conclusion

Preliminary tests confirmed the principal applicability of the assay to detect L-PheOMe with the enzyme cascade of alcalase, L-AAO and HRP. Optimal concentrations of these three enzymes and the substrate PheOMe were identified through optimisation of the assay at 200 μ L scale. Different concentrations of *Oa*ACL_R containing cell lysate were used in the detection of the racemisation of D-PheOMe under optimised conditions as summarised in Table 37. Despite the high background reaction it was possible to detect D-PheOMe racemisation with the photometric assay.

Table 37: Optimal assay conditions identified for the detection of AAER activity.

Assay component	Volume (μ L)	Final concentration
Alcalase	10	0.26 U mL ⁻¹
L-AAO	10	60 mU mL ⁻¹
HRP	0.6	28 U mL ⁻¹
KPi buffer (pH 5.8)	9.4	50 mM
D-PheOMe	30	5 mM
σ-dianisidine	40	0.2 mg mL ⁻¹
cell lysate	100	

The successful development of a functional assay for the photometric detection of PheOMe racemisation allows the high throughput screening of mutant libraries for improved AAE racemases.

8 Engineering of improved AAER activity

8.1 Introduction

The racemisation activity of two homologous ACLRs has been studied in detail in the previous chapters. *Oa*ACLR was shown to be active towards the model substrate phenylalanine methylester whereas *Rf*ACLR was not active towards this substrate. A detailed reaction mechanism was derived from structures of different reaction intermediates observed in *Rf*ACLR (Chapter 5). This revealed residues that are necessary for the catalysis, D210 and K267 as catalytic residues and K241 for substrate recognition.

The structural comparison of *Oa*ACLR and *Rf*ACLR showed differences in their substrate binding site. Additional to the differences in two active site residues, a structural and conformational deviation of the both enzymes was also observed. Of most interest are the two residues A51 and L293 in the *Oa*ACLR substrate binding site as they vary from the corresponding W49 and M239 in *Rf*ACLR. Site directed mutagenesis of these residues in *Rf*ACLR did not gain activity towards PheOMe. However, these two residues remain of interest for improving or introducing amino acid ester racemisation activity in ACLRs. As PheOMe racemisation activity was demonstrated for *Oa*ACLR emphasis was put on improving this already existing amino acid ester (AAE) racemisation activity. Instead of generating single mutations by rational design, saturation mutation libraries of the two residues were generated and screened for improved amino acid ester racemisation.

8.2 Materials and methods

The photometric activity assay to screen for amino acid ester racemisation activity was used under standard conditions as described in Chapter 2.2.9. Saturation mutation libraries were generated in position 51 and 293 as outlined in Chapter 2.2.4. Enzymes were produced and purified according to Chapter 2.2.5 and 2.2.6. Kinetic parameters for the AAE racemisation reaction were measured with the standard HPLC assay (Chapter 2.2.8).

8.3 Results and discussion

8.3.1 Generation of saturation mutagenesis libraries

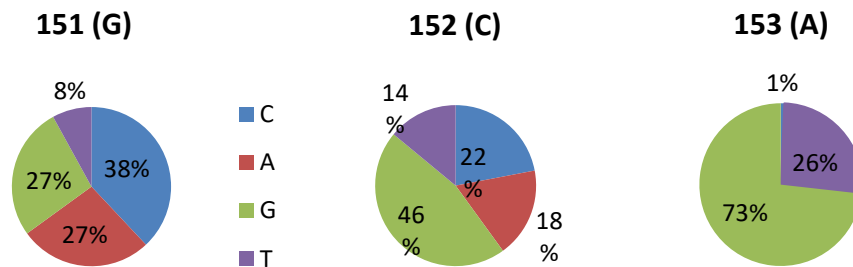
Site directed saturation mutations were introduced in position 51 (Sat-51) and 293 (Sat-293) of the amino acid sequence of *Oa*ACLR. Degenerate NNK primers were used for inverse PCR as described in Chapter 2.2.4. For inverse PCR the forward primer contained the mutation to

be incorporated in the plasmid DNA (Table 38). Using NNK primers theoretically results in 32 codons for 20 amino acids. Covering the library three-fold and at 95% was described as sufficient to find improved variants²⁰⁷ which correspond to 96 mutants used for the screening for improved activity.

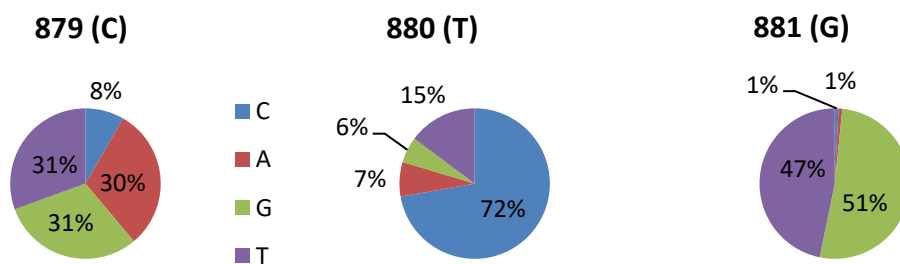
Table 38: Primers for the generation of a saturation mutagenesis library. NNK stands for the degenerate codon used to introduce saturation mutations.

Position of mutation	Forward primer (5' -> 3')
<i>OaACLR</i> - A51	TGAGCGGTAGC NNK GGTCCGGCAGCA
<i>OaACLR</i> - L293	CCGGCATTGT NNK CAGACCACCG

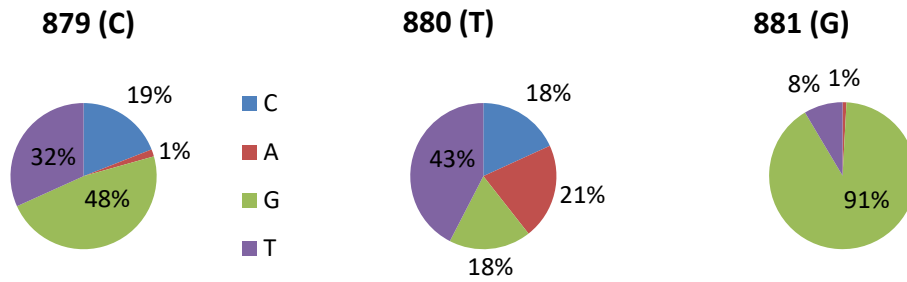
Approximately 100-300 colonies grew after transforming *E. coli* Stellar cells with the product of the inverse PCR procedure. The whole of the colonies were combined in water and the plasmids were isolated to be analysed by sequencing. The presence of the different bases was analysed by the sequencing chromatogram. As described by Reetz *et al.* the peak height can be related to the relative concentration of the respective base.²⁰⁸ The different concentrations of the bases in each position are summarised in Figure 105.



Position 51



Position 293, library 1



Position 293, library 2

Figure 105: Distribution of the four bases in the target positions for saturation mutagenesis.

Position 51 in the *Oa*ACLR amino acid sequence encodes an alanine residue which corresponds to the codon GCA in the DNA sequence (position 151-153). For position L293 this corresponds to the codon CTG in the position 879-881 in the DNA sequence. The saturation library obtained for the position A51 shows good distribution of the bases in each position. The theoretical distribution (25% N, 25% N, 50% K) is practically not achievable with PCR-based mutation techniques due to biases through the use of polymerases and primer sequences.²⁰⁸ Comparing the saturation libraries 1 and 2 of *Oa*ACLR-L293 library 1 showed a better degeneracy of the bases. In library 2 only 1% adenine in position 879 and only 8% thymine in position 881 are present which decreases the quality of this library. Thus, library 1 was selected for further use for the screening for AAER activity.

After picking clones and cultivating the libraries in *E. coli* cells (Chapter 2.2.5), samples were taken and sequenced to analyse the distribution of amino acids in the saturation mutagenesis libraries (Figure 106). 15% of each library was sequenced which corresponds to 14 *Oa*ACLR-mutants for each library.

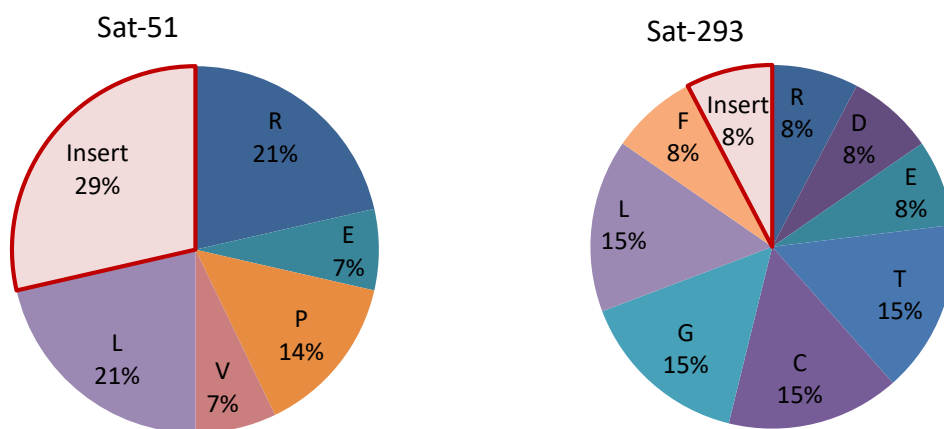


Figure 106: Quality of saturation mutant libraries. The percentage distribution of amino acids (single letter code) is shown in the respective position of the saturation mutagenesis library of *Oa*ACLR. Insert: primer insertion.

Full coverage of the amino acids (each of the 20 amino acid is present) for the sample size of 14 corresponds to 70% of all amino acids. The *Oa*ACLR-51 saturation library only covered 36% of possible amino acids according to the sample size. Furthermore, 29% of the samples of this library contained a primer insertion which led to a shift in the reading frame. These factors point out the low quality and low coverage of the Sat-51 saturation library. Despite several trials to obtain other Sat-51 libraries, the tested library was the only library that could be obtained from inverse PCR with the used primers. Therefore, this library was used for screening for improved AAER activity.

*Oa*ACLR-293 saturation library covered 40% of the possible amino acids which is 62% coverage at the respective sample size. Primer insertions only occurred in one of the tested mutants. Compared to the Sat-51 library, Sat-293 is of higher quality and was used for AAER screening.

8.3.2 Cultivation and screening of *Oa*ACLR saturation mutant libraries

The growth of *E. coli* BL21 (DE3)-wt*Oa*ACLR in 96 deep well plates was monitored at different shaking speeds. TB autoinduction medium was used for cultivation at 37°C for 24 h by shaking at 250, 400, 800 and 1000 rpm. The distribution of the OD_{600 nm} over the 96 wells was measured (Figure 107).

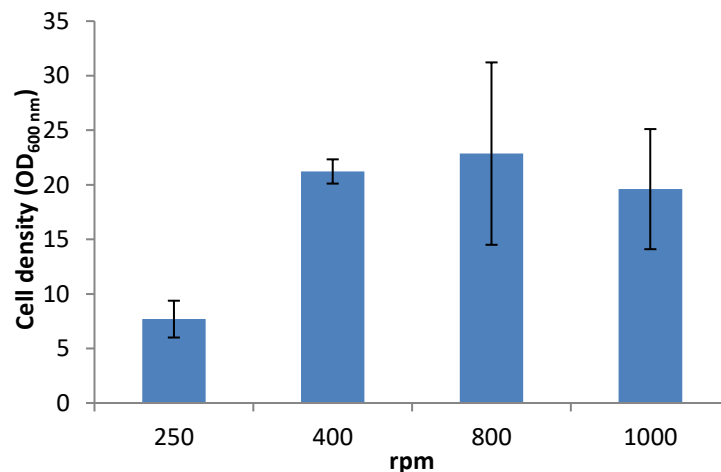


Figure 107: Growth of *E. coli* BL21-*Oa*ACLR in 96 deep well plates in TB autoinduction medium at different rpm. Growth at 800 rpm from *E. coli* BL21-*Oa*ACLR-Sat-A51

Shaking at 250 rpm did not give sufficient mixture of the cell culture resulting in low cell growth due the sedimentation of cells at the well bottom. Cultivation at 400 rpm gave the best results for evenly distributed cell growth. At this shaking speed the distribution of growth in the different wells was smallest and an OD_{600 nm} >20 was reached. Shaking at 1000 rpm gave

uneven distribution over the 96 wells and lower cell growth especially in wells in the middle of the plate. To reach optimal growth of *E. coli* BL21 expressing *OaACLR* saturation libraries 400 rpm can be used for the cultivation of the saturation mutagenesis libraries.

E. coli cells harbouring *OaACLR*-Sat-51 and *OaACLR*-Sat-293 were incubated at 37°C for 24 h in 96 deep-well blocks to test the cultivation of the saturation libraries. Overexpression of the *OaACLR* variants was induced by lactose present in the autoinduction medium and the OD_{600 nm} was measured after 24 h of incubation time (Figure 108).

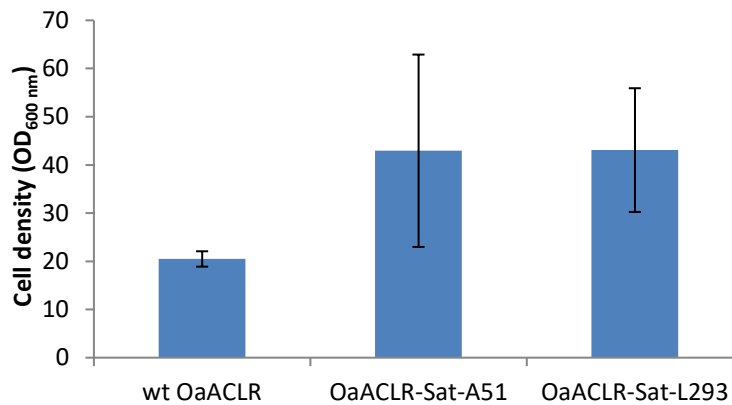


Figure 108: Cell growth of *E. coli* BL21 (DE3) cell overexpressing *OaACLR* mutants after 24 h incubation in 1 mL autoinduction medium at 37°C at 400 rpm.

E. coli cells overexpressing saturation mutants of *OaACLR* reached a higher OD_{600 nm} after 24 h incubation time. Noticeable is the high deviation (± 20 OD_{600 nm}) that was measured for the saturation libraries. The low deviation of ± 1.6 OD_{600 nm} for *E. coli* cells expressing wt *OaACLR* can be explained with the equal impact of the enzyme expression on the cells. The cells expressing different variants of *OaACLR* are differently affected by the overexpression which can result in different effects on the cell growth. The synthesis level varies for each mutant and differently influences the biosynthesis of other proteins of the host cell.

After overexpressing the saturation libraries in *E. coli*, cell lysate from these cells was prepared and used in the screening assay as described in Chapter 2.2.9. The protein concentration of the cell lysate was detected with the BCA method and used to calculate activities for each mutant of the library (Figure 109).

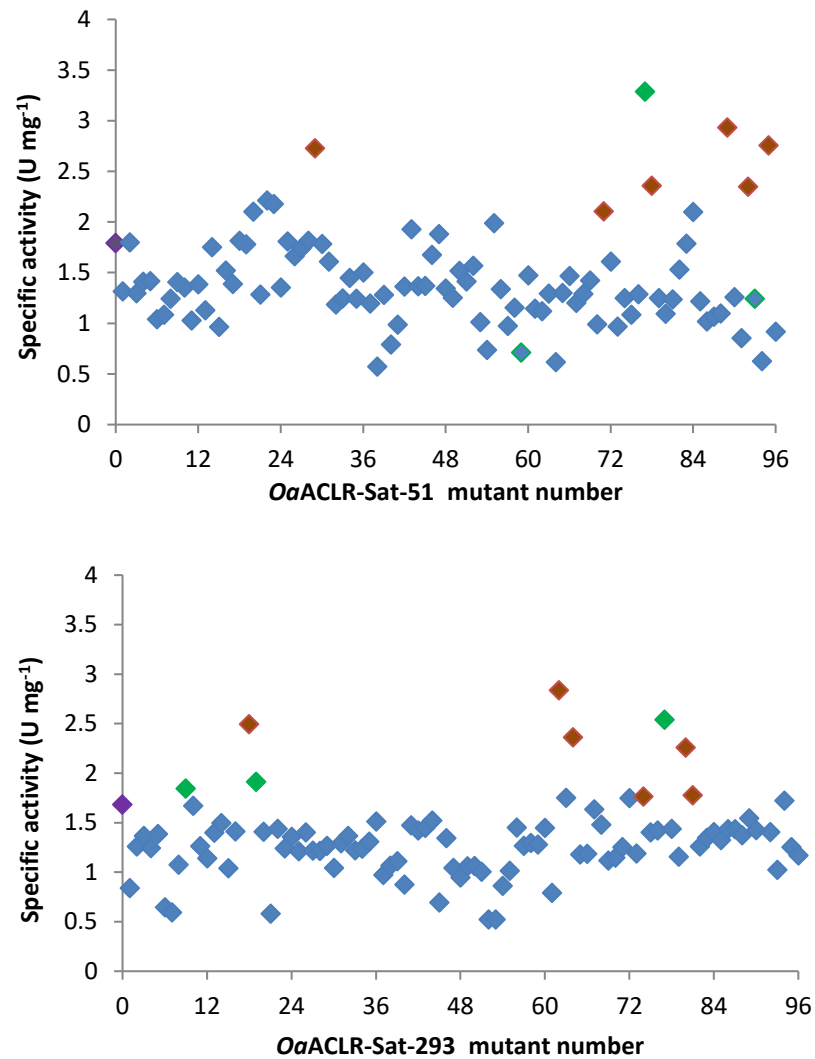


Figure 109: Screening for activity-improved *OaACLR* mutants. Activities measured for each mutant of the libraries *OaACLR-Sat-293* and *OaACLR-Sat-51*. The mutant number 0 depicted in purple shows the activity measured with wt *OaACLR*. Green indicated points represent reproducible positive hits. Points shown in amber were non-reproducible false positive hits.

The result of screening the two libraries demonstrates that most of the measured mutants showed lower activity than the wt enzyme (shown in purple). In the *OaACLR-Sat-293* library most mutants show an activity between 1-1.5 U mg⁻¹. The average activity of the tested mutants of this library was 1.3 ± 0.4 U mg⁻¹. For the *OaACLR-Sat-51* library similar result were observed with an average in activity of 1.5 ± 0.5 U mg⁻¹. The measurements were carried out in duplicates and the three best hits (shown in green) were selected for further analysis as discussed below. Unreproducible high activities can be explained by impurities in the assay from cell debris that were accidentally transferred into the assay solution.

8.3.3 Purification and activity of positive hits from AAER screening

The best hits from the AAER screening of the *Oa*ACLR-Sat51 library were sequenced and identified as *Oa*ACLR-A51L, *Oa*ACLR-A51V and *Oa*ACLR-A51E. For the saturation mutagenesis library in position 293 following mutation were sequenced: *Oa*ACLR-L293F, *Oa*ACLR-L293T and *Oa*ACLR-L293C. All six *Oa*ACLR mutants were purified by IMAC (Figure 110) and stored at -20°C (with 20% v/v glycerol) until further activity characterisation.

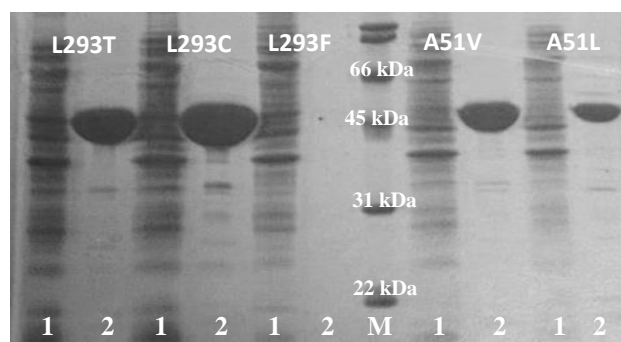


Figure 110: Purified *Oa*ACLR variants after IMAC purification. 1: cell extract, 2: purified enzyme.

Table 39: Purification yield and activity of best hits from AAER screening.

Position	Library No.	Mutation	Activity in screening assay U mg^{-1}	Purification yield (mg g^{-1})	Purification yield (mg L^{-1})
wt <i>Oa</i> ACLR			0.96 ± 0.12	0.86	3
<i>Oa</i> ACLR-A51	E12	L	1.21	0.35	1
	C8	V	1.24	0.10	0.3
<i>Oa</i> ACLR-L293	E10	E	3.29	0.22	0.9
	B3	T	2.49	2.2	6
	A2	C	1.84	1.7	5

The purification of *Oa*ACLR-L293F and *Oa*ACLR -A51E was repeated and gave yields of 0.49 mg g^{-1} , respectively 0.22 mg g^{-1} purified enzyme. The purified *Oa*ACLR mutants were used for the activity determination towards ACL and PheOMe. As the standard HPLC assay allows more accurate activity measurements it was used with purified enzymes to determine conversions for L-ACL or specific activities for L-PheOMe (Figure 111 and Figure 112).

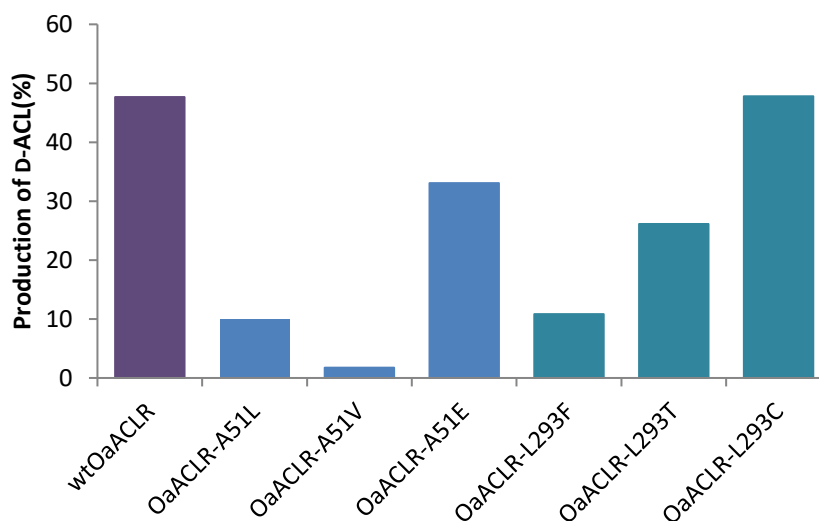


Figure 111: Conversion of L-ACL (50 mM) to D-ACL catalysed by different *OaACL R* mutants after 15 min incubation time. The reactions were carried out under standard conditions with enzyme amounts between 0.03-0.27 mg.

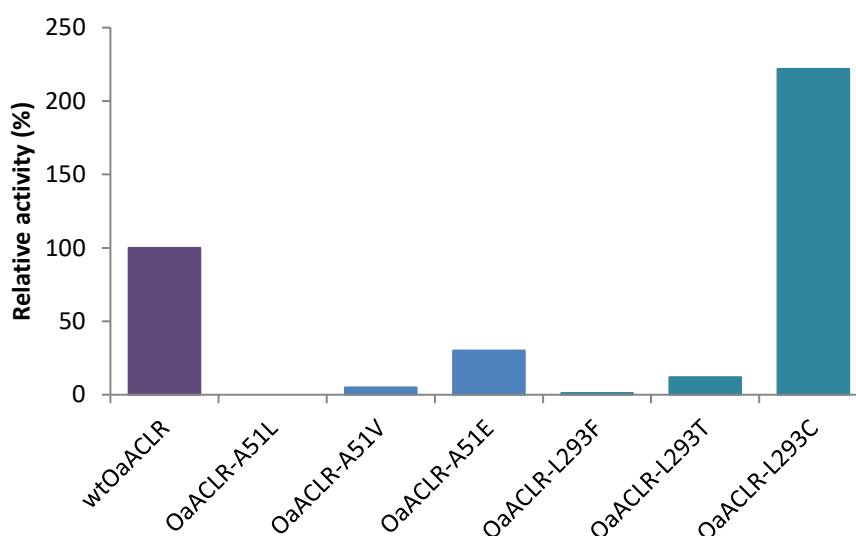


Figure 112: Relative activity of *OaACL R* mutants towards L-PheOMe (10 mM). Reactions were carried out under standard conditions with 0.06-0.22 mg enzyme. Specific activities were calculated from the production of D-PheOMe over time and the amount of enzyme used in the reaction.

All three tested mutants in the position A51 resulted in reduced activity towards ACL and PheOMe compared to wt *OaACL R*. The role of the residue in this position has been investigated in Chapter 6.3.2.1. Changing the residue in the position A51 to a tryptophan unexpectedly resulted in reduced activity rather than better substrate binding and improved activity. As discussed in the previous chapter this residue has a crucial role in substrate binding in *OaACL R*. Furthermore, the residue in this position is conserved throughout ACLRs as either alanine or tryptophan.¹⁸⁶ Therefore it is not surprising that randomly changing the residue in position 51 did not give an improved *OaACL R* variant. Substitutions to hydrophobic

side chains in *OaACLR-A51V* and *OaACLR-A51L* resulted in drastically reduced activity. It is remarkable that from these both mutations the exchange to leucine abolishes activity towards PheOMe but shows higher activity towards ACL. The bigger side chain, leucine, might improve binding of the smaller substrate ACL but sterically hinder the binding of PheOMe in the active site. Interestingly, the bulky and negatively charged residue glutamic acid was least detrimental for activity towards both substrates. Glutamic acid is a flexible residue and therefore might adapt its conformation for substrate binding.

Especially in the case of the saturation library in position 51 the quality of the library could have limited the identification of improved mutants. The coverage of 36% of the 20 amino acids in the sat-51 library is rather low for a saturation mutant library. All three selected best hits represented a mutant found when sampling the quality of the library. Altogether, this suggests that some mutations were not present in the library and therefore were not included in the screening. Additionally, the nature of the screen is somewhat limiting in finding improved mutants. Due the high background reaction in the cell lysate, the screening selects two factors: Firstly, improved AAER activity over the background reaction and secondly improved expression yield of *OaACLR* which also leads to overcoming the background. However, for following evolution rounds the background reaction would become less relevant once an improved mutant was found.

The mutations L293F and L293T lead to activity reduced *OaACLR* mutants, and *OaACLR-L293F* showed lower activity to both tested substrates. With 222% activity of the wt enzyme *OaACLR-L293C* proved to be the only activity improved variant among the tested *OaACLR* mutants. This mutant was then characterised and compared to the wt *OaACLR* as described in the next section.

8.3.4 Comparison of *OaACLR-L293C* and wt *OaACLR*

8.3.4.1 Activity and kinetic parameters of *OaACLR* and *OaACLR-L293C*

The improved *OaACLR-L293C* mutant was further characterised in its racemisation activity. At first the conversion of L-PheOMe of *OaACLR-L293C* and wt *OaACLR* was compared implementing the HPLC assay (Figure 113).

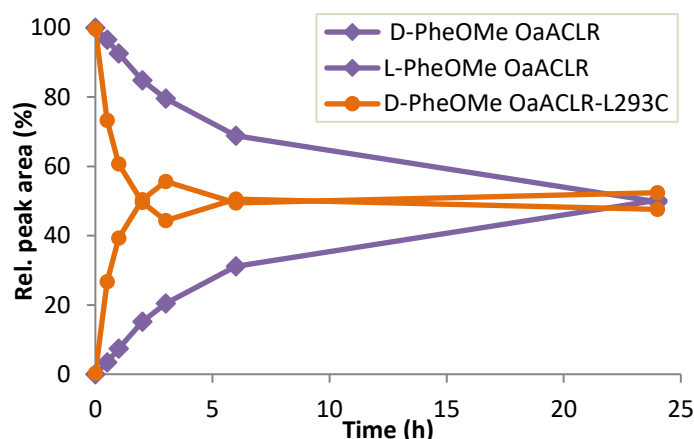


Figure 113: Conversion of L-PheOMe (10 mM) catalysed by purified *OaACLR* (0.082 mg) and *OaACLR*L293C (0.220 mg). Reactions were carried out under standard conditions in a total reaction volume of 100 μ L (100 mM KPi, pH 7.0) at 30°C for 24 h.

PheOMe was racemised much faster by *OaACLR*-L293C than by the wt enzyme. The racemisation was complete after 2 h (49.7 % D-PheOMe) when using *OaACLR*-L293C for the reaction. In contrast, the racemisation was complete after 24 h using the wt enzyme. The specific activity of *OaACLR*-L293C (28.3 U mg^{-1}) was calculated as 2.4 fold higher than for the wt enzyme (11.9 mg^{-1}). This result is in accordance with the result obtained from the assay screening in which *OaACLR*-L293C (1.8 U mg^{-1}) showed 1.8 fold activity of the wt enzyme (1.0 U mg^{-1}) in cell lysate. The faster conversion of PheOMe can be explained by a general higher activity of the new *OaACLR* variant and different inhibitory constants of the two enzymes (Table 40). However, the two enzymes were used at different concentrations for the racemisation. *OaACLR*-L293C was used in a 3.7 fold higher concentration which might be a reason for its higher activity even though specific activities were calculated. To judge the difference of the racemisation of the both enzymes, kinetic parameters for the racemisation of L-PheOMe were determined (Figure 114 and Figure 115) and summarised in Table 40. The activities for *OaACLR* and *OaACLR*-L293C were determined at different L-PheOMe concentrations and plotted according to Michaelis-Menten and substrate inhibition equations (Equation 1).

a) Michaelis-Menten equation

$$y = \frac{V_{max} * x}{K_m + x}$$

y: velocity

x: substrate concentration

V_{max} : Maximal velocity

K_m : Michaelis-Menten constant

K_i : Inhibitory constant

b) Substrate inhibition equation

$$y = \frac{V_{max} * x}{K_m + x * 1 + \frac{x}{K_i}}$$

Equation 1: Non-linear regression for curve fittings from kinetic measurements. a) Michaelis-Menten equation; b) Equation for kinetics with substrate inhibition.

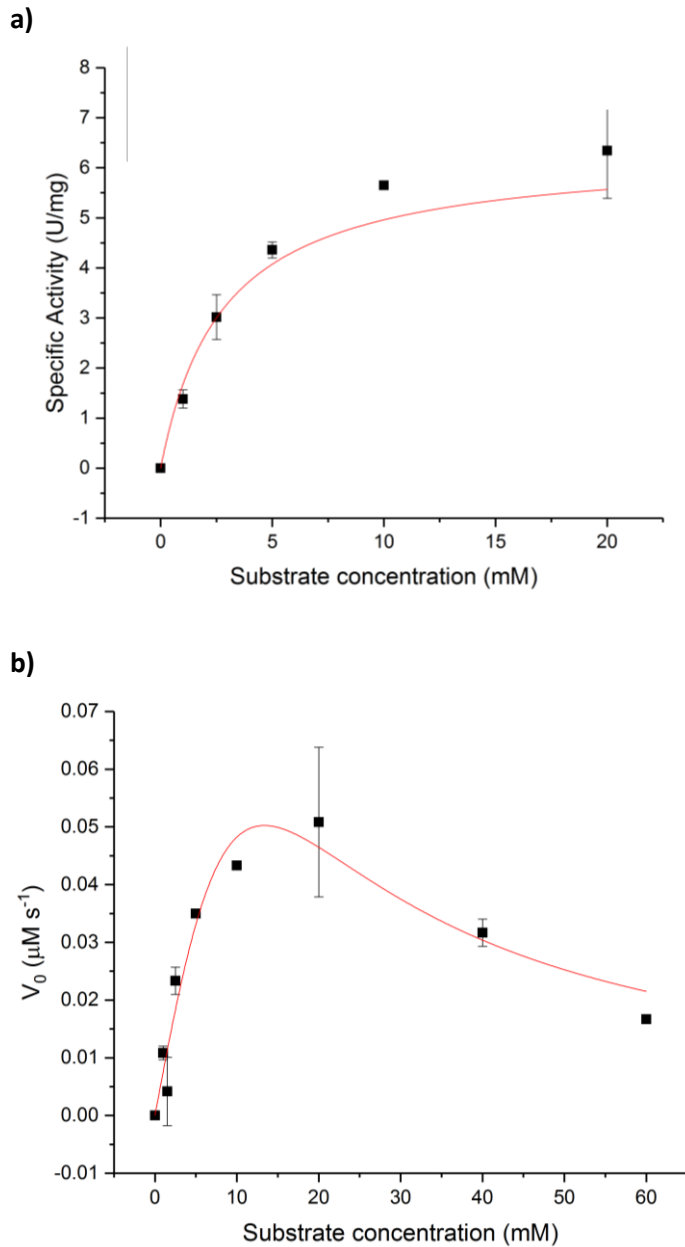


Figure 114: Non-linear regression of activities measured for *Oa*ACLR with different concentrations of L-PheOMe. Enzyme concentration in the reactions was between 0.022-0.028 mg. a) Fitting according to the Michaelis-Menten equation; b) Fitting with the substrate inhibition model.

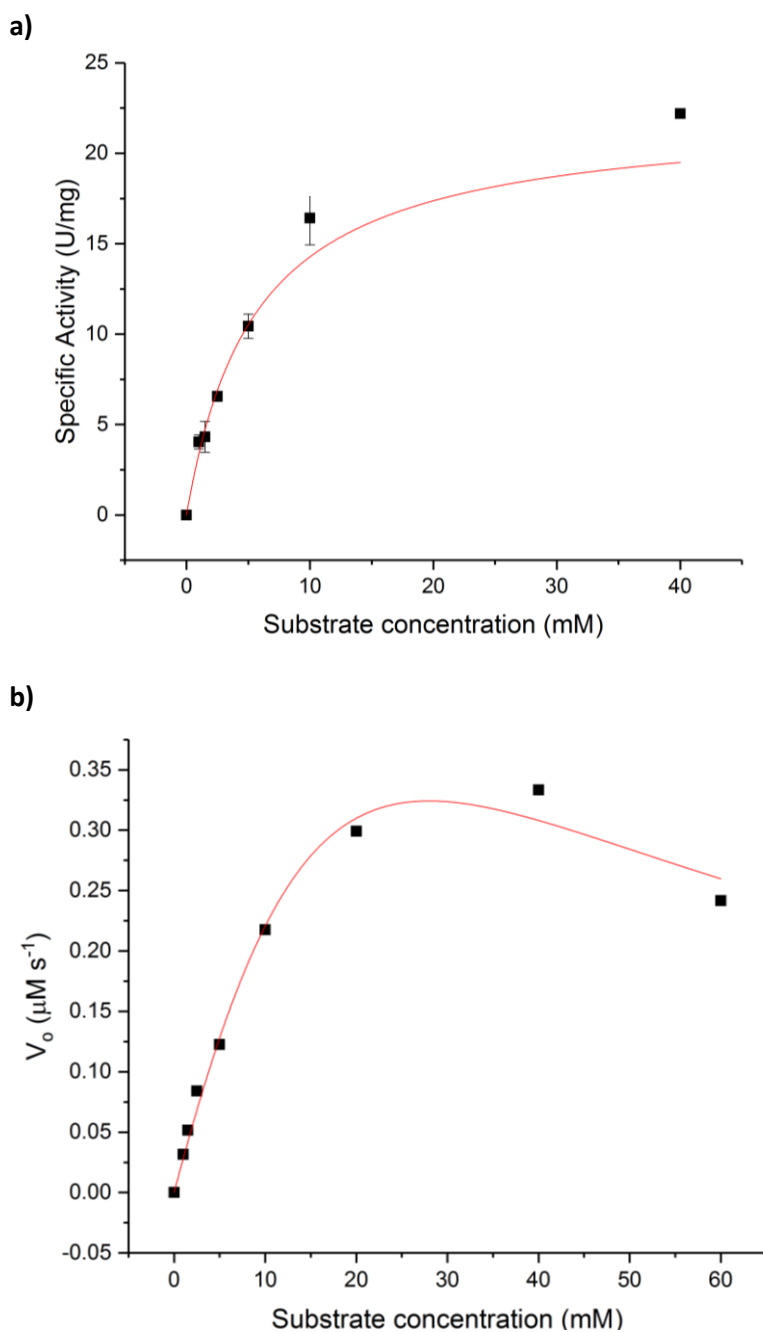


Figure 115: Non-linear regression of activities measured for *OaACLR-L293C* with different concentrations of L-PheOMe. Enzyme concentration in the reactions was between 0.022-0.028 mg. a) Fitting according to the Michaelis-Menten equation; b) Fitting with the substrate inhibition model.

Table 40: Summary of kinetic parameters determined for *OaACLR* variants towards L-PheOMe. K_m and V_{max} were obtained from non-linear fitting according to the Michaelis-Menten equation. K_{cat} and K_i were obtained from non-linear fitting according to the substrate inhibition model.

	K_m (mM)	V_{max} (U mg ⁻¹)	K_{cat} (s ⁻¹)	K_{cat}/K_m (mM ⁻¹ s ⁻¹)
<i>OaACLR</i>	2.8	6.4	0.020	0.007
<i>OaACLR-L293C</i>	5.6	22.2	0.145	0.026

The kinetic parameters clearly verify the improved activity of *Oa*ACLR-L293C. The catalytic efficiency (K_{cat}/K_m) is increased 3.7 fold for *Oa*ACLR-L293C comparing to the wt enzyme. Maximal activity for the improved variant was measured as 22.2 U mg⁻¹ at a concentration of 40 mM substrate. Contrary, V_{max} for *Oa*ACLR is 6.2 U mg⁻¹ at 20 mM substrate concentration and is 3.4 fold lower than *Oa*ACLR-L293C velocity. Substrate inhibition occurred at lower concentrations (>20 mM) and drastically affects *Oa*ACLR with a K_i of 0.35 mM. Inhibition of *Oa*ACLR-L293C was less severe (K_i 12.8 mM) and started at higher concentrations (>40 mM). A loss in activity of 67 % was observed in the wt enzyme in the range from 20 to 60 mM substrate concentration. For *Oa*ACLR-L293C substrate inhibition started at 40 mM L-PheOMe and activity decreased only 14 % in the range from 40 to 60 mM substrate concentration. Fittings with substrate inhibition gave inconsistent results, particularly for K_m and V_{max} (Appendix 10.5). Especially the modelling of the *Oa*ACLR curve for substrate inhibition gave a low R^2 value (0.94) implying that the wrong model was used. The observed inhibition might not be substrate inhibition but a competitive inhibition through the hydrolysis product of PheOMe. However, the substrate inhibition model gave the best fit as modelling to a competitive or non-competitive inhibition did not give any fits for both curves.

8.3.4.2 Substrate scope of *Oa*ACLR and *Oa*ACLR-L293C

The activity towards other amino acid derivatives was tested to evaluate the impact of the mutation L293C on the substrate scope of *Oa*ACLR (Table 41)

Table 41: Conversions of different substrates with *Oa*ACLR and *Oa*ACLR-L293C after 1 h reaction time under standard HPLC assay conditions.

Substrate	Conversion (%)	
	<i>Oa</i> ACLR	<i>Oa</i> ACLR-L293C
D-phenylglycine methylester	1.2	1.6
L-phenylglycine methylester	1.1	1.6
D-phenylalanine methylester	4.2	15.3
L-phenylalanine methylester	2.0	20.2
L-phenylalanine	0.0	0.0
L-phenylalanine amide	1.3	17.4

Comparing the conversions of different substrates with the two *Oa*ACLR variants showed that the mutation L293C resulted in an overall improved variant of *Oa*ACLR. Noticeable is that for all tested phenylalanine derivatives conversion was improved (3-13 times). The conversion of phenylglycine methylester was only slightly improved by the factor 1.5 with *Oa*ACLR-

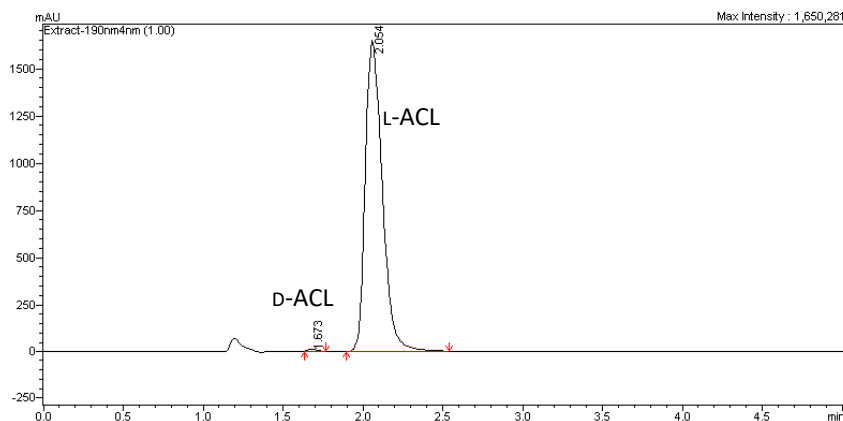
L293C. The improved activity of *Oa*ACLR-L293C did not yield activity towards phenylalanine hence the overall substrate scope was not changed. As conversions and not specific activities were measured detailed comparisons of preference for D- or L- enantiomers are difficult. As a trend, similar conversions were measured for both enantiomers suggesting that both enzymes are not enantioselective.

8.3.4.3 Discussion of the basis of the improved activity of *Oa*ACLR-L293C

Summarising the results of the characterisation of *Oa*ACLR-L293C shows that this enzyme is improved in different characteristics. The expression level of *Oa*ACLR-L293C is enhanced resulting in a two-fold higher purification yield compared to the wt enzyme. The purification yield of *Oa*ACLR-L293C (5.0 mg L^{-1}) is now even higher than the yield obtained for *Rf*ACLR (2.2 mg L^{-1}).

The determination of kinetic parameters revealed that K_m values are in the same range (2.8 and 5.6 mM) indicating similar binding affinity of the enzymes towards PheOMe. However, V_{\max} and K_{cat} are significantly improved, demonstrating the higher turnover number of *Oa*ACLR-L293C. The kinetic parameters verify a higher reactivity of the enzyme which suggests that the cysteine in position 293 might act as a more reactive catalytic acid/base residue in the catalysis. The double mutant *Oa*ACLR-D210A-L293C was generated to investigate the impact of the replacement of leucine with cysteine in the position 293 on the catalysis. As discussed in Chapter 5 aspartate in position 210 was identified as catalytic residue of *Rf*ACLR and replacement with alanine resulted in inactive enzyme. Activities of *Oa*ACLR-D210A and *Oa*ACLR-D210A-L293C were determined with ACL to test if the mutation L293C can rescue the racemisation activity of the enzyme (Figure 116).

a)



b)

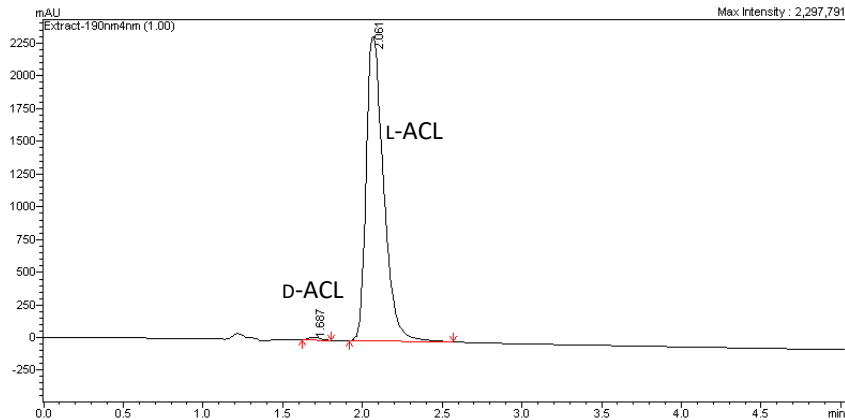


Figure 116: a) Chromatogram of conversion of L-ACL by *OaACLR-D210A* after 24 h b) Chromatogram of conversion of L-ACL by *OaACLR-D210A-L293C* after 24 h. Reactions were carried out under standard reaction conditions for the HPLC assay.

The measurement after 24 h reaction time showed a conversion of only 0.5% for both, *OaACLR-D210A* and *OaACLR-D210A-L293C*. This confirms the inactivity of both variants with the mutation D210A. The conversion of *OaACLR-D210A* variants is comparable to the low conversion of 4.4 % obtained with *RfACLR-D210A* after 24 h reaction time. This result confirms the catalytic role of D210 in ACLRs. Furthermore, the results clarify that cysteine in position 293 is not directly involved in the catalysis as activity could not be rescued by this mutation.

The previous structural analysis demonstrated that the residue in position 293 reaches from one subunit into the active site of the other subunit. The residue in position 293 is likely to be involved in the dimerization and the change of leucine to cysteine might enhance the dimer formation of the subunits. The sulphur of the cysteine could have a role in the dimer formation interactions, which also might give explanation for the increased expression level of *OaACLR-L293C*. Interestingly, the structurally similar residue threonine caused the opposite effect, it reduced expression and activity of *OaACLR-L293T*.

The case of an enhanced dimer formation of *OaACLR-L293C* might also yield improved stability. Increase of storage stability was not observed, *OaACLR-L293C* showed 88% compared to 92% residual activity of *OaACLR* after 5 weeks of storage with glycerol at -20°C. However, this condition was found as optimal storage condition (Chapter 3.3.5) and under other conditions, such as higher temperatures or in organic solvents, the stability might be different for the both enzyme variants.

8.4 Conclusion

Saturation mutagenesis libraries were cloned, expressed and screened using a high-throughput assay which was developed before (Chapter 7). Screening the mutant library of position 51 did not identify an improved mutant which might be due to the poor quality of the library or high background reactions in the screening assay. Nevertheless, characterisation of the activity of three different *OaACLR* mutations in the position 51 enabled the discussion of the role of the residue in this position. Screening a mutant library in position 293 resulted in identification of the improved variant *OaACLR-L293C*. This mutant was characterised in comparison to the wt enzyme and showed 3.4-fold improved activity towards phenylalanine methylester and an overall higher activity towards similar substrates. The new introduced cysteine in position 293 does not act as catalytic residue as demonstrated in a rescue experiment of the inactive double mutant *OaACLR-D210A-L293C*. The role of cysteine in the enhancement in activity might be facilitating dimerization of the subunits, however, this hypothesis needs to be proven by further experiments.

9 Conclusions and future work

The three main objectives of this work were firstly to clone, express and purify homologous ACLRs in order to characterise ACLRs with focus in their racemisation activity, in particular towards amino acid esters. The second objective was to investigate the reaction mechanism of ACLRs by combining structural and mutational analysis. The third objective was to use the obtained structural information for structure-guided engineering of amino acid ester racemisation activity in ACLRs.

The three homologous ACLRs, namely *Ao*ACLR, *Rf*ACLR and *Oa*ACLR, were selected to be investigated in detail within this work. These ACLRs were successfully cloned into an expression vector and optimal conditions for the heterologous overexpressed in *E. coli* cells were identified. The racemases were successfully purified by a two-step chromatography method using Ni-affinity purification and size exclusion chromatography. The enzymes were purified to high purity, however, yields were moderate with maximal 15.3 mg L⁻¹.

The activity of the purified enzymes was tested towards the L-enantiomers of ACL, phenylalanine amide and phenylalanine methylester. All three racemases show high activity towards the natural substrate ACL, but *Oa*ACLR was about 10-fold reduced in activity towards ACL. *Rf*ACLR was tested with both enantiomers of ACL and did not demonstrate a preference for one enantiomer confirming results published for *Ao*ACLR.¹⁷⁹ All three enzymes racemised phenylalanine amide, again, *Oa*ACLR activity was an order of magnitude lower than the activities determined for *Ao*ACLR and *Rf*ACLR. Interestingly, out of the three tested ACLRs, *Oa*ACLR was the only enzyme that was active towards phenylalanine methylester. This activity is of particular interest for the evolution of amino acid ester racemisation activity.

The investigation of the basis of the difference in the substrate scope of *Oa*ACLR and *Rf*ACLR is of interest to gain information for the engineering of amino acid ester racemisation activity. The structure of *Rf*ACLR complexed with ACL revealed putative catalytic residues which were later confirmed as D210 and K267. The importance for the catalysis of aspartate in position 210 was established by mutational analysis of the alanine replacement mutant *Rf*ACLR-D210A and *Oa*ACLR-D210A. Evidence for the formation of different mechanism intermediates was obtained in activity-reduced *Rf*ACLR variants. The structure of the internal aldimine was captured in the mutant *Rf*ACLR-K241A. The structure of *Rf*ACLR-D210A revealed the presence of the geminal diamine intermediate. Furthermore, the formation of the achiral quinonoid intermediate was spectrophotometrically measured in the same mutant. A

reaction mechanism *via* the formation of a geminal diamine and quinonoid was proposed based on the observed intermediates.

The structure of native *Oa*ACLR was solved and compared to *Rf*ACLR. Differences in the sequence and the conformation of active site were observed which help to explain the different substrate spectrum of the two racemases. An aromatic cage is formed in *Rf*ACLR for highly specific binding of the natural substrate ACL. Despite the specific binding site in *Rf*ACLR, the structure of *Oa*ACLR revealed a more spacious and flexible active site. The tyrosine in position 139 was found to be flexible in *Oa*ACLR whereas the conformation of the corresponding tyrosine in *Rf*ACLR was conserved in all obtained structures. Differences in the residues in position 51 (alanine or tryptophan) and 293 (leucine or methionine) were highlighted in the superposed structures of *Oa*ACLR and *Rf*ACLR. To investigate the influence of the different residue reciprocal mutagenesis of the *Rf*ACLR active site to *Oa*ACLR was carried out. Additionally, the second shell residue in position 386 was investigated as this residue might have a potential role in π -electron stacking with active site residues. The reciprocal mutagenesis experiments did not gain further insight as all generated mutants were drastically reduced in activity. Nevertheless, this stresses the importance and complexity of molecular interactions of active and non-active site residues for the full function of enzymatic catalysis.

For the semi-rational engineering of AAER activity the positions 51 and 293 were selected as targets for saturation mutagenesis to improve the amino acid ester racemisation activity in *Oa*ACLR. A photometric assay for the detection of *N*-acetyl amino acid racemisation was adapted and optimised for the detection AAER activity towards the substrate phenylalanine methylester. This assay was used for the screening of two saturation libraries of *Oa*ACLR in position 51 or 293. The screening of 192 mutants identified one improved *Oa*ACLR mutant with the replacement of L293 with cysteine. This mutant was further characterised and compared the wt enzyme showing a 3.4-fold improved reaction rate for phenylalanine methylester. *Oa*ACLR-L293C is not only improved in activity towards phenylalanine methylester, but also for phenylalanine amide or phenylglycine methylester. The determination of kinetic parameters suggests that substrate binding is similar for both enzymes but the reaction rate and catalytic efficiency is higher for *Oa*ACLR-L293C. The cysteine in position 293 does not have a catalytic role in the racemisation reaction as the double mutant *Oa*ACLR-D210A-L293C was inactive. The cysteine in position 293 is more likely to be involved in interactions between both subunits and might enhance the dimer formation.

To gain further insight into intermolecular interactions in *Oa*ACLR and the substrate binding future work could focus on obtaining a structure of the *Oa*ACLR in complex with a substrate,

especially with phenylalanine methylester. Furthermore, a more detailed characterisation of *Oa*ACLR-L293C and comparison to the wt enzyme is of interest to elucidate the basis of the improvement of AAER activity. With the hypothesis of enhanced dimerization of this mutant, investigations into the stability of the enzyme might give evidence for this theory. The gained information can be used for further rounds of structure-guided engineering to gain higher AAER activities. Other residues in the active site, such as L21, L80 or V388 could be targeted for saturation mutagenesis to improve racemisation of amino acid esters.

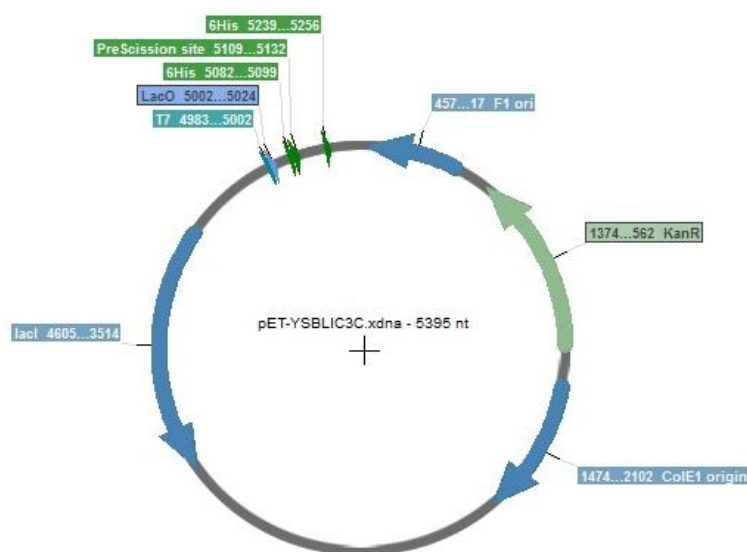
Having identified the catalytic residues, the investigation of the substrate recognition is also of interest. For the successful application of an AAE racemase in DKR towards an enantiopure amide product, it is of importance that the product is not racemised by the racemisation catalyst. Once higher AAER activity is established, residues for the amide recognition could be targeted to reduce the conversion of amino acid amides.

10 Appendix

10.1 Publication of this work

Frese, A., Sutton, P. W., Turkenburg, J. P., & Grogan, G. (2017). Snapshots of the Catalytic Cycle of the Industrial Enzyme α -Amino- ϵ -Caprolactam Racemase (ACLR) Observed Using X-ray Crystallography. *ACS Catalysis*, 7(2), 1045-1048.

10.2 Vector map of Lic3c vector



10.3 Gene sequences and corresponding amino acid sequences

1. Uniprot Q7M181: Alpha-amino-epsilon-caprolactam racemase (AAEC) from *Achromobacter obae*

>Q7M181

```
MTKALYDRDGAAGIQLKLRFFPLAISGGRGARLIEENGRELIDLSGAWGAASLGYGHPAIVAASAAAAANPAGAT
ILSASNAPAVTLAERLLASFPPEGTHKIWFHSGSDANEAAIRAIVKATGRSGVIAFAGAYHGCTVGSMAFSGHSV
QADAAKADGLILLPYDPYRNDPTGDAILTLLTEKLAAPAGSIGAAFIPIQSDGGLIVPPDGFLRFADIC
RAHGILVVCDEVKVLARSRLHCFEHEGFVPDILVLGKGLGGGLPLSAVIAPAEILDCAFAMQTLHGNPISAA
AGLAVLETIDRDDLPAMAERKGRLLRDGLSELAKRHLPIGDIRGRGLACGMELVCDRQSRPAPARAETAKLIYRAYQ
LGLVVYYVGMNGNVLEFTPPLTITETDIHKALDLDLDRAFSELSAVSNEEIAQFAGW
```

Synthetic Gene:

```
ATGACCAAAGCACTGTATGATCGTGATGGTGCAGCAATTGGTAATCTGCAGAAACTGCGTTTTTTTTCCGCTGGCAA
TTAGCGGTGGTGGTGGTGCACGCTGATTGAAGAAAATGGTTCGTGAACGATTGATCTGAGCGGTGCATGGGGTGC
AGCCAGCTGGGTTATGGTCATCCGGCAATTGTTGCAGCAGTTAGCGCAGCAGCAAAATCCGGCAGGCCAACCC
ATTCAGCGCAAGCAATGCACCGGCAGTTACCCTGGCAGAACGTCCTGCTGGCAAGCTTCCGGGTGAAGGCACCC
ATAAAATCTGGTTTTGGTCATAGCGGTAGTGATGCAAAATGAAGCAGCATAATCGTGCAATTTGTTAAAGCAACCGGTCG
TAGCGGTGTTATTGCATTTGCGGGTGCATATCATGTTGTACCGTTGGTAGCATGGCCTTTAGCGGTGCATAGTGTT
CAGGCAGATGCAGCAAAGCAGATGGTCTGATTCTGCTGCCGATCCGGATCCGATCGTCCTTATCGTAATGATC
CGACCGGTGATGCAATCTGACCCGCTGACCGAAAAACTGGCAGCAGTTCCGGCAGGTAGCATTTGGTGCAGCCTT
TATTGAACCGATTGAGAGTGATGGTGGCCTGATTGTTCCGCCTGATGGTTTTCTGCGTAAATTTGCAGATATTTGT
CGTGCCCATGGTATTTCTGGTTGTTTGTGATGAAGTTAAAGTTGGTCTGGCAGTAGCGGTCTGCTGCATTTGTTT
```

AACATGAAGTTTTTGTCCGGATATTCTGGTCTGGGTAAAGGTCTGGGTGGTGGTCTGCCGCTGAGCGCAGTTAT
 TGCTCCGGCAGAAAATCTGGATTGTCAAGCGCATTGCCATGCAGACCCTGCATGGTAATCCGATTAGTCAGCA
 GCCGGTCTGGCAGTTCTGGAAACCATTTGATCGTGACGATCTGCCTGCAATGGCCGAACGTAAGGTGCCTGCTGC
 GTGATGGTCTGTGAGAATGGCAAAACGTCATCCGCTGATTTGGTGATATTCGTGGTCCGGTCTGGCCTGTGGTAT
 GGAACCTGGTTTTGTGATCGTCAGAGCCGTGAACCGGCACGTGCAGAAAACCGCAAAACTGATTTATCGTGCCTATCAG
 CTGGGTCTGGTTGTGATTTATGTTGGTATGAATGGTAACGTGCTGGAATTTACCCCTCCGCTGACCATTACCGAAA
 CCGATATTATAAAGCACTGGATCTGCTGGATCGTGCATTTAGCGAACTGAGTGCAGTTAGCAATGAAGAAATTGC
 ACAGTTTGCAGGCTGGTAA

2. Uniprot N6UXY4: Putative PLP-dependent transaminase from *Rhizobium freirei*

>N6UXY4

MAGNLYGRDGAAGISLQKLRFFPLAVAGGQGARLVEEDGRELIDLSGAWGAASLGYGHPAIEAVSRAANPAGAS
 ILSASNAPAVALAERLTASFPRGTHKVVFGHSGSDANEAYRAITRATGRTGVIAFIGAYHGCTVGSMAFSGHSV
 QADAAKADGLILLPYPDFRYPYQDDPTGDAVLALLKERLAAVPAGSIAAAFIEPIQSDGGLIVPPDGFRLKFDIC
 RAHGISVVCDEVKVLARSRLHCFEHEGFVPDILVLGKGLGGGLPLSAVIAPAEILDCASAFAMQTLHGNPVCAA
 AGLAVLETIEAENLTTAAERKGLLREGLARLAEERHELIGDIRGRGLACGVELVRNRQSRERPARAETAKLIYRAYE
 LGLVLYYVGMNGNVLEMPPLTMTEDVRHAVNLLDQAFTELSTVSDTLVVSQFAGW

Synthetic Gene:

ATGGCAGGTAATCTGTATGGTCTGATGGTGCAGCAATTTGGTAGCCTGCAGAACTGCGTTTTTTTTCCGCTGGCAG
 TTGCCGGTGGTCAGGGTGCACGCTCGTTGAAGAAGATGGTCGCGAACTGATTGATCTGAGCGGTGCATGGGGTGC
 AGCCAGCCTGGGTTATGGTCATCCGGCAATTATTGAAGCAGTTAGCCGTGCAGCAGCAAATCCGGCAGGCGCAAGC
 ATTTCTGAGCGCAAGCAATGCACCGGCAGTTGCACTGGCAGAACGCTCTGACCGCAAGCTTTCCGGGTCTGGCACCC
 ATAAAGTTTGGTTTGGTCATAGCGGTAGTGATGCAATGAAGCAGCATACTGTCGAATTACCCGTGCAACCGGTGC
 TACCGGTGTTATTGCAATTTATTGGTGCATATCATGGTTGTACCGTTGGTAGCATGGCATTAGCGGTACATAGTGT
 CAGGCAGATGCAGCAAAAGCAGATGGTCTGATTCTGCTGCCGTATCCGGATCCGTATCGTCCGTATCAGGATGATC
 CGACCGGTGATGCAGTTCTGGCACTGCTGAAAGAACGCTGGCAGCAGTTCCGGCAGGTAGCATTGCAGCAGCCTT
 TATTGAACCGGATCAGAGTATGGTGGCCTGATTGTTCCGCCTGATGGTTTTCTGCGTAAATTTGCAGATATTTGT
 CGTGCCCATGGTATTAGCGTTGTTTTGTGATGAAGTTAAAGTTGGTCTGGCAGCAGTACCGGTCTGCATTTGTTTTG
 AACATGAAGTTTTTGTCCGGATATTCTGGTTCTGGGTAAAGGTCTGGGTGGTGGTCTGCCGCTGAGCGCAGTTAT
 TGCTCCGGCAGAAAATCTGGATTGTGCAAGCGCATTGCCATGCAGACCCTGCATGGTAATCCGGTTTTGTGCAGCC
 GCAGTCTGGCCGTTCTGGAAACCATTTGAAGCCGAAAATCTGACCACAGCAGCAGAACGTAAGGTAACCTGCTGC
 GTGAAGGCCTGGCACGCTGGCCGAACGTCATGAACGATCGGTGATATTCGTGGTCTGGTCTGGCCTGTGGTGT
 TGAACCTGGTTCTGTAATCGTCAGAGCCGTGAACCGGCACGTGCAGAAACCGCAAAACTGATTTATCGTGCATATGAA
 CTGGGTCTGGTCTGATTATGTTGGTATGAATGGTAATGTGCTGGAAATGACCCCTCCGCTGACCATGACCGAAG
 ATGAAGTTCTGCATGCAGTTAATCTGCTGGATCAGGCATTTACCGAACTGAGCACCCTTAGCGATACCTGGTTAG
 CC

3. Uniprot Q06K28: Putative amino acid amide racemase from *Ochrobactrum anthropi*

>Q06K28

MQTPLSLRERDARVIAEIGRLRFSPLSLIGGKGNRLIEEGGRSILDLSGSAGPAALGYGHPAIVEAVEKSVRDMAG
 ASLLLYPNEAAVSLAEDLLRITPGNGERRVWFHSGSDANDCAVRVLTAAKRSRIISFISYHGNLTGSMGISGH
 TAMHTLPRPGVLLLPYPDFRPRFSAEAVLELLDYHFATSCPPEQVAAVFIEPIILSDGGLVPPPAFLALQDRC
 RKHGILVVVDEVKVLGRGTGLMHCFQHEGLEPDMVVFVKGLGGGLPLSAVVGPQWMDHAPAVLQTTAGNPVATA
 AGRAVLNNTIERQGLAQRSERVGGIFADRLRRLSDKHSIIGDVRGRGLAIGVDLVSDRGSREPAPVTTTTAKIIRGY
 QLGAFTYVGLNANVLEFMPPLTLTEPEIDEAADIVDQAIGDVLGKVDSDVAHFMMW

Synthetic Gene:

ATGCAGACACCCTGAGCCTGCGTGAACGTGATGCACGTTATTGCAGAAATTTGGTCTGCTGCGTTTTTAGTCCGC
 TGAGTCTGATTGGTGGTAAAGGTAATCGTCTGATTGAAGAAGGTGGTCTGATCATTCTGGATCTGAGCGGTAGCGC
 AGGTCGGCAGCACTGGGTTATGGTCATCCGGCAATTTGTTGAAGCAGTTGAAAAAAGCGTTCTGATATGGCAGGC
 GCAACCTGCTGCTGATCCGAATGAAGCAGCAGTTAGCCTGGCAGAGATCTGCTGCGTATTACACCGGGTAATG
 GTGAACGTGCTGTTTTGGTTTGGTCAATAGCGGTAGTGATGCAATGATTTGTGAGTTCTGTTCTGACCCGACCA
 CAACGATAGCCGATATTATTAGCTTTATTTGGTAGCTATCATGGTAATCTGACCGGTAGTATGGGATATTAGCGGT
 ACCGCATGACCCATACCCCTGCCCTCGTCCGGGTGTTCTGCTGCTGCTTATCCGGATCCGTTTCGTCGCGTTTTT
 CAGCAGAAGCAGTCTGGAACCTGCTGGATTATCATTTTTGCAACCAGCTGTCCGCCTGAACAGGTTGCAGCAGTTTT
 TATTGAACCGATTCTGAGTATGGTGGTCTGGTTGTTCCGCCTCCGGCATTCTGGAAGCACTGCAGGATCGTTGT
 CGTAAACATGGTATTCTGGTTGTGGTTGATGAAGTTAAAGTTGGTCTGGGTCTGACCGGTCTGATGCATTTGTTTC
 AGCATGAGGGTCTGGAACCGGATATGGTTGTTTTTGTAAAGGCTGGGTGGTGGCCTGCCGCTGAGCCAGTTGT
 TGGTCCGAGTGGGTGATGGATCATGCACCGCATTTGTTCTGCAGACCACCGCAGGTAATCCGGTTGCCACCGCA
 GCAGTCTGTCAGTTCTGAATACCATTTGAACGTCAGGGTCTGGCACAGCGTAGCGAACGTTGTTGGTGGTATTTTTG

CAGATCGCCTGCGTCGTCTGAGCGATAAACATAGCATTATTGGTGATGTTTCGTGGTTCGTGGTCTGGCAATTGGTGT
 TGATCTGGTTAGCGATCGTGGTAGCCGTGAACCGGCACCGGTTACCACCACCGCAAAAAATCATTTATCGTGGTTAT
 CAGCTGGGTGCAGCATTACCTATGTTGGTCTGAATGCAAATGTGCTGGAATTTATGCCTCCGCTGACCCTGACCG
 AACCGAAATTGATGAAGCCGCAGATATGTTGATCAGGCAATCGGTGATGTACTGGATGGTAAAGTTGCAGATAG
 TGATGTTGCCCATTTTATGATGTGGTAA

10.4 Buffers for solubility screen

Table 42: Buffers used for solubility screen of RfACLR-W49A-M293L.

100 mM HEPES, 1 M MgSO ₄ , pH 7.0	1
100 mM HEPES, 100 mM sodium glutamate, 5 mM DTT, pH 7.0	2
100 mM HEPES, 100 mM KCl, pH 7.0	3
100 mM HEPES, 50 mM LiCl, 0.1 % CHAPS, pH 7.0	4
100 mM HEPES, 50 mM LiCl, 0.1 % deoxycholate, pH 7.0	5
100 mM HEPES, 50 mM (NH ₄) ₂ SO ₄ , 10 % glycerol, pH 7.0	6
100 mM K ₂ HPO ₄ /KH ₂ PO ₄ , 2.5 mM ZnCl ₂ , pH 4.3	7
100 mM K ₂ HPO ₄ /KH ₂ PO ₄ , 50 mM (NH ₄) ₂ SO ₄ , 0.05 % dextran sulfate, pH 6.0	8
100 mM K ₂ HPO ₄ /KH ₂ PO ₄ , 50 mM (NH ₄) ₂ SO ₄ , 1 % Triton X-10, pH 6.0	9
250 mM K ₂ HPO ₄ /KH ₂ PO ₄ , 0.1 % CHAPS, pH 6.0	10
100 mM potassium acetate, 50 mM NaCl, 0.05 % dextran sulfate, 0.1 % CHAPS, pH 5.5	11
100 mM sodium acetate, 1 M MgSO ₄ , pH 5.5	12
100 mM sodium acetate, 100 mM glutamine, 10 mM DTT, pH 5.5	13
100 mM sodium acetate, 100 mM KCl, 0.1 % <i>n</i> -octyl-β-D-glucoside, pH 5.5	14
100 mM sodium acetate, 50 mM LiCl, 5 mM CaAc, pH 5.5	15
100 mM triethanolamine, 100 mM KCl, 0.05 % dextran sulfate, pH 8.5	16
100 mM triethanolamine, 100 mM KCl, 10 mM DTT, pH 8.5	17
100 mM triethanolamine, 100 mM sodium glutamate, 0.02 % <i>n</i> -octyl-β-D-glucoside, 10% glycerol, pH 8.5	18
100 mM triethanolamine, 50 mM (NH ₄) ₂ SO ₄ , 10 mM MgSO ₄ , pH 8.5	19
100 mM triethanolamine, 50 mM LiCl, 5 mM EDTA, pH 8.5	20
100 mM Tris, 1 M (NH ₄) ₂ SO ₄ , 10 mM DTT, pH 8.2	21
100 mM Tris, 10 % glycerol, pH 7.6	22
100 mM Tris, 100 mM KCl, 0.1 % deoxycholate, 25 % glycerol, pH 7.6	23
100 mM Tris, 100 mM KCl, 2 mM EDTA, 1 % Triton X-100, pH 8.2	24
100 mM Tris, 100 mM sodium glutamate, 10 mM DTT, pH 8.5	25
100 mM Tris, 2 M NaCl, 0.1 % <i>n</i> -octyl-β-D-glucoside, pH 7.6	26
100 mM Tris, 50 mM NaCl, 10 % <i>i</i> PrOH, pH 8.2	27
100 mM Tris, 50 mM NaCl, 100 mM urea, pH 8.2	28
100 mM Tris, 50 mM NaCl, 5 mM CaAc, pH 7.6	29
100 mM Tris, 50 mM LiCl, pH 7.6	30

10.5 Data collection details for ACLR crystals

Table 43: Data collection and refinement statistics.

	Native <i>Oa</i> ACLR	Native <i>Rf</i> ACLR	<i>Rf</i> ACLR- <i>PheNH</i> ₂ Complex	<i>Rf</i> ACLR	<i>Rf</i> ACLR-K241	<i>Rf</i> ACLR-D210A
Ligand	No ligand	No ligand	PheNH ₂	L/D-ACL internal aldimine	ACL geminal diamine	ACL external aldimine
Data collection statistics						
Beamline	i04	i02	i04	i04	i04-1	i02
Wavelength Å	0.97949	0.97949	0.97949	0.97949	0.92819	0.97949
Space group	<i>P</i> 2 ₁ 1	<i>C</i> 2 ₁	<i>C</i> 2 ₁	<i>C</i> 2 ₁	<i>C</i> 2 ₁	<i>C</i> 2 ₁
Unit cell (Å)	a= 64.6 b= 135.0 c= 88.6 α=γ= 90.0, β=90.3	a= 87.6; b=76.5; c=58.6, α=γ= 90.0, β=113.1	a= 87.6 b= 76.8 c= 58.7 α=γ= 90.0, β=113.5	a= 87.7; b=77.7; c=57.6, α=γ= 90.0, β=112.7	a= 86.2; b=79.1; c=59.0, α=γ= 90.0, β=112.8	a= 86.1 b= 77.5 c= 58.5 α=γ= 90.0, β=113.7
Resolution Å	64.0–2.00 (2.06-2.00)	55.47-1.56 (1.77-1.56)	55.5-1.40 (1.45-1.40)	45.03-1.51 (1.54-1.51)	45.79-1.50 (1.53- 1.50)	55.27-1.93 (1.99- 1.86)
Unique reflections	105379 (8554)	49972 (3696)	66102 (6871)	55609 (2734)	57829 (2836)	29415 (2171)
Completeness (%)	98.5 (98.6)	98.9 (99.8)	98.1 (86.9)	99.6 (99.8)	99.2 (99.8)	99.3 (99.7)
Multiplicity	4.2 (4.3)	4.0 (4.1)	3.9 (2.6)	4.1 (4.2)	4.1 (4.2)	4.0 (4.0)
R _{merge}	0.11 (0.72)	0.06 (0.70)	0.07 (0.18)	0.03 (0.06)	0.03 (0.22)	0.22 (0.88)
R _{pim}	0.09 (0.53)	0.05 (0.60)	0.06 (0.14)	0.02 (0.05)	0.02 (0.18)	0.18 (0.74)
<i>I</i> /σ (<i>I</i>) ^a	7.6 (2.1)	12.0 (1.8)	21.0 (5.0)	33.9 (17.6)	26.1 (5.9)	4.9 (1.3)

Appendix

Refinement statistics						
R _{cryst} (%)	19.5	15.0	19.1	16.2	14.0	19.6
R _{free} (%)	23.0	18.5	23.1	19.5	16.7	25.0
Root mean square bond lengths (Å)	0.014	0.02	0.024	0.03	0.03	0.02
Root mean square bond angles (degree)	1.55	2.12	2.23	2.4	2.5	2.0
Average B main chain (Å ²)	28	17	12	13	14	13
Average B side chain (Å ²)	32	22	15	16	17	16
Average B water (Å ²)	32	32	25	26	26	16
Average B ligand (Å ²)	-	-	31	18	21	17

10.6 Separation of substrate enantiomers by chiral HPLC

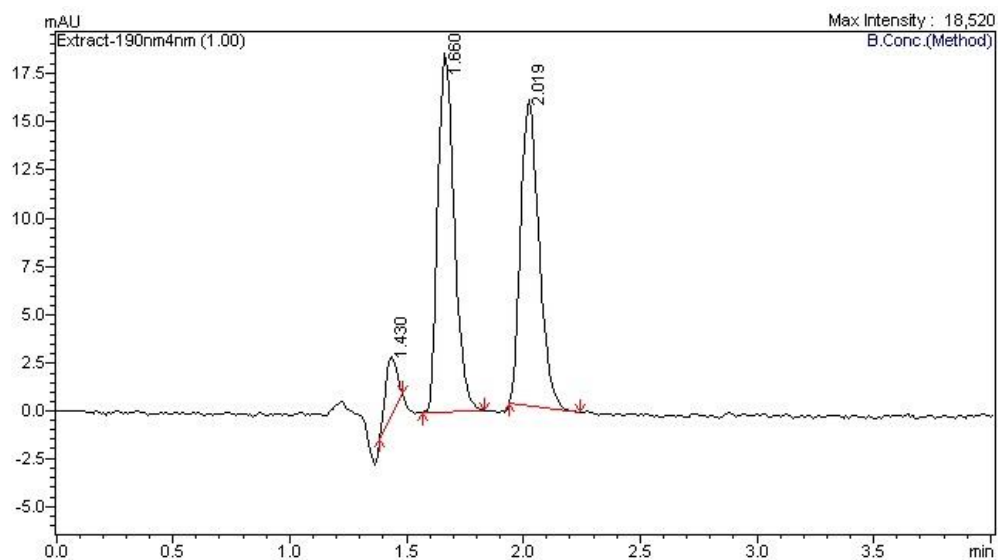


Figure 117: Separation of a mixture of D/L-ACL by chiral HPLC.

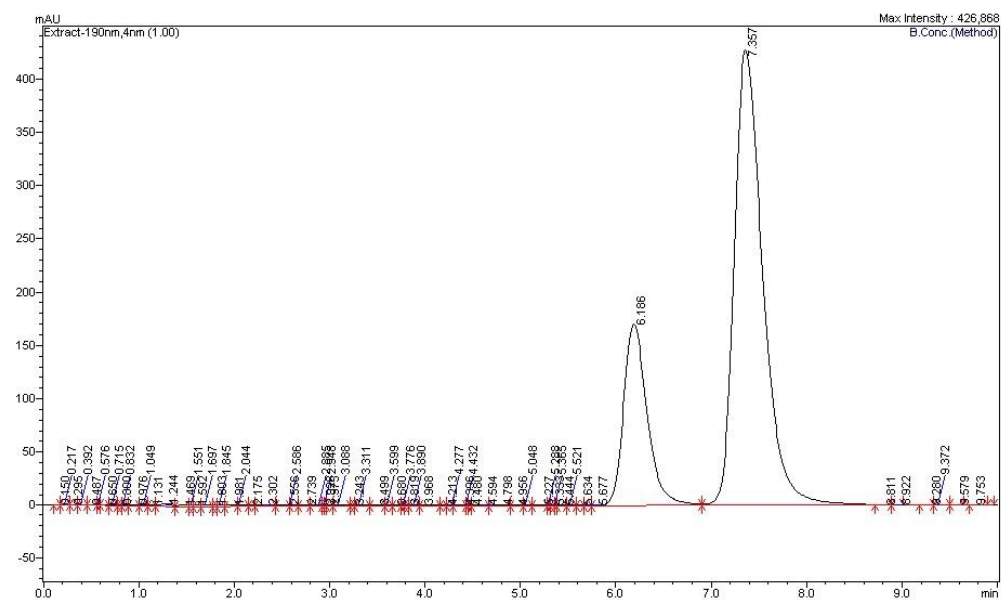


Figure 118: Separation of a mixture of D/L-PheNH₂ by chiral HPLC.

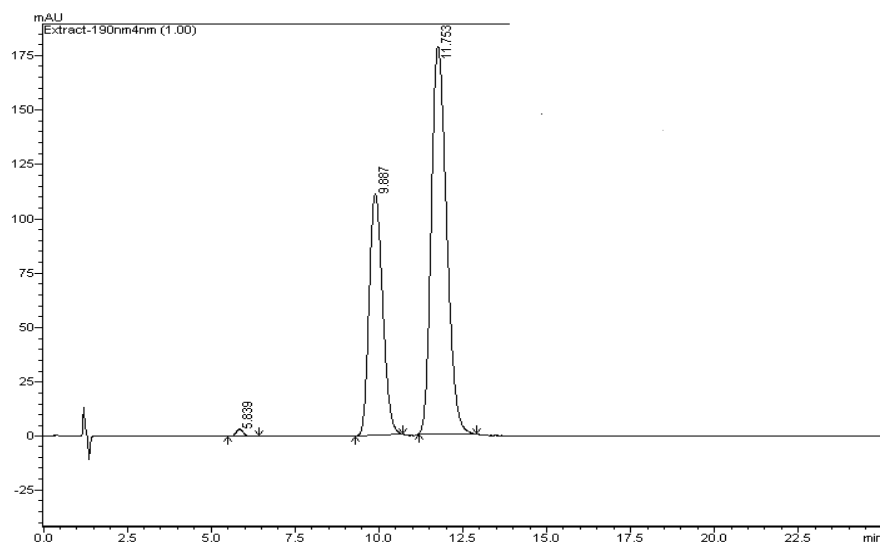


Figure 119: Separation of a mixture of D/L-PheOMe by chiral HPLC.

10.7 Kinetic parameters of *Oa*ACLR-L293C and *Oa*ACLR

Table 44: Kinetic parameters obtained from curves with non-linear fitting according to the Michaelis-Menten equation.

	K_m (mM)	V_{max} ($\mu M^{-1} s$)	K_i (mM)
<i>Oa</i> ACLR	2.8	0.05	n.d.
<i>Oa</i> ACLR-L293C	5.6	0.34	n.d.

Table 45: Kinetic parameters obtained from curves with non-linear fitting according to the substrate inhibition equation.

	K_m (mM)	V_{max} ($\mu M^{-1} s$)	K_i (mM)
<i>Oa</i> ACLR	464.7	3.5	0.38
<i>Oa</i> ACLR-L293C	60.8	1.7	12.9

Abbreviations

3D	Three-dimensional
AAO	Amino acid oxidase
API	Active pharmaceutical ingredient
AAE	Amino acid ester
°C	Degree Celsius
C(C)E	Crude cell extract
BCA	Bicinchoninic acid
BSA	Bovine serum albumin
BSAAR	Broad spectrum amino acid racemase
bp	Base pair
cm	Centimetre
CV	Column volume
ϵ	Extinction coefficient
<i>ee</i>	Enantiomeric excess
DOPA	L-3,4-dihydroxyphenylalanine
FAD	Flavin adenine dinucleotide
FT	Flow through
G	Guanine
GABA	γ -aminobutyric acid
HRP	Horse radish peroxidase
IPTG	Isopropyl β -D-1-thiogalactopyranoside
K	Keto
L	Litre
LIC	Ligation independent cloning
LB medium	Lysogeny broth
μ L	Microlitre
min	Minutes
MeOH	Methanol

mM	millimolar
mL	Millilitre
MWM	Molecular weight marker
N	Nucleotide
NAAR	N-Acetyl amino acid racemase
NAMN	Nicotinic acid mononucleotide
n.d.	not determined
nm	Nanometres
OD	Optical density
PAGE	Polyacrylamide gel electrophoresis
PEG	Polyethylene glycol
PMP	Pyridoxamine 5' phosphate
Rpm	Rounds per minute
SDS	Sodium dodecyl sulfate
Sp	Species
Subsp	Subspecies
T	Thymine
TA	Transaminase
TLC	Thin layer chromatography
TB medium	Terrific broth
U	Units
w/v	weight per volume

References

1. Soda, K.; Yoshimura, T.; Esaki, N., Stereospecificity for the hydrogen transfer of pyridoxal enzyme reactions. *Chem Rec* 2001, 1 (5), 373-384.
2. Heyl, D.; Harris, S. A.; Folkers, K., The Chemistry of Vitamin-B6 .6. Pyridoxylamino Acids. *J Am Chem Soc* 1948, 70 (10), 3429-3431.
3. Heyl, D.; Luz, E.; Harris, S. A.; Folkers, K., Phosphates of the Vitamin-B6 Group .3. Pyridoxamine Phosphate. *J Am Chem Soc* 1951, 73 (7), 3436-3437.
4. Wada, H.; Snell, E. E., Enzymatic Transamination of Pyridoxamine .2. Crystalline Pyridoxamine-Pyruvate Transaminase. *J Biol Chem* 1962, 237 (1), 133-&.
5. Eliot, A. C.; Kirsch, J. F., Pyridoxal phosphate enzymes: Mechanistic, structural, and evolutionary considerations. *Annu Rev Biochem* 2004, 73, 383-415.
6. Finkelstein, J. D.; Mudd, S. H.; Laster, L.; Irreverre, F., Homocystinuria Due to Cystathionine Synthetase Deficiency - Mode of Inheritance. *Science* 1964, 146 (364), 785-&.
7. Rios, A.; Amyes, T. L.; Richard, J. P., Formation and stability of organic zwitterions in aqueous solution: Enolates of the amino acid glycine and its derivatives. *J Am Chem Soc* 2000, 122 (39), 9373-9385.
8. Toney, M. D., Controlling reaction specificity in pyridoxal phosphate enzymes. *Bba-Proteins Proteom* 2011, 1814 (11), 1407-1418.
9. Dunathan, H. C., Conformation and Reaction Specificity in Pyridoxal Phosphate Enzymes. *P Natl Acad Sci USA* 1966, 55 (4), 712-&.
10. Jansonius, J. N.; Eichele, G.; Ford, G. C.; Kirsch, J. F.; Picot, D.; Thaller, C.; Vincent, M. G.; Christen, P.; Gehring, H.; Kirsten, H., Conformational-Changes during Catalysis by Mitochondrial Aspartate-Aminotransferase. *Fed Proc* 1981, 40 (6), 1757-1757.
11. Kirsch, J. F.; Eichele, G.; Ford, G. C.; Vincent, M. G.; Jansonius, J. N.; Gehring, H.; Christen, P., Mechanism of Action of Aspartate-Aminotransferase Proposed on the Basis of Its Spatial Structure. *J Mol Biol* 1984, 174 (3), 497-525.
12. Jansonius, J. N.; Eichele, G.; Ford, G. C.; Kirsch, J. F.; Picot, D.; Thaller, C.; Vincent, M. G.; Gehring, H.; Christen, P., 3 Dimensional Structure of Mitochondrial Aspartate-Aminotransferase and Some Functional-Derivatives - Implications for Its Mode of Action. *Biochem Soc T* 1984, 12 (3), 424-427.
13. Toney, M. D., Reaction specificity in pyridoxal phosphate enzymes. *Arch Biochem Biophys* 2005, 433 (1), 279-287.
14. Toney, M. D.; Hohenester, E.; Keller, J. W.; Jansonius, J. N., Structural and Mechanistic Analysis of 2 Refined Crystal-Structures of the Pyridoxal Phosphate-Dependent Enzyme Dialkylglycine Decarboxylase. *J Mol Biol* 1995, 245 (2), 151-179.
15. Sun, S. X.; Zabinski, R. F.; Toney, M. D., Reactions of alternate substrates demonstrate stereoelectronic control of reactivity in dialkylglycine decarboxylase. *Biochemistry-US* 1998, 37 (11), 3865-3875.
16. Malashkevich, V. N.; Strop, P.; Keller, J. W.; Jansonius, J. N.; Toney, M. D., Crystal structures of dialkylglycine decarboxylase inhibitor complexes. *J Mol Biol* 1999, 294 (1), 193-200.
17. Shaw, J. P.; Petsko, G. A.; Ringe, D., Determination of the structure of alanine racemase from *Bacillus stearothermophilus* at 1.9-angstrom resolution. *Biochemistry-US* 1997, 36 (6), 1329-1342.
18. Sun, S. X.; Toney, M. D., Evidence for a two-base mechanism involving tyrosine-265 from arginine-219 mutants of alanine racemase. *Biochemistry-US* 1999, 38 (13), 4058-4065.
19. Auld, D. S.; Bruice, T. C., Catalytic Reactions Involving Azomethines .7. Rates and Equilibria of Aldimine Formation with 3-Hydroxypyridine-4-Aldehyde and Alanine. *J Am Chem Soc* 1967, 89 (9), 2083-&.

20. Dixon, J. E.; Bruice, T. C., Comparison of Rate Constants for General Base-Catalyzed Prototropy and Racemization of Aldimine Species Formed from 3-Hydroxypyridine-4-Carboxaldehyde and Alanine. *Biochemistry-U.S.* 1973, *12* (23), 4762-4766.
21. Snell, E. E., Chemical Structure in Relation to Biological Activities of Vitamin-B6. *Vitam Horm* 1958, *16*, 77-125.
22. Seebeck, F. P.; Hilvert, D., Conversion of a PLP-dependent racemase into an aldolase by a single active site mutation. *J Am Chem Soc* 2003, *125* (34), 10158-10159.
23. Wang, N. C.; Lee, C. Y., Enhanced transaminase activity of a bifunctional L-aspartate 4-decarboxylase. *Biochem Biophys Res Commun* 2007, *356* (2), 368-373.
24. Graber, R.; Kasper, P.; Malashkevich, V. N.; Strop, P.; Gehring, H.; Jansonius, J. N.; Christen, P., Conversion of aspartate aminotransferase into an L-aspartate beta-decarboxylase by a triple active-site mutation. *J Biol Chem* 1999, *274* (44), 31203-31208.
25. Steffen-Munzberg, F.; Vickers, C.; Kohls, H.; Land, H.; Mallin, H.; Nobili, A.; Skalden, L.; van den Bergh, T.; Joosten, H. J.; Berglund, P.; Hohne, M.; Bornscheuer, U. T., Bioinformatic analysis of a PLP-dependent enzyme superfamily suitable for biocatalytic applications. *Biotechnol Adv* 2015, *33* (5), 566-604.
26. Catazaro, J.; Caprez, A.; Guru, A.; Swanson, D.; Powers, R., Functional evolution of PLP-dependent enzymes based on active-site structural similarities. *Proteins-Structure Function and Bioinformatics* 2014, *82* (10), 2597-2608.
27. Kern, A. D.; Oliveira, M. A.; Coffino, P.; Hackert, M. L., Structure of mammalian ornithine decarboxylase at 1.6 angstrom resolution: stereochemical implications of PLP-dependent amino acid decarboxylases. *Struct Fold Des* 1999, *7* (5), 567-581.
28. Milano, T.; Paiardini, A.; Grgurina, I.; Pascarella, S., Type I pyridoxal 5'-phosphate dependent enzymatic domains embedded within multimodular nonribosomal peptide synthetase and polyketide synthase assembly lines. *Bmc Struct Biol* 2013, *13*.
29. Capitani, G.; De Biase, D.; Aurizi, C.; Gut, H.; Bossa, F.; Grutter, M. G., Crystal structure and functional analysis of Escherichia coli glutamate decarboxylase. *Embo J* 2003, *22* (16), 4027-4037.
30. Sandmeier, E.; Hale, T. I.; Christen, P., Multiple Evolutionary Origin of Pyridoxal-5'-Phosphate-Dependent Amino-Acid Decarboxylases. *Eur J Biochem* 1994, *221* (3), 997-1002.
31. Momany, C.; Ernst, S.; Ghosh, R.; Chang, N. L.; Hackert, M. L., Crystallographic Structure of a Plp-Dependent Ornithine Decarboxylase from Lactobacillus-30a to 3.0 Angstrom Resolution. *J Mol Biol* 1995, *252* (5), 643-655.
32. Jansonius, J. N., Structure, evolution and action of vitamin B-6-dependent enzymes. *Curr Opin Struct Biol* 1998, *8* (6), 759-769.
33. Asada, Y.; Tanizawa, K.; Nakamura, K.; Moriguchi, M.; Soda, K., Stereochemistry of Ornithine Decarboxylase Reaction. *J Biochem-Tokyo* 1984, *95* (1), 277-282.
34. Asada, Y.; Tanizawa, K.; Sawada, S.; Suzuki, T.; Misono, H.; Soda, K., Stereochemistry of Meso-Alpha,Epsilon-Diaminopimelate Decarboxylase Reaction - the 1st Evidence for Pyridoxal 5'-Phosphate Dependent Decarboxylation with Inversion of Configuration. *Biochemistry-U.S.* 1981, *20* (24), 6881-6886.
35. Jackson, F. R., Prokaryotic and Eukaryotic Pyridoxal-Dependent Decarboxylases Are Homologous. *J Mol Evol* 1990, *31* (4), 325-329.
36. Christenson, J. G.; Dairman, W.; Udenfriend, S., Preparation and Properties of a Homogeneous Aromatic L-Amino Acid Decarboxylase from Hog Kidney. *Arch Biochem Biophys* 1970, *141* (1), 356-+.
37. Facchini, P. J.; Huber-Allanach, K. L.; Tari, L. W., Plant aromatic L-amino acid decarboxylases: evolution, biochemistry, regulation, and metabolic engineering applications. *Phytochemistry* 2000, *54* (2), 121-138.
38. Jakobs, C.; Jaeken, J.; Gibson, K. M., Inherited Disorders of Gaba-Metabolism. *J Inherit Metab Dis* 1993, *16* (4), 704-715.

39. Komatsuzaki, N.; Nakamura, T.; Kimura, T.; Shima, J., Characterization of glutamate decarboxylase from a high gamma-aminobutyric acid (GABA)-producer, *Lactobacillus paracasei*. *Biosci Biotech Bioch* 2008, *72* (2), 278-285.
40. Lundquist, I.; Panagiotidis, G.; Stenstrom, A., Effect of L-Dopa Administration on Islet Monoamine-Oxidase Activity and Glucose-Induced Insulin Release in the Mouse. *Pancreas* 1991, *6* (5), 522-527.
41. Songstad, D. D.; Deluca, V.; Brisson, N.; Kurz, W. G. W.; Nessler, C. L., High-Levels of Tryptamine Accumulation in Transgenic Tobacco Expressing Tryptophan Decarboxylase. *Plant Physiol* 1990, *94* (3), 1410-1413.
42. Berlin, J.; Rugenhagen, C.; Kuzovkina, I. N.; Fecker, L. F.; Sasse, F., Are Tissue-Cultures of *Peganum-Harmala* a Useful Model System for Studying How to Manipulate the Formation of Secondary Metabolites. *Plant Cell Tiss Org* 1994, *38* (2-3), 289-297.
43. Lee, S. G.; Hong, S. P.; Sung, M. H., Development of an enzymatic system for the production of dopamine from catechol, pyruvate, and ammonia. *Enzyme Microb Tech* 1999, *25* (3-5), 298-302.
44. Huang, J.; Mei, L. H.; Xia, J., Application of artificial neural network coupling particle swarm optimization algorithm to biocatalytic production of GABA. *Biotechnol Bioeng* 2007, *96* (5), 924-931.
45. Komatsuzaki, N.; Shima, J.; Kawamoto, S.; Momose, H.; Kimura, T., Production of gamma-aminobutyric acid (GABA) by *Lactobacillus paracasei* isolated from traditional fermented foods. *Food Microbiol* 2005, *22* (6), 497-504.
46. Plokhov, A. Y.; Gusyatiner, M. M.; Yampolskaya, T. A.; Kaluzhsky, V. E.; Sukhareva, B. S.; Schulga, A. A., Preparation of gamma-aminobutyric acid using E-coli cells with high activity of glutamate decarboxylase. *Appl Biochem Biotech* 2000, *88* (1-3), 257-265.
47. Kim, H. J.; Kim, Y. H.; Shin, J. H.; Bhatia, S. K.; Sathiyarayanan, G.; Seo, H. M.; Choi, K. Y.; Yang, Y. H.; Park, K., Optimization of Direct Lysine Decarboxylase Biotransformation for Cadaverine Production with Whole-Cell Biocatalysts at High Lysine Concentration. *J Microbiol Biotechn* 2015, *25* (7), 1108-1113.
48. Guan, C. G.; Ribeiro, A.; Akkermans, A. D. L.; Jing, Y. X.; vanKammen, A.; Bisseling, T.; Pawloski, K., Nitrogen metabolism in actinorhizal nodules of *Alnus glutinosa*: Expression of glutamine synthetase and acetylornithine transaminase. *Plant Mol Biol* 1996, *32* (6), 1177-1184.
49. de la Torre, F.; De Santis, L.; Suarez, M. F.; Crespillo, R.; Canovas, F. M., Identification and functional analysis of a prokaryotic-type aspartate aminotransferase: implications for plant amino acid metabolism. *Plant J* 2006, *46* (3), 414-425.
50. Stewart, J. D., Dehydrogenases and transaminases in asymmetric synthesis. *Curr Opin Chem Biol* 2001, *5* (2), 120-129.
51. Hwang, B. Y.; Cho, B. K.; Yun, H.; Koteswar, K.; Kim, B. G., Revisit of aminotransferase in the genomic era and its application to biocatalysis. *J Mol Catal B-Enzym* 2005, *37* (1-6), 47-55.
52. Malik, M. S.; Park, E. S.; Shin, J. S., Features and technical applications of omega-transaminases. *Appl Microbiol Biot* 2012, *94* (5), 1163-1171.
53. Kelly, S. A.; Pohle, S.; Wharry, S.; Mix, S.; Allen, C. C. R.; Moody, T. S.; Gilmore, B. F., Application of omega-Transaminases in the Pharmaceutical Industry. *Chem Rev* 2017, *118* (1), 349-367.
54. Grishin, N. V.; Phillips, M. A.; Goldsmith, E. J., Modeling of the Spatial Structure of Eukaryotic Ornithine Decarboxylases. *Protein Sci* 1995, *4* (7), 1291-1304.
55. Iwasaki, A.; Yamada, Y.; Kizaki, N.; Ikenaka, Y.; Hasegawa, J., Microbial synthesis of chiral amines by (R)-specific transamination with *Arthrobacter* sp KNK168. *Appl Microbiol Biot* 2006, *69* (5), 499-505.

56. Koszelewski, D.; Tauber, K.; Faber, K.; Kroutil, W., omega-Transaminases for the synthesis of non-racemic alpha-chiral primary amines. *Trends Biotechnol* 2010, 28 (6), 324-332.
57. Schatzle, S.; Hohne, M.; Redestad, E.; Robins, K.; Bornscheuer, U. T., Rapid and Sensitive Kinetic Assay for Characterization of omega-Transaminases. *Anal Chem* 2009, 81 (19), 8244-8248.
58. Hwang, B. Y.; Kim, B. G., High-throughput screening method for the identification of active and enantioselective omega-transaminases. *Enzyme Microb Tech* 2004, 34 (5), 429-436.
59. Faulkner, A.; Turner, J. M., Microbial Metabolism of Amino Alcohols - Aminoacetone Metabolism Via 1-Aminopropan-2-ol in *Pseudomonas* Sp Ncib 8858. *Biochem J* 1974, 138 (2), 263-276.
60. Jones, A.; Faulkner, A.; Turner, J. M., Microbial Metabolism of Amino Alcohols - Metabolism of Ethanolamine and 1-Aminopropan-2-ol in Species of *Erwinia* and Roles of Amino Alcohol Kinase and Amino Alcohol O-Phosphate Phospho-Lyase in Aldehyde Formation. *Biochem J* 1973, 134 (4), 959-968.
61. Veiga-da-Cunha, M.; Hadi, F.; Balligand, T.; Stroobant, V.; Van Schaftingen, E., Molecular Identification of Hydroxylysine Kinase and of Ammoniophospholyases Acting on 5-Phosphohydroxy-L-lysine and Phosphoethanolamine. *J Biol Chem* 2012, 287 (10), 7246-7255.
62. Cuetos, A.; Steffen-Munsberg, F.; Sanchez, J. M.; Frese, A.; Bornscheuer, U. T.; Hohne, M.; Grogan, G., Structural Basis for Phospholyase Activity of a Class III Transaminase Homologue. *ChemBiochem* 2016, 17 (24), 2308-2311.
63. Paiardini, A.; Contestabile, R.; D'Aguzzo, S.; Pascarella, S.; Bossa, F., Threonine aldolase and alanine racemase: novel examples of convergent evolution in the superfamily of vitamin B-6-dependent enzymes. *Bba-Proteins Proteom* 2003, 1647 (1-2), 214-219.
64. Samland, A. K.; Sprenger, G. A., Microbial aldolases as C-C bonding enzymes - unknown treasures and new developments. *Appl Microbiol Biot* 2006, 71 (3), 253-264.
65. Jungerma.Ka; Schmidt, W.; Kirchnia.Fh; Rupprech.Eh; Thauer, R. K., Glycine Formation Via Threonine and Serine Aldolase - Its Interrelation with Pyruvate Formate Lyase Pathway of One-Carbon Unit Synthesis in *Clostridium-Kluyveri*. *Eur J Biochem* 1970, 16 (3), 424-&.
66. Liu, J. Q.; Dairi, T.; Itoh, N.; Kataoka, M.; Shimizu, S.; Yamada, H., Diversity of microbial threonine aldolases and their application. *J Mol Catal B-Enzym* 2000, 10 (1-3), 107-115.
67. Nishiyama, T.; Kajimoto, T.; Mohile, S. S.; Hayama, N.; Otsuda, T.; Ozeki, M.; Node, M., The first enantioselective synthesis of imino-deoxydigitoxose and protected imino-digitoxose by using L-threonine aldolase-catalyzed aldol condensation. *Tetrahedron-Asymmetr* 2009, 20 (2), 230-234.
68. Nishiyama, T.; Mohile, S. S.; Kajimoto, T.; Node, M., Synthesis of thymine polyoxin C by using L-threonine aldolase-catalyzed aldol reaction. *Heterocycles* 2007, 71 (6), 1397-+.
69. Seebeck, F. P.; Guainazzi, A.; Amoreira, C.; Baldrige, K. K.; Hilvert, D., Stereoselectivity and expanded substrate scope of an engineered PLP-dependent aldolase. *Angew Chem Int Edit* 2006, 45 (41), 6824-6826.
70. Toscano, M. D.; Muller, M. M.; Hilvert, D., Enhancing activity and controlling stereoselectivity in a designed PLP-dependent aldolase. *Angew Chem Int Edit* 2007, 46 (24), 4468-4470.
71. Murphy, C. D.; O'Hagan, D.; Schaffrath, C., Identification of a PLP-dependent threonine transaldolase: a novel enzyme involved in 4-fluorothreonine biosynthesis in *Streptomyces cattleya*. *Angew Chem Int Edit* 2001, 40 (23), 4479-+.
72. Nozaki, H.; Kuroda, S.; Watanabe, K.; Yokozeki, K., Gene Cloning of alpha-Methylserine Aldolase from *Variovorax paradoxus* and Purification and Characterization of the Recombinant Enzyme. *Biosci Biotech Bioch* 2008, 72 (10), 2580-2588.

73. Tai, C. H.; Cook, P. F., Pyridoxal 5'-phosphate dependent alpha,beta-elimination reactions: Mechanism of O-acetylserine sulfhydrylase. *Accounts Chem Res* 2001, 34 (1), 49-59.
74. Du, Y. L.; Singh, R.; Alkhalaf, L. M.; Kuatsjah, E.; He, H. Y.; Eltis, L. D.; Ryan, K. S., A pyridoxal phosphate-dependent enzyme that oxidizes an unactivated carbon-carbon bond. *Nat Chem Biol* 2016, 12 (3), 194-199.
75. Singh, S.; Madzellan, P.; Banerjee, R., Properties of an unusual heme cofactor in PLP-dependent cystathionine beta-synthase. *Nat Prod Rep* 2007, 24 (3), 631-639.
76. Kabil, O.; Toaka, S.; LoBrutto, R.; Shoemaker, R.; Banerjee, R., Pyridoxal phosphate binding sites are similar in human heme-dependent and yeast heme-independent cystathionine beta-synthases - Evidence from P-31 NMR and pulsed EPR spectroscopy that heme and PLP cofactors are not proximal in the human enzyme. *J Biol Chem* 2001, 276 (22), 19350-19355.
77. Hernandez, S. B.; Cava, F., Environmental roles of microbial amino acid racemases. *Environ Microbiol* 2016, 18 (6), 1673-1685.
78. Corrigan, J. J., D-Amino Acids in Animals. *Science* 1969, 164 (3876), 142-&.
79. Montecucchi, P. C.; Henschen, A., Amino-Acid-Composition and Sequence-Analysis of Sauvagine, a New Active Peptide from the Skin of Phyllomedusa-Sauvagei. *Int J Pept Prot Res* 1981, 18 (2), 113-120.
80. Fujii, N.; Saito, T., Homochirality and life. *Chem Rec* 2004, 4 (5), 267-278.
81. Kaneko, I.; Yamada, N.; Sakuraba, Y.; Kamenosono, M.; Tutumi, S., Suppression of Mitochondrial Succinate-Dehydrogenase, a Primary Target of Beta-Amyloid, and Its Derivative Racemized at Ser Residue. *J Neurochem* 1995, 65 (6), 2585-2593.
82. Lin, C. H.; Yang, H. T.; Chiu, C. C.; Lane, H. Y., Blood levels of D-amino acid oxidase vs. D-amino acids in reflecting cognitive aging. *Sci Rep-Uk* 2017, 7.
83. Kawasaki, N.; Benner, R., Bacterial release of dissolved organic matter during cell growth and decline: Molecular origin and composition. *Limnol Oceanogr* 2006, 51 (5), 2170-2180.
84. Amelung, W.; Zhang, X.; Flach, K. W., Amino acids in grassland soils: Climatic effects on concentrations and chirality. *Geoderma* 2006, 130 (3-4), 207-217.
85. Kaufman, D. S.; Miller, G. H., Overview of Amino-Acid Geochronology. *Comp Biochem Phys B* 1992, 102 (2), 199-204.
86. Klumb, K.; Matzenauer, C.; Reckert, A.; Lehmann, K.; Ritz-Timme, S., Age estimation based on aspartic acid racemization in human sclera. *Int J Legal Med* 2016, 130 (1), 207-211.
87. Ebbers, E. J.; Ariaans, G. J. A.; Houbiers, J. P. M.; Bruggink, A.; Zwanenburg, B., Controlled racemization of optically active organic compounds: Prospects for asymmetric transformation. *Tetrahedron* 1997, 53 (28), 9417-9476.
88. Schnell, B.; Faber, K.; Kroutil, W., Enzymatic racemisation and its application to synthetic biotransformations. *Adv Synth Catal* 2003, 345 (6-7), 653-666.
89. Yamada, S.; Hongo, C.; Yoshioka, R.; Chibata, I., Method for the Racemization of Optically-Active Amino-Acids. *Journal of Organic Chemistry* 1983, 48 (6), 843-846.
90. Cuesta, S. M.; Furnham, N.; Rahman, S. A.; Sillitoe, I.; Thornton, J. M., The evolution of enzyme function in the isomerases. *Curr Opin Struc Biol* 2014, 26, 121-130.
91. Femmer, C.; Bechtold, M.; Roberts, T. M.; Panke, S., Exploiting racemases. *Appl Microbiol Biot* 2016, 100 (17), 7423-7436.
92. Yoshimura, T.; Esaki, N., Amino acid racemases: Functions and mechanisms. *J Biosci Bioeng* 2003, 96 (2), 103-109.
93. Servi, S.; Tessaro, D.; Pedrocchi-Fantoni, G., Chemo-enzymatic deracemization methods for the preparation of enantiopure non-natural alpha-amino acids. *Coordin Chem Rev* 2008, 252 (5-7), 715-726.
94. Pellissier, H., Dynamic kinetic resolution. *Tetrahedron* 2003, 59 (42), 8291-8327.

95. Huerta, F. F.; Minidis, A. B. E.; Backvall, J. E., Racemisation in asymmetric synthesis. Dynamic kinetic resolution and related processes in enzyme and metal catalysis. *Chem Soc Rev* 2001, 30 (6), 321-331.
96. Gruber, C. C.; Lavandera, I.; Faber, K.; Kroutil, W., From a racemate to a single enantiomer: Deracemization by stereoinversion. *Adv Synth Catal* 2006, 348 (14), 1789-1805.
97. Fee, J. A.; Hegeman, G. D.; Kenyon, G. L., Mandelate Racemase from *Pseudomonas-Putida* - Subunit Composition and Absolute Divalent Metal-Ion Requirement. *Biochemistry-U.S.* 1974, 13 (12), 2528-2532.
98. Neidhart, D. J.; Howell, P. L.; Petsko, G. A.; Powers, V. M.; Li, R. S.; Kenyon, G. L.; Gerlt, J. A., Mechanism of the Reaction Catalyzed by Mandelate Racemase .2. Crystal-Structure of Mandelate Racemase at 2.5-Å Resolution - Identification of the Active-Site and Possible Catalytic Residues. *Biochemistry-U.S.* 1991, 30 (38), 9264-9273.
99. Stecher, H.; Felfer, U.; Faber, K., Large-scale production of Mandelate racemase by *Pseudomonas putida* ATCC 12633: Optimization of enzyme induction and development of a stable crude enzyme preparation. *J Biotechnol* 1997, 56 (1), 33-40.
100. Strauss, U. T.; Kandelbauer, A.; Faber, K., Stabilization and activity-enhancement of mandelate racemase from *Pseudomonas putida* ATCC 12336 by immobilization. *Biotechnol Lett* 2000, 22 (6), 515-520.
101. Maggio, E. T.; Kenyon, G. L.; Mildvan, A. S.; Hegeman, G. D., Mandelate Racemase from *Pseudomonas-Putida* - Magnetic-Resonance and Kinetic Studies of Mechanism of Catalysis. *Biochemistry-U.S.* 1975, 14 (6), 1131-1139.
102. Felfer, U.; Goriup, M.; Koegl, M. E.; Wagner, U.; Larissegger-Schnell, B.; Faber, K.; Kroutil, W., The substrate spectrum of mandelate racemase: Minimum structural requirements for substrates and substrate model. *Adv Synth Catal* 2005, 347 (7-8), 951-961.
103. Hegeman, G. D.; Rosenber.Ey; Kenyon, G. L., Mandelic Acid Racemase from *Pseudomonas-Putida* - Purification and Properties of Enzyme. *Biochemistry-U.S.* 1970, 9 (21), 4029-&.
104. Li, R. S.; Powers, V. M.; Kozarich, J. W.; Kenyon, G. L., Racemization of Vinylglycolate Catalyzed by Mandelate Racemase. *Journal of Organic Chemistry* 1995, 60 (11), 3347-3351.
105. Strauss, U. T.; Faber, K., Deracemization of (+/-)-mandelic acid using a lipase-mandelate racemase two-enzyme system. *Tetrahedron-Asymmetr* 1999, 10 (21), 4079-4081.
106. Tatum, E. L.; Peterson, W. H.; Fred, E. B., Enzymic racemization of optically active lactic acid. *Biochem J* 1936, 30, 1892-1897.
107. Tatum, E. L.; Peterson, W. H.; Fred, E. B., Effect of associated growth on forms of lactic acid produced by certain bacteria. *Biochem J* 1932, 26, 846-852.
108. Hino, T.; Kuroda, S., Presence of Lactate-Dehydrogenase and Lactate Racemase in *Megasphaera-Elsdenii* Grown on Glucose or Lactate. *Applied and environmental microbiology* 1993, 59 (1), 255-259.
109. Stetter, K. O.; Kandler, O., Formation of DL-Lactic Acid by Lactobacilli and Characterization of a Lactic-Acid Racemase from Several Streptobacteria. *Arch Mikrobiol* 1973, 94 (3), 221-247.
110. Desguin, B.; Goffin, P.; Viaene, E.; Kleerebezem, M.; Martin-Diaconescu, V.; Maroney, M. J.; Declercq, J. P.; Soumillion, P.; Hols, P., Lactate racemase is a nickel-dependent enzyme activated by a widespread maturation system. *Nat Commun* 2014, 5.
111. Pepple, J. S.; Dennis, D., Lactate Racemase - Hydroxylamine-Dependent O-18 Exchange of Alpha-Hydroxyl of Lactic-Acid. *Biochim Biophys Acta* 1976, 429 (3), 1036-1040.
112. Desguin, B.; Goffin, P.; Bakouche, N.; Diman, A.; Viaene, E.; Dandoy, D.; Fontaine, L.; Hallet, B.; Hols, P., Enantioselective Regulation of Lactate Racemization by LarR in *Lactobacillus plantarum*. *J Bacteriol* 2015, 197 (1), 219-230.

113. Desguin, B.; Zhang, T.; Soumillion, P.; Hols, P.; Hu, J.; Hausinger, R. P., A tethered niacin-derived pincer complex with a nickel-carbon bond in lactate racemase. *Science* 2015, *349* (6243), 66-69.
114. Goffin, P.; Deghorain, M.; Mainardi, J. L.; Tytgat, I.; Champomier-Verges, M. C.; Kleerebezem, M.; Hols, P., Lactate racemization as a rescue pathway for supplying D-lactate to the cell wall biosynthesis machinery in *Lactobacillus plantarum*. *J Bacteriol* 2005, *187* (19), 6750-6761.
115. Billotklein, D.; Gutmann, L.; Sable, S.; Guittet, E.; Vanheijenoort, J., Modification of Peptidoglycan Precursors Is a Common Feature of the Low-Level Vancomycin-Resistant Vanb-Type Enterococcus D366 and of the Naturally Glycopeptide-Resistant Species *Lactobacillus-Casei*, *Pediococcus-Pentosaceus*, *Leuconostoc-Mesenteroides*, and *Enterococcus-Gallinarum*. *J Bacteriol* 1994, *176* (8), 2398-2405.
116. Handwerker, S.; Pucci, M. J.; Volk, K. J.; Liu, J. P.; Lee, M. S., Vancomycin-Resistant *Leuconostoc-Mesenteroides* and *Lactobacillus-Casei* Synthesize Cytoplasmic Peptidoglycan Precursors That Terminate in Lactate. *J Bacteriol* 1994, *176* (1), 260-264.
117. Zhang, X. Y.; Chung, L. W., Alternative Mechanistic Strategy for Enzyme Catalysis in a Ni-Dependent Lactate Racemase (LarA): Intermediate Destabilization by the Cofactor. *Chem-Eur J* 2017, *23* (15), 3623-3630.
118. Shrestha, R.; Lockless, S. W.; Sorg, J. A., A *Clostridium difficile* alanine racemase affects spore germination and accommodates serine as a substrate. *J Biol Chem* 2017, *292* (25), 10735-10742.
119. Tassoni, R.; van der Aart, L. T.; Ubbink, M.; Van Wezel, G. P.; Pannu, N. S., Structural and functional characterization of the alanine racemase from *Streptomyces coelicolor* A3(2). *Biochem Bioph Res Co* 2017, *483* (1), 122-128.
120. Nakatani, Y.; Opel-Reading, H. K.; Merker, M.; Machado, D.; Andres, S.; Kumar, S. S.; Moradigaravand, D.; Coll, F.; Perdigao, J.; Portugal, I.; Schon, T.; Nair, D.; Devi, K. R. U.; Kohl, T. A.; Beckert, P.; Clark, T. G.; Maphalala, G.; Khumalo, D.; Diel, R.; Klaos, K.; Aung, H. L.; Cook, G. M.; Parkhill, J.; Peacock, S. J.; Swaminathan, S.; Viveiros, M.; Niemann, S.; Krause, K. L.; Koser, C. U., Role of Alanine Racemase Mutations in *Mycobacterium tuberculosis* D-Cycloserine Resistance. *Antimicrob Agents Ch* 2017, *61* (12).
121. Wasserman, S. A.; Daub, E.; Grisafi, P.; Botstein, D.; Walsh, C. T., Catabolic Alanine Racemase from *Salmonella-Typhimurium* - DNA-Sequence, Enzyme-Purification, and Characterization. *Biochemistry-US* 1984, *23* (22), 5182-5187.
122. Willies, S. C.; White, J. L.; Turner, N. J., Development of a high-throughput screening method for racemase activity and its application to the identification of alanine racemase variants with activity towards L-arginine. *Tetrahedron* 2012, *68* (37), 7564-7567.
123. Harada, N.; Nishiyama, S.; Sato, K.; Tsukada, H., Development of an automated synthesis apparatus for L-[3-C-11] labeled aromatic amino acids. *Appl Radiat Isotopes* 2000, *52* (4), 845-850.
124. Fisher, S. L., Glutamate racemase as a target for drug discovery. *Microb Biotechnol* 2008, *1* (5), 345-360.
125. Israyilova, A.; Buroni, S.; Forneris, F.; Scoffone, V. C.; Shixaliyev, N. Q.; Riccardi, G.; Chiarelli, L. R., Biochemical Characterization of Glutamate Racemase - A New Candidate Drug Target against *Burkholderia cenocepacia* Infections. *PloS one* 2016, *11* (11).
126. Poen, S.; Nakatani, Y.; Opel-Reading, H. K.; Lasse, M.; Dobson, R. C. J.; Krause, K. L., Exploring the structure of glutamate racemase from *Mycobacterium tuberculosis* as a template for anti-mycobacterial drug discovery. *Biochem J* 2016, *473*, 1267-1280.
127. Malapati, P.; Krishna, V. S.; Nallangi, R.; Meda, N.; Srilakshmi, R. R.; Sriram, D., Lead identification and optimization of bacterial glutamate racemase inhibitors. *Bioorgan Med Chem* 2018, *26* (1), 177-190.

128. Lundqvist, T.; Fisher, S. L.; Kern, G.; Folmer, R. H. A.; Xue, Y. F.; Newton, D. T.; Keating, T. A.; Alm, R. A.; de Jonge, B. L. M., Exploitation of structural and regulatory diversity in glutamate racemases. *Nature* 2007, 447 (7146), 817-822.
129. Yagasaki, M.; Ozaki, A.; Hashimoto, Y., Enzymatic Production of D-Glu from L-Glu by *Lactobacillus-Brevis* Atcc-8287. *Biosci Biotech Bioch* 1993, 57 (9), 1499-1502.
130. Yagasaki, M.; Azuma, M.; Ishino, S.; Ozaki, A., Enzymatic Production of D-Glutamate from L-Glutamate by a Glutamate Racemase. *J Ferment Bioeng* 1995, 79 (1), 70-72.
131. Oikawa, T.; Watanabe, M.; Makiura, H.; Kusakabe, H.; Yamade, K.; Soda, K., Production of D-glutamate from L-glutamate with glutamate racemase and L-glutamate oxidase. *Biosci Biotech Bioch* 1999, 63 (12), 2168-2173.
132. Bae, H. S.; Lee, S. G.; Hong, S. P.; Kwak, M. S.; Esaki, N.; Soda, K.; Sung, M. H., Production of aromatic D-amino acids from alpha-keto acids and ammonia by coupling of four enzyme reactions. *J Mol Catal B-Enzym* 1999, 6 (3), 241-247.
133. Bae, H. S.; Hong, S. P.; Lee, S. G.; Kwak, M. S.; Esaki, N.; Sung, M. H., Application of a thermostable glutamate racemase from *Bacillus* sp SK-1 for the production of D-phenylalanine in a multi-enzyme system. *J Mol Catal B-Enzym* 2002, 17 (6), 223-233.
134. Asano, Y.; Endo, K., Amino-Acid Racemase with Broad Substrate-Specificity, Its Properties and Use in Phenylalanine Racemization. *Appl Microbiol Biot* 1988, 29 (6), 523-527.
135. Inagaki, K.; Tanizawa, K.; Tanaka, H.; Soda, K., Purification and Characterization of Amino-Acid Racemase with Very Broad Substrate-Specificity from *Aeromonas-Caviae*. *Agr Biol Chem Tokyo* 1987, 51 (1), 173-180.
136. Lim, Y. H.; Yokoigawa, K.; Esaki, N.; Soda, K., A New Amino-Acid Racemase with Threonine Alpha-Epimerase Activity from *Pseudomonas-Putida* - Purification and Characterization. *J Bacteriol* 1993, 175 (13), 4213-4217.
137. Miyamoto, T.; Katane, M.; Saitoh, Y.; Sekine, M.; Homma, H., Identification and characterization of novel broad-spectrum amino acid racemases from *Escherichia coli* and *Bacillus subtilis*. *Amino Acids* 2017, 49 (11), 1885-1894.
138. Espallat, A.; Carrasco-Lopez, C.; Bernardo-Garcia, N.; Pietrosevoli, N.; Otero, L. H.; Alvarez, L.; de Pedro, M. A.; Pazos, F.; Davis, B. M.; Waldor, M. K.; Hermoso, J. A.; Cava, F., Structural basis for the broad specificity of a new family of amino-acid racemases. *Acta Crystallogr D* 2014, 70, 79-90.
139. Ishiwata, K. I.; Fukuhara, N.; Shimada, M.; Makiguchi, N.; Soda, K., Enzymatic Production of L-Tryptophan from DL-Serine and Indole by a Coupled Reaction of Tryptophan Synthase and Amino-Acid Racemase. *Biotechnol Appl Bioc* 1990, 12 (2), 141-149.
140. Yorifuji, T.; Ogata, K.; Soda, K., Arginine Racemase of *Pseudomonas Graveolens* .1. Purification, Crystallization, and Properties. *J Biol Chem* 1971, 246 (16), 5085-&.
141. Matsui, D.; Oikawa, T., Detection and Function of the Intramolecular Disulfide Bond in Arginine Racemase: An Enzyme with Broad Substrate Specificity. *Chem Biodivers* 2010, 7 (6), 1591-1602.
142. Tani, Y.; Miyake, R.; Yukami, R.; Dekishima, Y.; China, H.; Saito, S.; Kawabata, H.; Mihara, H., Functional expression of L-lysine alpha-oxidase from *Scomber japonicus* in *Escherichia coli* for one-pot synthesis of L-pipecolic acid from DL-lysine. *Appl Microbiol Biot* 2015, 99 (12), 5045-5054.
143. He, M., Pipecolic acid in microbes: biosynthetic routes and enzymes. *J Ind Microbiol Biot* 2006, 33 (6), 401-407.
144. Kourist, R.; Miyauchi, Y.; Uemura, D.; Miyamoto, K., Engineering the Promiscuous Racemase Activity of an Arylmalonate Decarboxylase. *Chem-Eur J* 2011, 17 (2), 557-563.
145. Gasmeyer, S. K.; Yoshikawa, H.; Enoki, J.; Hulsemann, N.; Stoll, R.; Miyamoto, K.; Kourist, R., STD-NMR-Based Protein Engineering of the Unique Arylpropionate-Racemase AMDase G74C. *ChemBiochem* 2015, 16 (13), 1943-1949.

146. Busch, F.; Enoki, J.; Hulsemann, N.; Miyamoto, K.; Bocola, M.; Kourist, R., Semiempirical QM/MM calculations reveal a step-wise proton transfer and an unusual thiolate pocket in the mechanism of the unique arylpropionate racemase AMDase G74C. *Catal Sci Technol* 2016, *6* (13), 4937-4944.
147. Cecere, F., Galli, G., Della Penna, G., Rappuoli, B., German Patent DE 2422737. 1976.
148. May, O.; Verseck, S.; Bommarius, A.; Drauz, K., Development of dynamic kinetic resolution processes for biocatalytic production of natural and nonnatural L-amino acids. *Org Process Res Dev* 2002, *6* (4), 452-457.
149. Lickefett, H.; Krohn, K.; Konig, W. A.; Gehrcke, B.; Sylдатk, C., Enantioseparation of 5-Monosubstituted Hydantoins by Capillary Gas-Chromatography - Investigation of Chemical and Enzymatic Racemization. *Tetrahedron-Asymmetr* 1993, *4* (6), 1129-1135.
150. Ishikawa, T.; Watabe, K.; Mukohara, Y.; Nakamura, H., Mechanism of stereospecific conversion of DL-5-substituted hydantoins to the corresponding L-amino acids by *Pseudomonas* sp strain NS671. *Biosci Biotech Bioch* 1997, *61* (1), 185-187.
151. Wiese, A.; Pietzsch, M.; Sylдатk, C.; Mattes, R.; Altenbuchner, J., Hydantoin racemase from *Arthrobacter aurescens* DSM 3747: heterologous expression, purification and characterization. *J Biotechnol* 2000, *80* (3), 217-230.
152. Sylдатk, C.; May, O.; Altenbuchner, J.; Mattes, R.; Siemann, M., Microbial hydantoinases - industrial enzymes from the origin of life? *Appl Microbiol Biot* 1999, *51* (3), 293-309.
153. Wilms, B.; Wiese, A.; Sylдатk, C.; Mattes, R.; Altenbuchner, J., Development of an *Escherichia coli* whole cell biocatalyst for the production of L-amino acids. *J Biotechnol* 2001, *86* (1), 19-30.
154. May, O.; Nguyen, P. T.; Arnold, F. H., Inverting enantioselectivity by directed evolution of hydantoinase for improved production of L-methionine. *Nat Biotechnol* 2000, *18* (3), 317-320.
155. Martinez-Rodriguez, S.; Andujar-Sanchez, M.; Neira, J. L.; Clemente-Jimenez, J. M.; Jara-Perez, V.; Rodriguez-Vico, F.; Heras-Vazquez, F. J. L., Site-directed mutagenesis indicates an important role of cysteines 76 and 181 in the catalysis of hydantoin racemase from *Sinorhizobium meliloti*. *Protein Sci* 2006, *15* (12), 2729-2738.
156. Suzuki, S.; Onishi, N.; Yokozeki, K., Purification and characterization of hydantoin racemase from *Microbacterium liquefaciens* AJ 3912. *Biosci Biotech Bioch* 2005, *69* (3), 530-536.
157. Heras-Vazquez, F. J. L.; Martinez-Rodriguez, S.; Mingorance-Cazorla, L.; Clemente-Jimenez, J. M.; Rodriguez-Vico, F., Overexpression and characterization of hydantoin racemase from *Agrobacterium tumefaciens* C58. *Biochem Bioph Res Co* 2003, *303* (2), 541-547.
158. Vanderdrift, L.; Vogels, G. D.; Vanderdrift, C., Allantoin Racemase - New Enzyme from *Pseudomonas* Species. *Biochim Biophys Acta* 1975, *391* (1), 240-248.
159. French, J. B.; Neau, D. B.; Ealick, S. E., Characterization of the Structure and Function of *Klebsiella pneumoniae* Allantoin Racemase. *J Mol Biol* 2011, *410* (3), 447-460.
160. Rodriguez-Alonso, M. J.; Clemente-Jimenez, J. M.; Rodriguez-Vico, F.; Heras-Vazquez, F. J. L., Rational re-design of the "double-racemase hydantoinase process" for optically pure production of natural and non-natural L-amino acids. *Biochem Eng J* 2015, *101*, 68-76.
161. Soriano-Maldonado, P.; Rodriguez-Alonso, M. J.; Hernandez-Cervantes, C.; Rodriguez-Garcia, I.; Clemente-Jimenez, J. M.; Rodriguez-Vico, F.; Martinez-Rodriguez, S.; Heras-Vazquez, F. J. L., Amidohydrolase Process: Expanding the use of L-N-carbamoylase/N-succinyl-amino acid racemase tandem for the production of different optically pure L-amino acids. *Process Biochem* 2014, *49* (8), 1281-1287.

162. Bommarius, A. S.; Drauz, K.; Klenk, H.; Wandrey, C., Operational Stability of Enzymes - Acylase-Catalyzed Resolution of N-Acetyl Amino-Acids to Enantiomerically Pure L-Amino-Acids. *Ann Ny Acad Sci* 1992, 672, 126-136.
163. Tokuyama, S.; Hatano, K.; Takahashi, T., Discovery of a Novel Enzyme, N-Acylamino Acid Racemase in an Actinomycete - Screening, Isolation, and Identification. *Biosci Biotech Bioch* 1994, 58 (1), 24-27.
164. Takahashi, T., Hatano, K., *EP 304021 B1* 1989.
165. Matsuyama, A., Tokuzama, S., *EP 1130108 A1* 2001.
166. Tokuyama, S.; Hatano, K., Cloning, DNA-Sequencing and Heterologous Expression of the Gene for Thermostable N-Acylamino Acid Racemase from *Amycolatopsis Sp Ts-1-60* in *Escherichia-Coli*. *Appl Microbiol Biot* 1995, 42 (6), 884-889.
167. Tokuyama, S.; Hatano, K., Purification and Properties of Thermostable N-Acylamino Acid Racemase from *Amycolatopsis Sp Ts-1-60*. *Appl Microbiol Biot* 1995, 42 (6), 853-859.
168. Palmer, D. R. J.; Garrett, J. B.; Sharma, V.; Meganathan, R.; Babbitt, P. C.; Gerlt, J. A., Unexpected divergence of enzyme function and sequence: "N-acylamino acid racemase" is o-succinylbenzoate synthase. *Biochemistry-Us* 1999, 38 (14), 4252-4258.
169. Sakai, A.; Xiang, D. F.; Xu, C. F.; Song, L.; Yew, W. S.; Raushel, F. M.; Gerlt, J. A., Evolution of enzymatic activities in the enolase superfamily: N-succinylamino acid racemase and a new pathway for the irreversible conversion of D- to L-amino acids. *Biochemistry-Us* 2006, 45 (14), 4455-4462.
170. Pozo-Dengra, J.; Martinez-Gomez, A. I.; Martinez-Rodriguez, S.; Clemente-Jimenez, J. M.; Rodriguez-Vico, F.; Heras-Vazquez, F. J. L., Racemization study on different N-acetylamino acids by a recombinant N-succinylamino acid racemase from *Geobacillus kaustophilus* CECT4264. *Process Biochem* 2009, 44 (8), 835-841.
171. Wang, W. C.; Chiu, W. C.; Hsu, S. K.; Wu, C. L.; Chen, C. Y.; Liu, J. S.; Hsu, W. H., Structural basis for catalytic racemization and substrate specificity of an N-Acylamino acid racemase homologue from *Deinococcus radiodurans*. *J Mol Biol* 2004, 342 (1), 155-169.
172. Thoden, J. B.; Ringia, E. A. T.; Garrett, J. B.; Gerlt, J. A.; Holden, H. M.; Rayment, I., Evolution of enzymatic activity in the enolase superfamily: Structural studies of the promiscuous o-succinylbenzoate synthase from *Amycolatopsis*. *Biochemistry-Us* 2004, 43 (19), 5716-5727.
173. Verseck, S.; Bommarius, A.; Kula, M. R., Screening, overexpression and characterization of an N-acylamino acid racemase from *Amycolatopsis orientalis* subsp *lurida*. *Appl Microbiol Biot* 2001, 55 (3), 354-361.
174. Baxter, S.; Royer, S.; Grogan, G.; Brown, F.; Holt-Tiffin, K. E.; Taylor, I. N.; Fotheringham, I. G.; Campopiano, D. J., An Improved Racemase/Acylase Biotransformation for the Preparation of Enantiomerically Pure Amino Acids. *J Am Chem Soc* 2012, 134 (47), 19310-19313.
175. Sanchez-Carron, G.; Fleming, T.; Holt-Tiffin, K. E.; Campopiano, D. J., Continuous Colorimetric Assay That Enables High-Throughput Screening of N-Acetylamino Acid Racemases. *Anal Chem* 2015, 87 (7), 3923-3928.
176. Soriano-Maldonado, P.; Las Heras-Vazquez, F.; Clemente-Jimenez, J. M.; Rodriguez-Vico, F.; Martinez-Rodriguez, S., Enzymatic dynamic kinetic resolution of racemic N-formyl- and N-carbamoyl-amino acids using immobilized L-N-carbamoylase and N-succinyl-amino acid racemase. *Appl Microbiol Biot* 2015, 99 (1), 283-291.
177. Fukumura, T., Enzymatic Conversion of DL-Alpha-Amino-Epsilon-Caprolactam into L-Lysine .4. Partial-Purification and Some Properties of Alpha-Amino-Epsilon-Caprolactam-Racemizing Enzyme from *Achromobacter-Obae*. *Agr Biol Chem Tokyo* 1977, 41 (8), 1509-1510.
178. Crosby, J., Synthesis of Optically-Active Compounds - a Large-Scale Perspective. *Tetrahedron* 1991, 47 (27), 4789-4846.

179. Ahmed, S. A.; Esaki, N.; Tanaka, H.; Soda, K., Racemization of Alpha-Amino-Delta-Valerolactam Catalyzed by Alpha-Amino-Epsilon-Caprolactam Racemase from *Achromobacter-Obae*. *Agr Biol Chem Tokyo* 1983, 47 (5), 1149-1150.
180. Ahmed, S. A.; Esaki, N.; Tanaka, H.; Soda, K., L-Alpha-Amino-Beta-Thio-Epsilon-Caprolactam, a New Sulfur-Containing Substrate for Alpha-Amino-Epsilon-Caprolactam Racemase. *Febs Lett* 1984, 174 (1), 76-79.
181. Ahmed, S. A.; Esaki, N.; Tanaka, H.; Soda, K., Mechanism of Inactivation of Alpha-Amino-Epsilon-Caprolactam Racemase by Alpha-Amino-Delta-Valerolactam. *Agr Biol Chem Tokyo* 1985, 49 (10), 2991-2997.
182. Ahmed, S. A.; Esaki, N.; Tanaka, H.; Soda, K., Mechanism of Alpha-Amino-Epsilon-Caprolactam Racemase Reaction. *Biochemistry-US* 1986, 25 (2), 385-388.
183. Asano, Y.; Yamaguchi, S., Discovery of amino acid amides as new substrates for alpha-amino-epsilon-caprolactam racemase from *Achromobacter obae*. *J Mol Catal B-Enzym* 2005, 36 (1-6), 22-29.
184. Okazaki, S.; Suzuki, A.; Mizushima, T.; Kawano, T.; Komeda, H.; Asano, Y.; Yamane, T., The Novel Structure of a Pyridoxal 5'-Phosphate-Dependent Fold-Type I Racemase, alpha-Amino-epsilon-caprolactam Racemase from *Achromobacter obae*. *Biochemistry-US* 2009, 48 (5), 941-950.
185. Yasukawa, K.; Asano, Y., Enzymatic Synthesis of Chiral Phenylalanine Derivatives by a Dynamic Kinetic Resolution of Corresponding Amide and Nitrile Substrates with a Multi-Enzyme System. *Adv Synth Catal* 2012, 354 (17), 3327-3332.
186. Payoungkiattikun, W.; Okazaki, S.; Nakano, S.; Ina, A.; H-Kittikun, A.; Asano, Y., In Silico Identification for alpha-Amino-epsilon-Caprolactam Racemases by Using Information on the Structure and Function Relationship. *Appl Biochem Biotech* 2015, 176 (5), 1303-1314.
187. Payoungkiattikun, W.; Okazaki, S.; Ina, A.; H-Kittikun, A.; Asano, Y., Characterization of an alpha-amino-epsilon-caprolactam racemase with broad substrate specificity from *Citricella* sp SE45. *J Ind Microbiol Biot* 2017, 44 (4-5), 677-685.
188. Shen, S.; Floss, H. G.; Kumagai, H.; Yamada, H.; Esaki, N.; Soda, K.; Wasserman, S. A.; Walsh, C., Mechanism of Pyridoxal Phosphate-Dependent Enzymatic Amino-Acid Racemization. *J Chem Soc Chem Comm* 1983, (2), 82-83.
189. Boesten, W. H. J.; Raemakers-Franken, P. C.; Sonke, T.; Euverink, G.J.W.; Grijpstra, P., *UD 7371555 B2* 2008.
190. Bonsor, D.; Butz, S. F.; Solomons, J.; Grant, S.; Fairlamb, I. J. S.; Fogg, M. J.; Grogan, G., Ligation independent cloning (LIC) as a rapid route to families of recombinant biocatalysts from sequenced prokaryotic genomes. *Org Biomol Chem* 2006, 4 (7), 1252-1260.
191. Cox, G.; Stogios, P. J.; Savchenko, A.; Wright, G. D., Structural and Molecular Basis for Resistance to Aminoglycoside Antibiotics by the Adenylyltransferase ANT(2'')-Ia. *Mbio* 2015, 6 (1).
192. Korbie, D. J.; Mattick, J. S., Touchdown PCR for increased specificity and sensitivity in PCR amplification. *Nature protocols* 2008, 3 (9), 1452-1456.
193. Spiliotis, M., Inverse fusion PCR cloning. *PloS one* 2012, 7 (4), e35407.
194. Korbie, D. J.; Mattick, J. S., Touchdown PCR for increased specificity and sensitivity in PCR amplification. *Nature protocols* 2008, 3 (9), 1452-6.
195. Kohlstaedt, L. A.; Lindwall, G.; Gardner, S.; Chau, M., A sparse matrix approach to the solubilization of overexpressed proteins. *Faseb J* 1997, 11 (9), A1043-A1043.
196. Matthews, B. W., Solvent Content of Protein Crystals. *J Mol Biol* 1968, 33 (2), 491-&.
197. Vagin, A.; Teplyakov, A., Molecular replacement with MOLREP. *Acta Crystallogr D* 2010, 66, 22-25.
198. Emsley, P.; Cowtan, K., Coot: model-building tools for molecular graphics. *Acta Crystallogr D* 2004, 60, 2126-2132.

199. Murshudov, G. N.; Vagin, A. A.; Dodson, E. J., Refinement of macromolecular structures by the maximum-likelihood method. *Acta Crystallogr D* 1997, *53*, 240-255.
200. Peter, A.; Torok, G.; Fulop, F., Effect of temperature on retention of cyclic beta-amino acid enantiomers on a chiral crown ether stationary phase. *J Chromatogr Sci* 1998, *36* (6), 311-317.
201. Smith, P. K.; Krohn, R. I.; Hermanson, G. T.; Mallia, A. K.; Gartner, F. H.; Provenzano, M. D.; Fujimoto, E. K.; Goeke, N. M.; Olson, B. J.; Klenk, D. C., Measurement of Protein Using Bicinchoninic Acid. *Anal Biochem* 1985, *150* (1), 76-85.
202. Skwirczynski, R. D.; Connors, K. A., Demethylation Kinetics of Aspartame and L-Phenylalanine Methyl-Ester in Aqueous-Solution. *Pharmaceut Res* 1993, *10* (8), 1174-1180.
203. Mutti, F. G.; Kroutil, W., Asymmetric Bio-amination of Ketones in Organic Solvents. *Adv Synth Catal* 2012, *354* (18), 3409-3413.
204. Brody, S.; Andersen, J. S.; Kannangara, C. G.; Meldgaard, M.; Roepstorff, P.; von Wettstein, D., Characterization of the different spectral forms of glutamate 1-semialdehyde aminotransferase by mass spectrometry. *Biochemistry-Us* 1995, *34* (49), 15918-15924.
205. Frese, A.; Sutton, P. W.; Turkenburg, J. P.; Grogan, G., Snapshots of the Catalytic Cycle of the Industrial Enzyme alpha-Amino-epsilon-Caprolactam Racemase (ACLR) Observed Using X-ray Crystallography. *Acs Catal* 2017, *7* (2), 1045-1048.
206. Chen, S. T.; Wang, K. T.; Wong, C. H., Chirally Selective Hydrolysis of D,L-Amino Acid-Esters by Alkaline Protease. *J Chem Soc Chem Comm* 1986, (20), 1514-1516.
207. Reetz, M. T.; Carballeira, J. D., Iterative saturation mutagenesis (ISM) for rapid directed evolution of functional enzymes. *Nature protocols* 2007, *2* (4), 891-903.
208. Hoebenreich, S.; Zilly, F. E.; Acevedo-Rocha, C. G.; Zilly, M.; Reetz, M. T., Speeding up Directed Evolution: Combining the Advantages of Solid-Phase Combinatorial Gene Synthesis with Statistically Guided Reduction of Screening Effort. *Acs Synth Biol* 2015, *4* (3), 317-331.